Field Cycling NMR Experiments with Hyperpolarized Multi-Spin-Systems

Dissertation

zur Erlangung des akademischen Grades des Doktors der Naturwissenschaften
(Dr. rer. nat.)
eingereicht im Fachbereich Biologie, Chemie, Pharmazie der
Freien Universität Berlin

vorgelegt in englischer Sprache
mit deutscher Zusammenfassung
von

Karsten Miesel

aus Birkenfeld (Pfalz)
August 2008

1. Gutachter: Prof. Dr. Hans-Martin Vieth

2. Gutachter: Prof. Dr. Hans-Heinrich Limbach

Disputation am 08.12.2008

Zusammenfassung

Es werden FT-NMR Experimente an skalar gekoppelten Spinsystemen mit Magnetfeldzyklisierung beschrieben, welche eine Unterscheidung von Wechselwirkungsparametern anhand ihrer Abhängigkeit vom externen Magnetfeld *B* erlauben. Der größte Teil der Arbeit befaßt sich mit Spinensembles weitab vom thermischen Gleichgewicht. Insbesondere Hyperpolarisation (HP) erzeugt durch chemisch induzierte dynamische Kernspinpolarisation (CIDNP) und T_1-Relaxation in Flüssigkeiten werden studiert. Die Feldzyklisierung ermöglicht das Studium der Relaxation individueller Protonen, die Bestimmung magnetischer Wechselwirkungsparameter der Vorläuferradikale in denen HP erzeugt wurde, sowie einen Polarisationstransfer zu bestimmten ausgewählten Protonen. Des weiteren erlaubt die Methode eine Unterscheidung der Mechanismen für die photoinduzierte CIDNP Bildung und eine Analyse der beteiligten Photoreaktionen.

Weil im niedrigen Magnetfeld die Kernspinzustände gekoppelter Spinsysteme kollektive Zustände aller beteiligten Spins sind, werden Phänomene wie Hyperpolarisation (HP) und Kernspinrelaxation zu Eigenschaften der gesamten Spinsysteme. Als Konsequenz werden die Magnetfeldabhängigkeiten der HP und T_1-Relaxation für stark gekoppelte Kerne ($2\pi J > \Delta\omega_L$) auf einer der inversen *J*-Kopplung entsprechenden Zeitskala tendenziell gleich. In den frequenzabhängigen Relaxationszeiten (NMRD) sind Stufen an den Feldstellen sichtbar, in denen die Larmor-Präzession der Größenordnung der *J*-Kopplung entspricht.

Im Falle nicht-adiabatischer Magnetfeldvariation oder Produktbildung treten Null-Quantenkohärenzen auf. Durch Variation des Zeitintervalls für freie Spinevolution werden diese durch nicht-adiabatische Feldvariation in Polarisation überführt, und können in den Amplituden der NMR-Signale als charakteristische Quantenschwebungen detektiert werden. Auf diese Weise kann durch Anwendung geeigneter Feldzyklisierung HP von ursprünglich polarisierten Kernen auf unpolarisierte Kerne sogar dann übertragen werden, wenn die beiden Kerne im Hochfeld nicht direkt, sondern nur über weitere Kerne indirekt miteinander gekoppelt sind. Positionen, an denen Kernspinzustände kreuzen, sind für eine effiziente Übertragung von HP von besonderer Bedeutung und in unterschiedlichen feldabhängigen NMR Experimenten als Minima oder Maxima zu beobachten. Je nach Wahl der zeitlichen Parameter für die Bildung der HP, die freie Spinevolution und die Feldschaltung werden unterschiedliche Polarisationsmuster detektiert.

Als weitere Folge der Gruppierung von Kernspinzuständen werden im Niederfeld Multiplett-Polarisationen beobachtet, die sich über das gesamte Spinsystem erstrecken. Die Amplituden

einzelner Linien innerhalb des Spin-Multipletts hängen charakteristisch vom RF Nachweiswinkel φ ab, und die Nutationsmuster werden durch Fourier-Zerlegung entlang φ analysiert. Bei dieser Technik wird das Spektrum entsprechend den unterschiedlichen Nutationsfrequenzen in Spektren verschiedener Ordnungen zerlegt, welche ausschließlich die gegenseitige Orientierung bestimmter Untergruppen gekoppelter Kerne wiedergeben.

Die beschriebenen Techniken werden auf die Photolyse der aromatischen Aminosäuren Tyrosin (NATyrOH) und Tryptophan (NATrpH) bei λ=308nm in wäßriger Lösung angewandt, welche zur CIDNP Bildung in den Aminosäuren sowie den Protonen des Lösungsmittels (HDO) führt. Anhand der Feldabhängigkeit (FD-CIDNP) und zeitaufgelöster Messungen im Hochfeld (TR-CIDNP) wird die Photophysik und -chemie analysiert. In basischer Lösung erfolgt die Ionisierung aus einem angeregten Singulett-Zustand, und führt zur Bildung von Radikalpaaren solvatisierter Elektronen (e^-_{aq}) mit den Radikalen $NATyrO^\bullet$ und $NATrpH^{\bullet+}$. Die Reduktion der ursprünglichen Aminosäuren durch e^-_{aq} führt zu selektiv deuterierten Aminosäuren und erklärt die starke Polarisation von HDO.

Die oben genannten Aminosäuren werden des weiteren in der Gegenwart geeigneter Farbstoffe, z.B. 2,2'-Dipyridyl (DP) und Anthrachinon-2-sulfonat (AQ2S) untersucht, was zur Bildung von spinkorrelierten Triplett-Radikalpaaren aus denselben Aminosäure Radikalen und Farbstoff-Radikalen führt. Unterschiedliche Kombination derselben Radikale in Paaren mit unterschiedlichen Farbstoff-Radikalen erlaubt einen Vergleich der Δg-Werte aus mehreren CIDNP Feldabhängigkeiten, so daß g-Werte höherer Genauigkeit für die untersuchten Radikale erhalten werden.

Die Mechanismen der effizienten CIDNP Bildung bei Änderung molekularer Beweglichkeit wird anhand der Photolyse zyklischer Ketone untersucht. In der festen Phase bildet sich keine Polarisation, was zeigt, daß die Mobilität der Moleküle eine Voraussetzung für die CIDNP Bildung ist. Unter eingeschränkter Mobilität in der plastisch kristallinen Phase von C_6D_{12} wird die mittlere Austauschwechselwirkung J_{ex} in den resultierenden Diradikalen tendenziell durch die Dimensionen der Matrix bestimmt. Die Photolyse von Aceton in flüssigem und plastisch-kristallinem C_6D_{12} zeigt bei gleich bleibender Photochemie eine abrupte Änderung im Polarisationsmechanismus von $S\text{-}T_0$ nach $S\text{-}T_-$ beim Phasenübergang. Ähnliche Werte für J_{ex} wie im Fall der zyklischen Ketone werden gefunden. In diesem Fall sind die zwei Radikale nicht über Bindungen verknüpft und die J_{ex} wird durch den Raum übermittelt.

Die Perspektiven zukünftiger Anwendungen feldabhängiger Messungen der magnetischen Resonanz werden diskutiert.

Abstract

FT-NMR experiments with scalar coupled multi-spin systems employing variation of the external magnetic field *B* are described, allowing one to discriminate interaction parameters because of their different dependence on *B*. The mayor part of the work deals with spin ensembles far away from their thermal equilibrium. In particular, hyper-polarization (HP) generated by means of chemically induced dynamic nuclear polarization (CIDNP), and T_1-relaxation in liquids (fast motional regime) are studied. Field cycling experiments are shown to open possibilities for detailed studies of the relaxation behavior of individual protons, to provide access to the magnetic properties of the precursor radicals in which HP was formed, and for a proton site specific transfer of HP. Furthermore, the method allows one to differentiate mechanisms of CIDNP formation and the analysis of photoreactions.

In low field the nuclear spin states of coupled multi-spin systems are collective states and hyper-polarization (HP) and spin-relaxation become properties of the entire spin system. As a consequence, field dependences of HP and T_1-relaxation tend to become similar for nuclei fulfilling the condition of strong scalar coupling J ($2\pi J > \Delta\omega_L$), within a time that corresponds to the inverse J-coupling. In nuclear magnetic relaxation dispersion (NMRD), this results in stepwise features being observed in the field regions where the Larmor precession ω_L becomes comparable to the J-coupling.

Zero-quantum-coherences are shown to occur in the spin density matrix upon non-adiabatic field variation and product formation (radical recombination). Variations of the time interval for free spin-evolution reveal characteristic quantum beats in the amplitudes of NMR signals after the coherences are transferred into polarization by non-adiabatic field variation. This way, HP is coherently transferred from primarily polarized spins to particular target spins within coupled spin systems by devising appropriate field cycling schemes, even in case the two spins are not noticeably coupled by spin-spin interaction in the high field of the spectrometer but only through a chain of coupled spacer-spins. Positions where nuclear spin states anti-cross are of particular significance for efficient transfer of HP. Depending on the timing of field cycling, maxima and minima are observed in these regions in various kinds of field dependent NMR experiments. The outcome of the experiments depends on the timing for the formation of HP, for free spin-evolution and for the field switches.

Another consequence of the grouping of spin-levels in low field is that multiplet CIDNP is observable over entire multi-spin systems. The intensities of individual lines within multiplets characteristically depend on the RF-flip angle of the detection, and their nutation patterns are

analyzed by means of Fourier expansion with respect to the flip angle. This technique separates the multiplet effects belonging to different sub-sets of nuclei by their nutation frequency (harmonic order) and yields spectra that exclusively reflect the mutual alignment of several coupled spins.

The techniques described are applied to the analysis of the photolysis of the aromatic amino acids tyrosine (NATyrOH) and tryptophan (NATrpH) at λ = 308 nm in aqueous media. Their photolysis proceeds with the formation of CIDNP in the parent amino acids and in the residual protons of the solvent (HDO). From the field dependence of CIDNP and its time dependence at high magnetic field (TR-CIDNP), the photo-physics and -chemistry is analyzed. Ionization occurs from electronic singlet states, and is most efficient in basic solution, yielding solvated electrons (e^-_{aq}) and the radicals $NATyrO^{\bullet}$ and $NATrpH^{\bullet+}$. Reduction of the parent amino acids by e^-_{aq} and subsequent reaction steps yield selectively deuterated amino acids and explains the strong CIDNP observed for HDO.

The abovementioned amino acid radicals are further investigated in the presence of different triplet sensitizers, e.g. 2,2'-dipyridyl (DP) and anthraquinone-2-sulfonic acid (AQ2S), yielding the same amino acid radicals in spin correlated triplet radical pairs with the radicals of the dyes. Various combinations of the amino acid and dye radicals allow a comparison of the Δg-values from several CIDNP field dependences. Because of their inter-dependence, each g-value is extracted from more than a single field-dependence, and values of higher accuracy are obtained for the radicals under study.

The mechanisms for efficient CIDNP formation upon restriction of molecular mobility are investigated on the photolysis of cyclic ketones. In the solid phase, no CIDNP is detected, and molecular mobility is found as a prerequisite for the formation of CIDNP. When confined by a matrix of plastic crystalline C_6D_{12}, the average exchange interaction, J_{ex}, in the resulting bi-radicals tends to be determined by the matrix dimensions. When acetone is photolyzed in liquid and plastic crystalline C_6D_{12}, the photo-chemistry of the primary events remains the same, but the mechanism of CIDNP formation abruptly changes from S-T_0 to S-T_- at the phase transition, giving rise to comparable values for J_{ex} as in the case of the cyclic ketones. In this case, the two radicals are not connected via a network of chemical bonds, and J_{ex} is thus transmitted through space.

The prospects of further applications of field dependent magnetic resonance techniques are discussed.

Abbreviations and Symbols

a	isotropic hyperfine coupling
a_{eff}	effective hyperfine coupling
AQ2S	anthraquinone-2-sulfonic acid
B	magnetic field
B_0	field of NMR detection
B_1	radio frequency field
B_{ev}	intermediate field (for free spin evolution)
B_{pol}	polarization field
B_r	relaxation field
CIDEP	chemically induced dynamic electron polarization
CIDNP	chemically induced dynamic nuclear polarization
DNP	Dynamic nuclear polarization
DP	2,2’-dipyridyl
FD-CIDNP	field dependent CIDNP
HFC	hyperfine coupling
ISC	inter system crossing
J_{ex}	electronic exchange interaction
$J_{ex,eff}$	effective exchange interaction
J_{i-j}	scalar coupling between spin i and spin j
J_z	total spin projection quantum number
M_z	total z-magnetization
n	integer number (e.g. number of spins)
NATrpH	N-acetyl tryptophan
NATyrOH	N-acetyl tyrosine
NMR	nuclear magnetic resonance
NMRD	nuclear magnetic relaxation dispersion
NOE	Nuclear Overhauser effect
P_i	population of state i
R_B	Bohr radius
RF	radio frequency
T_1	longitudinal relaxation time

T_2	transversal relaxation time
TR-CIDNP	time resolved CIDNP
UV	ultra violet
E	energy
Ω_{rs}	coherence frequency between states *r* and *s*
ϕ	spin-spin coupling angle
φ	RF flip angle
σ_C	cross relaxation rate
τ	time interval
τ_c	correlation time
τ_{ev}	time interval for spin evolution
τ_{fv}	field variation time
τ_L	irradiation time
τ_p	pulse length
ω_L	Larmor frequency

Content

1 Introduction

Molecules in excited states are commonly encountered during or shortly after their formation in chemical reactions and can be investigated by optical spectroscopy, involving the electric component of electromagnetic radiation. What is less commonly known among chemists is, that the intermediates and products may also exhibit spin states which are far off thermal equilibrium, which are accessible via their magnetic moments. This is usually the case for reactions involving paramagnetic intermediates, i.e. molecules with unpaired electron spins. The field of ‘Spin Chemistry’ is engaged with investigations concerning the effects of the magnetic field on the outcome of chemical reactions. It covers magnetic field effects on reaction rates, yields, and on the quenching of fluorescence. The probably most important experimental tools to the spin chemist, however, directly probe the spin states of intermediates or products of radical reactions; these are Chemically Induced Dynamic Electron Polarization (CIDEP) and Chemically Induced Dynamic Nuclear Polarization (CIDNP). These phenomena origin from the selection rules for intersystem crossing and the fact that the making and braking of chemical bonds (or electron and hydrogen transfer) must preserve spin angular momentum (Wigner’s rules). Surveys on these subjects can be found in [1, 2]. Analysis of electron and nuclear spin polarization by these means allows a unique insight into the elementary steps of radical reactions.

CIDNP is a manifestation of the spin selection rule in radical reactions and is associated with spin transitions in radical reactions induced by magnetic interactions (Zeeman and hyperfine interaction). As a result of spin transitions in radical pairs, their recombination probability is affected by the weak magnetic interactions. Starting from a chemical non-equilibrium situation, the chemical equilibrium is established by leaving a transient disequilibrium in the nuclear spin states. Because nuclear spin relaxation is relatively slow (in the order of seconds) this non-equilibrium polarization can be probed by nuclear magnetic resonance (NMR) long after the radical reaction is over. The NMR spectra of the reaction products then exhibit anomalous signal intensities which are related to the magnetic interaction parameters in the radical pair state, thus containing information on the short lived intermediates of the reaction. The most common application of the CIDNP technique has therefore always been the analysis of the intermediates of radical reactions.

The present work is exclusively devoted to photo-chemically generated radical pairs (photo-CIDNP). Photoreactions play a key role in numerous biological processes and industrial

applications. An important industrial application is the UV-induced polymerisation reactions for the production of various polymers. Similar reactions are involved in the curing of certain types of glues and dental inlays. The most prominent example for light induced processes in biology is the photosynthesis of cyanobacteria and plants, the probably most efficient way of the conversion of light energy into chemical energy which is finally stored in the form of sugars.

A heavily debated question falling into the field of spin chemistry is whether ordinary (or environmental) magnetic fields can exert an appreciable influence on chemical and biochemical reactions, e.g. whether an excessive use of cellular phones can be harmful. Recently, the attention on magnetic field effects on the radical pair dynamics in very weak magnetic fields has increased, because anisotropic field effects as potential mechanisms controlling magnetoreception in migratory birds are discussed [3-6]. Cryptochromes, a flavoprotein family, in the bird's eye have been proposed to provide the radical pairs for the successful orientation in the earth magnetic field, consisting of a flavin and a tryptophan radical.

The directed motion of living organisms as a response to light irradiation (phototaxis) is also conciliated with the action of cryptochromes [7, 8]. Amino acids radicals, in particular those of tyrosine and tryptophan, are probably also involved in preserving genetic information by the scavenging of nucleotide-derived radicals of the DNA, which are produced e.g. by intense UV-light.

Because of the central role of the effects of electron and nuclear spins and of their magnetic interactions for the course of photochemical reactions, and for the formation of nuclear spin polarization, there is an obvious demand for probing CIDNP as a function of the external magnetic field. Different mechanisms for CIDNP formation are usually well differentiated by their characteristic dependence on the external magnetic field. In addition, the CIDNP field dependence usually bears information on the magnetic interaction parameters, thus allowing a characterization of very short lived radicals, which are sometimes elusive to electron paramagnetic resonance spectroscopy (EPR).

Field cycling NMR is a technique that has almost exclusively been used for acquisition of NMR relaxation dispersion (NMRD) in the past. With this type of experiments, the longitudinal and transversal relaxation to thermal equilibrium is probed at variable magnetic field (as a function of Larmor precession frequency). Information on molecular motion on time scales much shorter than the NMR time scale is usually extracted [9]. More recently, a new variation of NMR field cycling has enabled a more detailed investigation of the high

resolution NMR spectra recorded at high magnetic field, after the sample is ‘prepared’ at low magnetic fields [10, 11]. The mechanical field cycling apparatus allows the acquisition of FT-NMR spectra after conducting chemical reactions at arbitrary magnetic field. Moreover, it provides possibilities for several precisely controlled field switches prior to the detection of nuclear polarization in the field of the cryomagnet.

During the last decades NMR has evolved to the probably most valuable tool for elucidation of molecular structure due to its high content of information. Each group of equivalent nuclei in a given molecule gives rise to a separate signal in the NMR spectrum, and the position and shape of these signals is correlated with the chemical surrounding of the nucleus. This renders photo-CIDNP a particularly promising technique for elucidating the role of magnetic fields on radical pair reactions of biological interest since the product molecules are well differentiated when using NMR spectroscopy.

A mayor drawback of NMR spectroscopy is certainly its notoriously low sensitivity. When probing nuclear spins at thermal equilibrium, one is left with polarizations of about 10^{-4} to 10^{-5} at room temperature and the large field provided by modern cryomagnets. This shortcoming of the NMR technique is particularly incisive for medical applications, limiting the possibilities of magnetic resonance imaging (MRI) and microscopy [9, 12]. The potentials of functional MRI techniques depend decisively on suitable ways for boosting their sensitivity by the creation of hyper-polarisation (HP). Dynamic polarization methods prepare the spin states in the object under study to overcome problems resulting from the signal to noise ratio, still allowing to apply any possible pulse sequence for detection.

There are several other ways for generating HP besides the CIDNP technique [1], such as para hydrogen induced polarization (PHIP) [13] and different ways of optical nuclear polarization (ONP) or Overhauser-type experiments [14, 15]. Most importantly, MRI of the lung has been considerably advanced by the use of hyperpolarized noble gases as a contrast agent [16]. However, irrespective of the means by which means the non-equilibrium nuclear polarization is obtained, it is usually necessary to transfer it to the target nuclei which one desires to observe.

Field cycling NMR in combination with HP techniques enables not only investigations of radical reactions by generating nuclear polarization at arbitrary field but also the study of polarization and coherence transfer phenomena induced by switching the external field. Because the technique is relatively new, the effects of switching the external field on the polarized high resolution NMR spectra are not yet elucidated. In part, this work contributes to a more thorough understanding of such effects on the observed polarization patterns. Besides

of the expected merits of field cycling CIDNP within the field of spin chemistry, i.e. for the elucidation of radical reactions and the magnetic interaction parameters of the involved radicals, it shall be shown that the technique deserves additional appreciation for the possibility of transferring HP to nuclei that are initially not polarized.

1.1 Outline

In the next chapter (chapter 2) the reader is provided with some theoretical background, which shall help in understanding the techniques and observations described thereafter. The radical pair theory of CIDNP formation will be outlined, which forms the basis for an understanding of the generation of nuclear spin polarization during radical reactions. It is limited to a rather qualitative picture of the phenomena of CIDNP formation. Even though it might be considered too basic, the parameters that determine the appearance of a typical liquid state NMR spectrum will be briefly introduced in the second section of chapter 2. They are crucial for the understanding of virtually any type of field cycling experiment discussed in this work and can thus not be omitted.

This work is an almost entirely experimental approach of obtaining insight into the phenomena that are responsible for the outcome of different kinds of field cycling experiments. The experimental techniques are subject to chapter 3. Here, the experimental set-ups for the acquisition of time resolved and field dependent CIDNP spectra, as well as some modifications made during the work are described in detail, and the timing scheme commonly used for obtaining CIDNP field dependences is introduced.

The remaining part of the thesis is arranged according to the different aspects that determine the observed polarization patterns, these are: i) the peculiarities of CIDNP field dependences arising from the field cycling process and HP transfer phenomena, ii) the analysis of polarization patterns upon the variation of the detection flip angle (RF pulse length), and iii) the combination of time resolved and field dependent CIDNP techniques for the elucidation of photochemical processes of biological interest.

The polarization of particular nuclei in a given molecule depends on the energetic ordering and grouping of nuclear spin states. Chapter 4 is devoted to the effects of the changes in the ordering of states during variation of the external magnetic field. Besides the redistribution of polarization at low magnetic field, the coherent transfer of hyper-polarization by controlled

fast field switches into regions of level-anti crossings within nuclear spin states is investigated for the first time.

These effects can not be expected to be limited to experiments employing hyper-polarization, since any NMR experiment employs disequilibria in nuclear spin populations to enable its detection. In particular, the effects of changes in the ordering of spin states fast and slow field switches on observed CIDNP patterns, and the influence of the energetic arrangement of nuclear spin states on the T_1 relaxation dispersion of individual proton sites in small molecules will be explored.

The spin-spin couplings in hyperpolarized molecules are known to manifest themselves in particular NMR patters termed ‘multiplet effects’, which characteristically depend on the RF flip angle of detection (the length of the detection pulse). A convenient method for a detailed analysis of multiplet effects in complex spin systems is the Fourier expansion of the nutation pattern. This technique is explored experimentally in chapter 5, where nutation patterns are studied for CIDNP generated at different magnetic fields.

Finally, in the last chapter (chapter 6), photochemical and -physical aspects of particular radical reactions are explored by CIDNP. In the first section, photolysis reactions of the aromatic amino acids tyrosine and tryptophan are investigated. Here, the parallel application of time resolved and field dependent techniques provide a detailed insight into the processes following photo-ionization of these compounds, and the mechanism responsible for large polarizations observed on the solvent molecules (HDO).

The same amino acids are investigated in radical pairs with different sensitizing molecules (dyes) in the second part of chapter 6. This comparative study allows a reliable referencing for the relation of the CIDNP high field maxima with the g-factor differences in the radical pairs under study, and provides further insight into the properties that govern the formation of CIDNP low magnetic fields.

In all the reactions discussed until the very last part of the thesis (chapter 6.3), the exchange interaction, i.e. the energetic difference between the electronic singlet and triplet states, is negligible because the radicals in the pair are separated by diffusive displacement before their reencounter. The effects of geometrical confinement on the mechanism of CIDNP formation are studied in section 6.3. The CIDNP field dependences of biradicals formed during Norrish type I cleavage of cyclic ketones have been studied in some detail before, and it was shown that the position of maximum polarization scales with the length of the biradicals [11]. In the present work, this investigation is extended to CIDNP formation of different types of ketones in liquids and plastic crystalline matrix. It is shown that in the plastic crystalline matrix all

ketones under study are polarized by the S-T$_-$-mechanism, and the exchange interaction (J_{ex}) between the radical centres appears to be governed by the dimensions of the host lattice rather than by the size of guest molecules.

2 Theoretical Background

In this chapter, some theoretical models and tools for an understanding of the experimental results presented in chapters 4 to 6 shall be given. In the first part (chapter 2.1), the formation of nuclear spin polarization during radical reactions is discussed. Here, it is the evolution of the electron-nuclear spin density matrix, $\hat{\sigma}$, in the radical pair (RP) state which has to be considered in order to provide understanding of the peculiarities of chemically induced dynamic nuclear polarization (CIDNP). Particular attention is paid to the influence of the external magnetic field since the mayor part of this work deals with the field dependence of CIDNP.

Upon radical recombination to diamagnetic products, the large electronic spin interactions are 'switched off' and the preparation of the nuclear spin system is complete. Then, it is solely the spin evolution in the nuclear spin system, described by the nuclear spin density matrix, $\hat{\rho}$, which has to be considered. The first section of chapter 2.2 is therefore devoted to the quantities that describe liquid state NMR spectra in general, which turned out to be crucial for the outcome of virtually any field cycling NMR experiment. Changes in the relative energies of spin-states in complex multi-spin systems do not only manifest themselves in the NMR patterns of CIDNP spectra polarized at variable magnetic field , but also determine the patterns observed in other hyper-polarization experiments such as Para Hydrogen Induced Polarization (PHIP) [17], i.e. spin polarization that is formed in catalytic hydrogenation reactions of multiple bonds with para-H_2 at high (PASADENA) [18] and low (ALTADENA) [19] magnetic fields.

Controlled switching of the external magnetic field provides a tool for the redistribution and the directed transfer of hyper-polarization (HP) to target nuclei which do not initially exhibit spin polarization. The necessary conditions and underlying mechanisms for an efficient transfer of HP in field cycling experiments will be discussed in some detail.

In addition, the field dependence of longitudinal relaxation to thermal equilibrium (often termed T_1 relaxation dispersion or nuclear magnetic relaxation dispersion (NMRD)) of spins in coupled multi-spin systems of small molecules in liquid solution is subject to related phenomena. The theoretical background for a prediction of NMRD data of individual nuclei in the fast motional limit from their T_1 relaxation times at high magnetic field will be briefly described in the end of chapter 2.2.

2.1 CIDNP Formation

The term ‘CIDNP’ describes the observation of extraordinary polarization patterns in NMR spectra that reflect the non-equilibrium population of nuclear spin states in the products of chemical reactions. The phenomenon was first reported in 1967 simultaneously by two groups of researchers. Bargon et al. [20] observed emission lines in the NMR spectra taken during the thermal decomposition of peroxide compounds. Anomalous intensities of NMR lines were also seen by Ward and Lawler [21] while they studied reactions of lithium alkyls with alkyl halides by NMR. In both cases, it was immediately realized that the observed polarization was associated with the occurrence of free radicals in the solutions under study. It is therefore surprising that the phenomenon has not been observed earlier, because NMR had already evolved to a widely spread technique for the investigation of chemical reactions, and CIDNP is observable in a wide variety of reactions involving radical intermediates.

While CIDNP was initially rather attributed to electron-nuclear cross-relaxation (Over-hauser-Effect), it took until 1969 before an understanding of the underlying physics for these NMR spectra was underway. It was two groups that both contributed decisively to the development of a theory to explain the observations. Kaptein and Osterhoff [22, 23] on one hand, and the group around Closs [24, 25] on the other, independently worked on a similar model that is nowadays referred to as the ‘Radical Pair Model’ (RPM). The RPM is not only able to explain CIDNP, but simultaneously explains the unusual polarization patterns in transient electron paramagnetic resonance (EPR) spectra (CIDEP spectra).

The RPM is based on the idea of a radical pair in a so-called ‘cage’, and a nuclear spin selective intersystem crossing with successive recombination from a defined multiplicity. In both groups experiments were carried out in parallel that unambiguously confirmed the validity of their model, and it still serves to explain the phenomena of a variety of experiments such as time resolved CIDEP or SNP (Stimulated Nuclear Polarization). For completeness, it should be mentioned that alternative theories have been developed such as the triplet mechanism [26] that are, however, of minor importance for the present work and will therefore be disregarded.

Another important step in the theoretical description of CIDNP was done by Adrian [27, 28], who first realized the importance of diffusive reencounters of the radical pair (RP) in the formation of nuclear spin polarization. He questioned whether the RP, while hold together in the solvent cage, would have sufficient time between separation and recombination for nuclear spin selective intersystem crossing induced by the hyperfine interaction (HFI).

While the substantial part of investigations in the theoretical field of the formation of spin polarization was completed, CIDNP has developed to a useful tool for the investigation of radical reactions. This holds in particular for the analysis of physical and chemical processes of light induced reactions by photo-CIDNP. Here, a fundamental advantage comes into play, namely that the starting point of the chemical reaction is well defined by the incident light, and with the development of efficient light sources (pulsed lasers), the time resolved CIDNP (TR-CIDNP) method became a tool for the investigation of the kinetics during the radical pair stage.

From the theoretical point of view, the magnetic field effects associated with the formation and observation of CIDNP are also largely considered to be understood, disregarding that available experimental data of CIDNP field dependence were for a long time restricted to very few cases, which mostly dealt with the CIDNP formation in bi-radicals.

In the following, some of the theoretical models indispensable for the qualitative understanding of CIDNP formation shall be reviewed; most of these models are described in more detail in two books on these topics [1, 2], and in the original papers cited along with the text.

2.1.1 The Radical Pair Mechanism

A photochemical free radical reaction. A typical scheme of the radical pair mechanism (RPM) for photo-CIDNP is outlined in figure 2.1.1. It is applicable to qualitatively explain the formation of nuclear spin polarization observed in most of the experiments presented in this work. However, the RPM alone is not sufficient for a quantitative analysis of CIDNP spectra in terms of magnetic interaction parameters of the radicals involved, or the dependence of the CIDNP signal on time. Hence, the RPM only forms the basis for further theories, some of which shall be introduced below.

Consider a molecule, here a dye molecule denoted with D in figure 2.1.1, is brought into its excited state by the absorption of a photon. This is usually an excited singlet state, given, that the ground state was also a diamagnetic molecule (singlet-state). The light excitation is then followed by inter system crossing to an excited triplet state (ISC) and the separation into a radical pair (RP). These pairs are called *geminate* radical pairs due to the simultaneous generation of the two radicals. This may happen upon the homolytic cleavage of a covalent bond, or upon charge transfer by means of electron or hydrogen atom transfer from a second

molecule. In figure 2.1.1, it is a second molecule denoted as AH (for a protonated amino acid). Most of the reactions investigated in this work deal with reactions that fit into this pattern. However, the letters D and A could in principle denote any other electron donor and acceptor molecules, respectively. The RP generation takes place from either a singlet or a triplet state, and for photo-CIDNP both, singlet and triplet precursors are possible.

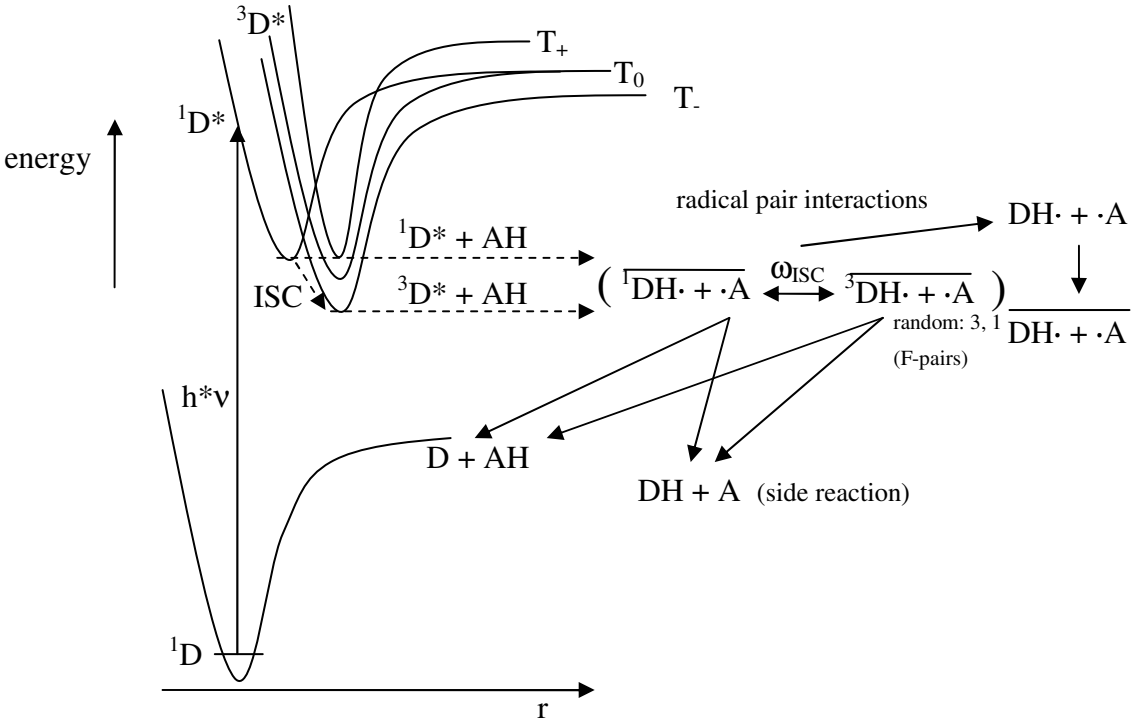

Figure 2.1.1: Typical scheme of a photochemical radical pair reaction (in part adopted from ref.: [2]). The radical pairs indicated on the right side are energetically not necessarily ordered in the indicated way.

Once the radical pair is generated it is referred to as a singlet- or triplet born radical pair. It initially remains correlated with the electron spins oriented anti-parallel (singlet: *S*) or parallel (triplet: *T*), and their spin correlation is usually indicated by an over-bar (see fig. 2.1.1). The radical pair may undergo a variety of chemical reactions, as indicated in figure 2.1.1. In the primary solvent cage, the original reactants may be restored, which in our case are usually a dye D and an amino acid AH, or disproportionate to form new products. Alternatively, the radicals can diffuse apart and loose their correlation, yielding free radicals. The free radicals are subject to subsequent reactions, such as fragmentation or abstraction, but eventually they will all recombine in pair-wise encounters. The RP formed by the random encounter of two independent (free) radicals is called F-pair to be distinguished from the geminate RP.

In order to observe a polarization on the nuclei, e.g. protons with spin ½, their magnetic moment must be involved in a magnetic interaction during the process of the radical reaction. The primary singlet-triplet intersystem crossing takes place due to spin-orbit interaction,

leading to polarization on the electron spins sometimes observable by EPR. In the radical pair, the magnetic interactions of the unpaired electrons with the external magnetic field (Zeeman interaction), their coupling with each other (exchange interaction), and their interaction with the magnetic nuclei (hyperfine interaction, HFI) are the requisites for nuclear spin polarization. The nuclear spins are involved during the process of singlet-triplet mixing (S-T-mixing) in the RP state as they can influence the rate of intersystem crossing, ω_{ISC}. Since this influence is the reason for the formation of CIDNP it shall be discussed here in more detail. In the following some peculiarities of the S-T-mixing are introduced.

Quantum mechanical description of S-T mixing. During the lifetime of the RP the spin dynamics is described by the time dependent Schrödinger equation [29]:

$$\frac{\partial \hat{\sigma}}{\partial t} = i\left[\hat{H}, \hat{\sigma}\right] \quad , \tag{2.1.1}$$

with the time dependent electron-nuclear spin density operator $\hat{\sigma}(t)$ (observable, hermitian), for which a singlet-triplet representation of the electronic spins is convenient. A system consisting of two electron spins and an arbitrary number of nuclear spins is then described by the direct product of the electron spin eigen-basis and the Zeeman basis for the nuclear spins coupled to the electrons by the hyperfine coupling (HFC). The electronic basis-functions are as follows (stationary eigen-states):

$$\begin{aligned} \left|T_+\right\rangle &= \left|\frac{1}{2},\frac{1}{2}\right\rangle \\ \left|T_-\right\rangle &= \left|-\frac{1}{2},-\frac{1}{2}\right\rangle \\ \left|T_0\right\rangle &= \frac{1}{\sqrt{2}}\left(\left|\frac{1}{2},-\frac{1}{2}\right\rangle + \left|-\frac{1}{2},\frac{1}{2}\right\rangle\right) \\ \left|S\right\rangle &= \frac{1}{\sqrt{2}}\left(\left|\frac{1}{2},-\frac{1}{2}\right\rangle - \left|-\frac{1}{2},\frac{1}{2}\right\rangle\right) \end{aligned} \quad . \tag{2.1.2}$$

Each of these functions is connected to a number *i* (or *j*) of nuclear spins $\left|m_i\right\rangle$ and $\left|n_j\right\rangle$ (*m* for those coupled to one, and *n* for those coupled to the other electron). Here, we only deal with spin-½ systems (protons), meaning that their eigenvalues are $m_i, n_j = \pm\frac{1}{2}$ (with ½ = α, –½ = β) that denote a proton spin oriented parallel or anti-parallel to the external magnetic field, respectively. The spin Hamiltonian $\hat{H}_M$ describing the intermediate RP state contains the exchange interaction (J_{ex}), the electron Zeeman interaction, and the hyperfine interactions. With the energies in units of $\hbar$, it is given by the equation [30]:

$$\hat{H}_M = -J_{ex}(r)\left(2\hat{S}_1 \cdot \hat{S}_2 + \frac{1}{2}\right) + \beta_0\hbar^{-1}\left(g_1\hat{S}_1 + g_2\hat{S}_2\right)B_{pol} + \sum_n a_{1n}\hat{S}_1\hat{I}_{1n} + \sum_m a_{1m}\hat{S}_2\hat{I}_{2m} \quad , \quad (2.1.3)$$

where S_1 and S_2 are the electron spins of the two radicals, and $2J_{ex} = (E_S - E_T)$ is the singlet triplet splitting. B_{pol} is the external magnetic field; g_1 and g_2 are the electronic g-factors of radicals 1 and 2, a_{1n} and I_{1n} are, respectively, the isotropic hyperfine structure constant and the nuclear spin of the n^{th} nucleus of radical 1, and a_{2m} and I_{2m} the analogous quantities for radical 2. The anisotropic terms of the Hamiltonian are usually neglected, because the time between separation and re-encounters of the radicals is anticipated to be long enough to average these terms to zero.

In addition to the quantum mechanical description by the spin Hamiltonian (formula 2.1.3), the evolution of the spin density matrix is determined by the chemical reaction and relaxation described by classical rate processes in terms of the stochastic Liouville equation [2]:

$$\frac{\partial\hat{\sigma}}{\partial t} = -i\hat{\hat{L}}\hat{\sigma} - \hat{\hat{K}}\hat{\sigma} - \hat{\hat{R}}\hat{\sigma} - \hat{\hat{W}}\hat{\sigma} \quad , \quad (2.1.4)$$

where the Liouville (super-)operator is given by:

$$\hat{\hat{L}} = \hat{H} \otimes \hat{E} - \hat{E} \otimes \hat{H} \quad . \quad (2.1.5)$$

In the Liouville formalism, the rates of chemical reactions into and from the RP are described by $\hat{\hat{K}}$, the electron spin relaxation is given by the relaxation matrix $\hat{\hat{R}}$ (very similar to that in the case of nuclear spin relaxation described in the end of chapter 2.2) [31], and $\hat{\hat{W}}$ describes the molecular dynamics during the live time of the RP.

Depending on the timescales of the processes described by the Liouville equation as compared to the spin dynamics, not necessarily all of the matrices have to be taken into account. In general, two time scales can be distinguished, i.e. the formation of geminate CIDNP that takes place within several nanoseconds, and the polarization formed in F-pairs during microseconds to seconds.

The rate operator $\hat{\hat{K}}$ however, is indispensable for the description of CIDNP formation, as it projects the nuclear spin polarization formed in the radicals onto the states in the diamagnetic product, which is finally observed in the NMR spectrometer. Molecular dynamics is of particular interest for the modulation of J_{ex} in case of the flexible biradicals studied in chapter 6.3, but the discussion there remains on a qualitative level, and the operator $\hat{\hat{W}}$ shall therefore not be discussed in more detail here. For the systems investigated in the present work, the relaxation operator $\hat{\hat{R}}$ is insignificant.

The initial spin density matrix (at $t = 0$), directly after the RP is formed is given by $\hat{\sigma}(0)$, and the reaction rates described by the operator $\hat{\hat{K}}$ are those from the RP state into the singlet state of the product molecule, k_S, and the reaction into a local triplet state, k_T. These transitions suffice to explain the formation of CIDNP in most cases, and their description by classical rates is justified as they occur instantaneously on the timescale of the considerably slower spin dynamics in the RP state, i.e. the frequency of singlet-triplet evolution, ω_{ISC}. The spin evolution is then practically 'frozen' during the transitions into the quantum states of the system. The spin density matrix after a time t, $\hat{\sigma}(t)$, is obtained by numerically solving the Liouville equation (2.1.4) in order to determine the non-equilibrium populations of nuclear spin states. The simplifications and approximations for modelling CIDNP field dependences are discussed at the end of this chapter (2.1.5). First it shall be examined in more detail how CIDNP is generated at arbitrary magnetic field.

Formation of CIDNP at variable magnetic field. The Hamiltonian in equation (2.1.3) includes terms which depend on the external magnetic field (Zeeman terms), and terms that do not depend on the external field. It is therefore obvious that the spin dynamics, and thus the frequency of the singlet-triplet evolution, ω_{ISC}, depend on the strength of the external field with respect to the interactions in the RP (in particular the HFC). Figure 2.1.2 schematically shows the energies of the electronic eigen-functions (S, T_-, T_0, T_+) as a function of the external field. The relative energetic positions of the eigen-levels change with the external field and accordingly, different ranges of the external field can be distinguished.

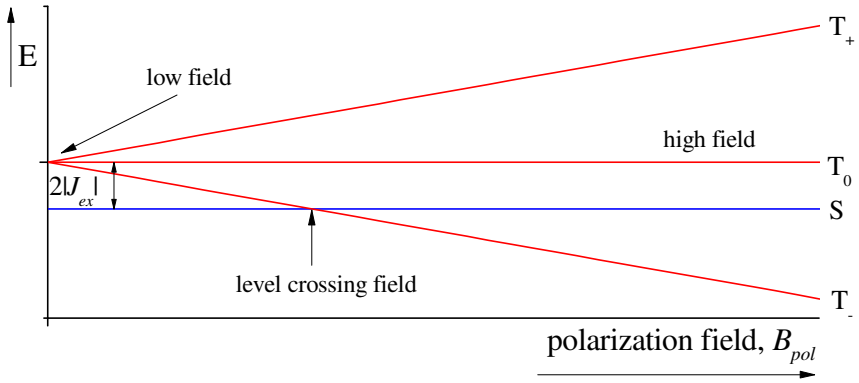

Figure 2.1.2: Schematic representation of the electronic energy levels upon variation of the external magnetic field (for the case J_{ex}<0).

In low fields, i.e. when $g\beta B_{pol}$ is much smaller than both, the hyperfine interaction a and the electronic exchange interaction J_{ex}, the energetic contributions of the nuclear spins to CIDNP formation can generally not be neglected. The process responsible for low-field CIDNP is discussed in chapter 2.1.4. In the level-crossing region, the electronic exchange interaction J_{ex} matches the external field. The S and the $T_{+/-}$ state become degenerate, and singlet triplet mixing then predominantly occurs between these levels (see chapter 2.1.2).

The fields in which the Zeeman energy of an unpaired electron exceeds the HFC, $g\beta B >> a$ are commonly referred to as 'high fields'[1]. During the life time of the RP, the hyperfine interaction is thus the scaling factor for B to be considered as strong or weak. In high field, the electronic Zeeman interaction splits the RP triplet term into three sublevels as depicted in figure 2.1.2. These levels are shown once more as a function of the inter-radical distance r in figure 2.1.3. Here, the repulsive (anti-bonding) triplet state in the radical pair is shown, whereas in figure 2.1.1, the sublevels of the bonding triplet state of the dye molecule are seen.

As the two radicals (geminate pair or F-pair) diffuse apart and the inter-radical distance (r) grows, the mutual exchange interaction $J_{ex}(r)$ between the two electrons becomes smaller. J_{ex} vanishes eventually upon the separation more than a few molecular diameters (~10Å), and S and T_0 states become energetically degenerate, and they stay degenerate until infinite distance (r_∞). This enables singlet triplet mixing by hyperfine interactions and the difference terms of electronic Zeeman energies (Δg).

If the radicals were separating slowly, which they do not, they would follow the adiabatic energy levels shown as dotted lines in the inset on the left side of figure 2.1.3. Instead, the separation occurs 'instantaneously' by dissociative vibration or simple diffusion with respect to the time scale of the magnetic interactions responsible for singlet triplet mixing, i.e. the typical hyperfine coupling of $\Delta\omega = 10^8$ rad/s (HFC of the CH_3-radical) corresponding to $\Delta t = 10^{-8}$s being much longer than the separation takes. Hence, the magnetic interactions responsible for S-T mixing are usually without any effect during the pair separation, leaving the populations of the electronic energy levels untouched.

[1] Note that this definition differs from the one that is used when the redistribution of CIDNP in the diamagnetic product molecules is discussed (chapter 2.2). There, it is the strong coupling condition for nuclear spins (formula 2.2.5) limiting the high field range.

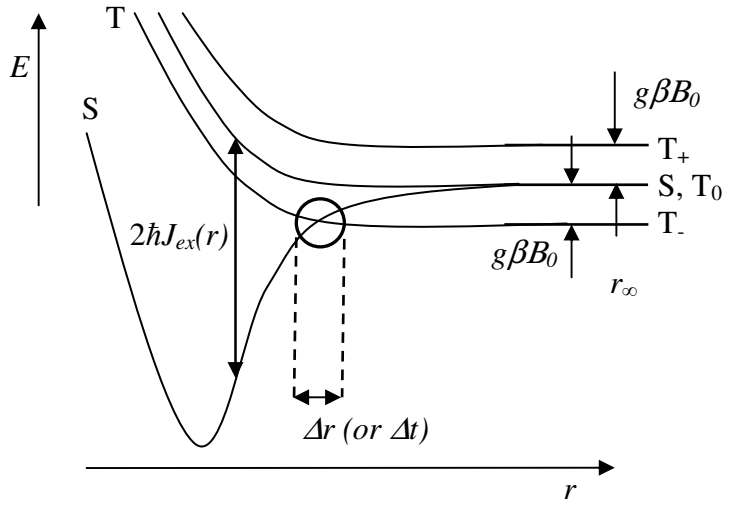

Figure 2.1.3: Scheme of electronic energy level splitting in the RP at high magnetic fields.

Different mechanisms for CIDNP formation can thus be distinguished, namely whether J_{ex} vanishes during diffusive displacement of the radicals, or whether the radicals remain coupled. The latter case, called the S-$T_{+/-}$-mechanism of CIDNP formation, shall be discussed briefly in the following (2.1.2). Thereafter the case of $J_{ex} \approx 0$ will be discussed in more detail (2.1.3), since most of the experiments in the present work are performed in aqueous solutions, where the radicals rapidly diffuse apart. The formation of CIDNP at low fields in the absence of J_{ex} is discussed in the end of this chapter (2.1.4).

2.1.2 The S-$T_{+/-}$-Mechanism

The exchange interaction, J_{ex}. In the characterization of biological charge transfer systems, e.g. photosynthetic reaction centres, the electronic exchange interaction is thought to play an important role, because the electronic coupling between the involved states is one factor that governs the process of charge separation in the RP state in these systems [32]. The exchange interaction arises from the fact that electrons are indistinguishable once they come close to each other. The exchange interaction is defined as half of the energetic difference between the anti-symmetric and the symmetric wave-functions (singlet and triplet states):

$$2J_{ex} = {}^1E - {}^3E \quad . \tag{2.1.6}$$

A theoretical prediction of its sign and magnitude is quite complicated, and an exact solution may only be found for simple molecules. In more complex organic molecules and in particular in their RP states the energetic differences (^1E - ^3E) can be quite small and little

contributions can change the relative positions of the singlet with respect to the triplet states, and the actual value of J_{ex} is difficult to predict.

Considering the two electrons in a RP to reside in two different molecular orbitals, *a* and *b*, the total wave-function may be found as a superposition of the two orbitals ('valence-bond approximation') [33]. The integral S_{ab} gives the overlap of the two wave-functions. This function is also called the exchange integral and is proportional to the square root of J_{ex} [34]:

$$J_{ex} \propto S_{ab}^{\ 2} \quad . \tag{2.1.7}$$

For orthogonal orbitals, J_{ex} is positive, meaning that the triplet is below the singlet state, while for the more general case of non-orthogonal orbitals this does not hold and the situation is more complicated.

In principle, different mechanisms for transmitting a scalar coupling between the two electron spins may be considered: The interaction may be transmitted directly (through space), or upon the involvement of other electrons (through bond), or it may involve surrounding solvent molecules [35]. The latter case is usually referred to as 'super exchange'. Typically, the exchange interaction can range up to several Tesla in RP's depending on the inter-radical distance *r*. In good approximation, the different contributions to J_{ex}, and thus the overlap of the two wave-functions decrease exponentially with the distance *r*:

$$J_{ex}(r) = J_{ex,0} \cdot e^{-\alpha r} \quad . \tag{2.1.8}$$

Calculations for the H_2-molecule confirm the exponential distance behaviour [34].

Experimentally, the exchange interaction manifests itself in e.g. time-resolved EPR and CIDEP spectra and plays a significant role in their interpretation. Its exact contribution to these spectra is, however, not directly accessible and other contributions render its extraction model-dependent. The CIDNP field dependence can yield the exchange interaction in sign and magnitude, and provides an indirect but model-free experimental access.

Determination of J_{ex} by field dependent CIDNP. Under certain circumstances the radicals can remain for a considerable time in the region denoted as Δr in figure 2.1.3, namely if the viscosity of the solution is sufficiently high, or by electrostatic inter-radical attraction. Also in case of geometrical constraints, e.g. when the RP is formed in micelles or in a crystal lattice or if the radical sites are bound to each other by a chain of chemical bonds, J_{ex} can remain finite. In the acyl-alkyl biradicals generated during the photolysis of different kinds of cyclic ketones in liquids and in plastic crystalline matrix discussed in chapter 6.3, the radical sites can not always diffuse freely with respect to each other, and S-T mixing occurs predominantly between the T_- and the S state. Within the region Δr, S-T_- transitions must generally be taken

into account. In this case, the unpaired electrons remain coupled by the exchange interaction, J_{ex}, and the most effective mixing occurs when their difference in energy ($2J_{ex}$) matches the external field (see G.L. Closs in ref. [2]):

$$2|J_{ex}| = g\beta B_{pol} \quad . \tag{2.1.9}$$

Hence, a particularly attractive application of measuring CIDNP as a function of the external magnetic field is the determination of the average electronic exchange interaction between two radical centres, because the probability of ISC and therefore that of radical recombination passes through a maximum at the anti-crossing field. The efficiency of singlet triplet mixing scales with the HFC ($\omega_{ISC} \approx a$), which forms the coupling element between the states $T_{+/-}$ and S. In chapter 6.3 J_{ex} in of acyl-alkyl bi-radicals is studied in liquids and plastic crystalline matrices by their CIDNP field dependence.

In contrast to the S-T_0 mechanism introduced in the next section (2.1.3), nuclear spin polarization arises from so-called spin 'flip-flop processes', in which an electron and a nucleus simultaneously change their spin states, thereby *creating* a net nuclear spin polarization once the electronic spin states are ordered. This means that for each RP changing its electronic spin state from T_0 to S, a nucleus coupled to it by HFC also changes its spin state from $|\alpha\rangle$ to $|\beta\rangle$ (or vice versa upon conservation of the total spin). Hence, large nuclear spin polarization can be achieved even after long times. (In the S-T_0-mechanism, nuclear spin polarization is not *created*, but the reaction products are *sorted* according to their nuclear spin states and the two decay channels for the RP's ($|\alpha\rangle$ and $|\beta\rangle$) tend to cancel each other (see 2.1.3).)

Depending on the sign of J_{ex}, the singlet level either crosses the T_- state ($J_{ex} > 0$) or the T_+ state ($J_{ex} < 0$) (see also fig. 2.1.2). The phase of the CIDNP signal is emissive (*E*) in the case either of positive J_{ex} and a singlet precursor or negative J_{ex} and triplet precursor. Absorptive CIDNP is expected for positive J_{ex} and a triplet precursor and for negative J_{ex} and singlet precursor. Note, that the sign of HFC has no effect on the phase of the polarized spectrum. This fact allows one to interpret CIDNP spectra by their polarization patters in terms of the prevailing mechanism of CIDNP formation (S-$T_{+/-}$ or S-T_0). An example is the observed change of the polarization pattern of acetone, when passing the phase transition from the liquid into the plastic crystalline phase of cyclohexane, discussed in chapter 6.3 and ref. [36].

2.1.3 The S-T_0 Mechanism

In the case of the two radical sites diffusing apart, the electronic exchange interaction vanishes ($J_{ex} \approx 0$), and at high field both the electronic T_+ and T_- states are energetically decoupled from S and T_0. In good approximation, the electronic T_+ and T_- states can be considered as pure eigen-states of the system, and for them no time evolution has to be considered. In contrast, the S and T_0 states are energetically degenerate (see fig. 2.1.3). Neglecting the exchange interaction, the radical pair spin Hamiltonian (equation 2.1.3) becomes:

$$\hat{H}_M = \beta_0 \hbar^{-1} \left(g_1 \hat{S}_1 + g_2 \hat{S}_2 \right) B_{pol} + \sum_n a_{1n} \hat{S}_1 \hat{I}_{1n} + \sum_m a_{1m} \hat{S}_2 \hat{I}_{2m} \quad , \qquad (2.1.10)$$

and the spin evolution in the RP can be studied irrespective of the molecular motion, only depending on the g-factors and hyperfine couplings in the two radicals. Accordingly, S-T_0 transitions are induced by the difference of Zeeman radical frequencies (the Δg mechanism), and the difference of spin resonance frequencies belonging to different hyperfine components in the EPR spectrum (the hyperfine mechanism). In radical pairs with both radicals giving rise to a single line in the EPR spectrum (no hyperfine spitting) at exactly the same frequency (identical radicals), in principle no S-T_0 transitions can occur.

Because of the first term in equation 2.1.10, which measures the difference in Zeeman energy between the two radicals, the system has a magnetic field dependence. The rate of intersystem crossing (which is roughly proportional to ω_{ISC}) depends on the difference in Larmor precession frequencies of the two electron spins, and for two nuclear spin configurations ($|\alpha\rangle$ and $|\beta\rangle$) the difference in rates is largest in magnetic fields, B_{pol}, that fulfill the condition:

$$2\Delta g \beta \hbar^{-1} B_{pol} = a \quad . \qquad (2.1.11)$$

After some time, the difference in the precession frequencies leads to dephasing of the spins and hence to inter system crossing. This process controls the details of nuclear spin polarization in the reaction products which are initially formed. As an experimental consequence, it follows that a proton CIDNP experiment run at 60MHz may yield far better signal to noise ratio than if it is run in a modern expensive 600MHz machine, and the magnetic field dependence of CIDNP hence yields information on the magnetic interaction parameters (g-factors and hyperfine couplings) in the RP.

Typically, the two radicals in the pair can recombine only in their combined singlet state, given that the product molecule has a singlet ground state. This means, they have to remain together (correlated) long enough within a solvent cage for the triplet multiplicity to ‘rephase’

and thereby cross over into the singlet state. If this singlet-triplet mixing takes too long, the radicals may escape the solvent cage before re-phasing occurs, and thereafter engage into some other types of reactions giving rise to so-called escape products. Recombination of the primarily formed radicals results preferentially from that fraction of intermediate triplet radical pairs, which contain a nuclear spin configuration that is favourable for the conversion to the electronic singlet state. Escape products will be formed from those radicals that possess nuclear spin states unfavourable for a change of their triplet state. Because this corresponds to a nuclear spin sorting process, often the expression 'spin sorting' is used for the S-T_0 mechanism.

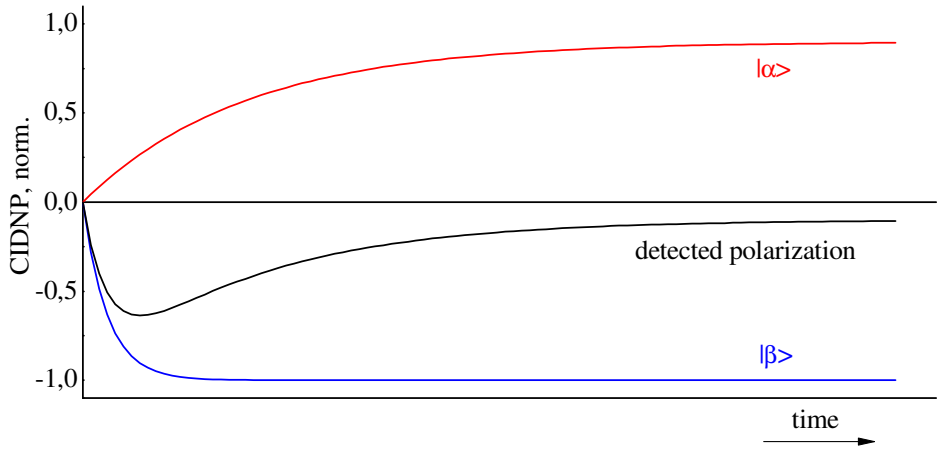

Figure 2.1.4: Typical time dependence of geminate CIDNP in the S-T_0 (spin-sorting) mechanism.

From the above, one may get the impression that after longer times nuclear spin polarization can not arise if no additional reaction pathways are available, because CIDNP formed in the reaction products with one nuclear spin configuration will be eventually cancelled by those with the other configuration once all intermediates have reacted to the same products. This situation is illustrated in figure 2.1.4: The initially formed products give rise to emissive CIDNP (|β>, blue curve). They are followed by those that initially remain in the triplet state with nuclear spin polarization of the opposite sign (|α>, red curve). Their sum (black curve) tends to cancel after longer times, e.g. under continuous irradiation conditions.

An additional way of creating a non-equilibrium nuclear spin polarization, however, arises from the nuclear spin lattice relaxation during the different life-times of the two above-mentioned channels. This renders the cancellation incomplete, and even after long times significant CIDNP can be detected. The 'stationary' value of CIDNP probed, i.e. the sum of the two channels (black curve in fig. 2.1.4) after long times, is then often much smaller than if

the polarization probed shortly after the laser pulse. This holds, if only the recombination of geminate RP's is considered but not the polarization formed in F-pairs at much later times.
A typical time evolution for geminate CIDNP is the black curve in figure 2.1.4. It is possible to map out such curve by variation of the time delay between a single laser pulse applied prior to the RF-detection, a method which is usually referred to as 'time resolved CIDNP' (TR-CIDNP). Here, nuclear spin polarization is probed on the microsecond timescale, the CIDNP intensities evolve as a function of the reaction rates of the radicals with each other, the paramagnetic nuclear spin lattice relaxation rates in the RP state, and also depend on the probabilities of reencounters. A theoretical approach for the quantitative extraction of the parameters determining the CIDNP transients developed by Vollenweider et al. [37].
The only experiment performed in a time resolved mode in this work, the photolysis reaction of tyrosine, is described in chapter 6.1. There, an attempt of estimating kinetic parameters (reaction rates) for some of the reactions following ionization of the amino acid from the CIDNP transients is undertaken. In most experiments discussed in this work, CIDNP is probed as a function of the external field under 'pseudo cw-illumination' (after many laser pulses). For them, in principle the polarization after long times has to be considered.

Role of Diffusion in CIDNP Formation. Within the RP lifetime of less that 10ns in low viscosity solution (before cage reaction or separation), usually no significant changes of spin multiplicity will occur, because the frequency of S-T mixing, ω_{ISC}, is usually far to low. It has been first recognized by Adrian [27], that the identity of the RP may be retained during the lengthy process of S-T evolution when Noyes' concept of a secondary cage recombination [38] is applied. In this process, the radicals which fail to undergo the primary cage reaction may diffuse apart freely, and the S-T mixing can proceed. Some of these radicals will separate forever, but it can be shown that there is a considerable probability for the reencounter of the same two radicals, which has been derived to be about 1/3 [2]. For a RP which separated in a triplet state the probability for recombination is proportional to the rate of inter system crossing, and finally the rate of formation of products in nuclear spin state *ab* (with *a* being the nuclear spin configuration of radical 1 and *b* that of radical 2) is also proportional:

$$\mathrm{P}_R^{(T)}(ab) = 0.2k_S\sqrt{\left\langle|\omega_{ISC}|\tau_D\right\rangle} \quad , \qquad (2.1.12)$$

where k_S is the rate constant expressed as the probability of a pure singlet state to react when a certain distance is reached, i.e when they get a chance to react, and τ_D is the live time of diffusive displacement. Analogously, equations can be derived for singlet born radical pairs or those that form upon random encounters (F-pairs) (see F.J. Adrian in ref. [2]).

As a quantitative result of the diffusion controlled recombination of radicals, the polarizations depend on the factor $\sqrt{(|\omega_{ISC}|\tau_D)}$, showing that large polarizations can be produced, even if the singlet-triplet inter-conversion is slow. This is the consequence of the considerable probability for the re-encounter of the same two radicals.

Qualitative models need to include the dependences of reaction probability on RP multiplicity and the S-T mixing rate ω_{ISC}, and lead to the CIDNP rules which shall be introduced in the following.

Net Effect. A simple but efficient analysis of CIDNP spectra can be obtained by two empirical rules, which have been formulated by R. Kaptein in 1971 [39], known as the 'Kaptein rules' of CIDNP. These rules allow the prediction of the sign (or 'phase') of polarization (emission or absorption) observed upon radical reactions by NMR spectroscopy. In most cases, the same rules also apply to the polarization patterns observed at high fields in the field cycling apparatus. A negative sign (-) of the resonance line is symbolized by E (emission), and a positive sign is symbolized by A (absorption).

The first rule predicts the sign of net-CIDNP formed by the S-T_0 mechanism. When the g-factor of the two radicals in the pair differs, the sign of the resonance lines in the CIDNP spectrum is determined by four decisive parameters, according to

$$\Gamma_n = (\mu)(\varepsilon)(\Delta g)(a) \quad . \tag{2.1.13}$$

Here, μ denotes the initial electron spin multiplicity of the radical pair at its formation (+ for triplet, - for singlet), ε the type of reaction leading to the observed product (+ for cage recombination, - for recombination after escape), $\Delta g = g_1 - g_2$, the difference in g-factors of the two radicals (g_1 is the g-factor of the radical with the nucleus under observation), and a the sign of hyperfine coupling (between the electron and the observed nucleus). The sign product of these four parameters determines, whether the phase, Γ_n, of the polarization for nucleus n is in absorption (+) or in emission (-).

This rule applies strictly when the radicals recombine to yield products in the singlet state, for recombination into the triplet state the rule has to be amended, or alternatively ε has to take the spin multiplicity of the products into account. Likewise, the so-called 'high-field multiplet effect' can be predicted by the formulation of a simple rule.

Multiplet Effect. In addition to the net-CIDNP effect formed during electronic S-T_0-transitions, the same mechanism can produce so-called multiplet effects in high magnetic

fields, providing that the spin system under investigation contains scalar coupled nuclear spins. Such case is not evaluated in this work, but it is briefly introduced for the sake of completeness. For simplicity, the case of two nuclear spins possessing a large HFC to the unpaired electron of the same radical is considered. In the case of $(g_1\text{-}g_2) \approx 0$ or when $(g_1\text{-}g_2)\beta\hbar^{-1}B_{pol} << a$ and $J_{ex} \approx 0$, there is a difference in mixing frequencies, ω_{ISC}, for parallel and anti-parallel mutual alignment of the two nuclear spins. The two mixing frequencies are given by:

$$\omega_{ISC}(\uparrow\uparrow) = \pm\frac{a_{11} + a_{12}}{2}$$
$$\omega_{ISC}(\uparrow\downarrow) = \pm\frac{a_{11} - a_{12}}{2} \quad . \qquad (2.1.14)$$

Thus, for parallel and anti-parallel alignment of the nuclear spins, the different singlet-triplet mixing frequencies give rise to equal populations of the two parallel and anti-parallel nuclear spin states. Such situations are shown schematically in the nuclear spin energy level diagrams in figure 2.1.6 with the energy level diagrams on the left side and the corresponding stick spectra on the right side. Accordingly, the 'rules of Kaptein' (equation 2.1.13) are amended to predict the sign for multiplet CIDNP effects for the case of *J*-coupling among the nuclear spins:

$$\Gamma_{ME} = (\mu)(\varepsilon)(a_i)(a_j)(J)(\sigma_{ij}) \quad . \qquad (2.1.15)$$

Here, the meanings of μ and ε are the same as in formula 2.1.13, and $\sigma_{ij} = +1$ when the two spins are coupled to the same electron, and $\sigma_{ij} = -1$ when they are coupled to the electrons of different radical sites. Here, *J* is the sign of the nuclear spin-spin coupling (see also section 2.2). For $\Gamma_{ME} = +1$ one obtains a polarization with emission and absorption in low and high field of the NMR spectrum, respectively (E/A), and for $\Gamma_{ME} = -1$ a spectral pattern A/E (see figure 2.1.5).

If the S-T_0 approximation were valid down to very low field, the polarization of a radical pair with a single proton would become smaller and smaller and finally vanish at zero-field. In reality, however, the situation is more complicated, since the off-diagonal elements connecting the S states with T_+ and T_- must also be taken into account. The following section examines the features arising from the breakdown of the S-T_0 approximation at low magnetic field.

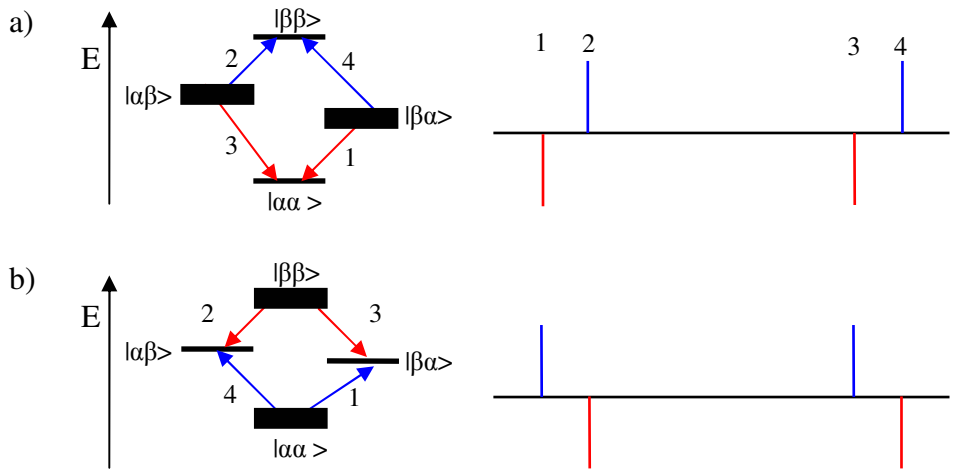

Figure 2.1.5: Multiplet polarization patterns in AB nuclear spin system in high magnetic fields with a) $\Gamma_{ME} = -1$ and b) $\Gamma_{ME} = +1$.

2.1.4 Low-Field CIDNP

The field in which the Zeeman energy of an unpaired electron is either smaller than or comparable to the HFC is usually referred to as 'low field'. In low magnetic fields the singlet triplet evolution differs substantially from that in high magnetic fields. The three triplet states are mixed, and in principle all three channels of S-T transitions are open: S-T_+,T_0, T_-.

In low fields, the difference in radical g-values is of no importance for the S-T transition dynamics and hence the g-values can be considered equal. Instead, the RP dynamics is extremely sensitive to changes of hyperfine interaction and external fields. Around a few Millitesla, the HFC becomes comparable to the Zeeman splitting of the electrons. A qualitative picture of what will happen to a RP containing a single HFC at low magnetic field can be obtained by coupling a single proton to the RP. Assuming a positive HFC, one can construct the energy diagram shown in figure 2.1.6, consisting of eight states. The selection rules for mixing are such that state |Sα> mixes with |T_+β>, and |Sβ> mixes with |T_-α>. The mixing then occurs due to off-diagonal matrix elements of the HFC. For the sake of symmetry the process is similar to that described as the S-$T_{+/-}$ mechanism, simultaneously 'flipping' the electron and the nuclear spin. In the case of J_{ex} = 0 (T_0 and S degenerate), the energy splitting between the two sets of mixed states is not equal, and the degree of mixing between these

states also differs. Because the transition probabilities are related to the degree of mixing, the rate of $|T_+\beta\rangle \leftrightarrow |S\alpha\rangle$ is greater than $|T_-\alpha\rangle \leftrightarrow |S\beta\rangle$. Hence, if the precursor state of the RP was a triplet state, the population of $|S\alpha\rangle$ will be larger than that of $|S\beta\rangle$, giving enhanced absorption in the product. The opposite will be the case for a singlet precursor.

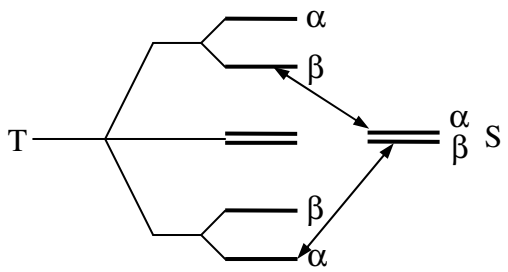

Figure 2.1.6: Energy levels of a one proton radical pair with $a_i > 0$ and $J_{ex} = 0$.

In summary, the above qualitative consideration also allows one to include some 'rules' for low field CIDNP, in addition to the Kaptein rules for high-field CIDNP. The following rules have been formulated by G.L. Closs in ref. [2]:

i. Singlet precursors give opposite polarization with respect to triplet precursors and uncorrelated RP's at *all* fields.
ii. A change in the sign of HFC changes the sign of the polarization at *all* fields.
iii. The sign of Δg does not influence the sign of the polarization only at *low* fields
iv. Escape products have opposite polarization from geminate recombination products at high field but the same polarization at *low* field.
v. For the case of a one-proton radical pair, and more general, for radical pairs in which the nuclear spins are not coupled among themselves the polarization goes to zero at zero field.

The latter of these rules necessitates to explain the often substantial net polarizations observed at the lowest available fields (B_{pol} = 0.1mT) in the present work. As will be shown further down (chapter 2.2), these observations are the consequence of the spin evolution in the diamagnetic reaction products before and during the process of field cycling, i.e. after CIDNP formation is complete. The rule formulated under v. is therefore not violated, it only turns out that a redistribution of CIDNP and the process of field cycling has to be taken into account.

The low field spin dynamics becomes considerably more complex when taking the exchange interaction into account. For RP's in which the radicals rapidly diffuse apart, it has however been shown, that J_{ex} may securely be neglected in order to explain the low field CIDNP effects [40, 41].

Zero-field multiplet effect. In zero-field, when there is no external axis of quantization, the internal magnetic fields in the radical pair are providing the axis of quantization for the spin angular momentum. In this case, the lowest triplet state is separated from the singlet state by the electronic exchange interaction, J_{ex} (see also fig. 2.1.2). The same holds for the nuclear spin states in the diamagnetic product: As the nuclear Zeeman interaction vanishes, only the scalar spin-spin coupling (*J*-coupling) remains. Very similar to electron spins, two coupled nuclear spins may be represented by a singlet-triplet eigen-basis. In this eigen-basis, the matrix elements of the scalar spin-spin couplings $2\pi J_{ij}\hat{\boldsymbol{I}}_i \cdot \hat{\boldsymbol{I}}_j$ are diagonal, and the singlet-triplet mixing may occur due to the off-diagonal elements in the HFC tensors. In low viscosity solutions, the electronic J_{ex}-coupling usually vanishes because of diffusive separation of the two radical centres, whereas the homo-nuclear *J*-coupling will always fulfill the condition for strong coupling ($J_{ij} >> \Delta\nu$) in low fields (see formula 2.2.4). The zero-field Hamiltonian, $\hat{H}_{zf}$, describing the singlet-triplet evolution under these conditions ($J_{ex} = 0$) contains the electron- and the nuclear spins coupled by HFC:

$$\hat{H}_{zf} = \sum_n a_{1n}\hat{\boldsymbol{S}}_1 \cdot \hat{\boldsymbol{I}}_{1n} + \sum_m a_{2m}\hat{\boldsymbol{S}}_2 \cdot \hat{\boldsymbol{I}}_{2m} \quad . \qquad (2.1.17)$$

Singlet-triplet transitions within the nuclear spin manifold are generally spin-forbidden. Whether the nuclear singlet or triplet states will be populated in the course of the radical reaction depends on the sign and magnitudes of HFC's in the radical pair state. In the case of two coupled nuclear spins, both possessing HFC's of comparable magnitude, this results in a selective population of the nuclear triplet states in case the two HFC's are of the same sign, and population of the nuclear singlet state in the case of the HFC's are of opposite sign. These two constellations and the resulting spectral patterns (stick spectra) expected in the case of an adiabatic field variation are depicted in figure 2.1.7. Only the transitions |1> ↔ |2> and |2> ↔ |4> can occur, and the spectral multiplet pattern consists of the outer lines only, while the inner lines do not contribute. Therefore, the zero-field multiplet pattern is often referred to as the "n-1 multiplet effect". The two lines appear in emission and absorption (E/A) and *vice versa* in the case that the nuclear spin triplet state is selectively populated.

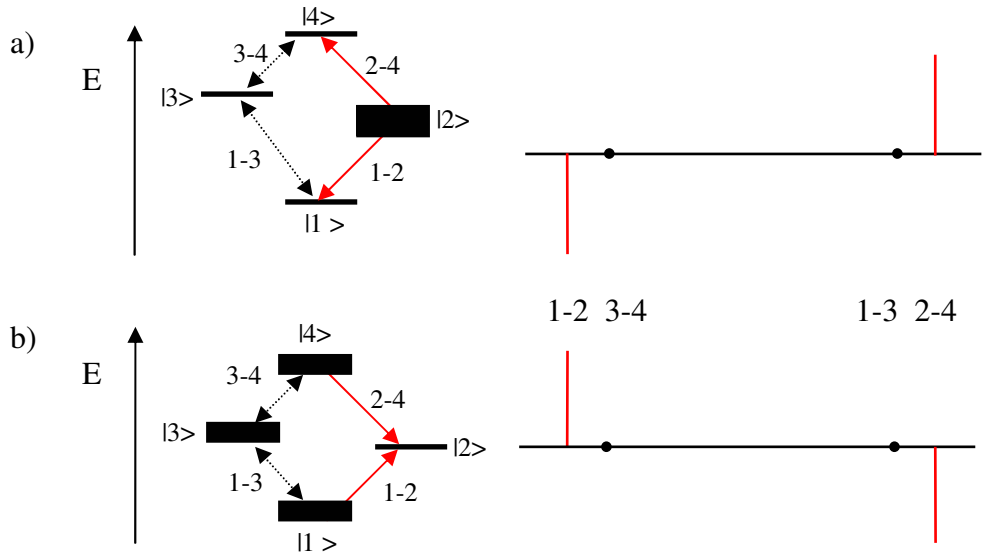

Figure 2.1.7: Zero-field multiplet effect (or n-1 multiplet effect) with selective population of a) nuclear spin singlet state and b) nuclear spin triplet state observed in high field after adiabatic field switch.

This is the case for the two β-protons in the amino acids under study (see chapter 6). When the hyperfine couplings of the two nuclear spins with the unpaired electron are of opposite sign, mainly the singlet nuclear spin level will be populated (as it is the case for the two pairs of equivalent aromatic protons in the tyrosine molecule). However, the zero-field multiplet effect is observable only when the populations formed at low field remain in the spin states possessing the same symmetry during the field switch, i.e. upon adiabatic sample transfer. Therefore, the observed polarization patterns in the two abovementioned cases can differ substantially.

Further peculiarities arise from the characteristic dependence of multiplet effects of different order (number of coupled spins) on the detection flip angle, which is discussed in chapter 2.2.4. A more detailed treatment of CIDNP formed at low magnetic fields can be found in ref. [42].

2.1.5 Modelling of CIDNP Field Dependences

From the introduction above it may be expected that calculations of the S-T_0 transition dynamics in order to predict the nuclear spin polarization at arbitrary fields are rather cumbersome. Nevertheless, a strategy for the determination of magnetic interaction

parameters from the field dependence of CIDNP has been developed and applied [40, 41, 43]. Modelling of the field dependent CIDNP data consists of three steps, and their quantitative evaluation is based on the numerical solution of Liouville equation (formula 2.1.4) for the electron-nuclear spin density matrix $\hat{\sigma}$ using the Green function approach [44] and uses several simplifications.

First, the approach makes use of the low-viscosity approximation [44, 45], which implies that the frequencies of electronic S-T mixing, ω_{ISC}, are small as compared to the time of diffusional displacement, τ_D, of the radicals in the pair:

$$\omega_{ISC}\tau_D << 1 \quad . \tag{2.1.18}$$

Within this approximation, the spin density matrix does not depend on the exchange interaction between the two radicals. Second, the semi-classical approximation suggested by Schulten and Wolynes [46] is applied. It uses an 'effective' magnetic field, i.e. an effective hyperfine coupling, a_{eff}, for those nuclei n that do not acquire significant polarization due to their small hyperfine couplings with the unpaired electron:

$$a_{eff} = \sqrt{\frac{2}{3}\sum_n a_n^2 I_n(I_n+1)} \quad . \tag{2.1.19}$$

It is applicable when $a_n << a_{eff}$ for any n. The values for the geminate CIDNP are then obtained by numerically calculating each element, $\hat{\rho}_{ij}$, of the density matrix of the diamagnetic product molecule for different configurations of the semi classical field [47].

The field variation from B_{pol} to B_0 is assumed to occur adiabatically. As mentioned above, under these conditions no net polarizations are obtained in 'zero field', because so far redistribution of polarization among strongly J-coupled spins before and during the sample transfer is not accounted for. These phenomena are subject of the second part of the theoretical section. By accounting properly for the multiplet effects of second order among pairs of coupled spins (n = 2, see chapter 5) it was possible to achieve a reasonable agreement between the experimental and calculated CIDNP field-dependences [41]. The simulations presented in chapter 6 finally reflect the CIDNP expected for the geminate recombination of the primary radical pairs. Quantitatively, low field CIDNP and high field CIDNP are affected differently by secondary effects such as the cancellation described in figure 2.1.4 or degenerate electron exchange (see e.g. reaction 6.2.6, chapter 6.2). Therefore, the low and high-field parts of the simulations are usually scaled separately.

As the approach has been extended to more and more nuclei, some substantial limitations became obvious, some of which are extensively discussed in chapter 4. The extraction of hyperfine couplings from the low field part of the field dependence in multi-nuclear radical

pairs remains problematic for the following reasons: Once it became possible to reduce the transfer time with a significantly lighter, newly developed NMR probe [48], it turned out that the sample transfer is not necessarily always adiabatic and the spin evolution in the diamagnetic product molecules during the actual change of external field (from B_{pol} to B_0) should be taken into account numerically. In addition, the primarily formed polarization on nuclei with significant HFC is redistributed among those nuclei that are strongly *J*-coupled to them in the diamagnetic product molecule. The information on the hyperfine couplings of individual spins is then lost.

However, a positive aspect of these limitations is the possibility of very efficient transfer of hyper-polarization to target nuclei by suitable field cycling schemes, for which a theoretical background shall be given in the following section.

2.2 Spin-Dynamics in Diamagnetic Product Molecules

After the formation of CIDNP is complete, i.e. typically after a few milliseconds when all the radicals have decayed, the spin-dynamics continues in the diamagnetic reaction products. The following considerations have general implications for NMR experiments that employ field cycling, irrespective of how hyper-polarization was formed or, if the nuclear spin system initially possesses thermal equilibrium.

In NMR of diamagnetic molecules only the nuclear spin states need to be considered, because the magnetic and electric influences of the rapidly moving electrons are averaged, so that the nuclei only sense the time average of the fields they generate. In return, the nuclear spin energies are so small that they will not affect the motions of the electrons within the molecule or even that of the whole molecule. In good approximation, the motions of the nuclear spins can be regarded as separate from that of the electrons which also obey the time-dependent Schrödinger equation (formula 2.1.1). Therefore, in the remaining part of the theoretical section, the changes of the *nuclear spin Hamiltonian*, $\hat{H}_n$, with the external field and the consequences for the evolution of the *nuclear spin density matrix*, $\hat{\rho}$ at variable field are discussed.

2.2.1 The Molecular Spin System

Nuclear Spin Hamiltonian for Liquid State NMR. The spectrometer usually[1] supplies two kinds of external fields, namely the very strong static field B_0, and a much weaker oscillating field B_1 which is perpendicular to it. In the absence of an RF-field (B_1), the properties of the molecular spin system are described by its time-independent spin Hamiltonian (in units of $\hbar$) [49]:

$$\hat{H}_n = -\sum_{i=1}^{N} \omega_{L,i} \hat{I}_{iz} + \sum_{i<j} 2\pi J_{ij} (\hat{\boldsymbol{I}}_i \cdot \hat{\boldsymbol{I}}_j) \qquad , \tag{2.2.1}$$

where $\omega_{L,i}$ is the chemically shifted Larmor precession frequency of the i-th spin, and J_{ij} the scalar spin-spin coupling (or J-coupling) between the i-th and the j-th spin. All molecules of the same isotopomeric species have the same Hamiltonian describing the molecular spin system.

[1] In the present work the situation is complicated by the fact that the 'static' field is variable (B_{pol} or B_{ev}), B_0 is referred to as the field where the NMR measurement is performed.

As has been tacitly assumed in the previous section, the molecules undergo rapid molecular motion in isotropic liquids, which is the case in the mayor part of this work. The interaction terms (chemical shift and *J*-coupling) then fluctuate in time. If the motion of molecules is sufficiently fast, the fluctuating terms of the Hamiltonian are replaced by a motionally averaged value, and those parts with zero time-average may securely be discarded. The discarded parts of the internal spin Hamiltonian are, however, responsible for the relaxation of the nuclear spin system. In case of protons this is in particular the dipolar coupling among spins.

In solids, the atomic motion is usually highly restricted and there is only little motional averaging, which is limited to motions of some molecular groups. Both inter- and intra-molecular spin interactions can then survive. In chapter 6.3, a special kind of molecular solid, namely plastic crystalline cyclohexane, is used to host guest molecules undergoing photochemical reactions. In these systems an unusual situation arises, because only the centres of gravity of the molecules are fixed with respect to the crystal lattice, but the molecules themselves rotate rapidly about their lattice sites, in many cases isotropically. Molecules that form plastic crystals are usually of spherical shape such as the football molecule C_{60} or adamantane. In these special systems, the rapid molecular rotation averages the *intra*molecular interactions to their isotropic values, while the averaging of *inter*molecular interactions is incomplete, since the molecular diffusion is slow.

For now, we shall stay with the interaction of the nuclei with the static external field (B_{pol} or B_0) and those of the nuclei with each other and the case of rapid molecular motion (effective averaging). At high magnetic fields, the spin dynamics are dominated by the large interaction with the external field, which tends to mask some of the components (x and y) of the internal spin interactions (*J*-couplings and chemical shift). Then, the 'secular approximation' of the internal spin Hamiltonian is valid, meaning that only the z-component has to be considered. It is thus not valid in the entire field region, and therefore often referred to as the 'high-field approximation'.

The chemical shift terms of the nuclear spin Hamiltonian represent the indirect magnetic interaction of the external magnetic field with the nuclear spins, through the involvement of electrons. The electrons in the molecule cause the local magnetic fields to vary considerably for different sites in the molecule. Because it is predominantly an intra-molecular interaction, the chemical shift is of mayor importance to chemical applications of NMR (determination of molecular structures).

In principle, the chemical shift interaction is represented by a 3x3 real matrix, the chemical shift tensor. However, within the secular approximation only the *z*-term of the chemical shift is retained, and in isotropic liquids the chemically shifted Larmor frequency ω_L of the nucleus *j* becomes:

$$\omega_{L,j} = -\gamma B_0(1+\delta_j) \quad . \tag{2.2.2}$$

Henceforth, the term δ refers to the isotropic chemical shift and does not depend on the orientation of the molecule with respect to the external magnetic field. It is simply the average of the three diagonal components in the chemical shift tensor. In very good approximation, the chemical shift δ is proportional to the external field B_0.

Another link between NMR and structural chemistry is provided by the indirect magnetic interactions of nuclear spins with each other, through the involvement of electrons, the spin-spin coupling (or *J*-coupling). Indicating the local electronic environment they are a direct manifestation of the chemical bond. The *J*-coupling is exclusively intramolecular, and two spins have a measurable *J*-coupling, only if they are linked together through a small number of chemical bonds.

As in the case of the chemical shift, the present work exclusively deals with the isotropic *J*-couplings, which are equal to the average of the diagonal elements of the *J*-coupling tensor. The term 'scalar coupling' indicates that the Hamiltonian for isotropic *J*-coupling is independent of molecular orientation. For the homo-nuclear case, the coupling between the spins *j* and *k* is:

$$\hat{H}_{jk}^{J} = 2\pi J_{jk}\hat{I}_{jz}\cdot\hat{I}_{kz} \quad . \tag{2.2.3}$$

The *J*-coupling has a sign, which is rather difficult to predict once the nuclei are coupled over two or more bonds. Unlike the chemical shift, the *J*-coupling is independent of the applied magnetic field.

Strong and weak coupling. A further simplification for the spin Hamiltonian can be made for isotropic liquids when the difference in chemical shift between two nuclei is much larger than the *J*-coupling among them. When the coupled spins precess at significantly different frequencies, interactions between transverse components of spin polarizations average out to zero and only the longitudinal components need to be included.

The scalar coupling between the spins is considered weak, when the nuclear spin interaction between them is much smaller than the difference in their Zeeman interaction with the external magnetic field:

$$2\pi J_{ij} << |\omega_{L,i} - \omega_{L,j}| \quad , \tag{2.2.4}$$

otherwise they are considered strongly coupled. In homo-nuclear spin systems, in particular of protons, formula 2.2.4 is by no means always satisfied and a secular approximation of the Hamiltonian is invalid.

Since the chemical shift frequency differences are proportional to the applied field, the weak coupling limit is more commonly encountered at high magnetic fields, while at low magnetic fields all proton spins will eventually become strongly coupled. In order to understand the outcome of field cycling experiments, one has to be aware that the relative strength of *J*-coupling, i.e the size of *J*-coupling with respect to the differential precession of the coupled spins changes significantly upon switching the external field.

Different regimes of the magnetic field may be distinguished according to the condition of strong coupling. In zero-field (or earth magnetic field), the Zeeman part of the Hamiltonian is no longer active, and one has to deal only with the *J*-coupling part of the Hamiltonian (formula 2.2.1), which is given by the strong coupling case for any pair of nuclei:

$$\hat{H}_J = \sum_{i<j} 2\pi J_{ij'} \left(I_x^i I_x^j + I_y^i I_y^j + I_z^i I_z^j \right) \tag{2.2.5}$$

As this Hamiltonian equally involves all three directions in space, it is responsible for a redistribution of polarization by 'isotropic mixing'. In this case, the spin density matrix evolves due to the *J*-couplings as the coupling element.

The strength of the spin-spin coupling at any given polarization field B_{pol} may be described by a coupling angle ϕ_{pol} :

$$\phi_{pol} = \frac{1}{2} \arctan\left(\frac{2\pi J}{\omega_{pol} \Delta\delta} \right) \quad , \tag{2.2.6}$$

and the condition of strong coupling is fulfilled when the angle approaches $\pi/4$.

The Zeeman states. The direct product Zeeman eigen-states of the *weakly* coupled spin Hamiltonian (formula 2.2.1) have the following energies:

$$\omega = -\sum_j \omega_{L,j}{}^0 m_j + \sum_{i<j} 2\pi J_{ij} m_i m_j \quad , \tag{2.2.7}$$

with $m_{i,j} = \pm 1/2$.

At high magnetic fields, a weakly coupled system of *N* spins-1/2 has 2^N stationary states given by the direct products of the Zeeman eigen-states of the individual spins. The state energies fall into distinct groups, distinguished by their value of total z-angular momentum quantum number, J_z. Small energy differences between the levels belonging to the same group are

caused by the differences in chemical shift and the *J*-couplings. The number of levels with a given value of J_z in a system on *N* spins-1/2 is equal to $N!/[(N/2- J_z)!(N/2+ J_z)]$.

In larger spin systems ($N \geq 3$), depending on the differences in chemical shifts, and on the values and mutual signs of the *J*-couplings, the eigen-levels within a group of levels with the same J_z can traverse through various level anti-crossings when the external field is varied. These crossings have important implications for the outcome of experiments in which the external field is varied. In addition, they may be employed as 'gates' for a coherent transfer of hyper-polarization among coupled nuclei, which will be explained in more detail further down.

2.2.2 Populations and Coherences

Ensemble of non-interacting spins-½. The spin-dynamics of an ensemble of molecules with the same molecular spin systems is described as a statistical mixture of states in terms of the spin density operator, $\hat{\rho}$. Here, only the physical interpretation of the components of the nuclear spin density matrix shall be briefly recalled. For the understanding of the microscopic states of individual spins, the terms 'polarization' and 'coherence' are introduced.

An ensemble of non-interacting spins-½ has two states with the z-angular momentum quantum numbers ±½ (called $|\alpha\rangle$ and $|\beta\rangle$), and the matrix representation of its density operator, may be written as follows [49]:

$$\hat{\rho} = \begin{pmatrix} \rho_{\alpha\alpha} & \rho_{\alpha\beta} \\ \rho_{\beta\alpha} & \rho_{\beta\beta} \end{pmatrix} = \begin{pmatrix} \overline{c_\alpha c_\alpha^*} & \overline{c_\alpha c_\beta^*} \\ \overline{c_\beta c_\alpha^*} & \overline{c_\beta c_\beta^*} \end{pmatrix} \quad . \tag{2.2.8}$$

The weighted average over the ensemble is indicated by the over-bars. The right-hand-side of this equation is called the density matrix that contains the quadratic product of the superposition coefficients c_α, c_β, and their complex conjugates.

The individual elements of the nuclear spin density matrix are described by the terms 'polarization' and 'coherence'. While the diagonal elements $\rho_{\alpha\alpha}$ and $\rho_{\beta\beta}$ are called the population of the states $|\alpha\rangle$ and $|\beta\rangle$, the off-diagonal elements, $\rho_{\beta\alpha}$ and $\rho_{\alpha\beta}$, are called the coherences between the states $|\alpha\rangle$ and $|\beta\rangle$. The coherences are classified by a quantum number called the coherence order, according to the difference in J_z between the two states connected by the coherence. The coherences in equation 2.2.8 are of the order -1 and +1, and are called (-1) and (+1)-quantum coherence, respectively.

The difference in spin state populations indicates a net *longitudinal* spin polarization, i.e. magnetization of the sample in the direction of the external field (by convention the z-axis). Thus, no net polarization in the direction of the external field arises, when the populations of the two states are equal ($\rho_{\alpha\alpha}=\rho_{\beta\beta}=1/2$).

The coherences indicate a net spin magnetization perpendicular to the external field, i.e a *transverse* spin polarization in the rotating frame, and the direction of the transverse spin polarization in the *xy*-plane is called the *phase* of the coherence.

The spin density operator represents a magnetization vector, *M*, indicating the magnitude and direction of the macroscopic net magnetization. The dynamics of the spin-1/2 ensemble correspond to the motion of the magnetization vector in space. The longitudinal component of the magnetization vector, M_z, is related to the population difference between the states, while the transverse components M_x and M_y are related to the (1)-quantum coherence between the states.

Coherences among coupled spin-states. In systems of coupled spins (multi-spin systems), additional types of coherence arise, that involve the mutual alignment of nuclear spins coupled by spin-spin interaction. The action of *J*-coupling thus introduces some new features into the nuclear spin density matrix. The influence of spin-spin coupling is indicated by the creation and destruction of correlations between the spin polarizations, which is of particular significance for the present work, because it means, that CIDNP detected for a particular nucleus, can not be regarded separately from the nuclei strongly coupled to it.

The coherences, ρ_{rs}, have precession frequencies which are equal to the difference of the energies of the involved states, *r* and *s*:

$$\nu_{rs} = (E_s - E_r)/h \qquad \text{or} \qquad \Omega_{rs} = (E_s - E_r)/\hbar \quad . \tag{2.2.9}$$

In practice, the precession of coherences is accompanied by decay, and in principle each coherence has a different characteristic de-coherence time, λ_{rs}, i.e. an exponential decay factor. The equation of motion of an individual coherence between time points t_a and t_b is then given by [49]:

$$\rho_{rs}(t_b) = \rho_{rs}(t_a)\exp\{(i\Omega_{rs} - \lambda_{rs})(t_b - t_a)\} \quad , \tag{2.2.10}$$

where Ω_{rs} is the coherence frequency (in the rotating frame), which depends on the chemical shifts and *J*-couplings of all nuclei involved in the multi spin system.

The size of the spin density matrix and thus the number of coherences increases very rapidly with the number of coupled spins in the spin system. For five coupled spins ½ for example there are already 220 (0)-quantum coherences (coherences of the order zero). The zero-

quantum coherences are of particular importance for the field cycling experiments, because coherences between states of different total z-projection quantum number J_z usually do not mix. In addition, the frequencies Ω_{rs} of coherences of higher order are way too high to be observed, and will usually be smeared out prior to their conversion into populations necessary for NMR detection.

By the application of different pulse sequences, the coherences may be transferred among each other, along a network of chemical bonds or into polarization for the NMR detection. In this work it is shown how controlled fast switches of the external field can also serve the purpose of selectively exchanging coherences and populations in coupled multi-spin systems upon the involvement of level anti-crossings.

2.2.3 Detection of Nuclear Spin State Populations

The density operator allows an ensemble of isolated spins-1/2 to be specified using four numbers (see formula 2.2.8), and the stochastic Liouville equation (formula 2.1.4) can predict the state of the spin ensemble at any point in time if the initial state is known. Leaving the spin system undisturbed for a long time, in contact with the molecular surroundings, it is expected to reach thermal equilibrium. For the large number of spins involved in NMR, the values for populations and coherences are then obtained from statistics. In thermal equilibrium, the coherences between all states are zero. The populations obey the Boltzmann distribution, which causes the lower energy eigen-states to be slightly more populated than the higher ones, and the difference in population between the states depends on their energy difference as compared to the available thermal energy.

When a radio frequency pulse is applied, the spins experience two magnetic fields: the static field generated by the magnet (B_0), and an oscillating RF-field from the excitation coil (B_1) which is many orders of magnitude smaller. Because the oscillating field is resonant with the precession of the spins it has strong influence on the spins when the pulse is applied long enough.

A measure of the amplitude of the on resonance part of the RF-pulse is the nutation frequency, ω_{nut}, which is defined as follows:

$$\omega_{nut} = \left| \frac{1}{2} \gamma B_1 \right| \quad . \tag{2.2.11}$$

The nutation frequency tells at which time the magnetization vector *M* is turned from z to –z and back to z by interaction with the RF field. The bandwidth of the pulse is proportional to the nutation frequency and hence to the peak RF amplitude.

The effect of the pulse on the ensemble of spins is usually expressed as the RF flip angle, φ, which is proportional to the nutation frequency ω_{nut} and the length of the applied pulse, τ_{rf}:

$$\varphi = \gamma B_1 \tau_{rf} \quad . \tag{2.2.12}$$

In practice, a significant change in spin polarization is achieved after several microseconds of RF irradiation. In an ordinary FT-NMR experiment, a single 90°-pulse converts the differences in populations into (+/-1)-quantum coherences which are detected by recording the FID.

It is of particular importance for this work, to notice that an additionally applied field changes can modify the spin density matrix in a manner that both, populations and coherences are affected. It turns out that the action of field cycling (the field switch) can also affect the populations of certain energy levels and the coherences between these energy levels, which are influenced by the process of the field change.

The intensities of individual NMR lines within a given multiplet (and also the amplitudes of the coherences) characteristically depend on the detection flip-angle (formula 2.2.12). The detection of non-thermal populations by FT-NMR shall be introduced in more detail in the following.

Flip angle dependence of non-thermal populations. The thermally polarized spin-system is characterized by the populations being proportional to total-spin-angular momentum, $\hat{I}_z$, i.e the energetic ordering of the spin states (Zeeman order). Accordingly, the populations may be probed directly by a one-pulse experiment, with the response giving a characteristic sine-dependence of the signal intensity on the detection flip angle, independent of the complexity of the coupling pattern of the nuclear spin system [50]. In contrast, evaluating the population numbers of individual spin levels in dynamically polarized spin systems by means of FT-NMR faces some difficulties, because only for very small pulse angles, φ, and in the case of non-selective pulses, the spectral intensities of lines reflect the population differences of the involved pair of levels as in cw-NMR. In addition spin-spin coupling is often small or the lines are broad so that a resolution of neighbouring lines is impossible.

When the nuclear spin levels are populated dynamically, and possess a symmetry that differs from that at the detection field, as it is for instance the case for the CIDNP multiplet effects introduced in chapter 2.1, the FT-NMR spectrum exhibits lines in absorption and in emission.

Such populations are generally referred to as a 'non-equilibrium state of the first kind' [51], in case the spin-density operator commutes with the Hamiltonian (providing the spin-density matrix is diagonal in the eigen-basis of the Hamiltonian). The diagonal elements in the spin density matrix then depend on the coupling pattern in the nuclear multi-spin system, and represent the populations of the individual energy levels. The intensity of a single line (transition) in the NMR-spectrum, L_{ij} , does not only depend on the populations of the two states P_i and P_j connected by this transition, but also on the populations of all other states coupled to them. For example, the line-intensities that result for the four transitions in a strongly coupled two-spin system are [51]:

$$
\begin{aligned}
L_{12} &= \frac{1}{2}\sin\varphi\left(\cos^2\left(\frac{\varphi}{2}\right)(1+\sin 2\phi)(P_2-P_1)-\sin^2\left(\frac{\varphi}{2}\right)\cos^2 2\phi(P_3-P_2)+\sin^2\left(\frac{\varphi}{2}\right)(1+\sin 2\phi)(P_4-P_2)\right)\\
L_{24} &= \frac{1}{2}\sin\varphi\left(\cos^2\left(\frac{\varphi}{2}\right)(1+\sin 2\phi)(P_2-P_1)+\sin^2\left(\frac{\varphi}{2}\right)\cos^2 2\phi(P_3-P_2)+\cos^2\left(\frac{\varphi}{2}\right)(1+\sin 2\phi)(P_4-P_2)\right)\\
L_{13} &= \frac{1}{2}\sin\varphi\left(\cos^2\left(\frac{\varphi}{2}\right)(1-\sin 2\phi)(P_3-P_1)+\sin^2\left(\frac{\varphi}{2}\right)\cos^2 2\phi(P_3-P_2)+\sin^2\left(\frac{\varphi}{2}\right)(1-\sin 2\phi)(P_4-P_3)\right)\\
L_{34} &= \frac{1}{2}\sin\varphi\left(\cos^2\left(\frac{\varphi}{2}\right)(1-\sin 2\phi)(P_3-P_1)-\sin^2\left(\frac{\varphi}{2}\right)\cos^2 2\phi(P_3-P_2)+\cos^2\left(\frac{\varphi}{2}\right)(1-\sin 2\phi)(P_4-P_3)\right)
\end{aligned}
\tag{2.2.13}
$$

Here, φ denotes the NMR flip angle (according to formula 2.2.12), and ϕ the coupling angle between the two nuclear spins which depends on the *J*-coupling among the spins with respect to the chemical shift difference (see formula 2.2.6). The values P_1 to P_4 are the populations of the individual spin levels. Hence, in order to determine the non-equilibrium populations of these levels, a single experiment at e.g. = 90° does not suffice, and the line-intensities have to be probed at different flip angles. The spectral pattern of two coupled spins may be probed by two experiments at different φ, and the relative populations P_1 to P_4 determined by suitable combinations of the equations 2.1.13. Vollenweider and Fischer [52] showed that in this case the net and multiplet CIDNP effects are obtained by taking the sum and the difference of two spectra taken at φ = 45° and 90° respectively, since their nutation pattern consist of terms varying as $\sin\varphi$ and $\sin 2\varphi$.

The case of two strongly coupled nuclear spins (AB-system) is fulfilled for the two protons in the β-position of the *N*-acetylated amino acids studied in the present work (tryptophan and tyrosine) only to a first, relatively crude, approximation. In the more general case of many coupled nuclear spins, more experiments would have to be performed depending on the number of spins involved. Facing complex multi-spin systems of organic molecules it may turn out that the suitable (proper) flip angles become difficult to hit and/or to predict.

In the case of *N* coupled polarized nuclei, the distribution of population over the multi-level system is determined not alone by all net polarizations,

$$\left\langle \hat{I}_{\alpha z} \right\rangle = Tr\left\{ \hat{I}_{\alpha z} \hat{\rho} \right\}, \qquad (\alpha = 1, \ldots, N) \tag{2.2.14}$$

and the average mutual orientation of each pair of spins (multiplet polarization)

$$\left\langle \hat{I}_{\alpha z} \hat{I}_{\beta z} \right\rangle = Tr\left\{ \hat{I}_{\alpha z} \hat{I}_{\beta z} \hat{\rho} \right\}, \qquad (\alpha, \beta = 1, \ldots, N \quad , \quad \alpha \neq \beta) \tag{2.2.15}$$

but also by higher order entanglement. It is thus necessary to also determine the following expectation values:

$$\left\langle \hat{I}_{\alpha z} \hat{I}_{\beta z} \hat{I}_{\gamma z} \right\rangle = Tr\left\{ \hat{I}_{\alpha z} \hat{I}_{\beta z} \hat{I}_{\gamma z} \hat{\rho} \right\} \qquad (\alpha, \beta, \gamma = 1, \ldots, N \quad , \quad \alpha \neq \beta \neq \gamma)$$

$$\left\langle \hat{I}_{\alpha z} \hat{I}_{\beta z} \hat{I}_{\gamma z} \hat{I}_{\delta z} \right\rangle = Tr\left\{ \hat{I}_{\alpha z} \hat{I}_{\beta z} \hat{I}_{\gamma z} \hat{I}_{\delta z} \hat{\rho} \right\} \quad (\alpha, \beta, \gamma, \delta = 1, \ldots, N \quad , \quad \alpha \neq \beta \neq \gamma \neq \delta)$$

$$\ldots \tag{2.2.16}$$

In order to determine these quantities, the following method was proposed by K. L. Ivanov [53]. Here, it is assumed that the RF-pulse is homogeneous and non-selective with respect to all ^{1}H $\Delta\left\langle \hat{I}_z \right\rangle = \pm 1$ transitions. For systems of N weakly coupled non-selectively excited spins ½ the flip angle dependence of the spectral line corresponding to the transition $|i\rangle \rightarrow |j\rangle$ between states $|i\rangle$ and $|j\rangle$ (the nutation pattern) is given by the following equation [50]:

$$L_{i \rightarrow j}(\varphi) = \sin\varphi \sum_{(rs)} \left(\sin\frac{\varphi}{2} \right)^{2\Delta_{ij,rs}} \left(\cos\frac{\varphi}{2} \right)^{2N - 2\Delta_{ij,rs} - 2} L^{(0)}_{r \rightarrow s} \tag{2.2.17}$$

It is important to note that the FT-NMR signal intensity does not only depend on the population difference between states $|i\rangle$ and $|j\rangle$, but also on the population differences between other states. Here, $L^{(0)}_{r \rightarrow s} = (P_s - P_r)/2$ is the standard intensity of the fully selectively excited NMR transition $|r\rangle \rightarrow |s\rangle$ determined by the difference between their populations, $\Delta_{ij,\,rs}$ is the so-called spin-flip number [50] equal to the number of spin ½ flips, required to make the state transitions $|i\rangle \rightarrow |j\rangle$ and $|r\rangle \rightarrow |s\rangle$ coincide. Consequently, only the signals corresponding to the so-called parallel transitions[1] affect each other. The expression 2.2.17 of the N-spin non-equilibrium system can be written as a Fourier series consisting of N sine terms:

$$L_{i \rightarrow j}(\varphi) = \sum_{n=1}^{N} A^{(n)}_{i \rightarrow j} \sin n\varphi \tag{2.2.18}$$

The amplitudes of the harmonics, $A^{(n)}_{i \rightarrow j}$, then appear as the coefficients of the Fourier series expansion of the periodic function $L_{i \rightarrow j}(\varphi)$. The expression for the NMR line intensity at the n^{th} harmonic is derived in ref. [53]. One may thus represent the flip angle dependent NMR

[1] Those transitions that involve the same nucleus; the parallel transitions of a system of four coupled spins are coloured accordingly in fig 4.0.2

spectra (2.2.17) of the *N*-spin system in two dimensions, one being the spin precession frequency, and the second being the number of the harmonic, *n*. The *N*-th harmonic then contains only the *N*-th order multiplet polarization, and consequently the higher order expectation values are resolved in the second dimension, and the quantities (2.2.14), (2.2.15) and (2.2.16) become accessible.

Thus, the average mutual alignment of *N* coupled spins may be analysed by taking many spectra at different flip angles and decompose them by a Fourier series. This yields spectra of different order *n*, carrying the characteristic contributions of $\sin n\varphi$ to the flip angle dependent spectra and thus reflect solely the alignment of *n* coupled spins.

The applicability of this approach is confirmed by suitable experiments in chapter 5. There, it is further shown that vanishing multiplet effects of different orders with increasing magnetic field are related to the fulfillment of the strong coupling condition (formula 2.2.4) by different sub-sets of nuclear spins, the changes in the relative ordering of the spin states, and the occurrence of level anti-crossings within them. The analysis of multiplet patterns at variable magnetic field by this approach may be helpful - or sometimes even an important step - in the development of suitable polarization transfer schemes for complex multi-spin systems that employ field cycling, since a 2D-nutation analysis can reveal further information on their coupling topology.

2.2.4 Mixing of Populations and Coherences in Field Cycling Experiments

Redistribution of polarization among strongly coupled spins. In most experiments described in this work, substantial CIDNP of nuclei is observed at low polarization fields that do not show any polarization in the high field of the spectrometer.

De Kanter and Kaptein have already considered the redistribution CIDNP in low magnetic fields due to scalar spin-spin coupling [54]. When spins are coupled sufficiently strongly (see strong coupling condition, formula 2.2.4), the eigen-states of the spin system are not characterized by the states of individual spins, but rather represented by collective states. Such collective states are calculated for several ‘groups’ of coupled spins in the N-acetyl-tryptophan molecule in chapter 4.0. Polarization, formed on particular nuclei in the radical pair stage manifests itself in a more complex redistribution of population among coupled spins. As a result, also the nuclei coupled strongly to those with considerable HFI that form the ‘origin’ of polarization can show strong CIDNP when observed in high field.

In the work of de Kanter and Kaptein [54] the period of light irradiation, τ_L, has been assumed to be rather long as compared to the reciprocal coupling between the interacting spins in the diamagnetic product molecule ($\tau_L >> 1/2\pi J$). Therefore they neglected the role of spin coherences (represented by off-diagonal elements of the respective spin density matrix) formed. However, with the use of intense laser irradiation it is possible to shorten τ_L to the limit that $\tau_L \leq 1/2\pi J$. In this case, spin coherences can no longer be neglected, and the detection of such coherences is presented in chapter 4 and has been published in ref. [55].

Here, we shall consider the effect of CIDNP redistribution in a pair of coupled spins, since the case of two coupled spins can be tackled analytically. The elements of the spin density matrix $\hat{\sigma}$ at a given magnetic field B_{pol} depend on the spin evolution in the precursor radical and can be expressed by the density matrix, $\hat{\rho}$, in the radical pair projected onto its electronic singlet state. This quantity can be conveniently written in the two-spin Zeeman basis [41]:

$$|1\rangle = |\alpha\alpha\rangle, \quad |2\rangle = |\alpha\beta\rangle, \quad |3\rangle = |\beta\alpha\rangle, \quad |4\rangle = |\beta\beta\rangle . \tag{2.2.19}$$

The values for $\hat{\sigma}$ are obtained by solving the stochastic Liouville equation (formula 2.1.4). For two spins-½, the spin eigen-states $|i\rangle$ in the diamagnetic product are then given by:

$$|1\rangle = |\alpha\alpha\rangle, \quad |2\rangle = \cos\phi|\alpha\beta\rangle - \sin\phi|\beta\alpha\rangle, \quad |3\rangle = \sin\phi|\alpha\beta\rangle + \cos\phi|\beta\alpha\rangle, \quad |4\rangle = |\beta\beta\rangle \tag{2.2.20}$$

at B_{pol} have the following populations P_i resulting from CIDNP [41]:

$$\begin{aligned} P_1 &= n_{\alpha\alpha}, \quad P_2 = \cos^2\phi\, n_{\alpha\beta} + \sin^2\phi\, n_{\beta\alpha} + \sin 2\phi\, \mathrm{Re}\{\sigma_{\alpha\beta,\beta\alpha}\}, \\ P_3 &= \sin^2\phi\, n_{\alpha\beta} + \cos^2\phi\, n_{\beta\alpha} - \sin 2\phi\, \mathrm{Re}\{\sigma_{\alpha\beta,\beta\alpha}\}, \quad P_4 = n_{\beta\beta} \end{aligned} \quad . \tag{2.2.21}$$

These state populations are the diagonal elements of the spin density matrix $\hat{\rho}$ of the diamagnetic reaction product. The populations n_{ij} are those in the two-spin Zeeman basis (eq. 2.2.19). Here, the mixing angle ϕ of the states $|2\rangle$ and $|3\rangle$ depends on the coupling strength J and the quantity $\Delta\omega_L$ at the polarization field (see formula 2.2.6).

Independent whether the transfer from B_{pol} into the detection field B_0 occurs in the adiabatic regime or not, the condition of strong coupling inevitably leads to a redistribution of polarization between the two nuclei. Only if the mixing angle ϕ approaches 0, i.e. if the spins are weakly coupled at B_{pol}, no polarization is transferred.

The ratio of polarization of the strongly coupled nuclei I_1 and I_2 depends on the timing of the process of field cycling and becomes

$$\frac{\langle I_{2z}\rangle}{\langle I_{1z}\rangle} = \frac{1-\cos 2\phi}{1+\cos 2\phi} \tag{2.2.22}$$

in the case of an adiabatic field variation, and

$$\frac{\langle I_{2z}\rangle}{\langle I_{1z}\rangle} = \frac{1-\cos^2 2\phi}{1+\cos^2 2\phi} \tag{2.2.23}$$

in the case of sudden field variation [56], i.e. no spin evolution during the field variation (some peculiarities of the field switch are discussed in more detail further down). For the sake of simplicity, it shall be assumed that only the first spin, I_1, is initially polarized, while the second spin, I_2 is not. In any case, the ratio of polarization between the two coupled spins reaches a value of 1 at very low field, where the condition of strong coupling with $\phi = \pi/4$ is practically always fulfillled. In the case of weak coupling at high field, the transfer becomes negligible, and in the intermediate field range the efficiency of polarization transfer depends on the strength of spin-spin coupling with respect to the chemical shift difference and the rate of sample transfer.

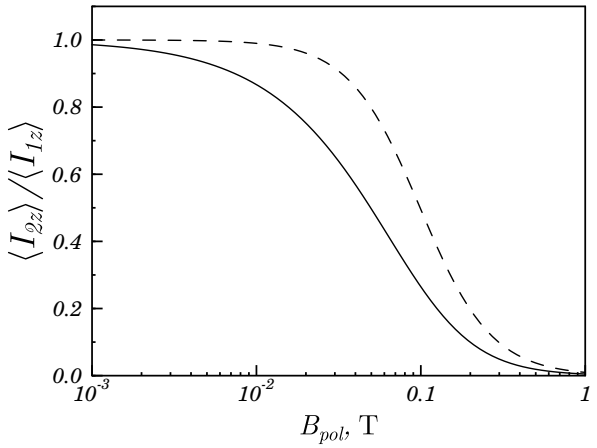

Figure 2.2.2: Polarization transfer efficiency as a function of the external field for the cases of adiabatic (solid line) and sudden (dashed line) field variation for a two-spin system with only the first I_1 spin being polarized directly, and the second spin I_2 acquiring CIDNP due to strong spin-spin coupling at B_{pol} (τ_L, $\tau_{ev} > J_{ij}^{-1}$). Parameters of calculation: J = 3Hz and $\Delta\delta$= 0.5ppm. From ref.: [56].

For a realistic set of parameters, the polarization transfer efficiency for the two cases of adiabatic and sudden field switches is depicted in figure 2.2.2. When the sample transfer occurs neither adiabatic nor sudden, an intermediate between the two curves may be expected. Experimentally, the redistribution of polarization manifests itself in similar low-field CIDNP of the coupled protons in the aromatic moieties of tryptophan and tyrosine (see chapter 4.2 and 6.2) irrespective of whether they exhibit significant hyperfine couplings in the corresponding radicals or not.

The redistribution does, however, not occur instantaneously and crucially depends on the timing scheme of the experiment. For an efficient transfer of polarization between the two

nuclei, the sample transfer either has to proceed adiabatically ($J\tau_{fv}\geq 1$) [1], or the redistribution is accomplished during finite irradiation or waiting times. The criteria for the polarization transfer can then be summarized as follows [56]:

$$J \geq \Delta\nu \text{ at } B_{pol} \quad \text{and} \quad J\tau_L, J\tau_{ev}, J\tau_{fv} \geq 1 \quad , \tag{2.2.24}$$

and the time for an efficient transfer of polarization may be estimated to J^{-1}.

In this case, the polarization transfer proceeds upon the evolution of coherences, the off-diagonal elements in the spin density matrix. These are usually formed at B_{pol}, because the nuclear spin eigen-states of the radicals do not coincide with those in the reaction products [57-59], and the Hamiltonian changes abruptly during the radical recombination. Alternatively, coherences may be created from polarization by appropriate pulse sequences or field switches. For the case considered here (two coupled spins-1/2) the frequency of the zero-quantum coherence between state $|2\rangle$ and $|3\rangle$ is [49]:

$$\frac{\Delta E_{23}}{\hbar} = \Omega_{23} = \sqrt{(2\pi J)^2 + (\Delta\delta \cdot \omega_{pol})^2} \quad . \tag{2.2.25}$$

In case, the irradiation time τ_L is chosen short ($\Omega_{23}\tau_L<<1$), the signal amplitudes exhibit beatings while the field is kept at the same value (during an additionally introduced waiting time for the spin evolution, τ_{ev}, after irradiation). Neglecting the decay of coherences, the ratio of polarization of nucleus 1 and nucleus 2 and the total net polarization, $\langle I_z \rangle$ becomes [56]:

$$\begin{aligned} \frac{\langle I_{1z} \rangle}{\langle I_z \rangle} &= 1 - \sin^2 2\phi \cdot \frac{1-\cos(\Omega_{23}\tau_{ev})}{2} \\ \frac{\langle I_{2z} \rangle}{\langle I_z \rangle} &= \sin^2 2\phi \cdot \frac{1-\cos(\Omega_{23}\tau_{ev})}{2}. \end{aligned} \tag{2.2.26}$$

When changing the irradiation time from very short ($\Omega_{23}\tau_L<<1$) to very long ($\Omega_{23}\tau_L>>1$) times, the beatings are washed out, due to the phases being shifted in time from one laser pulse to the next. The coherences eventually vanish, even without taking decoherence into account, and the following ratios of expectation values are obtained [56]:

$$\begin{aligned} \frac{\langle I_{1z} \rangle}{\langle I_z \rangle} &= 1 - \frac{\sin^2 2\phi}{2} \cdot \left[1 - \frac{\sin(\Omega_{23}\tau_L)}{\Omega_{23}\tau_L} \right] \\ \frac{\langle I_{2z} \rangle}{\langle I_z \rangle} &= \frac{\sin^2 2\phi}{2} \cdot \left[1 - \frac{\sin(\Omega_{23}\tau_L)}{\Omega_{23}\tau_L} \right]. \end{aligned} \tag{2.2.27}$$

In both cases, variation of τ_L or variation of τ_{ev}, the polarization is redistributed between the two nuclei during a time that is in the order of the reciprocal coupling strength (J^{-1}). In figure 2.2.3 the polarization of the first and the second spin with respect to the total net polarization

are shown as functions of irradiation and evolution times (τ_L and τ_{ev}). The characteristic beatings of the signal amplitudes are a manifestation of the zero-quantum coherence between the states $|2\rangle$ and $|3\rangle$ with a frequency proportional to the difference in energy between these states.

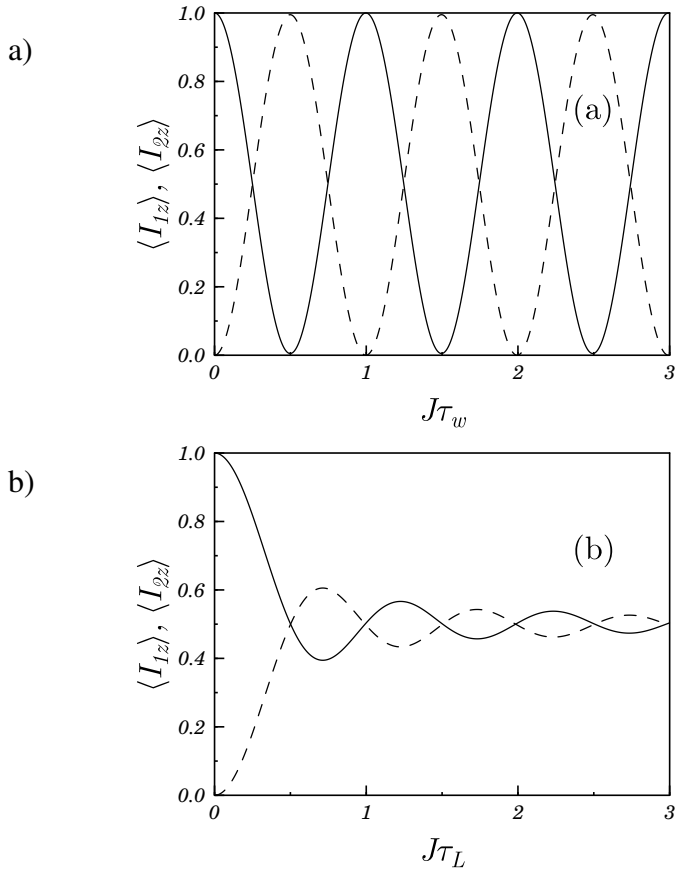

Figure 2.2.3: Polarization of spin I_1 (solid line) and I_2 (dashed line) normalized by dividing it by the total polarization $\langle I_z \rangle$ as functions of a) τ_{ev} and b) τ_L at B_{pol} = 10mT. Parameters of calculation: J = 3Hz anf $\Delta\delta$= 0.5ppm from ref.: [56].

As a matter of fact, the polarization patterns observed at B_0 are substantially affected by the sample transfer. Only the two limiting cases of a fully adiabatic or a sudden field switch can be treated analytically, whereas in complicated homonuclear multi-spin systems the sample transfer may be expected to occur in an intermediate regime for certain energy levels, which shall be discussed in more detail in the following.

The Field Cycling Process. The initial form of the density matrix depends on the peculiarities of CIDNP formation, which have been introduced in the first part of this chapter (2.1). During CIDNP formation, both polarizations and coherences may be formed by the rapid change of the Hamiltonian during radical recombination [59]. After the formation of CIDNP at arbitrary

magnetic field, the diamagnetic products have to be transported from the polarization field B_{pol} into the detection field B_0. Because nuclear polarization formed at B_{pol} consecutively decays with the spin-lattice relaxation time T_1, it is desirable to rapidly transfer the diamagnetic products into the high field for detection in order to conserve the polarization. On the other hand, however, the sample transfer should be slow if one wishes that the populations remain in their eigen-states during the transfer. As it is already seen in figure 2.2.2, the outcome of the field cycling experiment can differ substantially in the two limiting cases of an adiabatic and a sudden field variation.

In the fully adiabatic case, the Hamiltonian changes so slow that the populations always follow their time dependent eigen-states. This means, that the population of the state of the highest energy at B_{pol} remains in the state of the highest energy at B_0, and that of the second highest energy at B_{pol} in the state of the second highest energy at B_0 and so forth. It is then only necessary to know to which values of J_z the high-field transforms of the eigen-states at B_{pol} correspond. For this purpose the eigen-states of the Hamiltonian (formula 2.2.2) are evaluated analytically at arbitrary magnetic field. For instance in chapter 4.0, the eigen-values for different sub-ensembles containing up to 5 proton spins in the tryptophan molecule are computed as a function of the external field.

In the adiabatic regime, the coherences also remain in the off-diagonals of the spin density matrix and thus do not manifest themselves in the spectrum. For two groups of protons coupled by a spin-spin coupling J, the time τ_{fv} for a fully adiabatic field change has been estimated to be at least the inverse of the J-coupling [1]. On the basis of this estimate, the field switch has usually been assumed to always occur in the adiabatic regime [11, 40, 41], and only be violated in the case of small couplings or high transfer rates (actually a value of $J \approx 3$Hz is small enough when $\tau_{fv} = 0.3$s).

In the case that the field switch occurs suddenly, no spin evolution occurs during the field switch. The density matrix formed at B_{pol} then has to be projected onto the high field states, and the density matrix elements are as follows:

$$\rho_{rs}^{hf}(t) = \sum_{k,l} \left\langle r_{hf} \middle| k \right\rangle \left\langle l \middle| s_{hf} \right\rangle \rho_{kl}(t) \quad . \tag{2.2.28}$$

Knowing the density matrix at B_{pol} (i.e. the populations of the various eigen-states on one hand and the correlation to the high field states on the other) one is in the position to compute the corresponding theoretically expected polarizations of the individual nuclear spin states. In any case, the populations of the states at B_0 may be calculated by taking the trace of the final density matrix.

In reality, the situation is more complicated. Depending on sign and magnitude of the spin-spin couplings and the differences in chemical shift, level anti-crossings may occur within the groups of states with the same total spin projection, J_z. This changes the order of energy levels upon variation of the external field. Moreover, the field variation occurs non-linearly. In this work it turned out that the field variation does not necessarily always occur in the adiabatic regime and that other factors than the values of *J*-coupling alone limit the adiabatic regime of the field cycling process. This shall be briefly evaluated for a realistic case of the field variation from a field of level-anti-crossing to the detection field, B_0.

When restricting the consideration to a two-level system, the probability for a non-adiabatic field switch, P_{NA}, through an avoided crossing can be evaluated by means of the Landau-Zener theory [60-62] as follows:

$$P_{NA} = e^{-2\pi\cdot\Gamma}$$
$$\Gamma = \Delta\tau_{fv}\Delta E_{rs} = \frac{\Delta\tau_{fv}}{1/\Omega_{rs}} \quad , \qquad (2.2.29)$$

with $\Delta\tau_{fv}$ being a measure of the duration of interaction, e.g. the field variation through the region of level-crossing. The coherence frequency, Ω_{rs}, is the frequency of oscillations between the two adiabatic energy states. The Landau-Zener formula (2.2.29) gives only a very crude estimate whether a non-adiabatic transition has taken place during the traversal through the interaction region, since it is derived using approximations which are unrealistic under the actual experimental conditions: It assumes the perturbation (the field switch) and the energy separation to change linearly in time, and that the coupling element in the Hamiltonian matrix is independent of time. However, it may be expected, that only for large energy gaps ΔE_{rs} between the two states *r* and *s* and slow field variation, τ_{fv} the crossings of energy levels are avoided and no mixing of the populations between the states occurs ($\Delta\tau_{fv}\Delta E >> 1$).

Here, only one example shall be briefly analyzed, in order to show, that the sample transfer in the current field cycling set-up is not necessarily always in the adiabatic regime as it has formerly been assumed [40, 41], when the changes in the nuclear spin-systems with the external field have not been considered.

The energy difference, ΔE, between two of the four eigen-levels with J_z = -1 for the spin sub-system of the tryptophan molecule, consisting of the two β-protons, the α-proton and H2 is plotted in figure 2.2.4 a). Below (fig. 2.2.4 b)), a realistic time-field profile for the field change from B_{pol} = 0.32T to B_0 with a moderate transfer time of ~0.6s is shown[1]. At B_{pol} =

[1] The four corresponding energy levels are shown in chapter 4 (figure 4.0.4), and in chapter 3.2 the program for calculating time-field profiles is briefly described.

0.32T, the α-proton of N-acetyl-tryptophan (NATrpH) acquires significant polarization in CIDNP field cycling experiments, despite the fact that no HFC is expected for this proton position. The observed polarization is attributed to a level anti-crossing in this region. The parameter Γ (according to formula 2.2.29) is calculated in the bottom (fig. 2.2.4 c)), showing that the small energy differences within manifolds with the same total spin projection, J_z, render the field switch highly non-adiabatic (Γ<<1) in almost the entire region. Only at the start and the end of the process Γ is above 1. Under these conditions, it is thus not acceptable to assume the sample transfer to occur in the adiabatic regime, and considerable mixing of state populations has to be expected.

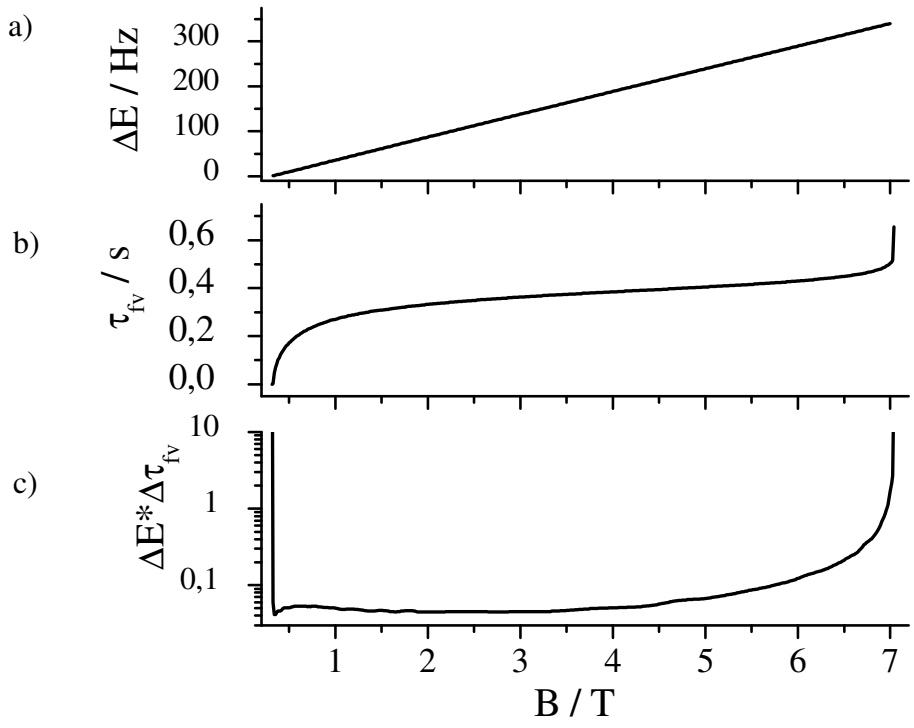

Figure 2.2.4: a) Energy difference between two nuclear spin energy levels in N-acetyl-tryptophan, |ββαβ> and |βαββ> of the protons β1, β2, α, and H2, respectively, possessing a level anti-crossing at B = 0.321T. b) Realistic timing scheme for a field cycling experiment starting at B_{pol} = 0.325T with a total transfer time τ_{fv} = 600ms to B_0 = 7T. c) Landau-Zener parameter, Γ, for the adiabaticity of the field switch calculated for increments of ΔB = 0.013T.

Besides of the mixing of populations, another peculiarity should be considered in the anti-crossing region. Not only the populations between the coupled states can mix, but also the coherences among them are mixed into the populations during the process of field cycling. The coherences observed for the experimental example discussed above are shown in chapter

4.3. The rise of the external field during the process of field cycling can act like a highly selective pulse for certain energy levels which happen to be in resonance with the field switch. Within these levels, populations and coherences can be exchanged during the process of field cycling, which is explored experimentally in some detail in chapter 4.

For a given field increase profile, such as it is shown in figure 2.2.4, the actual adiabatic efficiency is only accessible through a computer simulation of the spin evolution under the time dependent Hamiltonian. For a quantitative interpretation of the spectral patterns detected after CIDNP formation at low magnetic field, it is thus necessary to numerically evaluate the spin evolution during irradiation and sample transfer. Analytically, only the two cases of a fully adiabatic or a sudden sample transfer are relatively easy to treat. These two limiting cases may be considered e.g. for modelling of the T_1 relaxation dispersion of N-acetyl tryptophan in chapter 4.1, for which the theory shall be introduced in the following.

2.2.5 Spin Relaxation in Scalar Coupled Multi-Spin-Systems

As discussed above, the differences in the ordering of spin states at variable magnetic field, i.e. fulfillment of the strong coupling condition (formula 2.2.4) and the occurrence of level anti crossings, govern the spin evolution at variable magnetic fields. The same factors manifest themselves in the longitudinal relaxation times (T_1) of individual spins at variable magnetic field when probed by field cycling NMR.

In chapter 4.1 the NMR relaxation dispersion (NMRD) data for the individual protons in N-acetyl tryptophan is discussed. A strategy for the modelling of the NMRD curves was developed by K. L. Ivanov and shall be outlined here. It is based on the relaxation theory introduced by A. Redfield [31], and is described in some detail in refs. [63, 64]. In the simplest case, the rate of a nuclear spin to attain thermal equilibrium R_1 is assumed to occur due to random fluctuations of the external magnetic field, ΔB, and is given by:

$$R_1 = \frac{1}{T_1} = (\Delta B)^2 \frac{\tau_c}{1+(\omega_L \tau_c)^2} \quad , \tag{2.2.30}$$

where τ_c is the correlation time of random molecular motions, and ω_L is the Larmor precession frequency (see formula 2.2.2). One factor that is known to cause a field dependence of the relaxation behaviour is the random field fluctuations ΔB that can vary with the external field. This is usually the case when the relaxation is dominated by e.g. chemical shift anisotropy, since the chemical shift is roughly proportional to the external magnetic

field. Chemical shift anisotropy is known to be small in protons, and a field dependent ΔB shall be disregarded here.

Because ω_L depends on the external field according to equation 2.2.2, the characteristic relaxation time, T_1, may also be magnetic field dependent. Different relaxation regimes may then be distinguished: When $\omega_L \tau_c << 1$ molecular motion is fast as compared to the Larmor precession frequency and vice versa if $\omega_L \tau_c >> 1$. From this fact, correlation times of molecular motions are often extracted, because in case that T_1 exhibits a stepwise feature in the relaxation dispersion at $\omega_L \tau_c \approx 1$, the molecular motion is on the time scale of the Larmor precession frequency. In the present work it is shown that this interpretation can be misleading, because the condition of strong coupling of the individual spins in the molecule under observation may lead to similar features in the NMRD data of individual protons. The N-acetyl tryptophan molecule in aqueous solution is not expected to undergo any changes in relaxation behaviour since, as a relatively small molecule, it remains in the fast motional regime ($\omega_L \tau_c << 1$) in the entire field range. Accordingly, the relaxation curves of the individual protons of NATrpH are modelled regardless of any changes in the motional regime, with the aim to elucidate the features that appear due to the changes in the molecular spin system, i.e. the relative strength of *J*-coupling of protons among each other. Hence, the dynamics of the spin-system is again described by the time-independent Hamiltonian in equation 2.2.1, which contains all the scalar spin-spin couplings of the protons with each other and their isotropic chemical shifts.

Relaxation is caused by modulations of the time-dependent part of the total Hamiltonian that account for random fluctuations of the magnetic field explored independently by each nucleus, and has the following form [50, 65]:

$$\hat{H}_e(t) = \left(\frac{\gamma}{2\pi}\right) \sum_{i=1}^{N} \left(B_{ix}(t)\hat{I}_{ix} + B_{iy}(t)\hat{I}_{iy} + B_{iz}(t)\hat{I}_{iz} \right) \quad , \tag{2.2.31}$$

with B_{ix}, B_{iy} and B_{iz} as the components of the random local fields for spin i. The system under investigation clearly fulfills the extreme narrowing case, with short correlation times of motion, τ_c, and the relaxation rate between two eigen-states of the spin system, r and s ($r \neq s$), becomes [50, 65]:

$$R_{rs} = 2\tau_C \left\{ \left| \langle r | H_e(t) | s \rangle \right|^2 \right\}_{Av} \quad , \tag{2.2.32}$$

denoting the averaging over time. The relaxation parameters, as defined in the Bloch equations then follow from the components for the stochastic local fields [50, 65]:

$$2\tau_C\left\{B_{ix}^2\right\}_{Av} = 2\tau_C\left\{B_{iy}^2\right\}_{Av} = 2\tau_C\left\{B_{iz}^2\right\}_{Av} = \frac{1}{T_1^i}, \qquad (2.2.33)$$

where T_1^i is the longitudinal relaxation time for the i^{th} spin. In case all spins in the molecular spin system are coupled only weakly (see formula (2.2.4)), the formula (2.2.33) immediately gives independent relaxation times for each spin *i*. In low fields however, where the condition of weak coupling is not fulfilled anymore the situation changes. For the molecular spin system of tryptophan it is shown experimentally (see chapter 4.1), that those spins, which are strongly coupled tend to relax together, and moreover, that the anti-crossings in the nuclear spin eigen-states can also manifest themselves in the NMRD curves as peaks or dips.

For the modelling of the measured relaxation dispersions for the individual spins in the rather complex spin sub-systems of coupled spins-½ in N-acetyl tryptophan it is assumed that the entire relaxation dispersion is obtained with a single experimental protocol. This experimental protocol is shown in the experimental part of chapter 4.1 (figure 4.1.1a)). It starts with the spin-system at thermal equilibrium in the high field of the spectrometer B_0. The theory assumes the field to be then switched instantaneously to the field, in which T_1 is probed, B_{int}, where the sample remains for a variable time τ_r, to attain its thermal equilibrium. This means that during the first field switch no spin evolution occurs, and that the high field populations are projected onto the states at B_{int} (according to formula (2.2.28)). The re-magnetization of the sample ($B_{int} \rightarrow B_0$) may then be considered for the two limiting cases of adiabatic and sudden field variation (see above).

In the first step, the energies of the eigen-states for the multispin-system are calculated for the high field of the spectrometer (B_0), where the individual elements of the spin density matrix are given by the equilibrium polarizations, $p^0{}_\mu$:

$$\rho_{\mu\nu}^{hf} = p_\mu^0 \delta_{\mu\nu} \quad . \qquad (2.2.34)$$

Here, $\delta_{\mu\nu}$, is the Kronecker delta[1], and the value of the *z*-projection of the total spin of the system in this state, I_z^μ determines the μ-th eigen-state population:

$$p_\mu^0 = \frac{1}{Z_0}\exp\left(-\frac{h\nu I_z^\mu}{kT}\right) \approx \frac{1}{Z_0}\left(1+\frac{h\nu I_z^\mu}{kT}\right) = \frac{1}{Z_0}\left(1+\frac{\gamma B_0 \hbar I_z^\mu}{kT}\right), \qquad (2.2.35)$$

with Z_0 being the partition function, so that the trace of the density matrix $\hat{\rho}$ is equal to unity, *k* is the Boltzmann constant and *T* is the absolute temperature, and the high temperature approximation ($kT >> h\nu$) is used.

[1] with $\delta_{\mu\nu}=0$ if μ≠ν, and $\delta_{\mu\nu}=1$ if μ=ν

Furthermore, calculations are restricted to the diagonal elements of the spin density matrix $\hat{\rho}$, while the off-diagonal elements (the coherences) and their evolution are neglected, which is reasonable because those states being connected by zero-quantum coherences have similar populations throughout the entire field range. The problem is then confined to the column of its diagonal elements **p**:

$$\mathbf{p} = \begin{pmatrix} p_1 \\ p_2 \\ \vdots \\ p_n \end{pmatrix} \quad , \tag{2.2.36}$$

which relax according to their relaxation matrix $\hat{R}$ from their starting value $\mathbf{p_0}$ (when starting at B_0) to their stationary value $\mathbf{p_{int}}$ (at B_{int}):

$$\frac{d\mathbf{p}(t)}{dt} = \hat{R}(\mathbf{p}(t) - \mathbf{p}_{\text{int}}), \qquad \mathbf{p}(t=0) = \mathbf{p}_0 . \tag{2.2.37}$$

While the off-diagonal elements of the relaxation matrix are given by equation (2.2.32), the diagonal elements are as follows:

$$R_{\mu\mu} = -\sum_{\mu \neq \nu} R_{\mu\nu} = -\sum_{\mu \neq \nu} R_{\nu\mu} \quad . \tag{2.2.38}$$

The stationary values of **p** are the column of equilibrium values at $B = B_{int}$.

$$p_{\mu}^{\text{int}} \approx \frac{1}{Z_0}\left(1 + \frac{\gamma_\mu B_{\text{int}} \hbar I_z^{\mu}}{kT}\right) \quad . \tag{2.2.39}$$

Equation (2.2.39) is then solved numerically, and the T_1 times for the individual spins are obtained by analyzing the evolution of their z-magnetizations, $M_i(t)$, which are the expectation values of the operators $\hat{I}_{iz}$:

$$M_i(t) = \left\langle \hat{I}_{iz} \right\rangle (t) = Tr\left\{\hat{I}_{iz}\hat{\sigma}(t)\right\} \tag{2.2.40}$$

at the observation field.

Generally, because the transitions between many different states are involved, the relaxation behaviour of a single nucleus (or a group of magnetically equivalent nuclei) can not be expected to be described by a single exponential. However, an estimation of the T_1-time of spin i can be obtained by the numerically integrating the magnetization decay over the time:

$$T_1^i = \frac{1}{M_R - M_{\text{int}}} \int_0^{\infty} (M_i(t) - M_{\text{int}})dt \quad , \tag{2.2.41}$$

where M_R and M_{int} are the starting and final magnetizations, respectively. Here, the equilibrium magnetizations at both fields are:

$$M_0 = \frac{1}{4} \cdot \frac{\gamma B_0 \hbar}{kT}; \qquad M_{\text{int}} = \frac{1}{4} \cdot \frac{\gamma B_{\text{int}} \hbar}{kT} \quad . \qquad (2.2.42)$$

The values of T_1^i obtained by this procedure will be compared to the experimentally obtained values for N-acetyl tryptophan in chapter 4.1. The good agreement of the experiment with this relatively simple theory clearly shows that the features observed in the NMRD data of individual spins in the fast motional regime depend on the peculiarities of the molecular spin system, i.e. the relative strength of *J*-coupling among the spins. In fields where the strong coupling condition is fulfilled, the coupled spins tend to relax with the same rates.

3 Experimental

For the interpretation of CIDNP spectra in terms of the underlying photochemical and photo physical processes, a combination of different experimental techniques is often necessary. While most CIDNP investigations of photoreactions in the past have been performed using steady state illumination (cw-CIDNP), meaning that the sample is continuously irradiated during the acquisition of the NMR spectrum, with the use of pulsed lasers CIDNP techniques became more elaborate. Sometimes only the so-called 'geminate' spectrum, i.e. the CIDNP spectrum taken immediately after the laser pulse, contains the valuable information about precursor states and ratios of hyperfine couplings. This requires the acquisition of CIDNP spectra in a time-resolved mode (TR-CIDNP). Here, a kinetic profile is obtained with a microsecond time resolution by variation of the delay between laser flash and observation pulse. During this work a TR-CIDNP set-up was constructed that enables complementation of the knowledge from field-dependent CIDNP measurements with those from time resolved spectra. For the ease of comparison they are acquired at the same spectrometer frequency (300MHz) and the radicals are generated with lasers operating at the same wavelength (308nm). This set-up shall be briefly described in the first section of this chapter (3.1)
In the second part (3.2), the experimental set-up for the acquisition of high resolution NMR and CIDNP spectra as a function of the external magnetic field (FD-CIDNP) will be described. Because almost all experiments during this work were performed with this spectrometer, and because it is still quite unique, it shall be explained in some more detail. Some modifications were undertaken and its specifications have improved during the last years. In particular, the implementation of a lock unit (chapter 3.2.1) and the automation of field cycling experiments (chapter 3.2.2) enabled new types of experiments, thus providing new insights into field cycling NMR.

3.1 Time Resolved CIDNP Set-up

The idea to acquire CIDNP spectra in a time resolved mode goes back to experiments of Schäublin, A. Wokaun and R. R. Ernst in 1977 [58]. When such experiment was first performed, the duration of the light irradiation (~2.5ms) limited the time resolution to milliseconds. Since pulsed lasers that typically provide less than 10ns pulse width (e.g.

excimer lasers) are commonly in use, the RF-pulse for observation usually determines the time resolution. Hence, the technique was extended into the radical stage on the time-scale of microseconds by P. J. Hore *et.al.* [66], and with the aid of booster amplifiers even into the sub-microsecond regime by G. L. Closs and R. J. Miller [67]. Hence, TR-CIDNP is not a new experimental technique, and the present version of the setup does not differ considerably from those employed in Oxford or Novosibirsk [68]. It will therefore be described only briefly here.

In figure 3.1.1, a typical timing scheme of a TR-CIDNP experiment is shown. It starts with the removal of background (usually Boltzmann) polarization. The purpose of it is to measure solely the polarization that the products acquire upon their intermediate paramagnetic stage. For the experiment presented in chapter 6.1 it was particularly important to achieve an efficient and at the same time reproducible saturation of the solvent (HDO) line. It turned out that a single pulse long pulse of ~300μs (as schematically indicated in the timing scheme in figure 3.1.1) fulfills these requirements quite well: it saturates the water signal reproducibly to less than 5% in its amplitude. The pre-saturation is followed by a short laser pulse and a variable delay time. Finally, for different delay times conventional NMR spectra are acquired by means of an RF-detection pulse followed by the free induction decay (FID).

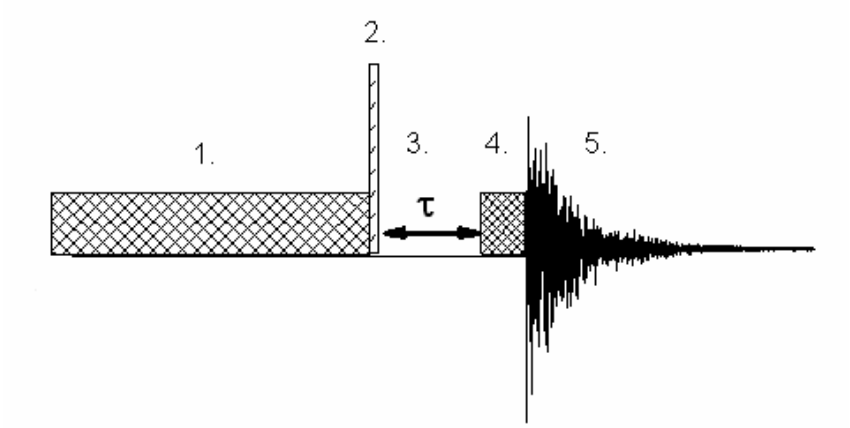

Figure 3.1.1: Timing scheme of a TR-CIDNP experiment with microsecond time resolution: 1. RF-presaturation pulse(s), 2. laser pulse, 3. variable delay, 4. RF-detection pulse, 5. free induction decay (FID).

Because the time resolution is limited by the length of the RF-pulse, usually short RF pulses (down to 30°) with a relatively high power are used, depending on the given requirements for the time resolution and the available CIDNP signal enhancement. However, presently the use of a 'class C' pulse amplifier does not allow switching the pulse amplitude between pre-saturation and detection. Therefore, the time resolution was limited by the long pulse for saturation, allowing a 90° pulse length of 3μs. Smaller flip angles may be used to improve

time resolution (minimum ≈ 1μs) at the expense of signal-to-noise ratio of the resulting spectra. One should be aware that fast transients are inevitably convoluted with the shape of the RF-pulse [69]. Only, if the CIDNP kinetics is slow enough to be approximated linearly within a rectangular pulse, one half of the applied RF-pulse length may be considered as the starting point of the observed kinetics. However, short RF-pulses can typically not be approximated as rectangular, and their centre of gravity is shifted towards later times.

The necessary modifications to run TR-CIDNP experiments were introduced on a 300MHz NMR spectrometer (Bruker CXP-300) which is equipped with a Tecmag computer for the data acquisition and a Macintosh computer running the MacNMR 5.5 PCI software. A scheme of the setup is shown in figure 3.1.2. It employs a XeCl excimer laser (type ATLEXC 160 Series from ATL), operating at λ=308nm. It provides single laser pulses with a duration of approximately 10 to 15ns, providing a power of 150mJ/per pulse. However, for the acquisition of pseudo cw-CIDNP spectra or other purposes it is also possible to apply the pulses with a repetition up to 200 Hz on the expense of pulse power.

With a fast photodiode the laser pulse was adjusted in time with respect to the RF-pulse, i.e. the laser pulse was placed at the beginning of the rise time (~0.3μs) of a 90° pulse. For the synchronisation, a digital delay and pulse generator (model DG 535 from Stanford Research Instruments, Inc.) is used.

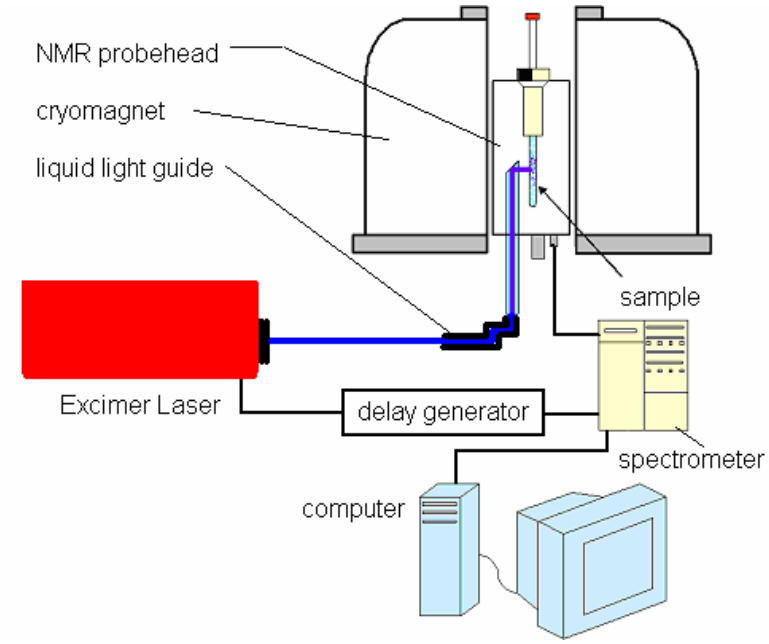

Figure 3.1.2: Scheme of the experimental set up for time resolved CIDNP measurements. In part from ref.: [70].

A flexible liquid light guide optimized for 308nm light (LUMATEC series 250) with a cross section of 5mm^2, is used to couple the light into a quartz rod placed in the probe head. The

advantages of this version lay in the facile adjustment of the optics. Alternatively, a system consisting of various lenses and mirrors is placed below the cryomagnet.

A 5mm high resolution ^{1}H-NMR probe (Bruker VSP 300) was modified for the time resolved photo-CIDNP measurements. It is equipped with a quartz rod that has been inserted through the whole probe and fixed with a small piece of Teflon and a nylon screw. A little 45° mirror was mounted in on its top so that the sample can be irradiated from the side through the NMR coil.

3.2 Field Cycling CIDNP Set-up

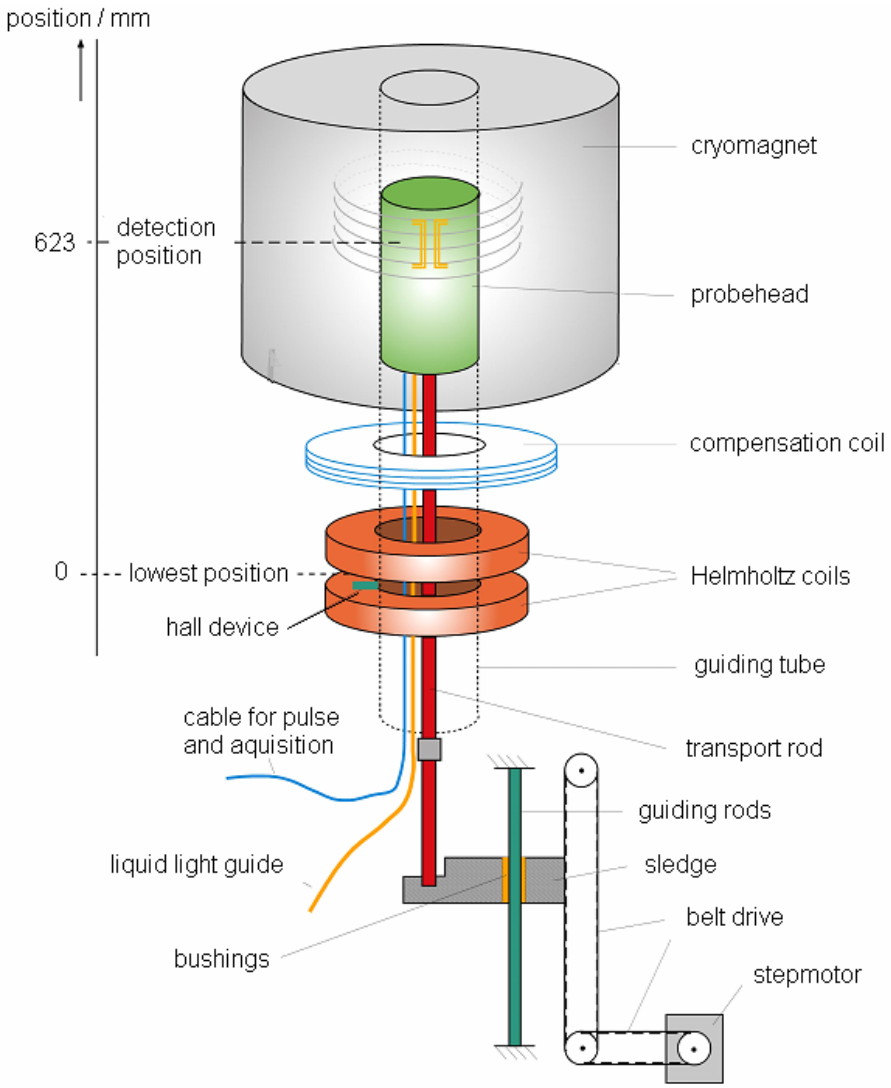

Figure 3.2.1: Scheme of the experimental set-up for field dependent CIDNP measurements (from ref. [48])

The field cycling spectrometer has been described in detail in refs. [10] and [11]. It employs fast field cycling covering a magnetic field of 0.1mT to 7T, allowing the acquisition of high

resolution NMR spectra of liquid samples and providing constant irradiation conditions over the whole field range. A schematic overview of the set-up is given in figure 3.2.1 In contrast to the time resolved setup it is not realized with a commercially available NMR machine, but on a homemade spectrometer [71].

The field cycling unit consists of a step motor (Phytron model ZSH 107-200-12.5) driving a system of belt drives that moves the whole NMR probe head along the bore of the cryomagnet (300MHz from Oxford Instruments). The positioning of the probe is computer controlled, and it can be placed with a precision better than 0.1mm at any desired position in the fringe field, or alternatively in a pair of Helmholtz coils placed under the cryomagnet. This auxiliary magnet and the step motor drive are shown in more detail on the photographs in figures 3.2.2a) and b), respectively.

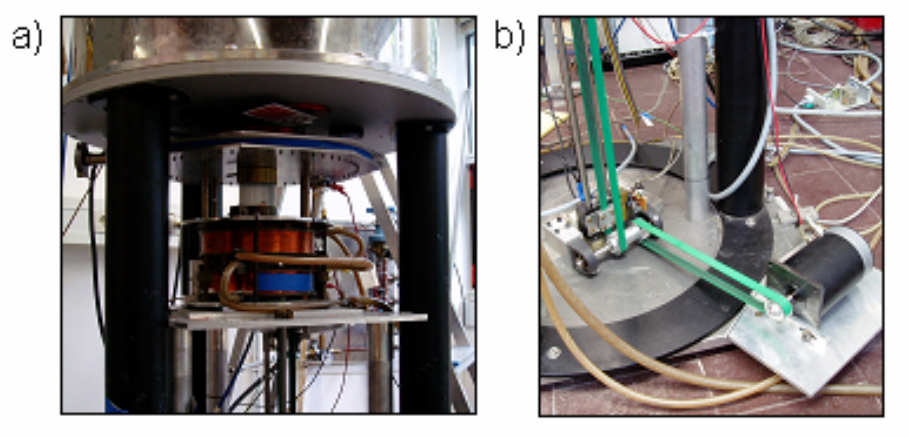

Figure 3.2.2: Photographs of: a) Helmholtz coils placed under the cryomagnet and b) step motor driven belt drives for the positioning of the probe head.

Because at low magnetic field sharp features in the CIDNP field dependencies are likely, a higher homogeneity over the sample volume and a more precise adjustment of external field are desired than it is available in the fringe field of the cryomagnet. Therefore, magnetic fields between 0.1mT to 100mT are set by control of the electric current through the electromagnet. The field is set by a control unit B-H11C with a power supply B-MNC4 both from Bruker. It can be set by steps of 0.1mT and the homogeneity is better than 0.05mT across the sample. Above 100mT the field homogeneity is given by the shape of the fringe field and its gradient across the sample. In figure 3.2.3 the profile of the field along the bore axis and its first derivative (the gradient) are plotted against the probe position. It was obtained by mounting a hall device on the transport rod (red in fig. 3.2.1) instead of the probe head and placing it in different positions in the fringe field of the cryomagnet. The curves slightly deviate from

those obtained in the work of S. Grosse [11], where a larger maximum gradient (~75 T/m) than that presently found (~55 T/m) has been determined around the same field.

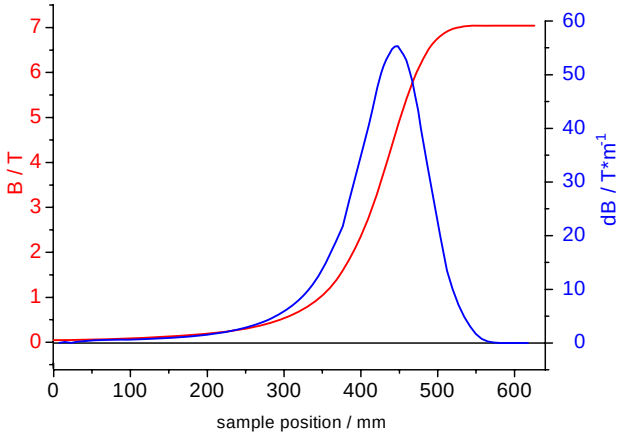

Figure 3.2.3: Field profile and gradient along the bore axis of the cryomagnet.

The additional compensation coil indicated in figure 3.2.1 is connected in series to the Helmholtz pair and compensates the residual fringe field of the electromagnet for an undisturbed NMR detection when the electromagnet is switched on. Inside the Helmholtz pair, an additional anti-Helmholtz pair corrects for the gradient which the fringe field of the cryomagnet causes at the sample position.

Sample irradiation is realized in a similar way as in the TR-CIDNP setup. It employs a flexible liquid light guide that is attached to the probe and routes the light into a quartz rod placed in the probe. Depending on the probe head utilized, the upper end of the quartz rod is either polished in a 41° angle, or it connects to a separate prism that reflects the light into the sample in the region of the coil. This method guarantees constant irradiation conditions over the whole field range. It further employs a pulsed XeCl excimer laser (Lambda Physics EMG 101 MSC) operating at 308nm. Alternatively, the sample irradiation can be performed with a high pressure mercury lamp.

A typical field cycling CIDNP experiment can be divided into three parts: i) the preparation of a defined spin state, ii) a spin evolution period and iii) the detection of the FT-NMR spectrum. As an example, the experimental protocol that is commonly employed to obtain a CIDNP field dependence is given in figure 3.2.4. In the first step a polarized nuclear spin state is prepared by irradiation of the sample for a defined time, τ_L, at a pre-selected magnetic field, B_{pol}. Typically, the sample is then transferred during the time τ_{fv} from B_{pol} to the detection field B_0 where the detection is performed by a conventional NMR experiment that consists of

the RF pulse followed by the free induction decay. In field dependent CIDNP experiments discussed in this work, the different values for B_{pol} in the stray field were scrambled, and not successively decreased or increased, in order to avoid systematic errors from an incomplete correction of the loss of signal intensity in sets of experiments performed with the same sample.

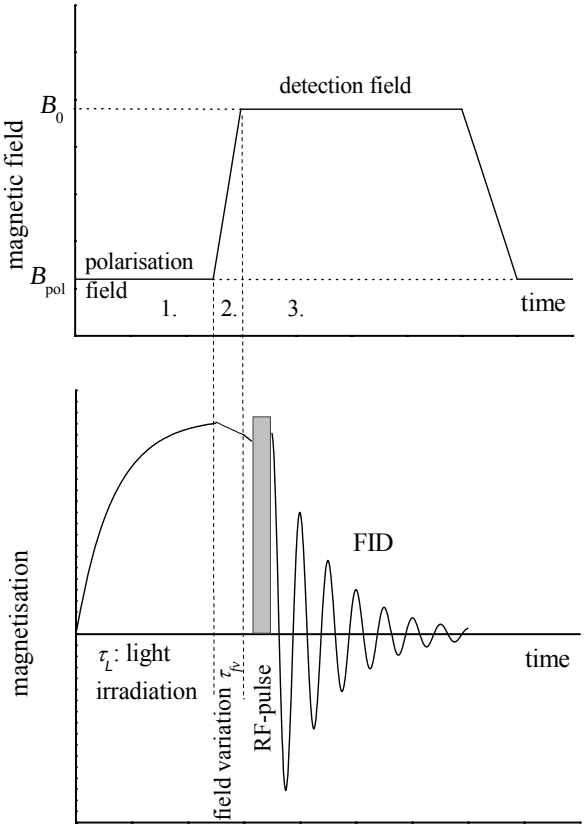

Figure 3.2.4: Typical timing scheme of a FD-CIDNP experiment: 1. laser irradiation for τ_L at B_{pol}, 2. Transfer of reaction products from B_{pol} to B_0 during τ_{fv}, 3. Conventional NMR detection by means of RF-pulse and FID.

The outcome of a field cycling experiment crucially depends on all three stages of the experiment which is shown in chapter 4 by several modifications of the timing scheme in figure 3.2.4. The modified experimental protocols are presented in the appropriate chapters together with the experimental results.

In the following, some modifications of the field cycling setup are described in more detail. In section 3.2.1 the realization of an external lock unit is described which was implemented and enabled monitoring the changes of the external field during the sample transfer. Thereafter, the automation of the field cycling process, which considerably facilitates the acquisition of data, and the modelling of time-field profiles are described in section 3.2.2.

3.2.1 The Lock Unit

The purpose of a lock system is to provide control over the magnetic field strength, B_0, by automatically compensating any minor variations caused by a drift in temperature or the change of other circumstances. Usually an internal lock is employed. It continuously detects the resonant frequency of a nucleus in the sample under study and adjusts the current in the z_0-shim (the shim that adds a constant field without any gradient across the sample) to compensate for slow changes of the main field. Because in the field cycling spectrometer, the sample under study is subject to fast field changes it can not be considered as a potential lock sample. This is also the reason, why the field cycling spectrometer was not equipped with a lock system.

The solution to this problem was developed together with F. Gubaydullin. It employs an external lock with an extra sample placed as close as possible to the position of the main sample while it is positioned in the cryomagnet. This way the lock sample experiences only the field changes that actually occur at the position of the NMR measurement. These requirements are complicated to fulfill since the whole probe is moved inside a guiding tube leaving practically no space for an additional sample and the circuitry of a lock system. This problem was solved as follows: A 15mm times 30mm large piece was carefully cut out of the bearing tube at exactly the same height where the NMR measurement is performed and continued with a 5mm wide slit for the feed cable up to where the probe head ends when it is positioned in the uppermost position. On picture a) in figure 3.2.5, the bearing tube for the probe with the notch can be seen; it already bears the lock circuitry and the coaxial feed cable. For the resonance circuit, a sample with D_2O was prepared and sealed into a capillary. A small amount of paramagnetic copper salt ($CuCl_2$) was added to the sample to provide a faster relaxation of the deuteron spins and thereby enable a faster correction of the field. The capillary was then bent (see fig. 3.2.5 b)); two 90° angles make sure that the sample remaining after the sealing procedure would fill the coil region completely. The coil itself is a 0.2mm copper cable, wound around the capillary and stabilized with acrylic glue. Finally, an appropriate capacitor was attached to the coil in-between the legs of the sample to obtain the resonance frequency of 46.05MHz for the deuteron spins. It is shown in figure 3.2.5 b). The whole circuit was wrapped up with a Teflon strip and then shielded with copper foil that is grounded together with the outer part of the feed cable (figure 3.2.5 c). This procedure yields a quite compact NMR probe that fits into the notch of the bearing tube with its 4mm walls

without getting in the way of the probe transfer after covering the inside of the bearing tube with some tape to smoothen its surface.

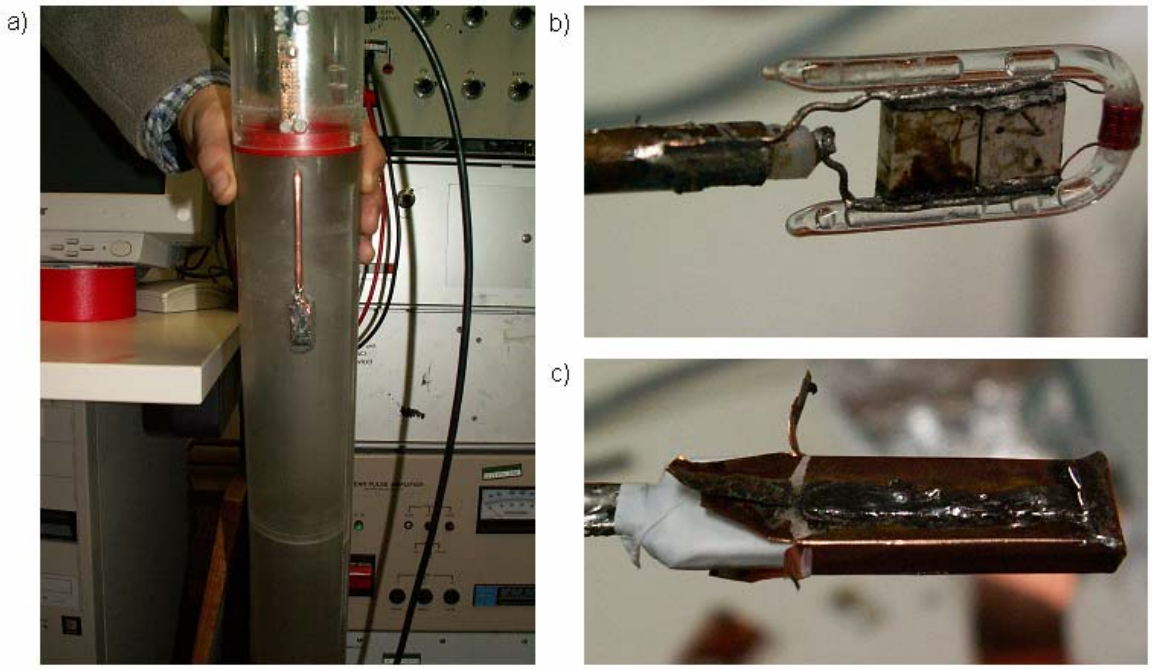

Figure 3.2.5: a) Bearing tube with notches for resonance circuit and feed cable, b) resonance circuit with sample and c) shielding of the lock circuitry

The electronic feed back loop system attached to the probe in principle works like that of any conventional lock system. A detailed description of its functioning is out of the scope of this work. The principle of the final lock system for the field cycling set-up is sketched once more in figure 3.2.6.

The lock system provides a possibility to monitor small changes of the actual field, when material (e.g. the probe head) is brought into the cryomagnet by reading the correction voltage applied to the z_0-shim. Measuring these changes has enabled creating a plastic mixture of diamagnetic and paramagnetic components having a total magnetic susceptibility $\chi = 0$. The proper mixing ratio was found by minimizing the field changes corrected by the lock system when the new material was placed at the probe position. Then, a probe head was designed, that is almost entirely made from this material [48]. Because this probe head does not induce significant changes of the field, by its transfer into the cryomagnet, the detection of NMR spectra shortly after the probe transfer was considerably improved. In addition, the specifications of the new probe have enabled shortening the field cycling times because of its lower weight.

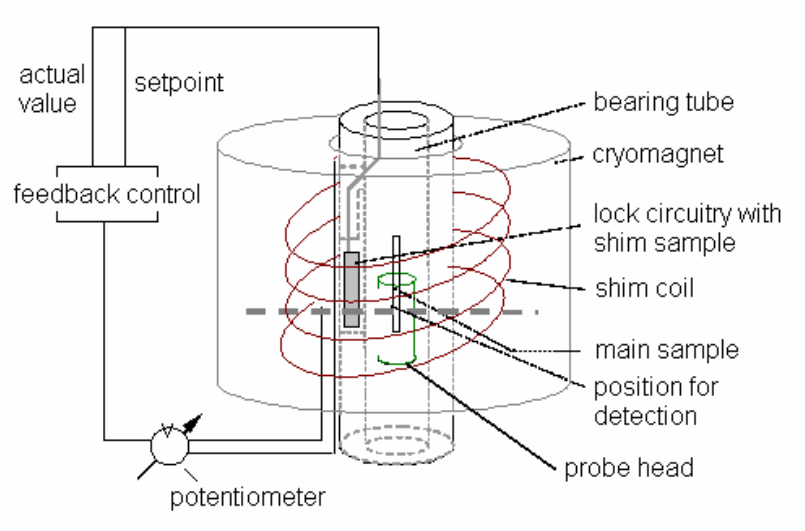

Figure 3.2.6: Principle idea and positioning of the lock system (from ref.[48])

3.2.2 Automation of Experiments and Modelling of Time-Field-Profiles

This section describes two new features for the field cycling set-up that involve computer programming. The first program enables a sequential acquisition of spectra upon variation of the intermediate probe head position on the field cycling spectrometer without manually reprogramming the step motor during the experiments, while the second program aims at a better understanding of the field cycling process itself. The modelling of time-field profiles that the sample explores during its transfer to the detection field forms a basis for a numeric simulation of the spin evolution during the field cycling experiment. Knowledge of these time-field profiles is a crucial step towards an extraction of quantitative information from CIDNP field dependences of coupled multispin systems.

Automation of field cycling experiments. The step motor of the field cycling unit is run by a programmable control unit (IPP 172-140) that features its own power supply and a programmable microprocessor. The control unit is connected to a Windows PC via a serial port (RS 232) and is reprogrammed interactively with a program running under Windows (IPCOMM) that allows the operator the storage of eight pre-selected positions for the probe head in the non-volatile memory of the control unit. A screenshot of the communication program IPCOMM window is shown in figure 3.2.7. Each of these positions is allocated with one value for the acceleration and deceleration ("Rampe"), and one for the speed ("Lauffrequenz") with which the probe is moved to the designated position. This means that

three programs for the absolute movement of the probe head are stored in the control unit via the so-called “SPS”. In addition, the program can be used to directly conduct a command for a change in position of the probe head in the fringe field.

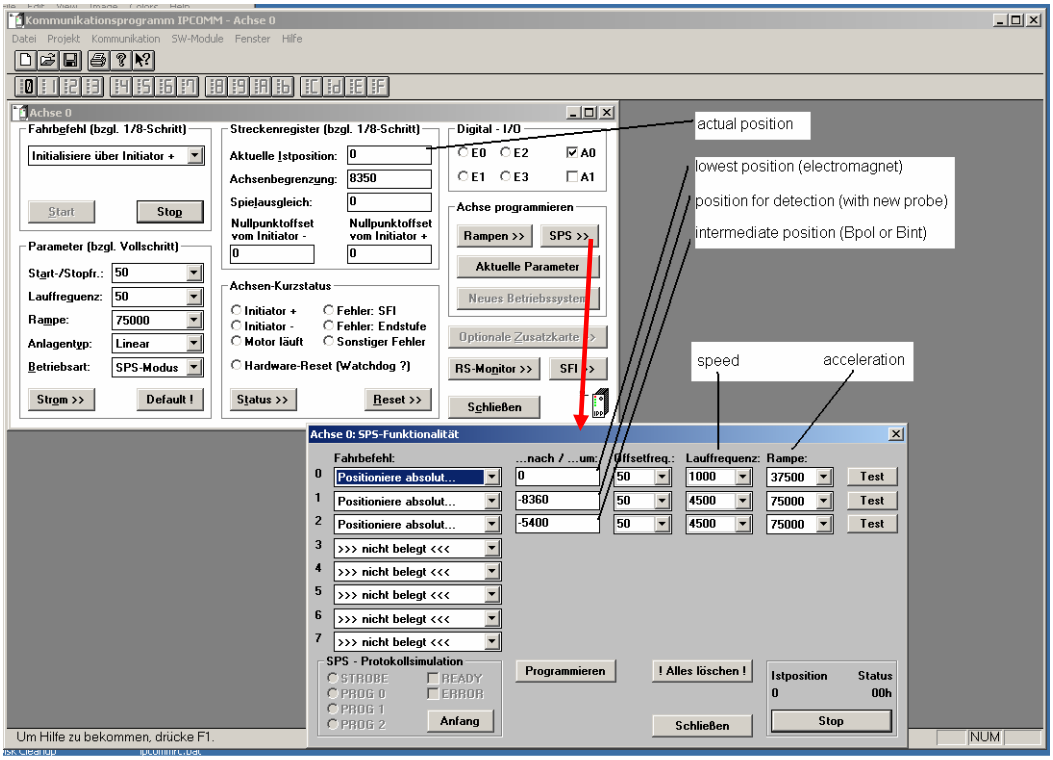

Figure 3.2.7: Screenshot of the IPCOMM interface to access the control unit.

Whenever the SPS-window (“SPS-Funktionalität” in fig. 3.2.7) is closed, the three stored programs might be called by a separate input at the control unit. This input makes use of a special communication protocol that codes up to eight different movements on a small number of cables. However, the programs for different movements of the probe are directly called by the computer of the spectrometer (CXP) via this input at the control unit using a single output line. Therefore, the pulses from the spectrometer that address to the different positions are coded according to the IPP protocol by a separate circuitry.

The movements of the probe head to three pre-selected positions can thus be conducted by the CXP computer via three different commands: ‘.godown’, ‘.goup’, and ‘.goint’, according to the positions programmed in the SPS-window. However, normally field cycling experiments are designed to explore parameters that change with the external magnetic field. It is therefore desirable to repeat the same experiment for different intermediate positions, i.e. at different fields for polarization, B_{pol}, or spin evolution, B_{ev}. In order to change this intermediate position, the operator of the field cycling spectrometer had to wait for the appropriate moment to change the intermediate probe position manually in the SPS window while the CXP

computer conducts the same experiment several times. Some of the measurements presented in this work would have been out of the scope under these conditions because their data collection takes several tens of hours.

The automation of the change of the intermediate position is realized by a program called “ipcommrc”, a remote control for the program ‘IPCOMM’. The program was developed in cooperation with my brother Thorsten Miesel and is written in the programming language ‘C++’. It uses the addresses of the buttons in the two windows shown in figure 3.2.7, which are usually activated by the operator of the spectrometer. When a change of the intermediate position is desired, the program calls the SPS-function via the button SPS in the parent window (red arrow in fig. 3.2.7). Then the new value is entered in the entry field for the intermediate position and the button ‘Programmieren’ is activated to change the program in the control unit. Finally, the SPS-window is closed via the ‘Schliessen’ button, to wait until the next change of the intermediate position is required.

Now, the ‘ipcommrc’ program only needs to know i) how many field cycles should be performed before the value in the SPS-window should be changed, and ii) the list of values in the order they should be entered. These parameters are defined in the initialization file (also given in the appendix). Here, the number of repetitions of the same field cycling protocol is given as ‘Wiederholungen’, and a path for the file with a list of the values is defined as ‘Wertedatei’, i.e. an ASCII file with a column of values between -1 and -8360 (zero is not recommended to use for a reason explained further down). In addition, the operator can define a path for a log-file, that enables him to check if the field cycles were performed in the desired way.

The program is constantly running in the background, while the CXP computer performs its field cycling experiments. It utilizes actual probe position, i.e. the number in ‘Aktuelle Istposition’ (see figure 3.2.7), in order to count the field cycles that are accomplished. By comparison to the number of desired repetitions given in the initialization file it accomplishes the proper number of experiments with the same intermediate position. The experiment should therefore always start and end at the same position. The program constantly (with the present settings every second) reads the actual probe head position, and writes it into a log file when it differs from the previous read value, whenever the value becomes zero it considers one experiment (repetition) accomplished.

With the program “ipcommrc.exe”, the operator of the field cycling spectrometer has a convenient way to run a diversity of different field cycling experiments that require a change of intermediate probe position from one experiment to the next. This change of intermediate

probe position is not only required for the acquisition of a common CIDNP field dependence. For example, the acquisition of NMRD data (see chapter 4.1) would be out of the scope without an automation of the change of intermediate probe position, where the sample attains thermal equilibrium.

Modelling of time-field profiles. During the work it turned out that a closer insight into the field cycling process itself is necessary for a better understanding of the CIDNP patterns observed in low and intermediate fields. The transport of coupled multi-spin systems from the field of polarization, B_{pol}, to the field of detection, B_0, can not be assumed to occur purely adiabatic or non-adiabatic. Actually, in the case of fast sample transfer to the detection field, it will be both adiabatic and non-adiabatic, depending on the group of nuclei considered, and the change of magnetic field they explore in time. An example for a completely different outcome of a field cycling experiment upon different transfer times is given in chapter 4.3. Therefore, usually a numerical modelling of the sample transfer process will be necessary to understand the NMR spectra obtained after the field cycling process. This requires the exact knowledge of the time-field profiles that the step motor creates for the sample in the fringe field of the cryomagnet for any given combination of acceleration, speed, starting, and final position of the sample.

From the parameters in the SPS-window in figure 3.2.7 and the shape of the fringe field in figure 3.2.3, any time-field profile can be calculated. The program that models the profiles is written in MATLAB. It starts with the program ‘startprofile.m’, that asks the operator for the starting and ending values (in 1/8 steps of the motor advance) of the field cycle and for the speed (1/8 steps*s^{-1}) and the ramp (1/8 steps*s^{-2}) allocated to it. The input values are to be taken from the ones programmed in the SPS-window shown in figure 3.2.7. It is therefore convenient to work with $1/8^{th}$ steps; one of such steps corresponds to 0.0753mm movement of the probe head.

From these values the total time of the field cycle is calculated. Four different cases are distinguished, depending on whether the sample is moved up or down and whether the probe reaches its maximum speed or not. For each of the four cases a different subprogram (e.g. ‘stepprofile1.m’) is executed that calculates the actual profiles in 1/8 steps over the time. For two typical cases the resulting time-space profiles are shown in figure 3.2.8.

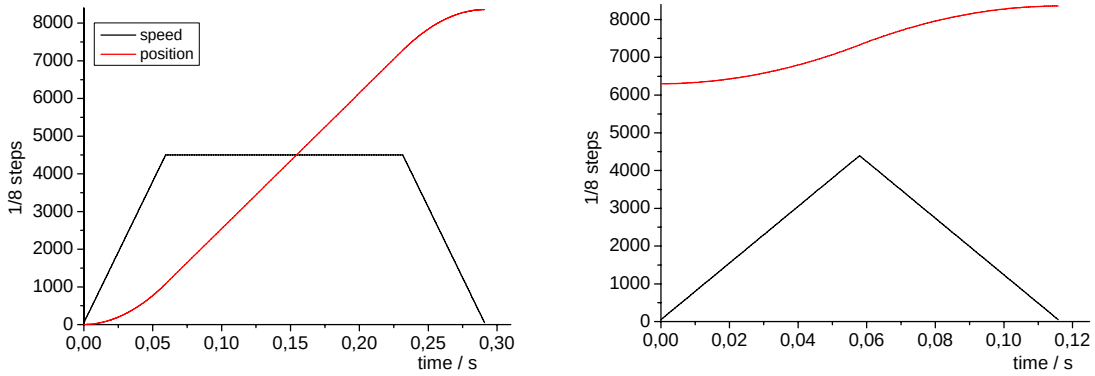

Figure 3.2.8: Calculated movements of the probe head along the bore axis of the cryomagnet: a) start=0, ende=8360, speed=4500, acceleration=75000, t_{tot} (calculated transfer time) = 0.2909s; b) start=6300, ende=8360, speed=4500, acceleration=75000, t_{tot} = 0.1159s. (1/8 step = 0.0753mm)

The parameters for the sample transfer simulated in fig 3.2.8 are realistic for the fast transfer of the new probe head [48]; they are actually taken from figure 3.2.7. The only difference between the two cases is the starting position (0 in fig. 3.2.8 a) and 6300 in fig. 3.2.8 b)). In the second case, the sample transfer from an initial field of about B=5T, the probe head does not reach the final speed indicated in the SPS-window (4500 1/8th steps/s).

After the movement of the probe head is calculated, it has to be correlated with the actual magnetic field that the sample explores on its way along the bore axis of the cryomagnet. This requires the shape of the actual fringe field from figure 3.2, which is provided by the ASCII file 'origSB.txt'. It has to be interpolated for the appropriate number of points, *n*, which is done by the subroutine 'makeBS'. After the program has successfully accomplished the calculation it gives the total time for the transfer, t_{tot} (= τ_{fv}), plots the calculated time-field profile (τ_{fv} over B_{fv}), and provides the user with the results in ASCII format in the file 'output.txt'. This file contains four columns in the following order: 1. time in seconds, 2. speed in 1/8th steps per second, 3.position in 1/8th steps, and 4. magnetic field / T.

The experiments described in chapter 4 will show that these time-field profiles inevitably have to be taken into account for the interpretation of the results. For most experiments introduced in chapter 4, such profiles are therefore given together with the description of the experiments.

4 Spin Dynamics at Arbitrary Magnetic Field

In Field Cycling NMR one probes properties of molecules that depend on the external magnetic field. This implies that the system under study is prepared at one field value, and probed at another, usually higher magnetic field in order to benefit from the considerable advantages of high field NMR. Our realization of this technique is described in some detail in the experimental part of this work (chapter 3.2). Besides of the elucidation of molecular properties, field cycling is used in hyper-polarization (HP) experiments, because it is often more efficient to polarize nuclear spins at low magnetic field in order to exploit the polarization for enhancing the notoriously low sensitivity of NMR spectroscopy probed at high field. Different ways of hyper-polarizing the spin system are known, such as optical pumping [15], Para Hydrogen Induced Polarization (PHIP) [13], or CIDNP [1]. When the nuclei are detected at the high magnetic field of the NMR spectrometer (B_0), while the system has been prepared in low magnetic field (B_{pol}), the acquisition of the spectrum requires the variation of the field. The nature of the field cycling process and its consequences for the appearance of the spectrum has hitherto not been paid much attention to.

This chapter shall provide an insight into the phenomena that can influence the outcome different kinds of field cycling experiments. It starts with the probably most common application of field cycling NMR, namely field dependent longitudinal relaxation times (T_1), also termed nuclear magnetic relaxation dispersion (NMRD). The effects will then be examined for hyper-polarized spin systems using CIDNP, a technique that conveniently allows polarizing certain spins-½ in a pre-selected magnetic field with a well defined starting point in time.

Because the chemical shift differences are proportional to the external field, whereas the spin-spin couplings remain constant, the energy differences between the states do not coincide at arbitrary magnetic field, which causes characteristic differences in the NMR spectra taken at different fields. In liquid samples, scalar spin-spin interactions act as the predominant interaction in low magnetic fields. Depending on the frequency offset of coupled spins in a given molecule at a field B, the condition of either strong or weak spin-spin coupling, J, is met (see chapter 2.2, formula 2.2.4).

In field cycling experiments, the sample will usually explore both, the case of strong and weak coupling being fulfilled as the external magnetic field is varied. Here, the terminology ‘low-field’ and ‘high-field’ shall be used depending on if the condition for weak scalar

coupling is fulfilled or not, since the present chapter is addressed to phenomena which compelled this terminology, i.e. the collective relaxation of strongly coupled spins, and the transfer of polarization and coherence among them. The radical reactions leading to the formation of HP are subject to chapter 6.

The effects of polarization and coherence transfer phenomena are, with a few exceptions, studied on the N-acetyl tryptophan (NATrpH) molecule. The photo-reactivity of this essential amino acid is of mayor importance for light driven processes in proteins and is thus of particular biological interest. It is easily polarized in reversible photoreactions with different suitable dyes (see chapter 6.2) and also exhibits CIDNP in the absence of a sensitizer (see chapter 6.1). As a nitrogen-containing aromatic amino acid, it displays a large variety of NMR parameters, i.e. ^{1}H-chemical shifts and spin-spin couplings. Together, this enables a facile observation of the various effects discussed in this chapter, which is certainly one reason, why all these effects were discovered in this rather complex spin system. However, most of the effects treated here have already been verified on simpler spin systems that allow a more exact theoretical description.

NMR parameters of N-acetyl tryptophan (NATrpH). The assignment of the NMR spectrum, meaning the identification of each spectral line with the transition responsible for it, is an essential prerequisite for an NMR investigation. It is hence of particular importance for the following sections, in which the T_1 relaxation dispersion curves (NMRD) and the polarization transfer phenomena due to strong coupling of spins is discussed.

The NMR spectrum of a molecule in liquid solution is characterized by a chemical shift for each magnetic nucleus and the scalar couplings between these nuclei that may be of positive or negative sign (see Hamiltonian in formula 2.2.1, chapter 2.2). Figure 4.0.1a) shows the structure of N-acetyl-tryptophan (NATrpH), and the upper trace in fig. 4.0.1b) shows a 300MHz ^{1}H-NMR spectrum in D_2O together with the assignment of signals to the different proton positions. The lower trace in figure 4.0.1 b) shows the simulation of the spectrum from which the NMR parameters were extracted. It was obtained with the NUTS software from ACORN, and table 4.0.1 displays the chemical shifts and the scalar spin-spin coupling constants used for the simulation.

The simulation includes all eleven protons, even though the N-acetyl group couples only very weakly to the other protons, so that the three equivalent protons of the N-acetyl group give rise to a sharp singlet at 1.78ppm. Small *J*-couplings (<0.2Hz) are not resolved by the spectrum, nevertheless they are included in the simulation to obtain approximately the desired

line width for the individual lines. The N-acetyl group was coupled weakly to the α-CH and the two diastereotopic β-CH_2-protons in order to obtain the desired line width. The smallest coupling revealed by the spectrum is that between H2 and H6 (J = -0.4Hz). In the discussion of the results in the following sections, only the couplings listed in table 4.0.1 will be considered, and smaller couplings (< 0.2Hz) are neglected.

a)

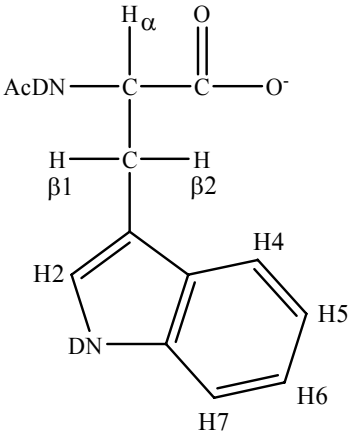

b)

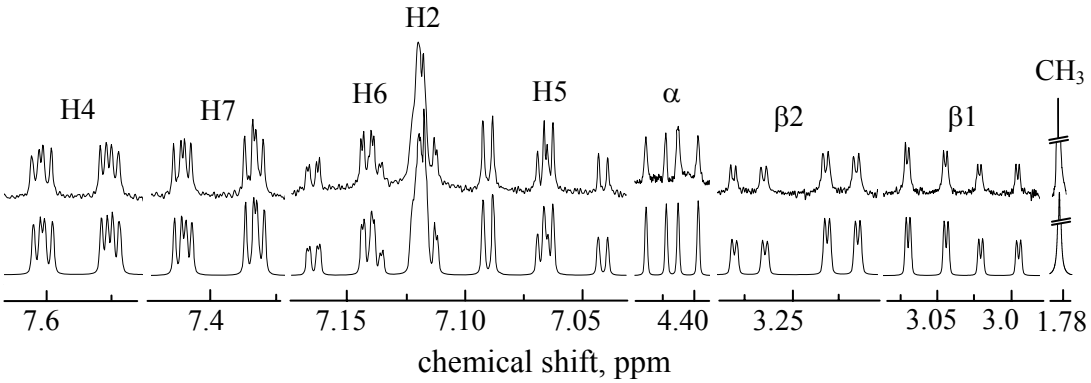

Figure 4.0.1: a) Structure of N-acetyl tryptophan b) 300MHz ^{1}H-NMR spectrum of N-acetyl tryptophan (upper trace) and simulation with the parameters listed in table 4.0.1 (lower trace).

	β1	**β2**	**α**	**H2**	**H4**	**H5**	**H6**	**H7**
σ / ppm	3.0330	3.2440	4.4170	7.1200	7.5895	7.0677	7.1400	7.3966
J / Hz	-							
β2	-14.8	-						
α	7.8	4.9	-					
H2	0.8	0.7	*<0.2*	-				
H4	*<0.2*	*<0.2*	*<0.2*	*<0.2*	-			
H5	*<0.2*	*<0.2*	*<0.2*	*<0.2*	8.0	-		
H6	*<0.2*	*<0.2*	*<0.2*	-0.4	1.2	7.0	-	
H7	*<0.2*	*<0.2*	*<0.2*	*<0.2*	0.8	1.1	8.3	-

Table 4.0.1: Simulation parameters for the spectrum shown in figure 4.0.1

As most large systems of coupled spins-½ the spectrum has a relatively high degree of degeneracy, since not every spin has a noticeable *J*-coupling to every other spin. This degeneracy has important practical consequences: It makes the spectrum still tractable and permits a division in two subsystems containing four proton spins each. They are marked with different colours (light blue and orange) in table 4.0.1. The spin-spin couplings also give rise to cross peaks in the homo-nuclear 2D-COSY spectrum of NATrpH[1] confirming the assignments in table 4.0.1, however, neither in the high resolution NMR spectrum in fig. 4.0.1, nor in phase sensitive COSY spectra, the signs of the small couplings ($J < 1$Hz) can be reliably extracted. It shall be seen that the detection off level anti-crossings in coupled multi-spin systems by field cycling experiments provides a new possibility to obtain the signs of very small couplings, which have hardly been accessible before.

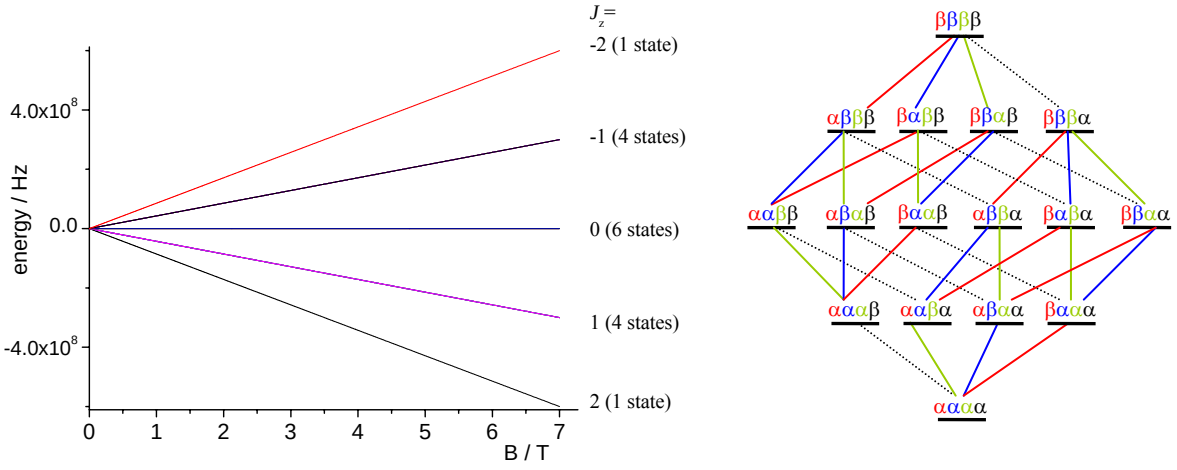

Figure 4.0.2: Zeeman energy levels in a four spin-½ system at arbitrary magnetic field. In high field, the states are grouped according to their total spin projection on the z-axis, J_z.

Knowledge of the NMR parameters listed in table 4.0.1 allows the calculation of energy levels of the two spin subsystems. The diagram in figure 4.0.2 shows the energy levels calculated for a system of four coupled spins-½ at arbitrary magnetic field, *B*. In the high field of the spectrometer, the state energies fall into distinct groups, distinguished by their value of total spin projection on the z-axis (J_z). An ensemble of four coupled spins-½ consists of $2^4 = 16$ different energy levels, which are shown on the right side of figure 4.0.2 together with the 32 possible single quantum transitions that are coloured differently according to the spins they involve.

[1] The homonuclear 2D-COSY spectrum was kindly provided by Dr. A. Schäfer, service division of the institute of chemistry, FU Berlin.

J_z can take five different values: 4/2 (1 state), 2/2 (4 states), 0 (6 states), -2/2 (4 states), -4/2 (1 state). The splitting between two states with $\Delta J_z = \pm 1$ is approximately $\gamma_N B/2\pi$, where γ_N is the proton gyromagnetic ratio. Note, that the product states of all four coupled nuclei indicated in figure 4.0.2 are not necessarily eigen-states, when the spins are strongly coupled. They only represent the eigen-states of the spin system in the weak coupling limit. When the spins are strongly coupled, the coherences between the eigen-states can generally not be neglected.

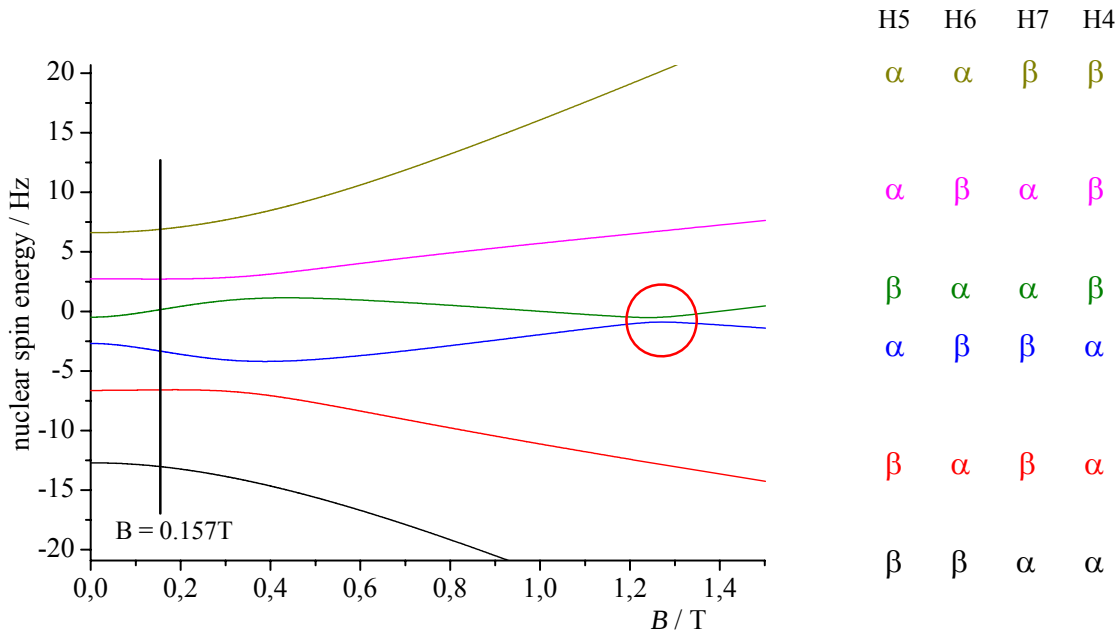

Figure 4.0.3: The six calculated energy levels in the manifold with $J_z = 0$ of the four spin system of NATrpH containing H4, H5, H6 and H7 (marked in orange in table 4.0.1). The field of B = 0.157T was chosen for some of the experiments discussed in chapter 4.3.

For the four protons of the six membered ring in the NATrpH molecule (H4, H5, H6 and H7), the six calculated energy levels in the manifold with $J_z = 0$ are plotted again in figure 4.0.3. Their degeneracy is lifted by differences in chemical shift and the spin-spin couplings among the individual protons, leading to additional splittings. Note the different energy scales in figure 4.0.2 and 4.0.3: While the difference between the states that belong to different manifolds is in the order of the Larmor precession frequency (300MHz at 7.04T), the energy differences seen in figure 4.0.3 are only some tens of Hertz in the low field part up to B = 1.5T. The alignment of the four spins in the different energy levels at high magnetic field is indicated in the table on the right side, and shall be helpful in the discussion of polarization transfer between the NMR signals that belong to particular nuclei in the NATrpH molecule.

Depending on the NMR parameters listed in table 4.0.1, the individual energy levels undergo characteristic changes when the external field is varied. It can be seen, that two energy levels closely approach each other at B = 1.27T (red circle in fig. 4.0.3). A correct prediction of such level anti crossing requires the proper sign of the scalar couplings. Two additional anti-crossings are seen around 0.36T and 0.38T, but the energy levels do not approach each other as close as they do at 1.27T. When approaching lower fields, all energy levels come closer and closer, until all levels anti cross at zero-field.

Before looking at the consequences of the distances between the energy levels and the predicted level anti-crossings for T_1 dispersion curves (chapter 4.1) and CIDNP field dependences (chapter 4.2) of individual spins, the other sub spin-system of NATrpH containing four spins shall be introduced. It contains the proton in position 2 in the aromatic system of the indole moiety, which couples stronger to the two CH_2-protons in β-position than to any of the other aromatic protons. Furthermore, the CH-proton in α-position is taken into account, because it is coupled to the β-protons with about 5 and 8Hz (see table 4.0.1).

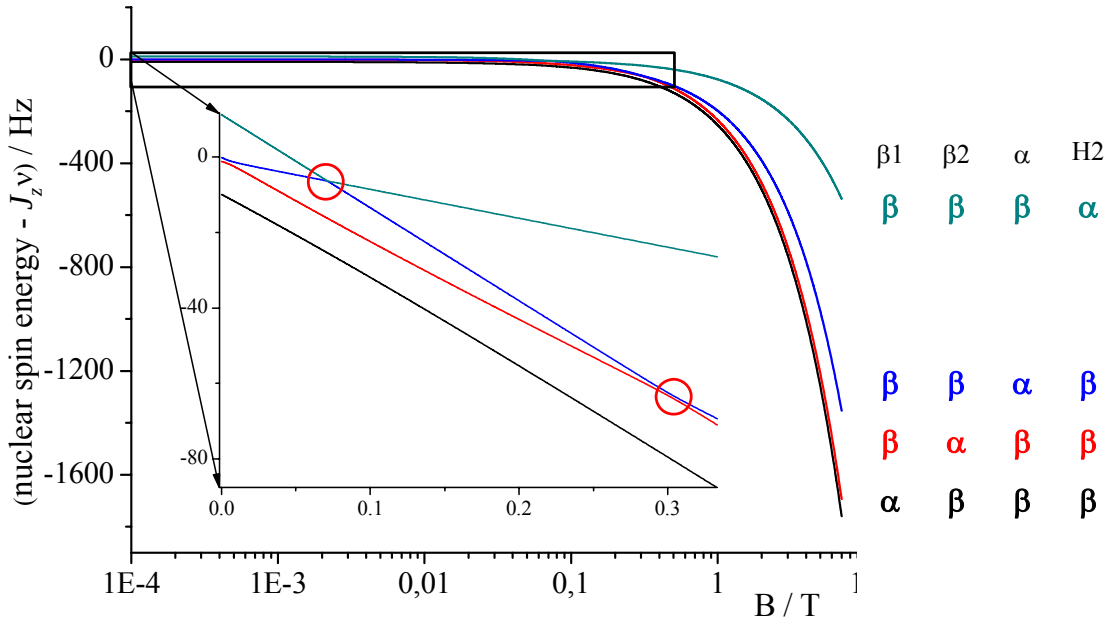

Figure 4.0.4: Calculated energy levels in the four spin system of the protons H2, β1, β2 and α in the manifold with total spin projection J_z = -1. The inset shows the area between 0 and 0.33T enlarged (The Zeeman energy, $J_z\nu$, was subtracted.)

The Zeeman splitting in the second four spin system under consideration is analogous to that presented in figure 4.0.2. Here, the calculations predict two level anti-crossings to occur in the

manifold with J_z = -1. To visualize the level-crossings, the Zeeman energy, $\gamma_N B J_z / 2\pi$, which is the same for all four levels in a given manifold, was subtracted. It can be seen, that the energetic difference between the states at fields below 0.4T is only a few tens of Hz. The two level anti-crossings occur at B = 0.071T and at B = 0.32T. In this manifold, the energy differences between the four levels in high field (B = 7T) roughly reflect the chemical shift differences between the signals for the individual protons in the NMR spectrum.

When the field is varied between 0.1mT and 7T, the changing chemical shift differences, i.e. the effective strength of spin-spin couplings and the level anti-crossings will inevitably manifest themselves in the polarized spectra and the relaxation behaviour of the homo-nuclear spin-½-systems. An inclusion of the entire spin system (without the N-acetyl group) containing eight spins would lead to 2^8 = 256 energy levels and consequently to more crossing energy levels. However, most of these energy levels are almost degenerate and the two spin subsystems of four spins each should provide a sound basis for the following discussions and allow a general understanding of the spin dynamics in diamagnetic molecules at arbitrary magnetic field that influence the outcome of the field cycling experiments.

4.1 Spin Relaxation in Coupled Multi-Spin Systems – Proton T_1-Dispersion of N-acetyl-tryptophan in D_2O

An important application of field cycling NMR spectroscopy is the determination of longitudinal relaxation times T_1, as they open a possibility to probe molecular motion over a wide range of timescales, ranging from picoseconds to several seconds. Spin-lattice relaxation is induced by random fluctuations of the local magnetic field that take place on the timescale of the Larmor frequency ($\omega_L = \gamma_N B$). Qualitatively, the correlation time, τ_C, indicates how long it takes before the random field changes sign. For rotating molecules in a liquid, τ_C is in the range of tens of picoseconds to several nanoseconds. If the transverse field fluctuates rapidly, τ_C is short, and the spectral density function, $\tau_C/(1+(\omega_L\ \tau_C)^2)$, is broad. For a fluctuating random field, ΔB, the transition probabilities are proportional to the spectral density at the Larmor frequency, and the spin lattice relaxation rate, R_1, is equal to twice the mean transition probability per unit time between the states. In the simplest case, relaxation may then be described in terms of equation 2.2.30 (chapter 2), which is also known as the Redfield approximation [31].

In principle, NMRD data provide experimental access to correlation times, τ_C, which characterize molecular motion. For small molecules, however, the time-scale of molecular motion is always faster than the Larmor precession, and the molecules remain in the fast motional regime ($\omega\tau_C << 1$) in the entire field range. Thus, in the present case in principle no changes in relaxation rates are expected upon field variation between 100 μT and 7 T, since τ_C for the tumbling of the NATrpH molecule is expected in the range of 100 picoseconds.

What has been left unexplored is the effect of scalar spin-spin couplings on relaxation dispersion of solutes in liquids because conventional field cycling spectrometers usually do not provide the resolution of high field liquid-state NMR spectrometers. Therefore, usually only one common relaxation time is explored for all protons in a given molecule, and thus only one relaxation mechanism is then assigned to a group of nuclei, which in fact are exhibited to quite different environments in the molecule. In the present work it will be shown that this approach is oversimplified and can be misleading, because the T_1 relaxation dispersions for individual protons in multi-spin-systems can be quite different.

Motional narrowing in liquid-state NMR in combination with slow sample rotation gives one the possibility to resolve all the resonances belonging to individual protons. The field cycling spectrometer described in chapter 3.2 provides these benefits, and allows one to differentiate

between signals from individual positions in fairly complex organic molecules of biological interest. For the NATrpH molecule the assignment of the high resolution NMR spectrum was given in the previous section, and the possibility of precise field variation provides the T_1 values for the individual spectral components at arbitrary field.

The condition of strong coupling of spins (formula 2.2.4, chapter 2.2) affects the NMRD data of individual sites in the molecule: as the spin-spin coupling becomes comparable or larger than their chemical shift difference, the eigen-states are collective states of the spin system, and the coupled spins tend to relax together. Moreover, they display well-pronounced features that are related to level anti-crossings that occur in fields, where the coupling between protons match their chemical shift differences. These features have previously been unexplored, since usual field-cycling spectrometers do not provide site-specific data.

For modelling the experimentally obtained T_1-dispersions, only random fluctuations of the local field are considered. This means that the field experienced by a particular spin depends neither on its orientation, nor on the orientations of the spins in the vicinity. The fields are rather assumed to emanate from a source external to the spin system. This is a clearly incorrect assumption, ignorant of the states on which the particular relaxation mechanism acts. However, it will show that the T_1-relaxation dispersions of the individual protons in small molecules in liquids are largely independent of the actual relaxation mechanism, and are well described by stochastic field fluctuations. The theoretical approach is outlined in more detail in chapter 2.2.4 and in ref. [64].

Experimental

Nuclear spin-lattice relaxation rate constants were measured as a function of the external magnetic field with the field cycling spectrometer described in chapter 3.2. Depending on the magnetic field in which the relaxation rate is to be determined, two different experimental protocols were employed. The two experiments provide a large difference between starting and final (thermally equilibrated) magnetization, ($M_i(0)$-$M_{i,eq}$), for different ranges of the magnetic field, and thus provide a reasonable sensitivity for the detection of T_1-values over the whole field range. Realistic profiles of the experiments are sketched in figure 4.1.1 a) and b). For magnetic fields lower than five Tesla protocol a) was employed. Here, the sample under study is polarized in the high field of the NMR spectrometer (7.04T), then it is transferred into the auxiliary magnet (during τ_{fv1}) or alternatively into the fringe field of the

cryomagnet, where it is permitted to relax towards the low-field equilibrium for some variable time τ_r, afterwards it is returned during τ_{fv2} into the high field, where the remaining magnetization is detected by means of conventional Fourier transform spectroscopy with a 90°-detection pulse.

Protocol b) is used for magnetic fields higher than one Tesla, where the sample is initially kept in the fringe field at the lowest position corresponding to a magnetic field of about 48mT until thermal equilibrium is established. It is then transferred during the time τ_{fv1} to the intermediate field, B_r, and kept there for the relaxation delay, τ_r. Finally it is transferred into the high field of the NMR spectrometer where the FID is recorded in a similar fashion as in the first experimental protocol. In an intermediate field range (B_r = 1 to 5 Tesla) both methods where employed, showing that both techniques lead to essentially the same results. The two methods are thus complementary, and together they cover the complete range of evolution field values, B_r (0.1mT to 7T), with nearly constant sensitivity, provided by the large detection field and a line width of ~0.3 Hz. Spin lattice relaxation times at B_r = 7.04T can be obtained with higher accuracy by a conventional inversion recovery experiment (180°$_x$ - τ_r - 90°$_x$ - FID) without field cycling.

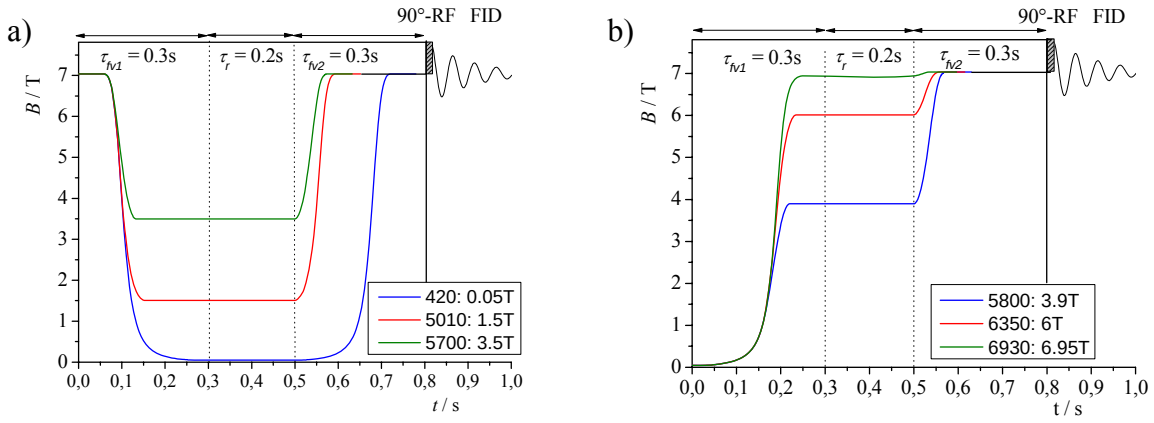

Figure 4.1.1: Realistic timing schemes for experimental protocols a) and b) used for the determination of T_1 at variable field by variation of τ_r. The legends show the stepmotor-values and the magnetic field, B_r.

Additional experiments were performed with a 180°-pulse followed by a variable delay, τ_w, prior to the first field variation (τ_{fv1}). This experimental protocol is analogue to that sketched in figure 4.1.1 a) (blue line), as it employs the same field cycling parameters. The auxiliary electromagnet was set to 5mT in order to study the exchange of magnetization at this field. The additional waiting time, τ_w, was introduced between the population inversion and field

cycling in order to see the influence of different amplitudes of the HDO lines on the relaxation behaviour of the solutes protons and vice versa.
In all experiments presented in this chapter, the sample was transferred with the highest currently available acceleration and speed, which results in transfer times of about 290ms for the 65cm difference between the auxiliary magnet and cryomagnet. The intervals, τ_{fv1} and τ_{fv2}, for the sample transfer were therefore always set to 300ms (see also fig. 4.1.1).
It was attempted to keep the temperature constant (~30°C) during the experiments by purging the probe with a stream of dry air. However, because the probe-head used for the experiments [48] is designed without a separate sample compartment that allows a precise temperature control, the temperature deviations were about +/-3 °C. This has an adverse effect on the accuracy of the relaxation data, since any relaxation mechanism to be considered is known to depend on the temperature.

Sample prepararation. N-acetyl-L-tryptophan (NATrpH) was used as obtained from Aldrich (Germany) and dissolved in 99.9% D_2O from Deutero GmbH (Germany). The concentration was 12 mM. NATrpH was used in such low concentration because of its poor solubility. The pH-value was set to 11 by addition of NaOD, it was chosen according to the pH-value mostly used for CIDNP experiments in this work. The solutions were purged with pure nitrogen gas prior to use in order to drive out dissolved oxygen, which can enhance relaxation rates because of its paramagnetic nature. Conventional 5mm NMR sample tubes were used and provided with a vortex plug in order to prevent sample shaking during the transfer. In addition it allows (for liquid state NMR) a relatively fast sample rotation of up to 100Hz to guarantee that the rotation remains constant during the field cycling process. The entire relaxation dispersion was measured with a single sample to avoid changes in proton concentration. Since relaxation caused by intermolecular dipole-dipole interaction depends on the number of spins per unit volume, the sample was sealed with PARAFILM® to avoid the exchange with H_2O in air.

Results and Discussion

Data reduction. For the determination of relaxation rates of individual NMR signals at arbitrary magnetic field, a group of peaks (a given multiplet) was integrated. Then, the

integrals of seventeen measurements with variable τ_r, ranging from 100ms to 60000ms, were fitted by an exponential function, containing three parameters,:

$$M_i(\tau_r) = \left(M_i(0) - M_{ieq}\right) \cdot e^{\tau_r / T_1} + M_{ieq} \quad . \tag{4.1.1}$$

The initial magnetization of the protons of type i, $M_i(0)$, is above the equilibrium magnetization M_{ieq} for experimental protocol a) and below M_{ieq} for protocol b). Some results of the fitting procedure are shown in figure 4.1.2 for the example of the H2-proton of the aromatic moiety of NATrpH.

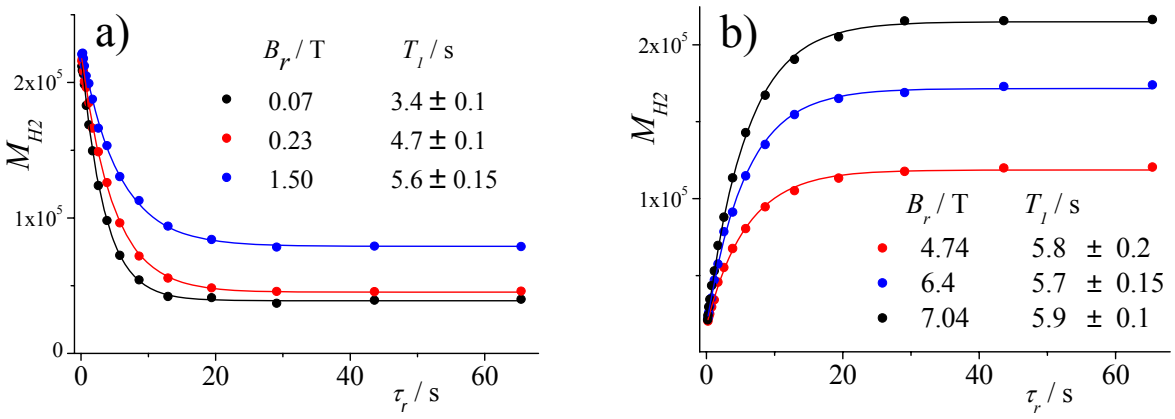

Figure 4.1.2: T_1 curves of H2 proton in NATrpH for variable B_r and mono exponential fits a) for protocol a) and b) for protocol b).

In an intermediate field, B_r = 2 to 5 T, both experimental protocols (see fig. 4.1.1a) and b)) were employed. Here, the statistical error becomes larger for both experimental protocols, because the difference between the initial and the final magnetization, $M_i(0)$-$M_{i,eq}$, is smaller. No systematic deviation in relaxation behaviour from one method to the other was found. Therefore, the two relaxation rates obtained where weighted by their errors (least squares) and then averaged. Relaxation rates obtained by protocol b) for less than 2T were completely discarded.

The T_1 relaxation dispersion for individual protons of NATrpH in D_2O. The T_1-values obtained in the above procedure were plotted against the external field B_r, and the result is presented in figure 4.1.3. Their accuracy depends on the width of the integration window, and for the aromatic protons it is estimated to be better than 10%. For H2, which gives a relatively narrow signal, T_1 has accuracy better than 5%. The T_1 times for the β-protons are relatively short, in high field they relax with a T_1 of 0.7 to 0.8s. In addition their splitting with each other, with the α-proton and H2 distributes their intensity over a wider range in the spectrum

(0.3ppm). Moreover, the decay of magnetization of β-protons is not described very well by a single exponential curve as will be discussed further down. Therefore, the T_1-values for the β-protons could only be extracted with accuracy of about 20%. For the α-protons, the error is between 15% and 30% and originates mainly from the vicinity to the HDO-line. This vicinity actually prevents the extraction of reliable T_1-values, and the dispersion for the α-proton is omitted. Many spectra suffer from artefacts, e.g rotational sidebands that overlap with the signal of the α-proton and the data do not allow a clear distinction of the underground from the water line on one hand, and cross relaxation effects as discussed further down on the other. The poor solubility of NATrpH in water, and hence the low concentration used in the experiments has an adverse effect on the precision of all T_1-values obtained.

In principle, the involvement of transitions between multiple states with different efficiency renders all magnetization decay curves multi-exponential. In most cases, however, the longitudinal magnetization attains its equilibrium value with a function that is well described by single rate constant. The fitting with a single exponential thus yields an 'effective T_1', which is henceforth simply referred to as T_1.

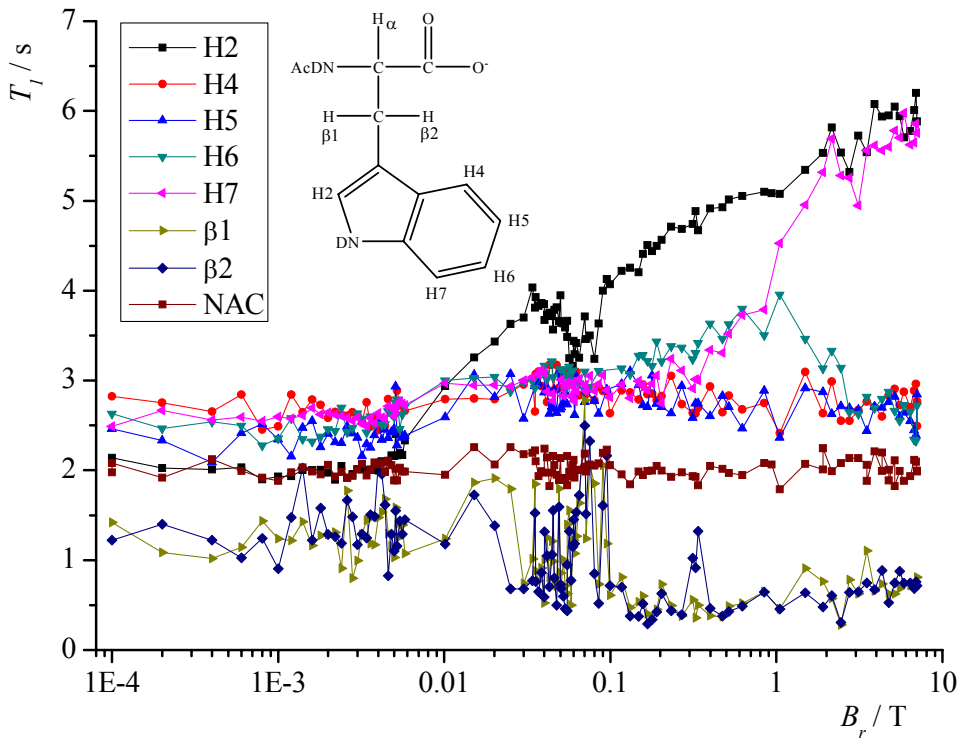

Figure 4.1.3: Experimental dispersion of longitudinal relaxation times (T_1) of the individual protons in N-acetyl tryptophan. The inset shows the structure of NATrpH.

In the high field of the spectrometer (B_0 = 7 T), the chemical shift differences between proton-sites are the largest, and spin-spin coupling is thus to be considered most weak. Here, the relaxation times for individual proton-sites vary between 0.7s for the β-protons to about 6s for H2 and H7. The T_1-values at high field qualitatively agree with the notion that relaxation is caused mainly by intra-molecular dipole-dipole interactions. Shortest relaxation times (~0.7s) are found for the two β-protons which are expected to be subject to the strongest dipolar interaction as they reside in vicinal position, while the slowest relaxation is found for the H2 proton with no other proton in its close vicinity, providing that the interaction with all other remote protons is weak. The similar values for the protons in the positions H5 and H6 (2.5s and 2.8s, respectively) correspond well to the close similarity of their proton neighbourhood. The significant difference in the T_1-values of H4 and H7 can be understood when the thermally equilibrated structure of the whole molecule in aqueous solution with the lowest energy is considered [72]: Due to the twisting of the peptide chain, the N-acetyl group resides in much closer vicinity to the proton in position 4 than to that in position 7, making the relaxation of H4 (2.8s) significantly faster than that of H7 (5.8s).

As the field is lowered, the T_1 times tend to become more similar. Below $B_r = 10^{-3}$ T, the relaxation times vary only between 1.2s for the β-protons and less than 3s for the aromatic protons. Both, increasing and decreasing T_1-times with the variation of external magnetic field are observed within the same amino acid molecule. As can be seen, the dispersions of the aromatic protons in the amino acid differ considerably from each other: Above B_r = 0.01T the relaxation rates of the protons in position 2 and 7 show a pronounced increase in T_1 with increasing Larmor frequency, whereas those in the positions 4, 5 and 6 are rather independent of the external magnetic field. In contrast to the aromatic protons, the T_1-values of the β-protons decrease (from ~1.2s to ~600ms) with higher external field. The α-proton relaxes with a T_1 of about 2.5s in low field and the relaxation time rises to roughly 4s at 7T. These observations contrast the expectation, that for all protons the dispersion curves are flat, because of the molecule remaining in the fast motional regime in the entire frequency range.

It should be pointed out, that only for the three magnetically equivalent methyl-protons (NAC), which are not considerably J-coupled to any other proton, the curve is indeed flat in the experimentally available field range ($T_1 \approx 2$s). All other curves show a strong dependence on the external magnetic field. This observation is taken as an indication that the shape of NMRD curves of these protons is related to the relative strength of their spin-spin couplings among each other, i.e. the fulfillment of the condition for strong coupling (formula 2.2.4, chapter 2.2).

The most remarkable peculiarity of the relaxation data shown in figure 4.1.3 is the fact that some curves traverse through minima and maxima as the external magnetic field is varied. Such features so far remained undiscovered in the field dependent relaxation rates of individual spins in coupled multi-spin systems. The observed extrema find their explanation in the occurrence of level anti-crossings of individual spin eigen-states in certain magnetic fields. For instance, at 0.32T the dispersion of the β2-proton shows a pronounced increase. This field coincides with an anti-crossing. It is also observed in CIDNP experiments with NATrpH (see fig. 4.2.6, chapter 4.2. and ref. [55]). Even more clearly seen is the dip around B_r = 0.06T in the relaxation dispersion of H2, which is also explained by a level anti-crossing. Both level crossings are calculated in figure 4.0.4 (chapter 4.0).
The above observations have lead to the development of a suitable theory, which permits a simulation of the measured NMRD data [63], and in the following, the above assumptions shall be verified by applying this theory to different spin-subsystems in the NATrpH molecule.

Calculation of T_1-dispersions for individual protons. The computational approach proving the above assumptions is based on the Redfield theory [31] and outlined in more detail in chapter 2.2.5 and in ref.: [63]. Because the inclusion of all eleven proton spins in the NATrpH molecule would be too complex, the dispersions are modelled for the individual protons with the following strategy: The spin-system is subsequently divided into different subsystems containing four and five protons according to table 4.0.1. For the two subsystems containing four spins, the decay of magnetization of the individual protons are calculated for arbitrary field for the case of sudden sample transfer, and T_1 is determined by integration (see chapter 2.2.5). Besides of the parameters in table 4.0.1 (scalar couplings and chemical shift differences), the relaxation times at high field for independently relaxing spins enter into the calculations. These values must not coincide exactly with those determined at B = 7T, since some of the couplings are still strong enough to cause a tendency of similar T_1-values.
For the first sub-system (H4, H5, H6 and H7), the results are displayed in figure 4.1.4 a). The decrease of T_1 for H7 between 7T and 0.3T is quite well reproduced by the calculations, and is thus attributed to the converging chemical shifts of the aromatic protons in the six-membered ring of NATrpH and to the relative strength of their scalar coupling among each other. The level anti-crossing at B = 1.27T (see fig. 4.0.3), manifests itself as a peak/dip in the calculations. In the case of an adiabatic field change, a stepwise feature would be expected in the level crossing region.

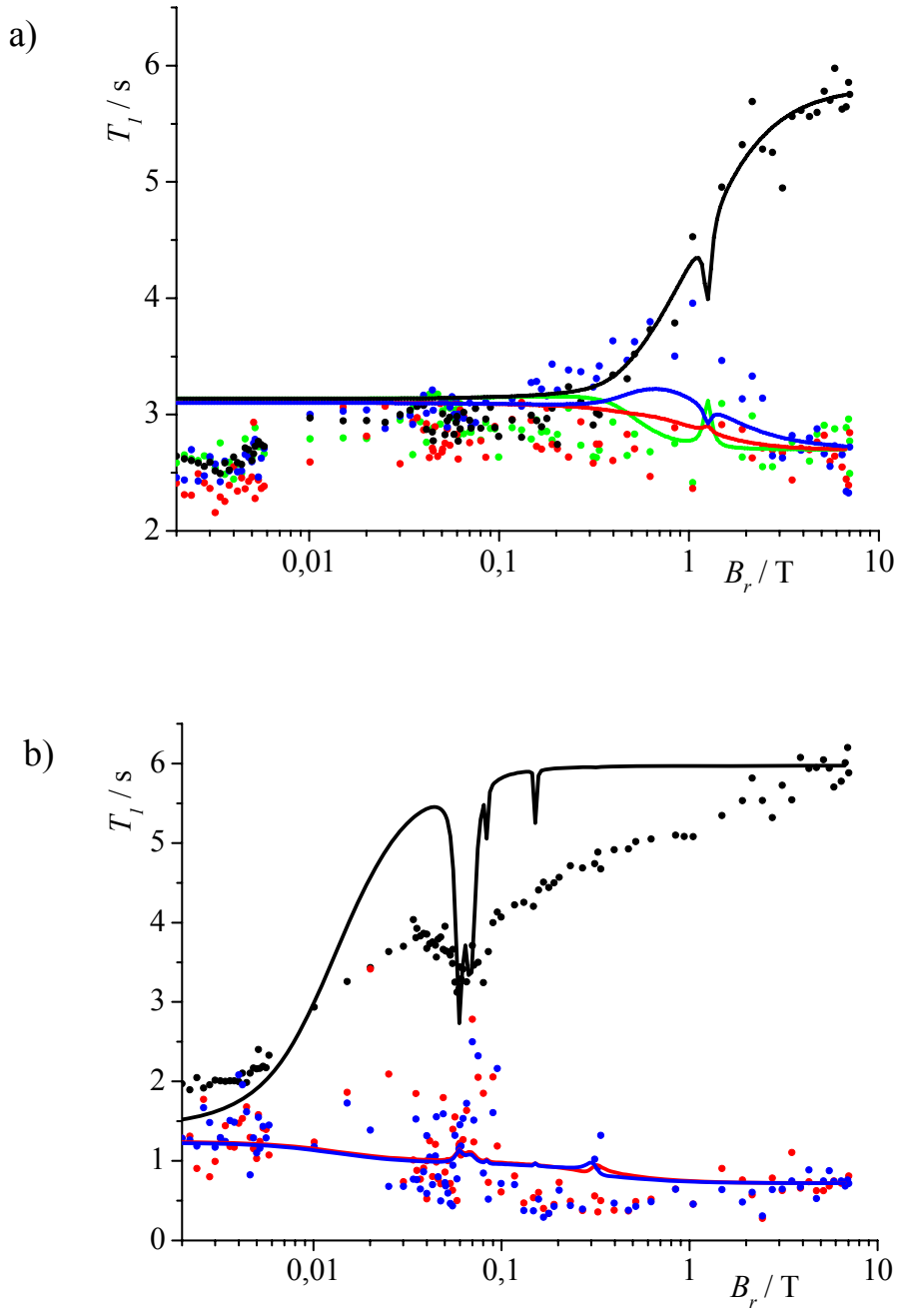

Figure 4.1.4: Simulations of T_1 relaxation dispersions with the NMR parameters from table 4.0.1 for spin sub-systems containing four spins each upon sudden sample transfer (straight lines) and comparison to the experimentally determined values from fig. 4.1.3. a) •: H4, •: H5, •: H6 and •: H7; b) •: H2, •: β1, •: β2 and α (not shown). The calculations are coloured accordingly.

The calculations further predict the dip on the dispersion on H7 to be accompanied by a peak on that of H4. In further experiments (not shown) it was tried to reproduce the predicted features at 1.27T, but they were not found. This anti-crossing lies in a region where the gradient over the sample (see figure 3.2.3) along the z-axis exceeds the width of the predicted

features, and without increasing the field homogeneity (or decreasing the sample volume) this peak is probably not accessible.

For the second four spin system, H2 with the two β-CH_2 protons and α-CH, the experimental data is compared to calculations assuming a sudden field change in figure 4.1.4 b). Here, a pronounced dip around B = 0.055T to 0.075T in the dispersion curve of H2 is predicted. This feature is seen quite well in the experimental data, and coincides with the anti crossing in the J_z = -1 manifold calculated in figure 4.0.4. The slight increase of T_1 from 0.7s to 1.3s when going to lower fields in the dispersion of the β-protons is also predicted by the calculations. The gradual decrease in T_1 of H2 between 7T and 0.005T is not reproduced by the calculations, where it remains roughly constant until 0.1T and then drops at B<0.1T when taking only four protons into account.

Qualitatively, most of the features in the T_1-dispersions of the individual protons are predicted quite well by the calculations, but apparently the approximation of dividing the large spin system into two subsystems of four spins is somewhat crude. A closer inspection of table 4.0.1 shows, that the two subsystems are coupled via the J = -0.4Hz coupling between H2 and H6. Since the signals of these two protons have almost the same chemical shifts (7.12 ppm and 7.14 ppm) it can be expected that this coupling manifests itself up to relatively high fields, in case the relaxation rate of the involved protons is slower than the inverse of their coupling. The dispersion curves were therefore modelled again with five spins for the case of sudden field variation and the results are displayed in figure 4.1.5. In general, a five spin system leads to 32 eigen-states, that are grouped according to their total magnetization, J_z (= 5/2 (1 state), 3/2 (5 states), 1/2 (10 states), -1/2 (10 states), -3/2 (5 states), 5/2 (1 state)).

First, consider the aromatic protons (H2, H4, H5, H6 and H7) in figure 4.1.5 a). The decrease of T_1 in the dispersion of H2 is much smoother and attributed to the coupling to H6, which has been omitted in the calculation above. Several level crossings are present between 0.1 and 7T, but the resulting peaks are probably not accessible due to the lack of field homogeneity. The fact that the dip in the experimental T_1 curve of H2 at 0.065T is not reproduced by the calculation is taken as a further indication that it results from the level crossing occurring in the spin sub-system containing the α and β-protons. Also, the decrease of T_1 for H7 when going down to 0.3T is seen very well. The increasing T_1 of H6 between 0.02 and 2T is more pronounced than if only four spins are taken into account. In low field, all relaxation times are overestimated by the calculations, probably because the coupling of H2 to the rapidly relaxing β-protons is neglected.

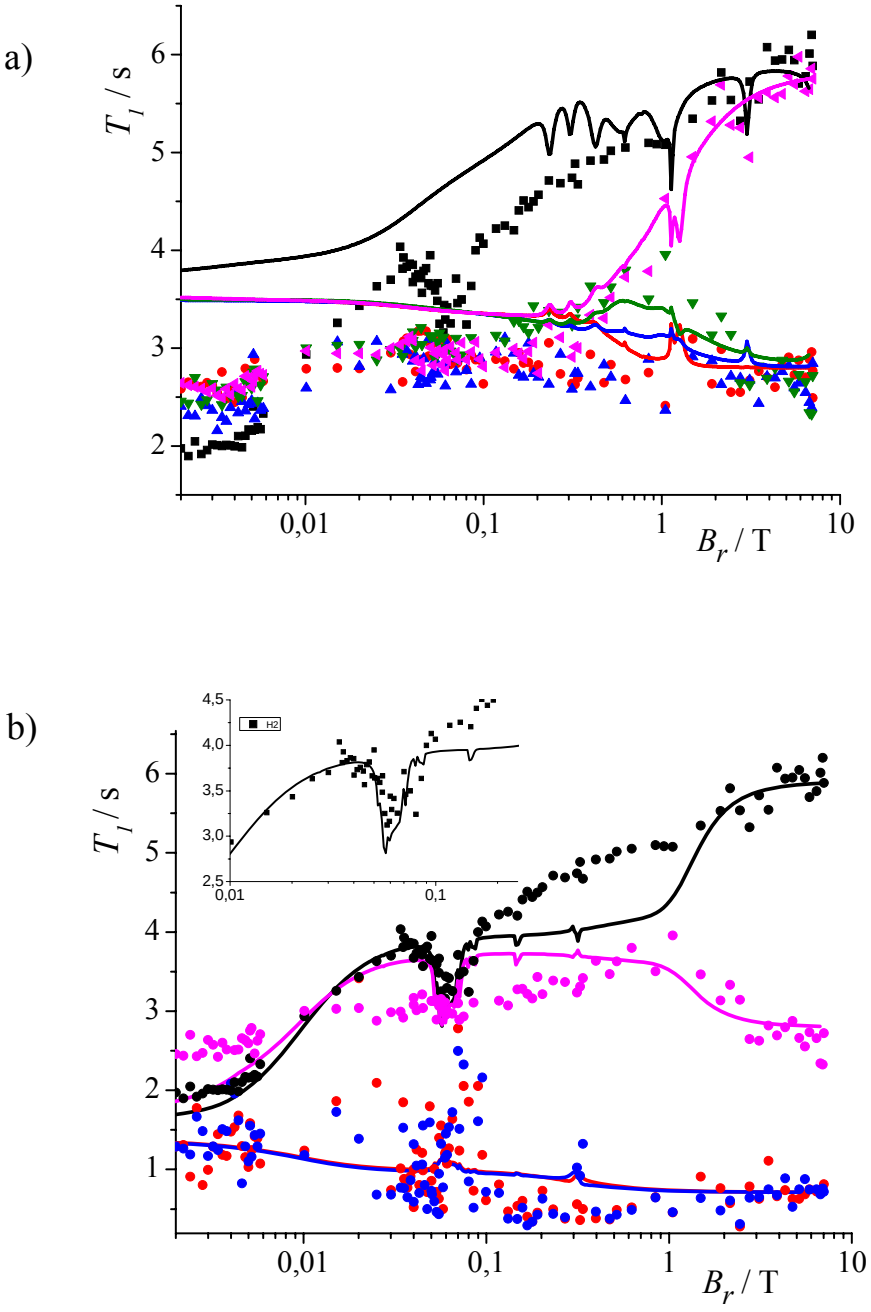

Figure 4.1.5: Simulations of T_1 relaxation dispersions with the NMR parameters from table 4.0.1 for spin sub-systems containing five spins each upon sudden sample transfer (straight lines) and comparison to the experimentally determined values from fig. 4.1.3. a) •: H4, •: H5, •: H6, •: H7 and •: H2; b) •: H2, •: H6, •: β1, •: β2 and α (not shown). The calculations with the parameters from table 4.0.1 are coloured accordingly. The inset shows the dip (0.06 to 0.07T) n the dispersion of the H2-proton.

In the second case, H6 was coupled to the previously considered four spin system of the β-CH_2-protons, the α-CH-proton and H2 and the results are displayed in figure 4.1.5b). In contrast to the case with only four spins taken into account, the dip around B_r = 0.065T in the

dispersion of H2 is more featureless and resembles the experimentally obtained dip much better (see inset in fig. 4.1.5 b)). The intermediate rise of H6 is only slightly overestimated by the calculations, when the coupling to the more rapidly relaxing protons H4 and H5 are not taken into account, but qualitatively reproduces the intermediate increase in T_1 between 0.01T and 2T quite well, and also the slight increase of T_1-values for the β-protons is predicted by the calculations.

Finally, the prevailing features of the experimental NMRD-data for the individual proton sites are reproduced quite well, and unambiguously reveal the connectivity between spin-spin couplings and relaxation behaviour. The results presented here thus evidence that stepwise features in T_1-dispersions of individual proton sites are caused by common relaxation of strongly coupled spins but not by a change of the time-scale of molecular motion. The theory predicts similar relaxation times for all strongly coupled spins in very low fields, while the experimental values show a difference. This shortcoming may probably be overcome by taking into account that the spin-spin couplings can not affect the relaxation immediately but take a finite time ($\sim J^{-1}$) to do so.

The same peculiarities may be expected to also influence the NMRD-data of other (larger) molecules, for which a change of motional regime would be expected to lead to similar features. The level anti-crossings calculated for the nuclear spin sub-systems in NATrpH are shown to result in sharp peaks and/or dips when the field is changed non-adiabatically.

Before the final conclusions are summarized in more detail, another feature of the individual relaxation curves shall be briefly discussed, i.e. the observation of multi-exponential relaxation curves for solvent and solute spins.

Exchange of magnetization between solvent and solute spins. A substantial part of the present work deals with the phenomena of transfer of hyper-polarization and coherences in systems of coupled spins-½ at low magnetic fields, and new (dynamic) mechanisms are introduced in the following sections (4.2 and 4.3). In the literature, the transfer of polarization in regions of anti-crossings has been usually referred to as a stochastic process, i.e due to relaxation. That such a stochastic process is indeed observed in terms of an intermolecular exchange of magnetization is now briefly shown on basis of a single set of experiments at low field (B_r = 5mT). The experiment introduced here, enables the determination of intermolecular cross relaxation rates in low magnetic fields and allows a clear distinction between this kind of process and the much more efficient, dynamic processes discussed in the chapters 4.2 and 4.3.

The relaxation behaviour of those protons of NATrpH which are presumed to have the highest mobility, namely the two CH_2-protons in β-position, the CH-proton in α-position, and the three protons of the methyl group of NATrpH, differs considerably from that of the aromatic protons. As an example, the magnetization decay curve for the acetyl group is given in figure 4.1.6. The following discussion is focussed mainly on the N-acetyl-line (NAC-line), because it is a sharp singlet around 2.1ppm for the three equivalent protons of the methyl group; its integration gives a better signal to noise ratio than any other signal of the amino acid and is thus suited best for an identification of the underlying phenomena. A closer inspection of its decay curve (fig.4.1.6) shows that the measured magnetization decays with (at least) two exponentials. However, the experimental data do not allow extracting two decay constants reliably.

The multi-exponential relaxation behaviour was clearly observed throughout the whole field range, and is not expected to be unique to the NATrpH molecule but also observable for other molecules. A systematic search for its reason has not yet been undertaken. Instead, the discussion of the multi-exponential relaxation behaviour was circumvented by introducing the term 'effective T_1-value ($T_{1,eff.}$)' for the result of a single exponential fit, as in the discussion above. Here, it is intended to explore the possible sources of the multi-exponential T_1-relaxation.

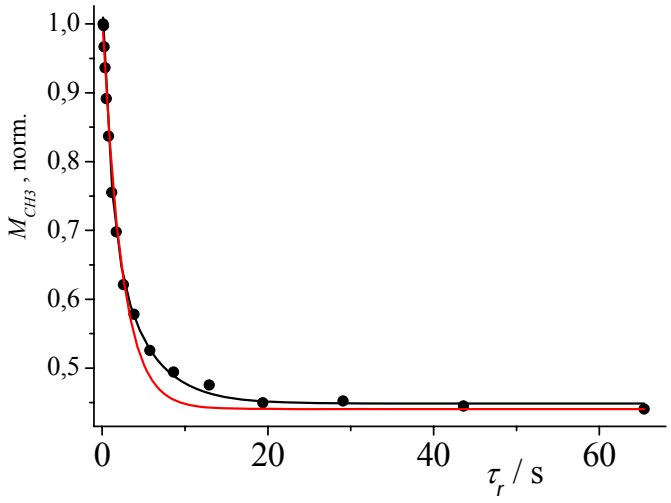

Figure 4.1.6: Multi-exponential decay of the N-acetyl signal at B_r = 0.02T. Mono- and bi-exponential fits are shown as red and black lines, respectively.

For the solvent line of the residual protons in the water, also characteristic deviations from a pure mono-exponential behaviour were noticed: In contrast to the relaxation curves of the amino acid protons, the largest deviations between the mono-exponential fits and the

measured NMR integrals of the HDO signal do not occur for the longest but for the shortest delay times, τ_r. The effect on the HDO-line is not very pronounced, which is probably why it is widely ignored in the literature.

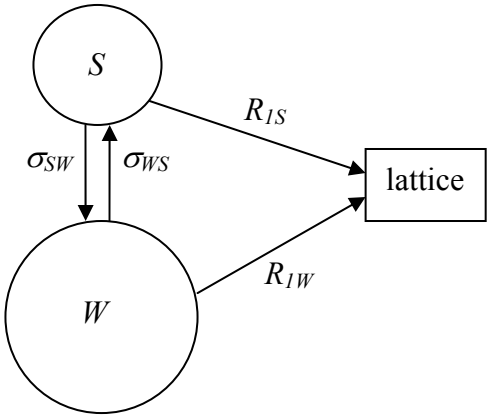

Figure 4.1.7: Diagram for magnetization exchange in aqueous amino acid solution.

For an understanding of the multi-exponential decay curves, the exchange of magnetization between solute and solvent molecules is considered. The diagram in figure 4.1.7 summarizes the essential features of the transfer of longitudinal magnetization between the two pools of proton spins. The magnetization is assumed to be transferred by secular dipolar interactions, usually loosely referred to as cross-relaxation arising from a 'flip-flop mechanism' [65]. In the simplest case, two spins relax each other by their mutual dipolar interaction (homo-nuclear NOE).

The two pools of spins involved are that of the amino acid protons, *S*, and the residual protons in the solvent, *W*. They interact with the lattice via their characteristic longitudinal relaxation rates $R_{1W} = 1/T_{1W}$ and $R_{1S} = 1/T_{1S}$. In addition the exchange of magnetization via the cross relaxation rates σ_{SW} and σ_{SW} is considered. The exchanged magnetization is mutually interdependent with $\sigma_{WS}=\sigma_{WS}\equiv\sigma_C$. It is a Solomon type equation [73], which formally describes the time dependence of the longitudinal magnetization M_S and M_W during relaxation:

$$\frac{d}{dt}\begin{pmatrix} M_S \\ M_W \end{pmatrix} = -\begin{pmatrix} \frac{1}{T_{1S}} & \sigma_{SW} \\ \sigma_{WS} & \frac{1}{T_{1W}} \end{pmatrix} \cdot \begin{pmatrix} \Delta M_S \\ \Delta M_W \end{pmatrix} \quad , \tag{4.1.3}$$

The magnetization decays (or rises) from the starting magnetization M_S^0 at $t=0$ to the equilibrium magnetization M_S^{eq}, and their difference is given by $\Delta M_S = M_S^0 - M_S^{eq}$. Equation 4.1.3 can be solved analytically by standard matrix diagonalization methods, and the solutions are as follows:

$$M_S(t) = M_S^{eq} + \Delta M_S e^{-\lambda_1 t} + \alpha\left(e^{-\lambda_2 t} - e^{-\lambda_1 t}\right)\Delta M_S + \sqrt{\alpha}\left(e^{-\lambda_2 t} - e^{-\lambda_1 t}\right)\Delta M_W \quad \text{and} \quad (4.1.4)$$

$$M_W(t) = M_W^{eq} + \Delta M_W{}^0 e^{-\lambda_2 t} + \alpha\left(e^{-\lambda_1 t} - e^{-\lambda_2 t}\right)\Delta M_W{}^0 + \sqrt{\alpha}\left(e^{-\lambda_2 t} - e^{-\lambda_1 t}\right)\Delta M_S{}^0 \quad , \quad (4.1.5)$$

with the coefficients

$$\lambda_1 \approx -\frac{1}{T_{1W}} - \alpha\frac{T_{1W} - T_{1S}}{T_{1W} \cdot T_{1S}} \quad \text{and} \quad \lambda_2 \approx -\frac{1}{T_{1S}} + \alpha\frac{T_{1W} - T_{1S}}{T_{1W} \cdot T_{1S}} \quad , \quad \alpha = \left(\frac{T_{1W} \cdot T_{1S} \cdot \sigma_C}{T_{1W} - T_{1S}}\right)^2 . \quad (4.1.6)$$

In general, each magnetization component M_i (i = *S, W*), will evolve in time as a sum of three exponential functions of which two are related to the cross relaxation rate, σ_C.

The applicability of this model is tested by variation of the relative starting magnetizations $M_S(\tau_r=0)$ and $M_W(\tau_r=0)$. These can be conveniently varied by introducing a 180°$_x$-pulse prior to the field cycling experiment outlined in figure 4.1.1 a). Between the population inversion and the field cycle, an additional waiting time, τ_w, was introduced. The resulting experiment is then as follows: 180°$_x$ - τ_w - τ_{fv1} - τ_r - τ_{fv2} - 90°$_x$ - FID.

At B = 7T the longitudinal relaxation time of the water protons in the sample under investigation (0.07% HDO in D_2O) is about T_{1W} = 25s, i.e. about 10 times longer than that of the amino acid protons. At 50G, the relaxation time is still considerably longer (T_{1W} (B_r = 50G) ≈ 11.4s). Because of their significant difference in relaxation rates, one can conveniently vary the relative starting amplitudes of the water signal and the amino acid signals. For NATrpH solutions a variation of proton concentration would be impractical because of its low solubility, and experiments with selective pulses would also be more laborious than the applied technique.

In figure 4.1.8, the results for seven different waiting times in high field, (τ_w = 0.1s to 22s), are shown; the experiments for 8s, 12s and 18s were performed twice for different τ_r. Depending on τ_w, the initial (τ_r = 0) amplitude of the water varies between -1 and 0.7 (fig. 4.1.8 a)), and the influence on the time evolution of the amino acid signals (fig. 4.1.8 b)-d)) is quite pronounced. The most significant influence is found for τ_w = 1s and τ_w = 4s: When the HDO line starts with negative amplitudes, the magnetization of the amino acid lines are passing through a minimum. While the position of these minima is given by the T_1-values for the individual lines, the amplitude of the minima is sensitive to the cross relaxation rate, σ_C.

The time profiles are fitted according to equations 4.1.4 for M_S and 4.1.5 for M_W, and the results are also presented in figure 4.1.8 (. The spin lattice relaxation times T_{1S} and T_{1W} are well determined because the curves are dominated by them. In addition, these values are known from the investigation presented above. Starting and final amplitudes of the curves in fig.4.1.8 solely depend on the spin lattice relaxation at high field (B = 7T), and were fitted by

mono exponentials, e.g. M_W (τ_r = 100ms) over τ_w. The rates of cross relaxation, σ_C for different spins S, in NATrpH are then the only variable left to be determined by simultaneously fitting the time evolution curves in figure 4.1.8 a) – d). Thus, each data set provides access to a single rate constant, σ_C, describing the exchange of magnetization (NOE) between certain proton sites in the sample.

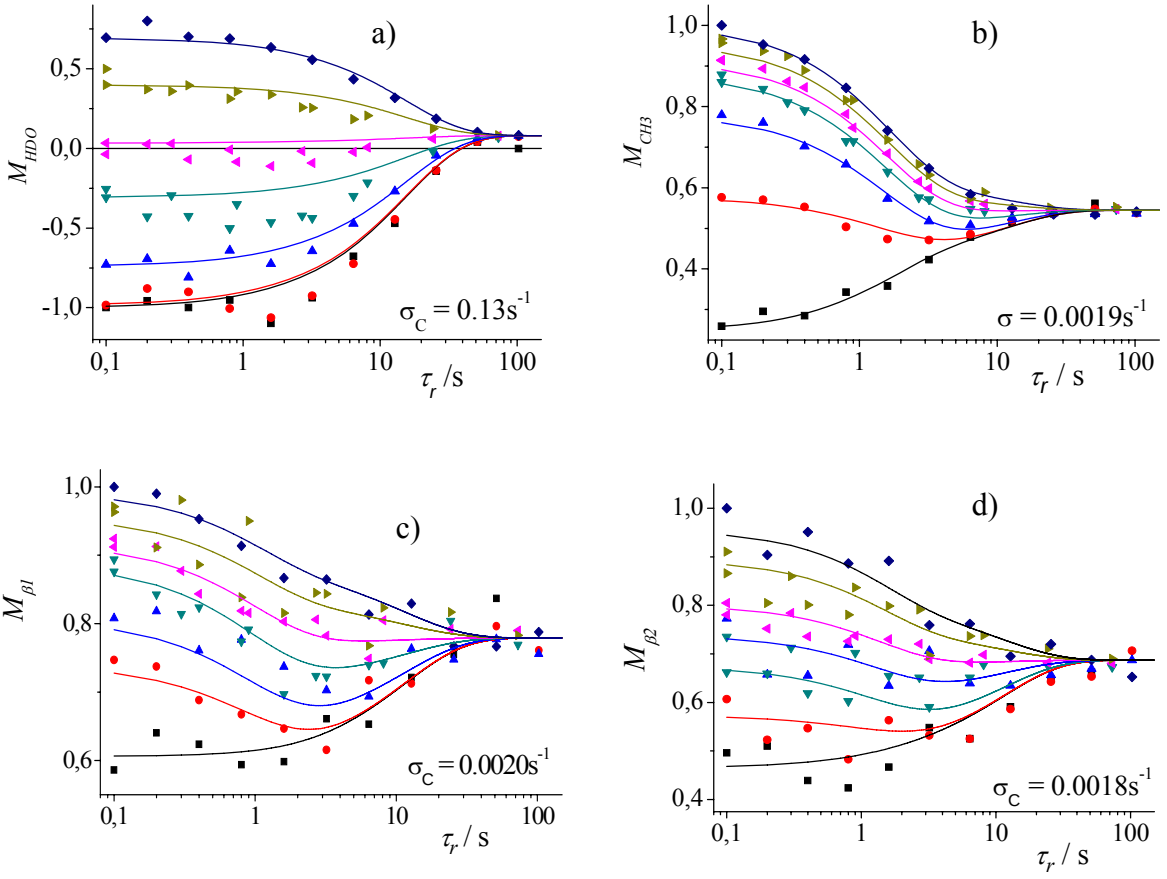

Figure 4.1.8: Time evolution of proton magnetizations, M_i, at B_r = 5mT for different starting magnetizations obtained by variation of the waiting time (τ_w) at B_0 after population inversion (180°-pulse). ■: τ_w = 0.1s, ●: τ_w = 1s, ▲: τ_w = 4s, ▼: τ_w = 8s, ◄: τ_w = 12s, ►: τ_w = 18s, ♦: τ_w = 22s. a) HDO; b) -CH_3; c) β1-CH; d) β2-CH. The signal intensities are normalized to -1 (τ_w = 0.1s) in case of HDO, and to +1 (τ_w = 22s) in the cases of -CH_3, β1-CH, and β2-CH.

The present experiments clearly prove that the magnetization kinetics of solvent and solute molecules is interdependent, and subject to considerable exchange of magnetization. The results are relatively well described by a simple model taking a classical rate constant, the cross-relaxation rate σ_C, for the exchange of magnetization into account, clearly showing that - at least in part - multi-exponential relaxation behaviour is caused by this exchange. However, better fits for the curves of HDO probably require more than a single cross

relaxation rate, because of the magnetization exchange with multiple sites in NATrpH. The experimental method is expected to be well suited for the determination of cross-relaxation rates at variable magnetic field and may serve to study magnetization exchange in larger bio-molecules, and provide information on the distribution and the mobility of water molecules in polypeptides or small proteins in the future.

Conclusions

For the first time, a site-specific study of proton relaxation in a coupled multi-spin-system of a small molecule in aqueous solution is presented. The common features of the experimental data and the calculated curves give evidence that the relaxation dispersions of coupled multi-spin systems are governed by their NMR parameters (scalar couplings and chemical shifts). Knowledge of the relaxation times in high field, where all spins are coupled most weakly, and the NMR parameters suffice for the description of the prevailing features of NMRD-curves of small molecules which remain in the fast motional regime in the entire frequency range.

In principle, NMRD-data can give information about prevailing relaxation mechanisms. Furthermore, certain mechanisms have been assigned to govern the nuclear spin relaxation on the basis of increasing or decreasing T_1-curves with increasing Larmor frequency. However, the findings presented in this chapter show clearly that care has to be taken when interpreting field dependent relaxation data of multinuclear spin systems, in particular when individual signals can not be assigned or overlap or when the number or range of investigated field values is small. For the NATrpH molecule in aqueous solution under ambient conditions, it is shown that significant changes in relaxation rates are observed for individual proton sites even in the absence of field dependent mechanisms of relaxation and constant spectral density of the fluctuating fields.

A better coincidence between the experimental and calculated curves may be expected, if more (all) coupled spins-½ were taken into account. Moreover, a quantitative description of the dispersions presented here, would require taking the actual time profile of the field variation into account, instead of assuming adiabatic or sudden field changes. The findings presented in this chapter have later been verified for simpler spin systems such as N-acetyl histidine, N-acetyl tyrosine and for the mono phosphates of adenosine and guanosine [64] in aqueous solutions, for which the entire spin systems were modelled. These results support the

assumption that the inclusion of all spins in the coupled multi-spin system gives a better coincidence of theory and experiment.

Furthermore, the magnetization kinetics for certain protons in the solute molecule show a characteristic dependence on the magnetization of the residual protons (HDO) in the solvent D_2O. This shows that the kinetics of magnetization can not solely be explained by intra-molecular dipole-dipole interactions, but also inter-molecular interactions are present. These interactions are clearly shown to cause an interdependent decay of magnetization and lead to the observation of multi-exponential relaxation. By a simple modification of the field cycling experiment, rate constants for the magnetization exchange between certain pools of protons become accessible.

One may speculate that the modulations of inter-molecular distances are the main channel of relaxation for HDO in D_2O. A more detailed study may provide access to the underlying mechanisms and the dependence of efficiency of magnetization exchange on the amount and the mobility of the protons in the surrounding of the amino-acid. Extending the investigation to the exchange of magnetization of bio-molecules with surrounding water-molecules may provide insight into location and mobility of HDO in proteins.

4.2 Redistribution of Polarization among Coupled Spins

In the previous chapter it was shown that scalar spin-spin couplings govern the appearance of field dependent relaxation data for individual spins, and that level anti-crossings between different nuclear spin states of coupled spin-systems manifest themselves as characteristic features in the T_1-dispersions of the individual NMR signals. The T_1-experiments probe the time in which the spin-system establishes thermal equilibrium, after it is brought into a non-equilibrium state. The non-thermal polarization of nuclear spins is often termed hyper-polarisation (HP) and provides an efficient way for enhancing the notoriously low sensitivity of NMR spectroscopy. For an efficient exploitation of HP it is often necessary to transfer the polarization from the primarily polarized spins to certain target spins.

It has been pointed out by de Kanter and Kaptein [54] that strong coupling leads to the transfer of CIDNP to nuclei that do not have any HFI in the transient radicals, and therefore do not show any polarization at high magnetic fields. It is thus expected that the condition of strong coupling causes a transfer of HP, and the purpose of this chapter is to elucidate the consequences of scalar spin-spin couplings in field cycling experiments with hyper-polarized spin systems.

Here, the effects are demonstrated on aromatic amino acids that exhibit photo-CIDNP after going through a radical reaction with a suitable dye. The polarization is then stored in the stable reaction products during the time of spin lattice relaxation and contains information on the elusive radical species involved.

In principle, field dependent CIDNP provides a possibility for the determination of the magnetic interaction parameters, i.e. hyperfine interaction (HFI) and g-factors in short lived radical species. The strategy for the determination has been outlined in chapter 2.1.5. In magnetic fields lower or comparable to the effective HFI, a_{eff} (see formula 2.1.19), of the radicals under study the CIDNP formation is governed only by the HFI. This can allow the extraction of HFI's from the field dependence of CIDNP. The HFI can then be used to extract the g-factors of the radicals which constitute the transient radical pair from the high field part of the field dependence. This strategy has been employed before [40, 41, 43], however, the method of extracting magnetic interaction parameters meets serious limitations when at low magnetic field the spins are coupled strongly ($J>>\delta\nu$) by scalar spin-spin coupling. Here, the redistribution of HP is discussed and hence the polarization of the strongly and weakly coupled spins shall be termed low-field CIDNP and high-field CIDNP, respectively, corresponding to strong or weak entanglement of the individual spin states in the reaction

products. This terminology is in contrast to that introduced in chapter 2.1.4, where the formation of CIDNP in the paramagnetic stage is discussed.

While the determination of chemical reaction pathways and extraction of the properties of the intermediates can become problematic, there is also a very positive aspect about the transfer of HP, since in many HP experiments it is desired to transfer the polarization from the initially polarized spins to certain target spins. Optimizing the conditions for an efficient and selective transfer of HP is central to its successful exploitation. A systematic experimental study on the redistribution of HP in coupled multi-spin system is necessary to understand the underlying phenomena and may provide new possibilities for guiding HP along desired pathways in coupled multi-spin systems by field cycling NMR. In particular, this chapter shall provide an insight into how spin-spin couplings can alter the polarization patterns observed at high magnetic fields i) after being formed in low field and ii) after being polarized in high field and two consecutive fast field switches to low field and back into the spectrometer field for detection. The latter experiment starts with a well defined polarization pattern, and allows a better separation of the initial HP and polarization that is transferred to potential target spins.

Experimental

In this chapter, two different kinds of experiments shall be discussed. The first part is focussed on the low field part of typical field dependent CIDNP experiments. This kind of experiment has been performed for many years in our laboratory and a typical timing scheme is given in chapter 3.2 (fig. 3.2.1). It is characterized by the irradiation time, τ_L, at a certain magnetic field, B_{pol}, followed by a rapid transfer of the sample to high magnetic field B_0, where the NMR is recorded by a $45°_x$ or a $90°_x$ RF-pulse. In this case the transfer of polarization can obstruct the elucidation of hyperfine coupling from the low field part of the field dependence. In return, the actually desired CIDNP field dependence may still be present and complicate the analysis of polarization transfer. To elucidate the effects of polarization transfer in more detail, it is necessary to separate these effects. It is thus desirable to have well defined starting conditions in the polarized spin system, such that certain spins are polarized while others are not, and the experiment was therefore modified.

The second kind of experiment discussed here basically parallels the protocol used for the acquisition of field dependent relaxation data (fig. 4.1.1 a)). The timing scheme of this

experiment employs two fast field switches and is shown in figure 4.2.1. Before the experiment, the background polarization is removed by a suitable waiting time (at least five times T_1 of the slowest relaxing nucleus) in low field. Then, the sample is transferred to the polarization field B_{pol} (= B_0), where it is irradiated by 308nm laser light for the time τ_L (0.4s). Directly after the irradiation (t = 0 in fig. 4.2.1), the probe is moved to a variable intermediate field, B_{ev}, during the time τ_{fv} (≤ 0.3s), and then transferred to the detection field B_0 where the NMR spectrum is acquired by a 90° RF-pulse. For the present case it was convenient to choose $B_{pol} = B_0$, and the transfer times from B_{pol} to B_{ev} and from B_{ev} to B_0 are chosen identical (~ 0.3s).

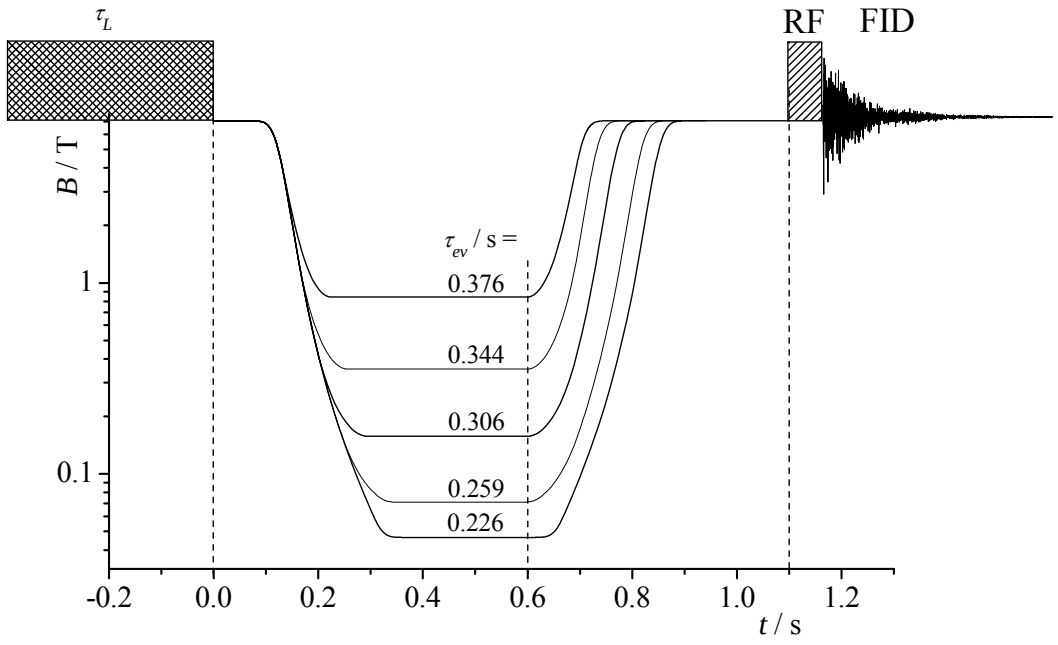

Figure 4.2.1: Realistic timing schemes for the investigation of polarization transfer in diamagnetic product molecules at variable magnetic field, B_{ev}. Here, $B_{pol} = B_0 = 7$T

In the experiment outlined in figure 4.2.1, the delay time between the irradiation and the second field change detection is kept constant ($\tau_{fv1} + \tau_{ev} = 0.6$s), and also the time between irradiation and 90°-RF detection pulse ($\tau_{fv1} + \tau_{ev} + \tau_{fv2} = 1.1$s), because this allows a convenient automation of the experiment. These time intervals are indicated as the dashed lines in figure 4.2.1. The changes in transfer times, τ_{fv}, to different values of B_{ev} lead to a slight variation of residence times (spin evolution time, τ_{ev}) at B_{ev} for the different experiments, when the polarization transfer is probed in the fringe field of the cryomagnet: the lower the field, the shorter the evolution time, τ_{ev}. For some experiments τ_{ev} was calculated

and is given in fig. 4.2.1. In contrast, for the transfer into the electromagnet (0.12T ≥ B_{ev} ≥ 10^{-4}T), the residence time at B_{ev} remains the same (0.226s); because the transfer time of the probe, τ_{fv} does not change.

Sample preparation. The samples used for the experiments are: a) 5mM of N-acetyl tyrosine (NATyrOH) at pH 11, b) 8 mM of NATrpH and 0.6 mM of anthraquinone-2-sulfonic acid (AQ2S) in D_2O at pH=11 and c) 2 mM of NATrpH and 1mM 4-carboxybenzophenone (CBP) at pH 11. The amino acids were purchased from Aldrich and the solvent (D_2O) from Deutero GmbH. All samples were purged with pure nitrogen gas prior to use to remove dissolved oxygen. The pH values were adjusted by addition of NaOD.

Results and Discussion

Redistribution of HP in low-field CIDNP experiments. The first experiment considered here is the photolysis of N-acetyl-tyrosine (NATyrOH) with 308nm laser light (sample a)). Polarization is formed in transient radical pairs consisting of the tyrosyl-radical and a solvated electron (e^-_{aq}). Further peculiarities of the chemistry following photo-ionization of NATyrOH are discussed in chapter 6.1.1. Here, it is only important that the photoreaction proceeds via the tyrosyl-radical (phenoxyl type). The tyrosyl radical carries a large HFC's on the protons closer to the phenolic oxygen (H3 and H5), and a much smaller HFC at the protons in positions 2 and 6. The ratio of HFC's may be estimated from the high field TR-CIDNP spectrum taken immediately after the laser pulse ('geminate spectrum'), which is: H3/5:H2/6 = 1:-0.27, see fig. 6.1.4 a)). This spectrum reflects solely the polarization formed in the primary radical pair, i.e. the tyrosyl radical and e^-_{aq}. However, when a sample of 5mM $NATyrO^-$ at pH 11 is irradiated for τ_L = 1.5s at low magnetic field, the two inequivalent pairs of protons show identical field dependences despite their remarkable difference in HFC's in the radical pair stage. This situation is shown in figure 4.2.2 a).

The spin-spin coupling between the protons in position 3/5 and 2/6 is about J = 8.5 Hz, and the similarity of the observed field dependences is attributed to the mixing of states during the rather long irradiation time (τ_L = 1.5s). This meets exactly the case that has readily been considered by de Kanter and Kaptein [54], namely that the period during which CIDNP is formed is rather long in comparison to the scalar coupling, J, between the two interacting

protons of the diamagnetic molecule ($\tau_L >> \frac{1}{2}\pi J^{-1}$). In ref. [54], the role of coherences (represented by off-diagonal elements of the respective spin density matrix) formed in low magnetic fields were completely neglected. This approximation finds justification, as the coherences have been washed out completely during τ_L. However, De Kanter and Kaptein considered the polarization transfer to occur instantaneously. That this is not correct, when the irradiation times are chosen shorter has recently been predicted theoretically by K. L. Ivanov. Subsequently it was shown in CIDNP experiments with adenosine monophosphate that the time for CIDNP redistribution can be roughly estimated to J^{-1} [56]. For the present case of the aromatic protons in NATyrOH, this corresponds to a time as short as 0.11s. The similarity of the field dependences in figure 4.2.2 a) is therefore not surprising, and the scalar coupling of spins obviously provides a very efficient way of polarization transfer between strongly coupled spins.

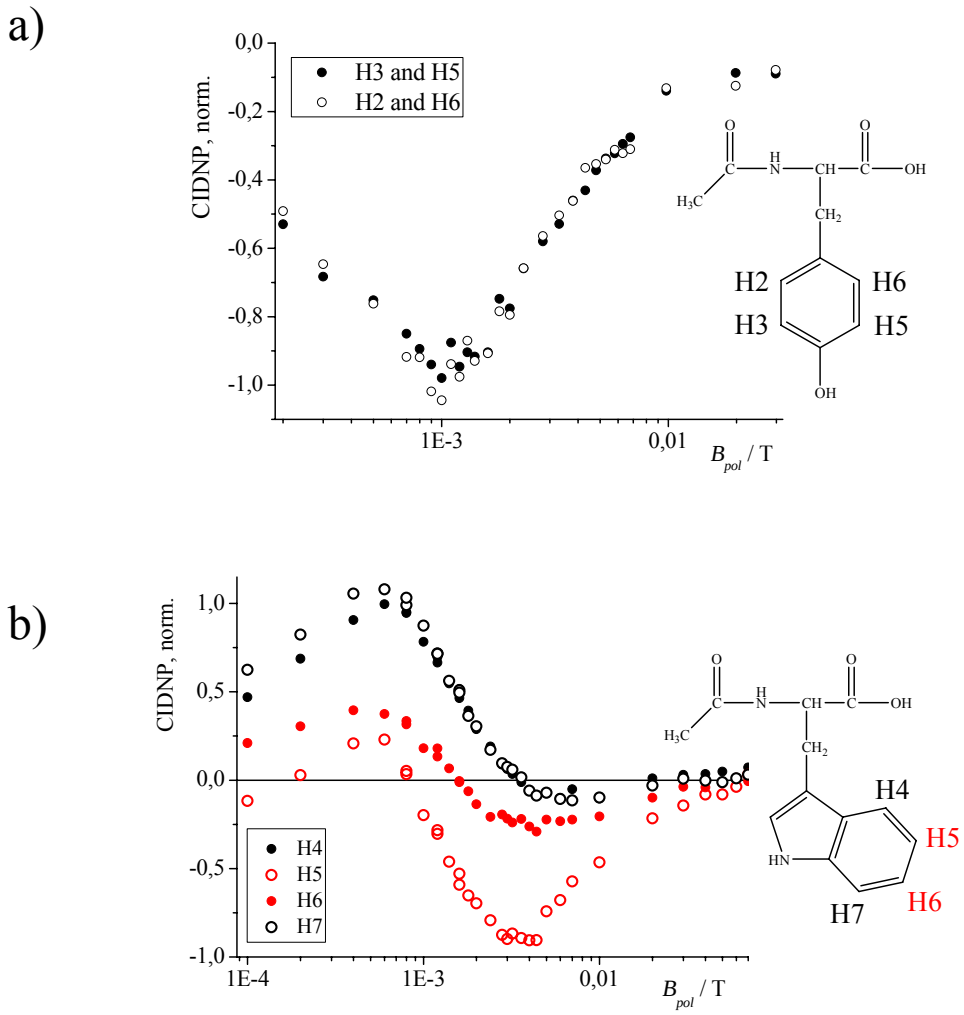

Figure 4.2.2: CIDNP field dependences of aromatic protons in a) $NATyrO^-$ and b) NATrpH. The directly polarized protons are shown with full, the indirectly polarized protons with open symbols. a) τ_L = 1s, $\tau_{fv} \approx$ 0.3s, 90° RF-pulse flip angle b) τ_L = 1s, $\tau_{fv} \approx$ 0.35s, 45° RF flip angle.

Of course, the redistribution of HP by strong scalar spin-spin couplings at low magnetic fields is not limited to the case of NATyrOH. The second example considered here is the redistribution of polarization in the N-acetyl tryptophan (NATrpH) molecule. During the reversible electron transfer reaction between the triplet excited dye AQ2S and NATrpH (sample b), see sample preparation on p. 94), CIDNP is formed on certain protons of the indole ring of NATrpH. As in the case above, only the protons that have considerable HFI in the radical stage are polarized in high magnetic fields. These are the protons in the positions 6, 4 and 2 of the indole ring and the two inequivalent β-CH_2-protons. The protons in the α-CH position and those in positions H5 and H7 do not have considerable HFI, and thus do not show 'high field CIDNP'. An example for the CIDNP pattern observed in high field is seen in figure 4.2.3 (second trace), which reflects the spin density distribution in the tryptophanyl radical cation ($NATrpH^{\bullet+}$) quite well. This assumption is supported by the time-resolved CIDNP spectrum detected immediately after the laser pulse [74], which is not affected by secondary bulk reactions.

CIDNP field dependences of the four protons of the six-membered ring (H4, H5, H6 and H7) are shown in figure 4.2.2 b). The scalar couplings between neighbouring aromatic protons are comparable to those in the case of NATyrOH and are listed in table 4.0.1. As long as the field is low enough that the scalar coupling is in the same order as the difference in Zeeman interactions (strong coupling condition), the eigen-states of the nuclear spin system are not the states of individual spins but the collective states of the entire spin system, which is factorized further into two subsystems, one comprising four spins of the H2-, the α-CH- and the β-CH_2-protons, and the other one comprising those of the six-membered ring (H4, H5, H6 and H7). Here, the discussion shall be restricted to the low field CIDNP in the six-membered ring, for which the energies of the collective states are shown in figure 4.0.3. The low-field part of the field dependences of these four protons is qualitatively different from the high field polarization pattern. All protons in the six-membered ring acquire significant polarization irrespective of their HFI, moreover their CIDNP field dependences are very similar and have their extrema at the same magnetic field. Since only two (H4 and H6) of the four protons have significant HFI in the radical state and are thus polarized directly, it is concluded that H5 and H7 are polarized by CIDNP transfer from other spins. The reason for the difference in amplitudes between e.g. H5 and H6 may be the consequence of an incomplete decay of coherences.

Qualitatively, the low field CIDNP patterns observed for $NATyrO^-$ and NATrpH can be explained as follows: At fields, B_{pol} below 0.3T the aromatic protons form strongly coupled

spin systems in both cases ($J>>\delta\nu$), since the couplings between the neighbouring protons are about 8Hz, and the differences in chemical shifts are less than 0.6ppm. Because the timing scheme of the experiments meets the condition so that $J\tau_L>1$, large CIDNP is observed on protons that do not have any HFI in the radical pair stage.

To investigate the efficiency of polarization transfer achievable by field cycling NMR techniques in more detail, and to gain a deeper insight into the underlying mechanisms, the experiment was modified and the results are discussed in the following.

High Field CIDNP with subsequent redistribution of polarization at arbitrary field. The experiment described in the following may be seen as a first attempt to devise new field cycling schemes in order to guide HP along certain pathways in coupled multi-spin systems. The experimental protocol is still relatively simple and was described above (see fig. 4.2.1). In the first step HP is formed at a pre-selected field, B_{pol} = 7T, the sample is then transferred into a variable field, B_{ev}, where the spin-system evolves for the time, τ_{ev}, and finally transferred into the field for NMR detection, B_0.

Here, HP is formed by CIDNP in the reversible electron transfer reaction between the photo-excited triplet dye CBP and NATrpH (sample c), see sample preparation on p.94 in the experimental section) at high field ($B_{pol} = B_0$ = 7T). Because the method for the formation of HP is not the focus of this chapter, the photo-cycle shall be outlined only briefly here. NATrpH is polarized by nuclear spin dependent intersystem crossing (*ISC*) in the radical pair formed after electron transfer from NATrpH to CBP:

$$CBP + NATrpH \xrightarrow{h\nu,ISC} {}^3CBP + NATrpH \rightarrow \overline{{}^3CBP^{\bullet-} + NATrpH^{\bullet+}} \xleftrightarrow{ISC} \overline{{}^1CBP^{\bullet-} + NATrpH^{\bullet+}} \rightarrow CBP + NATrpH^*$$

(The asterisk denotes the polarized reaction product.) The whole reaction cycle lasts less than 0.1ms, thus there are no radicals in the sample during evolution time τ_{ev} and field variation τ_{fv}. The initial compounds are restored to a high extend, and the polarization is formed very efficiently after a relatively short irradiation time (τ_L = 0.4s). Together, these circumstances make this photoreaction particularly attractive to study the spin evolution in the diamagnetic NATrpH molecule at intermediate field.

Once CIDNP is formed and all the radicals have decayed, the sample is transferred to the variable field B_{ev} and back to B_0. The first trace in figure 4.2.3 shows the NMR spectrum taken at Boltzmann equilibrium and the high field CIDNP spectrum is shown in the second trace. Without shuttling (i.e. $B_{pol} = B_{ev} = B_0$) the CIDNP spectrum exhibits polarization according roughly to the spin density distribution in $NATrpH^{\bullet+}$ [72] (see above).

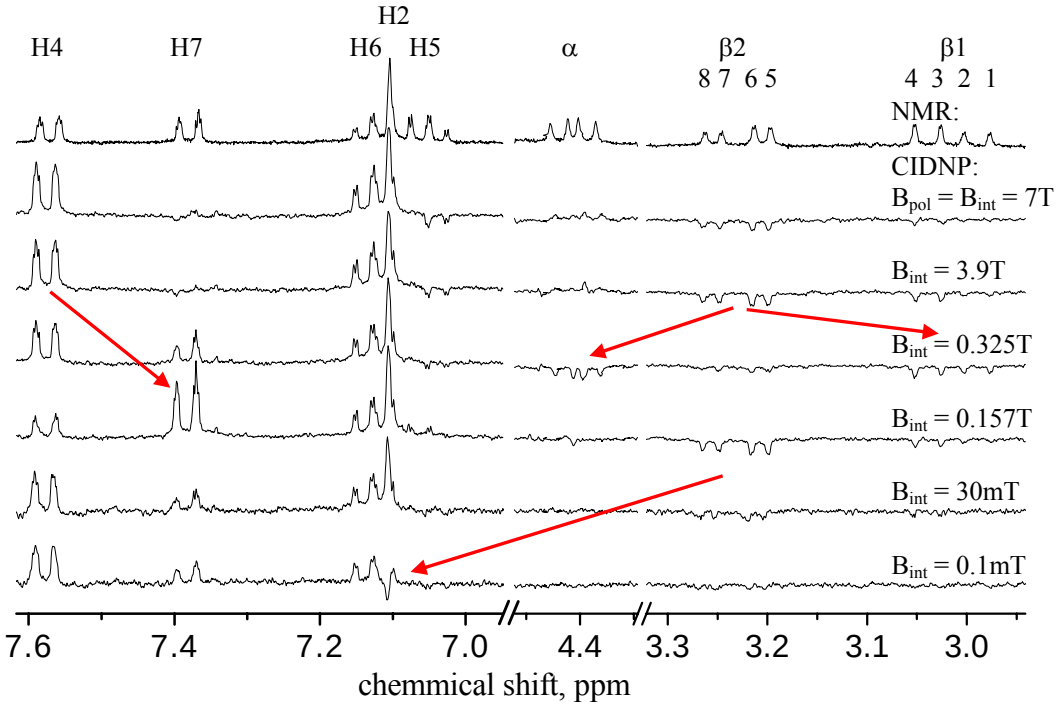

Figure 4.2.3: CIDNP difference spectra of the redistribution of polarization over the protons in NATrpH after photoreaction with 4-CBP in high field (B_{pol} = 7T) and two fast field switches (τ_L = 0.4s, τ_{fv} = 0.3s). Suggested polarization transfer pathways are indicated by the red arrows.

When the sample is rapidly transferred to B_{ev} = 3.9T and back to the detection field, the CIDNP pattern remains unchanged (fig. 4.2.3, third trace). Choosing lower fields for B_{ev}, the changes in the CIDNP pattern become rather pronounced, indicating that the strong coupling of spins is responsible for these changes. Shuttling the sample into a field of 0.325T and back to the detection field, results in very efficient transfer of polarization away from the β2-proton. It seems this polarization is distributed between the other β-proton (β1) and the α-proton. Comparing the CIDNP spectra with B_{ev} = 7T and B_{ev} = 0.325T, one can see that the polarization on the α-proton has even changed its sign. This field roughly coincides with a level anti-crossing field (see calculated energy levels in fig. 4.0.4). The comparison immediately suggests that the redistribution of HP at B_{ev} is not due to spin evolution in the radical pair stage but should be attributed to a redistribution of CIDNP in the diamagnetic reaction products, and furthermore, that the redistribution is particularly efficient in fields where the nuclear spin levels closely approach each other (anti-crossing field).

Taking even lower fields for B_{ev} leads to redistribution of polarization in the aromatic system of NATrpH. Most significant is the substantial gain in polarization of H7 at B_{ev} = 0.157T,

which is obviously accompanied by a loss of polarization on the H4 proton. After jumping to the lowest available field (B_{ev} = 0.1mT), the polarization on H2 turns from absorption to emission and no polarization is seen on the α- and the β-protons. Since the time between irradiation and data acquisition was kept constant, and the relaxation times of the β-CH_2 protons become rather longer at lower fields (see fig. 4.1.3), the loss of polarization on the β-protons can not be attributed to relaxation or cross relaxation. Instead, the emissive polarization is transferred very efficiently to the H2 proton (7.1ppm).

The peculiarities of polarization transfer in the indole ring by fast field switching are better seen in figure 4.2.4, where the integrals of the aromatic protons are plotted over B_{ev}. Choosing B_{ev} < 1T, the polarization pattern is significantly altered as compared to the pattern observed with $B_{pol} = B_{ev} = B_0$ = 7T. This observation suggests that efficient transfer of HP in this experiment also has its origin in the strong scalar coupling among the protons in the indole ring: A comparison with the previously discussed experiments shows, that at fields below 1T, the CIDNP field dependences (fig. 4.2.2 b)) of the aromatic tend to become similar, and the T_1-values of the individual proton sites (fig. 4.1.3) also tend to be equalized.

The ratios of HP obtained after a train of laser pulses (τ_L = 0.4s, 50 Hz) at 7T in the indole ring (H4 : H6 : H2 : H7 : H5) are about 1 : 0.75 : 0.4 : 0.07 : -0.07, respectively (when normalized to the initial polarization of H4). After two fast field changes to B_{ev} = 0.1mT and back to the detection field, they undergo a remarkable change to 0.75 : 0.4 : -0.1 : 0.4 : -0.07. Thus, neither the ratio of CIDNP on the individual protons, nor their sum is conserved. Interestingly, the polarization is not equalized as one could expect from their common relaxation times in low field or from the similarity of the CIDNP field dependences discussed in previous sections.

The residence time in the intermediate level anti-crossing fields is in the order 300ms, as can be seen from the calculated time profiles in figure 4.2.1. This time is rather short as compared to cross relaxation rates (see chapter 4.1, figure 4.1.8) that are several orders of magnitude slower and rule out a stochastic process to cause the transfer of HP. Furthermore, cross-relaxation would lead to equal polarizations for H4 and H7, and not to the overshoot seen in fig. 4.2.4.

Between 0.8T and 1.3T the polarization primarily formed on H4 is very efficiently transferred to H7. The exchange of polarization between H4 and H7 goes through a broad (the width is about 0.1T) maximum centred at B_{ev} = 0.157T, where a very efficient transfer takes place over five chemical bonds (see chemical structure in fig. 4.2.4), and the polarization is nearly fully transferred. The CIDNP on the protons positioned in-between (H5 and H6) is also affected by

the polarization transfer, showing less pronounced peaks and dips. The energy levels for the four spin-system comprising H4, H5, H6 and H7 are calculated in chapter 4.0 and shown in figure 4.0.3. It turns out that two nuclear levels within the $J_z = 0$ manifold closely approach each other at B = 1.27T with a splitting of 0.4 Hz. In high field these two states correlate with the Zeeman states |βααβ⟩ and |βααβ⟩ of protons H5, H6, H7, and H4, respectively.

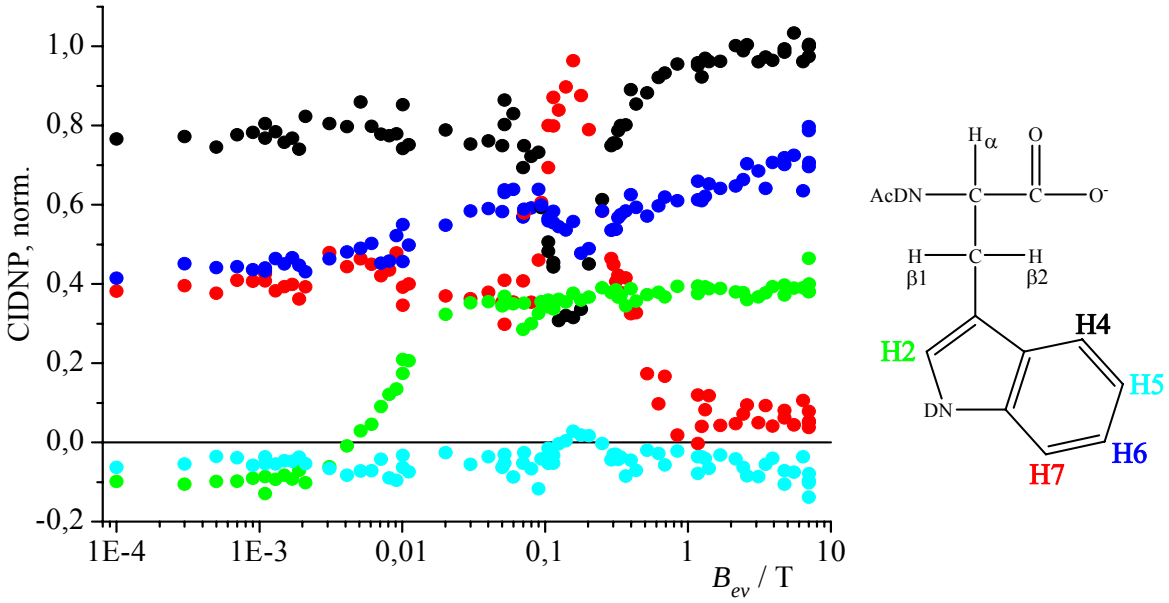

Figure 4.2.4: CIDNP redistribution in the indole ring of NATrpH after photoreaction with 4-CBP in high field (B_{pol} = 7T) and two fast field switches to B_{ev} (varied) and to B_0 = 7T.

The collective dynamic behaviour of all coupled nuclear spins is suspected to lead to the efficient transfer of HP, since the direct spin-spin coupling between H4 and H7 is as small as 0.8 Hz (see table 4.0.1). Obviously it is sufficient that they are coupled strongly via H5 and H6. This particular case of efficient transfer of HP is studied in more detail in chapter 4.3, where the transfer kinetics are probed upon slow and fast sample transfer. There it will also be shown, that the two abovementioned states are crucial to the process of transfer of HP in this case. For the α-proton, the redistribution of CIDNP after two fast field changes is partly shown in figure 4.2.6 c).

The experiment discussed here generally demonstrates the capabilities of new experimental protocols in field cycling NMR, for the efficient transfer of HP in coupled multi spin-systems. Because of the timing scheme of the experiment employing a fixed value of 1.1s for the two field switches and the spin evolution period in intermediate field ($2\tau_{fv}+\tau_{ev}$ = 1.1s), one can assume that the results cover only a very narrow window of possible polarization transfer

pathways in the coupled multi-spin system of NATrpH. It is anticipated, that a variation of the timing for different field values, B_{ev} and/or B_{pol} may open a variety of other transfer pathways, not only for the amino acid under investigation, but also in other molecules with spin-systems fulfilling the strong coupling condition at low or intermediate fields. Expanding the experimentally available range of B_{ev} to even lower fields should also open the possibility of transferring HP among hetero-nuclei.

Magnetic fields, in which the nuclear spin systems show anti-crossings, are of particular importance for the efficient transfer of HP. These fields manifest themselves in various kinds of field cycling NMR experiments, as will be briefly emphasized in the following section by comparing the results of different experiments for these particular field regions.

Manifestation of level anti-crossings in different field cycling experiments. In different kinds of field cycling experiments, one can find peaks or dips that occur at magnetic fields where the nuclear spin eigen-states anti-cross. These features are not restricted to the amino acid tryptophan, as shall be shown by comparing the present results to experiments on a second CIDNP-active amino acid, namely N-acetyl-histidine (NAHis).

The effects are demonstrated on two level-crossings showing up in the spin sub-system containing the two β-CH_2 protons, the α-CH-proton, and the H2-proton of NATrpH. The NAHis molecule contains a similar spin sub-system with the proton H4 ($\sigma_{H4(NAHis)}$ ~ 7.3ppm) located in a position similar to that of H2 in the case of NATrpH ($\sigma_{H2(NATrpH)}$ ~ 7.2ppm). Whereas the magnetic properties of the radical species of the two molecules differ considerably, the protons in α- and β-positions of the diamagnetic products have almost the same chemical shifts and spin-spin interaction constants. Figure 4.2.5 compares the structures of the two CIDNP active amino acids with their common four-spin system highlighted.

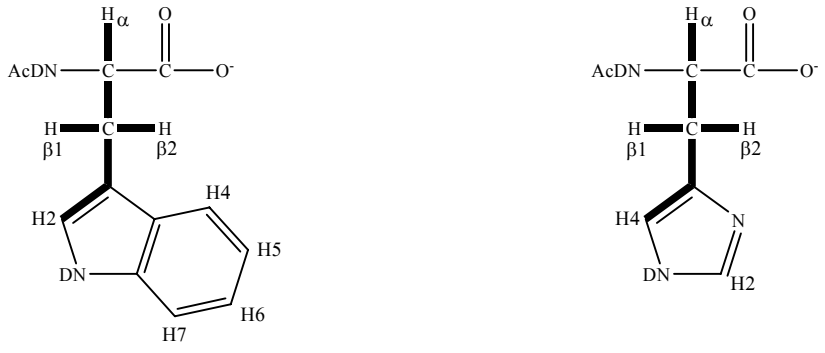

Figure 4.2.5: Structures of the two CIDNP active amino acids NATrpH (left) and NAHis (right) with their common spin-sub-systems highlighted.

The two level-crossing considered here occur in the J_z = -1 manifold and are calculated for NATrpH in chapter 4.0 (see fig. 4.0.4). The first one is located around $B \approx 0.3$ T and is shown in figure 4.2.6 a). In figure 4.2.6 b), the CIDNP field dependence of the α-proton obtained in the quenching reaction of tryptophan with 2,2'-dipyridyl (DP) (discussed in chapter 6.2.3) clearly shows a peak that coincides with the calculated anti-crossing at $B \sim 0.3$ T. This peak is accompanied by a dip in the field dependence for one of the β-protons (see fig. 6.3.10). It was reproduced in quenching reactions with other dyes, namely anthraquinone-4-sulfonic acid, 3-N-(carboxymethyl)lumiflavin (Flavin I), and 4-carboxybenzophenone, and also appears in the absence of a sensitizer (see fig. 6.1.6 a)). This observation has lead to the notion the sharp features do not have their origin in the radical pair stage, but in the diamagnetic reaction products. In CIDNP formed on the β-protons during the reaction of NAHis with DP [11] the dip is also discernable (fig. 4.2.6 b)), but it is not seen as clearly as on the α-proton in the case of NATrpH. CIDNP of the α-proton was not considered in ref. [11] because of its small HFC in the radical pair state.

In the experiment employing two field switches (with $B_{pol} = B_0 = 7$T as described in the previous section), an emissive feature is detected at the same field value ($B_{ev} = 0.3$T); this dip is shown in figure 4.2.6 c) and corresponds to the emissive polarization that can be seen on the signal at 4.4ppm in the spectrum shown in figure 4.2.3 (fourth trace). In addition, the T_1-value of one of the β-protons also shows a pronounced increase in the same field region (see fig 4.1.3). Together, these observations strongly indicate that the peaks and dips originate from the spin evolution in the diamagnetic product molecules in the regions of anti-crossings.

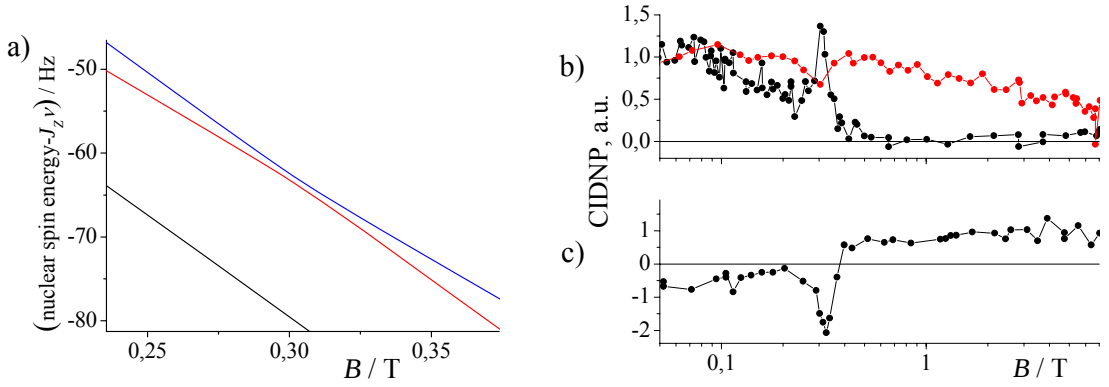

Figure 4.2.6: a) Calculated energy levels and crossing between the Zeeman spin states |ββαβ⟩ (blue) and |βαββ⟩ (red) of the NATrpH-protons β1, β2, α and H2, respectively. b) CIDNP field dependences of α-proton in NATrpH (black) and of the β-protons in NAHis (red, from ref. [11]). c) Hyper-polarization on the α-proton after CIDNP formation in high field ($B_{pol} = 7$T) and two consecutive fast field switches.

Another level-anti-crossing occurs between the states that correspond to the Zeeman states with the spin configurations |βββα⟩ and |ββαβ⟩, for the β1-, β2-, α- and H2-protons in NATrpH, respectively. It is located around B = 0.071T and the calculated energy levels are shown in figure 4.2.7 a) (and in fig. 4.0.4). Here, the proton in position 2 of NATrpH acquires significant polarization after the photoreaction with DP, as can be seen in figure 4.2.7 b). Correspondingly, emissive and absorptive features were detected on the H4-proton of NAHis in reference [11] at the exact same field value (see also fig. 4.2.6 b). These parallels further justify the comparison of the spin-sub-systems in tryptophan and histidine as done in fig. 4.2.5.

Finally, it is shown in figure 4.2.7 c) that features occur in the T_1-dispersions of NATrpH (H2) and NAHis (H4) at the exact same field value. They are thus both attributed to the level-crossings occurring in the similar spin-sub-systems of the two amino-acids. The T_1-dispersion for NATrpH is published in ref. [75].

The coincidence of the features with the calculated anti crossings shown in figure 4.2.6 and 4.2.7 indicate that the correct signs of spin-spin couplings were taken for the simulation of the NMR spectrum of NATrpH shown in figure 4.0.1. Similar features have been observed before in CIDNP field dependences of N-acetyl histidine (NAHis) in the work of S. Grosse [10, 11, 40] and can now be attributed to the corresponding level-crossings in NAHis, showing that the effects are not unique to the amino acid tryptophan.

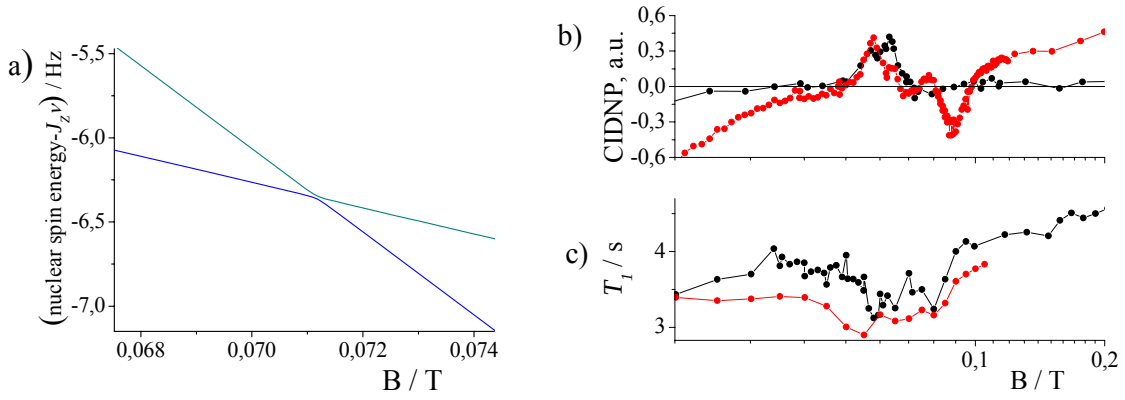

Figure 4.2.7: a) Calculated energy levels and crossing between the Zeeman spin states |βββα⟩ (green) and |ββαβ⟩ (blue) of the NATrpH-protons β1, β2, α and H2, respectively. b) CIDNP field dependence of the H2 proton in of NATrpH (black) and H4 of NAHis (red, from ref. [11]) c) NMRD of H2 proton in NATrpH (black) and H4 proton of NAHis (red).

The three-spin system consisting of two β-CH_2 protons and the α-CH proton is a pattern commonly encountered in virtually any naturally occurring amino acid. The anti-crossing at

~0.3T is found when taking only these three spins into account [55] and may thus provide an efficient way of channelling polarization to target nuclei in bio-molecules like proteins, as it may be applied in large spin systems such as chains of coupled homo-nuclear spins (e.g. methylene or methyl groups) in protein backbone or side chain experiments.
The peaks and dips that occur in different kinds of field cycling NMR experiments can now clearly be attributed to spin dynamics in the diamagnetic product molecules. In the next chapter, a more detailed insight into the nature of the spin evolution in the anti-crossing regions shall be provided.

Conclusions

The scalar coupling among spins provides an efficient way for the redistribution of HP. As a consequence the field dependence of CIDNP tends to be similar for the strongly coupled nuclei irrespective of their hyperfine coupling in the radical pair stage. Even at very low fields, i.e. when the condition for strong coupling among protons is practically always fulfilled, the redistribution of HP does not occur instantaneously but on the time scale of their reciprocal coupling, J^{-1}. This means that the time during which HP is formed is inevitably convoluted with the outcome of the field cycling experiment. Only if the time for irradiation, τ_L, is kept short with respect to the scalar coupling, the shape of the CIDNP field dependence in low field can provide information on the spin density distribution in the precursor radicals. In any other case this information is lost and attempts to extract HFC's for the individual proton sites in coupled spin-systems are to be considered with care.
As a positive aspect, however, the transfer of HP by field cycling NMR can be exploited for guiding HP from primary polarized spins to previously unpolarized spins. This transfer is possible even when the two spins are not coupled directly, but along chains of spacer spins in which each spin is coupled to its nearest neighbour. Thus, the transfer of HP in not restricted to spins that are coupled directly. It is possible to transfer HP via several spacer spins, i.e among spins that are not coupled significantly by scalar interactions (e.g. H4 and H7 in NATrpH).
The efficiency of HP transfer passes through minima and maxima when the field for the spin evolution is varied. Under certain conditions, it is possible to archive levels of HP on formerly unpolarized spins that is even above that of the primarily polarized spins, hence it is suspected that the transfer proceeds via coherences. This assumption shall be verified in chapter 4.3.

In various field cycling experiments, features are observable at the field values where level anti-crossings occur. Because the chemical shifts and scalar couplings are related to the structures of the molecules under study, those molecules that have similar structural features give rise to minima and maxima that occur at the same field values. They are observable for different molecules with similar sub-structures in NMRD data, CIDNP field dependences, and in the HP transfer experiments that employ two field switches. The positions level anti-crossings do not only provide information on the signs of even very small spin-spin interactions, which are hardly accessible by other NMR techniques, but they are also of particular importance for the efficient transfer of HP within coupled multi spin-systems as will be further shown in the next chapter.

4.3 Transfer of Coherence into Polarization by Fast Field Variation

In the previous section, it turned out that the transfer of hyper-polarization occurs particularly efficient within the regions where the energy sub-levels of a given manifold with the same total spin projection, J_z, anti-cross. In order to elucidate the dynamics of the polarization transfer processes in more detail it is necessary to record its kinetics, i.e. the spin evolution in the diamagnetic products of the radical reactions in which CIDNP is formed. The aim of this section is, to experimentally explore suitable conditions for an efficient transfer of HP by field cycling NMR in more detail, and to probe the physical limits of coherence transfer.

While the transfer of coherences (off-diagonal elements in the spin density matrix) among spin-states forms the basis for a variety of multi-dimensional NMR experiments [49], their role in field cycling experiments has hitherto not been established. In the present chapter it is demonstrated that the efficiency of polarization transfer found in the previous chapter is not only due the strong coupling condition among the spins being fulfilled, but a consequence of the transfer of coherences into polarization.

The quantum adiabatic theorem [76] tells that, when external parameters change very slowly a quantum system prepared in its eigen-state of the initial Hamiltonian evolves into one of the eigen-states of the final Hamiltonian if the rates of non-adiabatic transitions between different instantaneous eigen-states are negligible during the evolution. When changes of the Hamiltonian occur rapidly (non-adiabatic), the state also gains some dynamical phase factor (or coherence). Here, it is not the coherences excited by RF-pulses that are discussed, but coherences that are formed either during the recombination of radicals in the course of a photo-chemical reaction, or by non-adiabatic field switches in the process of field cycling.

It shall be shown that the sudden character of the changes in the Hamiltonian is a prerequisite for the conversion of polarization (differences in the diagonal elements of the spin density matrix) into coherences and vice versa. This is demonstrated experimentally by a variation of the velocity of the sample transfer in the field cycling schemes devised in the previous chapters. Manipulations in the timing schemes of field cycling experiments in terms of computer controlled passages to certain field values can be utilized for site selective polarization transfer and are of potential use for boosting the sensitivity of the method.

Experimental

Timing schemes. The first experiment discussed here, resembles that for the acquisition of a CIDNP field dependence (see chapter 3.2, fig. 3.2.4), with the only difference that after the generation of HP at certain field values, the spin-system is allowed to freely evolve during a variable evolution time, τ_{ev}, at B_{pol} (= B_{ev}) which is placed in-between sample irradiation and field variation. The experiment thus starts with a waiting time (~5*T_1) in low field, that is sufficiently long to destroy the background polarization. The sample is then moved quickly into a field, in which features such as peaks or dips have been detected during the acquisition of CIDNP field dependences. Then CIDNP is formed by irradiating the sample with a short train of laser pulses at 308nm, typically τ_L = 0.2s to 0.5s at a repetition rate of 50Hz. The formation of HP is followed by a variable delay time, τ_{ev}, at B_{ev} = B_{pol}. After the delay time, the probe is transferred rapidly (τ_{fv} ≈ 0.3s) into the detection field, where the FID is recorded by means of an RF-pulse.

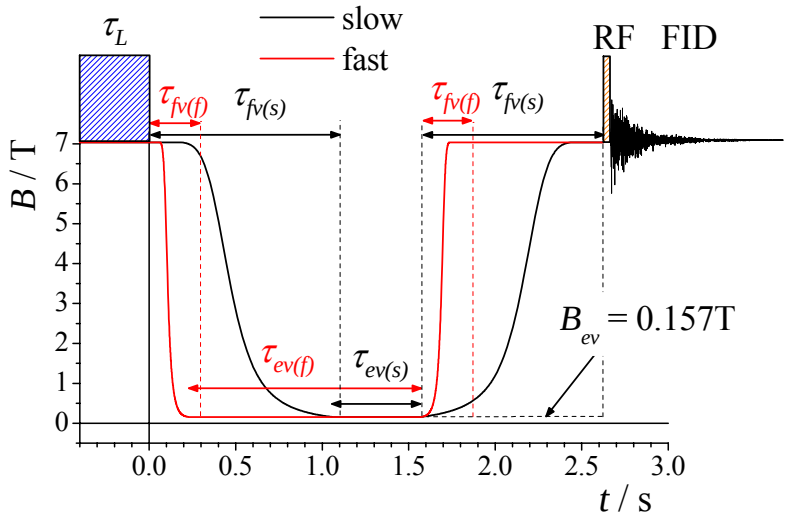

Figure 4.3.1: Realistic timing schemes for the comparison of HP transfer kinetics upon fast (τ_{fv} = 0.24s) and slow (τ_{fv} = 1.1s) field variation.

The second experiment parallels the one that has been introduced in the previous section (see fig. 4.2.1 and the red trace in fig. 4.3.1). Again, the background polarization is removed by keeping the sample in the lowest position, before CIDNP is formed in the high field of the spectrometer (B_{pol} = 7T). The sample is then quickly transferred to B_{ev} = 0.157T with τ_{fv} = 0.24s (at this field value a particularly efficient polarization transfer from H4 to H7 in NATrpH was found in chapter 4.2). Here the time τ_{ev} is varied, in order to record the kinetics

of the polarization transfer. Finally, the sample is moved back (τ_{fv} = 0.24s) to B_0 = 7T, where the FID is recorded.

For the third experiment introduced is this chapter realistic timing schemes are shown in figure 4.3.1. The experiment aims at the elucidation of the physical limitations for an efficient conversion of coherences into polarization, and is the only experiment for which the necessity of non-adiabatic field switches has hitherto been proved successfully. The sequence of experimental steps is the same as in the experiment described above, and involves two consecutive field changes after polarization is formed in the high field of the spectrometer (B_{pol} = 7T). Now, the experiment is performed twice with fast (red trace in fig. 4.3.1) and slow (black trace in fig. 4.3.1) field variation. In-between the two field switches, the time for free evolution of the spin system, τ_{ev}, is varied at B_{ev} = 0.157T. Finally the kinetics of the transfer of HP is detected by means of a 90°-RF-pulse and the acquisition of the FID.

Sample preparation. The samples are prepared according to the description in chapter 4.2. Coherence transfer experiments were performed with two different solutions: sample a) 2mM NATrpH and 1mM 4-carboxybenzophenone (CBP) at pH 11 and sample b) 5mM NATrpH and 2mM DP at pH 13.

Results and Discussion

Variation of the evolution time after irradiation in level crossing fields. Two level anti-crossings occur in the four spin system consisting of the two β-protons, the α-proton and the H2 of NATrpH. Their position is calculated using the NMR parameters of NATrpH listed in table 4.0.1. As described above they lead to characteristic features in different kinds of field cycling experiments. Similar features are also seen for the corresponding spin-sub-system in NAHis (see chapter 4.2).

In the experiment considered here, the spin evolution time, τ_{ev}, is varied after HP is formed near the level crossing regions in order to probe the kinetics of the transfer of HP. Because both level crossings occur in the same manifold (J_Z = -1) (see fig. 4.0.4), they are expected to affect each other in experiments were the field is swept through both of them. It is therefore straightforward to start with the simpler case, the level anti-crossing that occurs at higher field (B = 0.32T).

For the generation of HP at B_{pol} = 0.32T, sample a) (see sample preparation on p.108) was irradiated during τ_L = 0.2s. Figure 4.3.2 a) shows selected spectra for different delay times, τ_{ev}, after CIDNP is formed in the vicinity of the level crossing region (B_{pol} = B_{ev} = 0.32T). When the field is switched to the detection field, B_0, immediately after irradiation (τ_{ev} = 0s), the spectrum shown in the bottom is obtained. Here, the β-protons show a pronounced multiplet effect, while practically no polarization is discernable at the position of the signal for the α-proton (4.6 ppm). This is in accord with the expected polarization pattern, because the β-protons are located close to the indole ring, which carries large spin density above and below the plane of the aromatic system. In contrast, the more remote α-proton has only a small HFC in the radical pair state. When a short waiting time of τ_{ev} = 0.4s is introduced, the polarization pattern has changed significantly, and the signal of the α-proton acquires very high absorptive HP. Depending on the RF flip-angle for the detection, different polarization-patterns are achievable for the signal of α-CH: The pattern seen in figure 4.3.2 a), with the two α-lines in high field polarized stronger is obtained with a 270°-pulse. When a 90°-pulse is applied, all four α-lines are equally polarized, and with a 30°-pulse the two low-field lines show a higher signal (not shown).

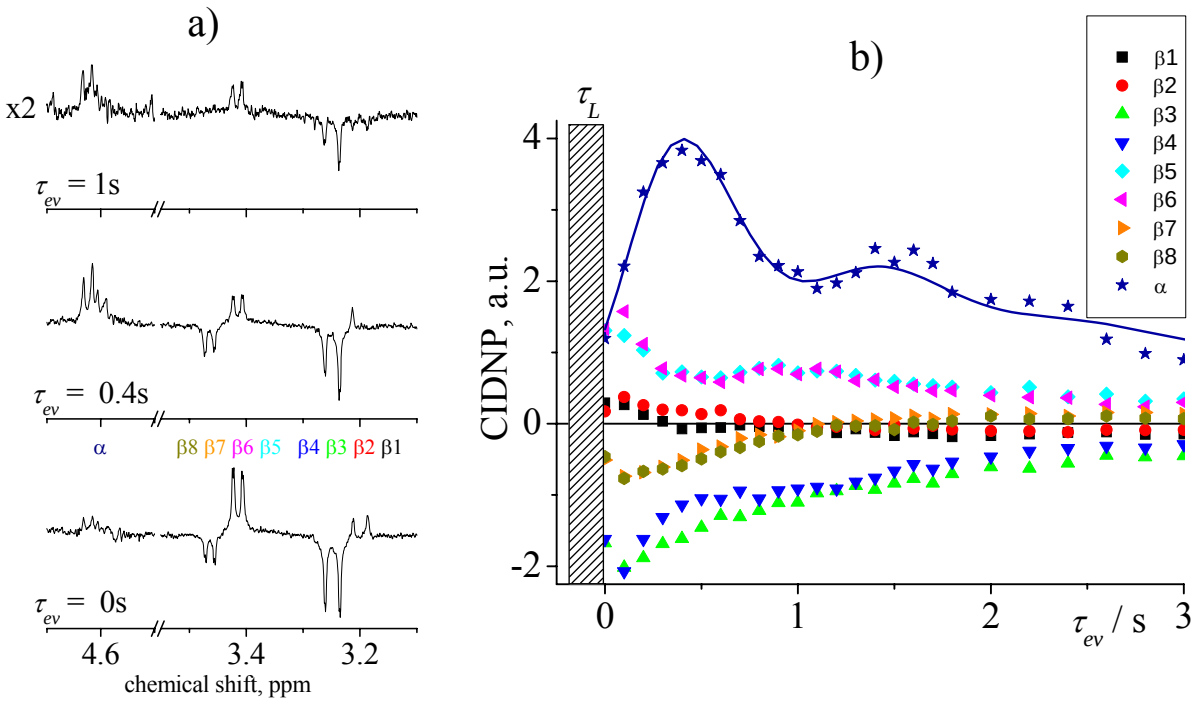

Figure 4.3.2: a) CIDNP-spectra of α-CH and β-CH_2 for different delay times, τ_{ev}, at B_{pol} = B_{ev} = 0.32T. b) Spin evolution of α-CH and β-CH_2 signals of NATrpH after photoreaction with CBP in the level crossing field (B_{pol} = 0.32T) and variable evolution time, τ_{ev}, after the CIDNP formation ($\tau_{fv} \approx$ 0.3s, φ = 270°).

At the same time, the amplitudes of the individual lines of the two β-protons also evolve unequally: while some lines have lost their polarization completely, others remained almost constant. The uppermost spectrum in figure 4.3.2 a) shows the situation after τ_{ev} = 1.2s. It is blown up by a factor of two since much of the polarization has already decayed due to relaxation. However, it is clearly seen that some of the lines (β1 and β2) changed their sign with respect to the initial polarization pattern. Such substantial changes in polarization pattern can certainly not be accounted for by the perception of cross relaxation, and an alternative explanation had to be found.

In figure 4.3.2 b) the integrals of individual β-lines and the total intensity of all four α-lines are plotted over τ_{ev} which was incremented in steps of 0.1s. It can be seen that the signals exhibit beatings, i.e. they contain contributions which oscillate when the evolution time, τ_{ev}, is varied. The periodic changes in signal amplitudes clearly indicate that the changes are due to dynamic quantum evolution of the system. The frequency of the oscillation seen on the α-signal agrees very well with the splitting of the anti-crossing energy levels ($\Delta E/h \sim 1$Hz) seen in fig. 4.2.6 a). These levels correspond to the Zeeman spin states $|\beta\beta\alpha\beta\rangle$ (blue) and $|\beta\alpha\beta\beta\rangle$ (red) of the NATrpH-protons β1, β2, α and H2, respectively. Thus, the coherence between these states can cause an exchange of magnetization between the CH-protons in the positions β2 and α.

At 0.32T, very efficient transfer of HP between the β2-proton and the α-proton is thus obtained by exploiting the coherence among the anti-crossing spin-states. In this field range, the chemical shift difference to the H2 proton is already so large that this proton is only weakly coupled to the β-protons. In ref. [55] it was shown that it suffices to reduce the calculation to the three spin-system of the two β-protons and the α-proton to arrive at the conclusions that concern the level crossing at 0.32T.

Before the observation of the quantum beats is explained in more detail, a second example for the experimental detection of oscillations in the signal amplitude shall be given. When NATrpH is polarized in the presence of 2,2'-dipyridyl as a sensitizer (sample b), see p.108), a peak is obtained in the CIDNP field dependence around B_{pol} = 0.062T (see figure 4.2.7 b), chapter 4.2). In contrast to the observation discussed above, this peak is exclusively detected with this particular sensitizer (DP), but not with any other dye. Nevertheless, its appearance is attributed to the quantum evolution in the diamagnetic NATrpH molecule.

Figure 4.3.3 shows how the amplitude of HP on the proton in position 2 of NATrpH grows on the timescale of some hundreds of milliseconds, i.e. when all the radicals in the solution have

already decayed. Again, the variation of the evolution time, τ_{ev}, shows the presence of quantum beatings with a frequency corresponding very well to the difference in energy levels at this field (B_{pol} = B_{ev} = 0.62T). The data for H2 in fig. 4.3.3 are fitted with a coherence frequency of $\Delta E/h$ = 1.5Hz. Because a relatively long irradiation time (τ_L = 0.5s) is necessary to obtain appreciable polarization in this field range, the beatings are only seen clearly for a quarter of a period because they tend to be washed out during τ_L. Nevertheless, this observation shows that the formation of coherences during the termination of the radical reaction is not unique to the level crossing at 0.32T, but that quantum beatings are also present near the level crossing region around 0.07T.

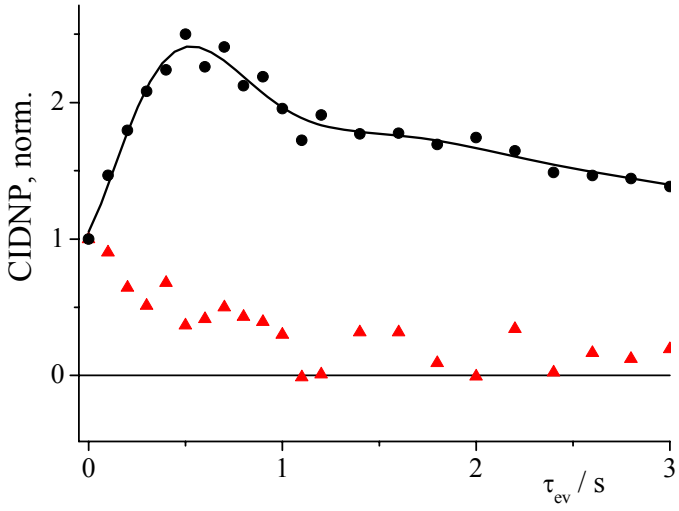

Figure 4.3.3: Evolution of HP in the NATrpH molecule after photoreaction with 2,2' dipyridyl (DP) at B_{pol} = B_{ev} = 0.062T. • : CIDNP of H2-proton, • : CIDNP of α-CH-proton.

Here, it is the Zeeman spin states |βββα⟩ and |ββαβ⟩ of the NATrpH-protons β1, β2, α and H2, respectively (see fig 6.2.7 a)), that anti-cross at B = 0.71T. The zero-quantum coherence thus opens a polarization transfer pathway between α-CH and H2, i.e. between two spins that are not noticeably coupled in the high field of the spectrometer. This assignment allows a qualitative explanation why the level crossing at 0.071T is only detected with DP, whereas that at 0.32T is detected in field dependent CIDNP experiments with any dye. During the photo-reaction of DP with NATrpH, HP of relatively large amplitude is generated on the α-proton in this field range (see fig. 6.2.9), which is unique to this reaction system.

The deviating polarization pattern of NATrpH with DP suggests that the photo-chemistry of this reaction system differs, but the actual difference remains open and is not subject to this

chapter. Here, only the evolution of HP in the product molecules should be discussed. Because neither the α-proton nor any other of the protons in the four spin sub-system under consideration acquires HP with other sensitizers than DP in this field range, no polarization is transferred to H2 in these cases.

In the work of S. Grosse [11], features in the CIDNP field dependence were observed for the H4-proton of NAHis in the same field region. These features can now be attributed to the anti-crossing that occurs in the corresponding spin-system of NAHis (see figs. 4.2.5 and 4.2.7a)), and in his work, also DP was used as a sensitizer. Because of the vicinity of the solvent line, no CIDNP was reported for the α-proton of NAHis in ref. [11], but the above considerations strongly suggest that it exists also in this reaction system.

Together with the observations presented in chapter 4.2, the peaks and dips observed in the field dependences of CIDNP are explained in the following way: Coherences that oscillate with the frequency $\Delta E/h$, corresponding to the difference in energy between different eigen-states of the spin system, are present after rapid changes of the Hamiltonian. These rapid changes are achieved by the process of CIDNP formation, because the nuclear spin eigen-states in the radical pair do not coincide with those of the reaction products. Thus, after the radical pair recombines coherences have formed. The coherences formed in fields where the spins form strongly coupled systems have hitherto been neglected when analyzing the polarized spectra. They are present after CIDNP formation and transferable into polarization by means of non-adiabatic field switches, B_{ev} to B_0. The field variation from B_{ev} = 0.32T to B_0 = 7T was discussed in some detail in the theoretical section (fig. 2.2.4, chapter 2.2).

It is important to emphasize that the time in which CIDNP forms has to be kept short, when the experiment is aimed at the observation of coherences, since these will only constructively interfere for a time that is considerably shorter than their respective frequency. Otherwise they will be washed out. In the following section it will be shown that coherences can not only be obtained during the recombination of radicals, but also by rapidly switching the field.

Variation of τ_{ev} in low field after CIDNP formation in high field. The experiment discussed here employs two fast field switches. A realistic timing scheme is given in figure 4.3.1. In chapter 4.2 it was shown, that HP formed at B_{pol} = 7T is exchanged very efficiently between the protons H4 and H7 in the six-membered ring of NATrpH by rapidly switching the field to B_{ev} = 0.157T and back to $B_0 = B_{pol}$ = 7T (see fig. 4.2.4). Tracing this particularly efficient transfer of polarization is possible by a set of experiments in which the system is allowed to develop freely during an evolution period, τ_{ev}.

The spin evolution during τ_{ev} at B_{ev} = 0.157T after photoreaction of NATrpH with CBP (sample a), see sample preparation on p.108) at B_{pol} = 7T is shown in figure 4.3.4. The signals of the protons H4 and H7 exhibit beatings that are exactly 180° out of phase. Periodic changes are also seen for the other aromatic protons, in particular for H5. The beatings in the signal amplitude of H4 and H7 have a frequency of approximately $\Delta E/h$ = 3.2 Hz and persist for several seconds with an amplitude that constitutes about half of their polarization. Those of H5 obviously contain more than a single coherence frequency. The amplitude of the oscillations is considerably larger than in the cases discussed above. These observations can be understood in the following way: Here, the coherence is not formed during the recombination of the radicals in the time interval τ_L, but during a much shorter time interval, namely the non-adiabatic variation of the magnetic field during the process of field cycling through a level crossing region.

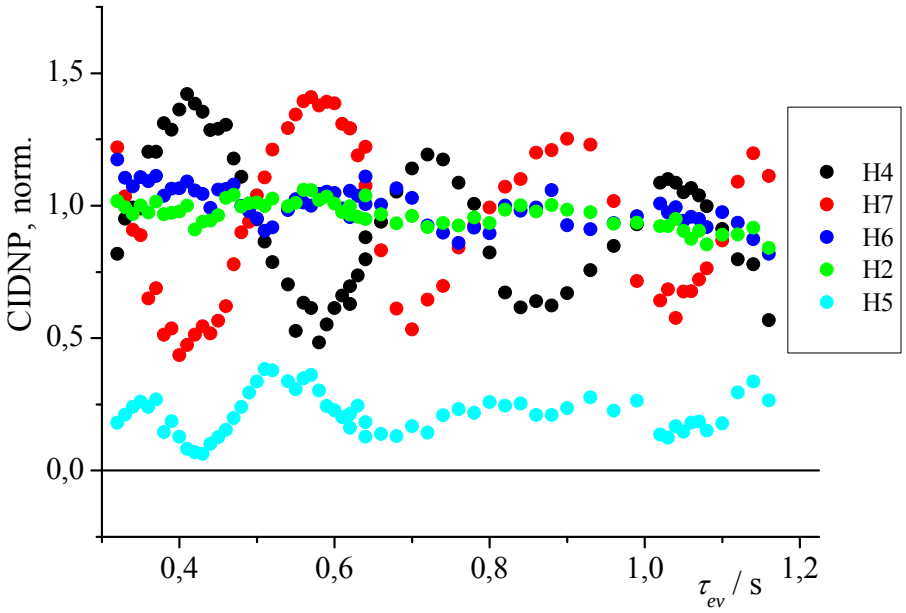

Figure 4.3.4: Spin evolution of the aromatic protons in the indole ring of NATrpH at B_{ev} = 0.157T after photoreaction with 4-CBP at B_{pol} = 7T and two fast field switches ($\tau_{fv1} = \tau_{fv2} \approx$ 0.3s, see fig. 4.3.1).

The spin-spin coupling between H4 and H7 is as small as 0.8 Hz (see table 4.0.1), while the beatings in fig. 4.3.4 have a frequency of 3.2 Hz. Qualitatively, the unprecedented polarization transfer between H4 and H7 over five chemical bonds can be explained when considering the energy levels of the spin states of the spin sub-system that consists of H4, H5, H6 and H7 of NATrpH (see fig. 4.0.3, chapter 4). The six energy levels in the manifold with total spin projection J_Z = 0 show several anti-crossings, one of which is located at B = 1.27T with a splitting of 0.4 Hz at the closest approach. At high field, the two crossing energy levels

correlate with the Zeeman states with projections |βααβ⟩ and |αββα⟩ of the protons H5, H6, H7 and H4, respectively. At B_{ev} = 0.157 T, the same energy levels have a distance of 3.2 Hz, which is exactly the frequency of the beats observed for H4 and H7. Although the beats are most pronounced for H4 and H7, it can be concluded that the whole four spin-system participates in the coherent evolution of HP, and that the 'spacer-spins' H5 and H6 act as a 'bridge' for the transfer the polarization over five chemical bonds.
Inducing coherence by the sudden field variation through a level-crossing, here at B = 1.27T, is thus well suited for the visualization of the coherences, because their observation is not obstructed by the finite irradiation time, τ_L.

Variation of the transfer time, τ_{fv}. It still remains to prove that the non-adiabatic field variation is an essential requisite for the efficient transfer of coherence into polarization and vice versa. For accomplishing this objective, the beatings of H4 and H7 in NATrpH (sample a)) after two fast field variations are chosen, because they last for several seconds with large amplitude, thus allowing one to repeat the experiment with slow sample transfer. A realistic timing scheme for this experiment is given in figure 4.3.1.
The beatings for H4 and H7 seen in fig. 4.3.5 a) are the same data as in figure 4.3.4. Here, the two curves are fitted with a single coherence frequency ($\Delta E/h$ = 3.2 Hz) and two decay constants for the coherence decay and for the loss of signal intensity (T_1). Figure 4.3.5 b) compares the spin evolution at B_{ev} = 0.157 T after CIDNP formation at the spectrometer field (B_{pol} = 7T) upon fast and slow sample transfer. Here, the delay between the second field jump (at t = 1.5s in figure 4.3.1) and detection pulse (at t = 2.6s in figure 4.3.1) was extended in order to consecutively probe the differences between slow and fast sample transfer under comparable conditions. This means that the RF-pulse was placed more than 2.5s after the irradiation. Thus, the coherences shown in figs. 4.3.5 a) and b) are affected differently by relaxation. However, it is clearly seen that the coherences are still present after 1.2s when the sample is transferred rapidly from B_{pol} to B_{ev} and back.
When using the slow cycling time, τ_{fv} = 1.1s, the beatings vanish, while some polarization remains. This behaviour is taken as a solid piece of evidence that the oscillations are caused by spin coherences and that the non-adiabatic field-variation is an essential prerequisite for an efficient conversion between coherence and polarization.

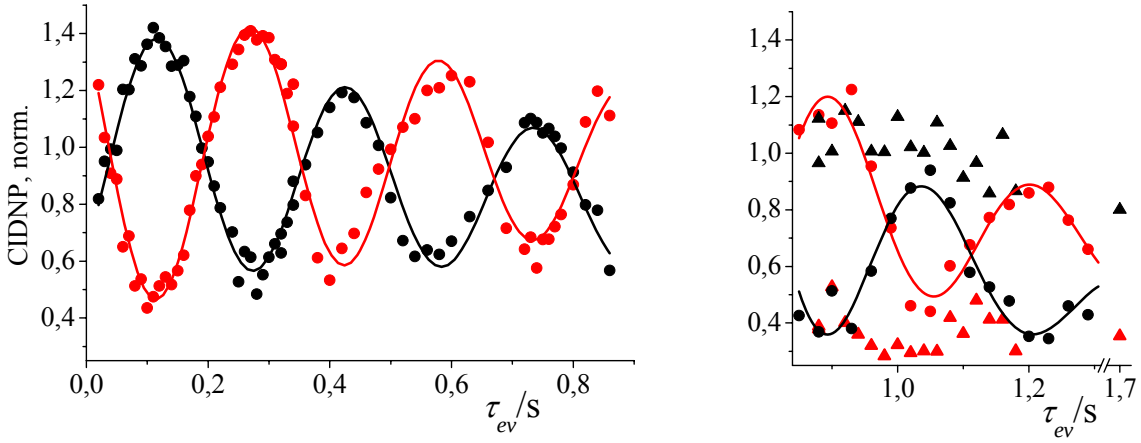

Figure 4.3.5: Dependence of H4 and H7 signal intensities on evolution time, τ_{ev}, at B_{ev} = 0.157T for a) fast field variation (τ_{fv} = 0.29s), •: H4; •: H7, and b) in comparison to slow field variation (τ_{fv} = 1.1s), ▲: H4; ▲: H7. For better comparison, the starting point τ_{ev}= 0 for the slow experiment is taken the same as for the fast experiment.

The first fast passage through the crossing converts polarization of the primarily polarized H4 and H6 at high field into coherence between the coupled states. The coherences oscillate with their characteristic frequencies during τ_{ev}, until the second non-adiabatic field variation in the vicinity of the crossing converts the coherence into polarization, which is observed in the FID after the RF-pulse. It appears that this conversion is particularly efficient in the present case, because the magnetic field gradient in the experimental set-up is relatively large in the level-crossing region around 1.27T (see fig. 3.2.3). The conditions in the present experiments are thus in favour of a sudden field variation, in particular, when the sample is transferred from B_{ev} = 0.157T to B_0 =7T within $\tau_{fv2} \approx$ 0.25s, because it has already reached its maximum speed at B = 1.27T.

Conclusions

The systematic study of the model system NATrpH revealed the following properties of an efficient transfer of HP among nuclei that fulfil the strong coupling condition at low magnetic fields. First, the timing schemes of the field cycling experiments are crucial for a good transfer of HP to non-polarized spins: The efficiency depends on the time interval of free evolution at low field, τ_{ev}, as well as on the time for the field variation from the evolution field B_{ev} to the detection field B_0, τ_{fv}.

Second, the transfer of HP is shown to be a coherent process with its kinetics exhibiting characteristic quantum beats. It is the zero-quantum coherences, i.e. those among spin-states with the same value of the total spin projection (J_z) that can be exploited for transferring HP because they oscillate with frequencies that are on the time scale of the field cycling experiments.

Nuclear spin coherences are shown to be formed i) during the recombination of radicals together with formation of CIDNP and ii) by non-adiabatic field switches through regions where the nuclear spin levels anti-cross. As a consequence characteristic features are found in HP field cycling experiments that may appear as peaks or dips (see chapter 4.2), depending on the timing scheme of the experiment. Regions where nuclear spin levels anti-cross, are of particular importance for a selective transfer of HP between particular nuclei.

Third, in low fields it is possible to coherently transfer HP between spins that show only very weak direct spin-spin coupling via several spacer-spins. The HP transfer process then is a coherent process of the whole multi-spin system in which all spins are coupled strongly to their nearest neighbours. Knowledge of the peculiarities in the multi spin-system under study, thus allows one to develop field cycling schemes that enable a selective transfer from initially polarized spins to certain target spins. Extending the available homogeneous magnetic field range to fields on the μT scale is anticipated to open similar opportunities for the transfer of HP to hetero-nuclei such as ^{15}N or ^{13}C and may help to overcome shortcomings from their low sensitivity, which is still the critical time constraint of magnetic resonance imaging (MRI) techniques for these nuclei. Finally, it is pointed out that the polarization transfer phenomena considered here are not unique to CIDNP and are expected to arise also in other low-field experiments on hyper-polarized spin systems. For example, the mechanism discussed above can also explain the ALTADENA experiments with long-range polarization transfer that has recently been reported [77].

5 Analysis of High Order Multiplet CIDNP by Fourier Expansion of Nutation Patterns

Polarized NMR spectra of molecules exhibiting spin-spin couplings generally reveal polarization patterns that can be separated into so-called net and multiplet contributions. While net CIDNP effects are represented by the intensities integrated over the entire multiplet signal belonging to a single spin with its scalar couplings, the multiplet CIDNP effects are characterized by the appearance of emissive and absorptive lines within one particular multiplet. They are obtained by taking the intensity differences of lines with equal transition probabilities within a given multiplet.

When the CIDNP intensities are detected by slow passage cw-NMR, the RF-excitation field is small and the intensities of spectral lines is directly proportional to the population differences of the nuclear spin levels associated with the transitions. In FT-NMR the polarization is read out by a non-selective excitation pulse. In this case, the so-called parallel transitions (transitions that involve the same spin) affect each other, and the pattern of the spectral intensities strongly depends on the spin flip angle, φ [50]. On resonance, φ is proportional to the amplitude of the RF excitation pulse, B_1, and to the length of the applied pulse, τ_{rf} (formula 2.2.12). The observed intensity of a particular transition in the FT-NMR spectrum carries pulse angle dependent contributions from all the other transitions in the same multiplet (see e.g. formulae 2.2.13), and the term nutation is commonly used for the flip angle dependent response to the monitoring RF-pulse [57].

The response of two coupled spins-½ to different excitation angles has been studied experimentally and theoretically in a sizable number of works, because their nutation patterns are relatively simple as they consist of $sin\varphi$ and $sin2\varphi$ terms only. Vollenweider and Fischer [52] showed, that for a system of two coupled spins-½ the sum and the difference of two spectra taken at $\pi/8$ and $\pi/4$ yield the net and multiplet CIDNP, respectively. However, for a system of N coupled spins this approach becomes rather complicated. In order to analyse the average mutual alignment of N coupled nuclei, in principle, N spectra of exactly set flip angles would have to be measured and appropriately superimposed. In such complicated superposition of spectra, the noise increases with the square root of the number of spectra involved.

Another possibility of separating net- and multiplet effects in polarized spin systems is the two dimensional J-correlated spectroscopy (2D-COSY) technique, because additional cross-

peaks arise solely from the multiplet polarization. This technique is commonly used in CIDNP investigations of protein structure [78], but in a normal COSY experiment, multiplet effects of higher order than N=2 do not give rise to any cross peaks and one would have to apply more pulses, thus increasing the complexity of the COSY experiment.

The approach presented here, has in principle been indicated in the work of Vollenweider and Fischer [52]. A straightforward extension of the idea to apply pulses of different angles has been worked out theoretically by K. Ivanov [53]. He suggested recording a series of spectra at a stepwise increased rotation angle, and to decompose this set by Fourier analysis into N harmonics. The n^{th} (n = 1,…, N) harmonic then represents the average mutual orientation of n spins, because their contribution to the flip angle dependent spectra depends on φ with $\sin n\varphi$. The theoretical considerations (see chapter 2.2.3 and ref. [53]) are, however, restricted to weakly coupled spin-systems in so-called first order non-equilibrium states, in which coherent superpositions (off diagonal elements of the spin density matrix) are absent, since those can be treated in a closed form.

More recently, it was shown theoretically that the idea of separating multiplet effects of higher order by the variation of the flip angle may be extendable to solids, where strong dipolar interactions are not averaged out completely and the spectral resolution does not allow separating the lines of individual transitions [79]. In a spin echo experiment, the echos in the x-y-plane are focussed in phase and out of phase for multiplet effects of odd and even order respectively, and the contributions of different orders can in principle be separated in the same way by variation of the detection pulse length.

In order to optimize the transfer of polarization to certain target nuclei along a specific pathway, it is desirable to trace the starting populations, P_i, of the individual energy levels i back. The knowledge of the contributions (amplitudes $A_{i\text{-}j}$) of multiplet effects of higher order to the CIDNP spectra is a prerequisite for the determination of the non-equilibrium populations P_i of the individual eigen-states in a coupled multi-spin system. The populations may be used to analyse the polarizing mechanism and hyperfine couplings in the precursor radicals.

In order to establish a general strategy for enhancing the sensitivity of NMR (or MRI) for biological and medical applications, a complete understanding of the appearance of the NMR spectra of multi-spin systems polarized at low magnetic fields is necessary. Thus, particular interest in the populations of the individual nuclear spin states arises from the findings discussed in chapter 4, because phenomena of polarization and coherence transfer by strong scalar coupling can be complicated by the complexity of the multi-spin systems.

The applicability of the analysis of multiplet CIDNP of higher orders *n* by Fourier expansion of flip angle dependent spectra is demonstrated on two prominent experimental examples. In the first case, CIDNP in the cyclic ketone cyclodecanone polarized in zero-field is considered, and the second example deals with the aromatic amino acid NATrpH, which has already been studied extensively in the previous chapter.

Experimental

Spectra with flip angle variation at variable magnetic field were recorded with the field cycling set up described in chapter 3.2. The timing scheme of the experiment is the same as the one used to acquire CIDNP field dependences and is schematically shown in figure 3.2.4. After the background polarization is removed by a suitable waiting time (~5*T_1) in low field, the sample is transferred to the polarization field B_{pol}, where it is irradiated for a time τ_L. Immediately after the irradiation, the sample is transferred to the detection field, B_0 (with τ_{fv} = 350ms for B_{pol} = 0.1mT), where FT-NMR spectra are detected with a single RF-pulse of stepwise increased length.

For the computer supported analysis, it is necessary that the increments in pulse length remain the same, and that a full period from 0 to 360° pulse length is acquired. In order to resolve harmonics of the order *n*, the acquisition of *n* spectra is the minimum requirement. It is therefore recommended to reduce the output power at the pulse amplifier, in order to lengthen the 360°-pulse to an extent that the flip angle can be conveniently incremented. For the present experiments, the pulse power was attenuated to obtain a 360° pulse length of approximately 25μs.

When the length of the applied RF-pulse is stepwise incremented in a CIDNP experiment, the spectral amplitude is successively reduced because of side reactions causing a depletion of the sample. Therefore, the spectra are corrected for the loss in signal amplitude prior to Fourier expansion.

Sample preparation. Sample a): 0.06M cyclodecanone in $CDCl_3$, sample b). 10mM NATrpH with 2mM anthraquinone-2-sulfonic acid (AQ2S) in D_2O, and sample c). 12mM NATrpH with 1.5mM DP in D_2O. All samples were purged with pure N_2 prior to use, and a teflon plug was inserted to avoid vortex formation and sample mixing during the transfer.

Results and Discussion

2D Analysis of nutations in the photoreaction of cyclodecanone in zero-field. The Norrish type I photoreaction of cyclodecanone is outlined in chapter 6.3 (see fig. 6.3.1), where the system is investigated in solid solutions of cyclohexane-d_{12}. The underlying photochemistry is, in part, the same in liquid solutions of $CDCl_3$ and shall not be discussed separately here. CIDNP is formed during the nuclear spin dependent recombination of the two radical centers in acyl-alkyl biradicals [1] generated by the irradiation with near UV light (S-T$_-$ -mechanism). The reaction is particularly well suited for the analysis of nutation patterns because it restores the starting compound to a relatively high extent. A second pathway for the termination is the H-atom abstraction from the β-position of the alkyl end of the biradical to give the unsaturated aldehyde dec-9-enal [80]. Here, the average mutual alignment of nuclear spins in both, the product of the cyclic photoreaction, that returns the original ketone (type I), and the 'side product', i.e. the unsaturated aldehyde, formed in the type II reaction shall be analyzed.
In biradicals, the radical centers stay linked by a polymethylene chain and thus can not diffuse appart. As a consequence the non-zero exchange interaction, J_{ex}, leads to a splitting of the electronic singlet and triplet levels in the biradical; while the external magnetic field determines the splitting between the triplet sub-levels. For the formation of nuclear spin polarization, three different ranges of the magnetic field have to be considered. In very high field ($B_{pol} >> 2 \left| J_{ex} \right| \gamma_e$), where γ_e denotes the gyromagnitic ratio of the electron, S-T_0 transitions prevail, and the spectral pattern reflects the spin density distribution in the transient acyl-alkyl biradical formed after α-cleavage of the cyclic ketone in the triplet state. The largest hyperfine couplings are expected at the alkyl and the acyl ends of the biradical, they can be estimated from corresponding values for analogous monaradicals (-2.2mT and 2.8mT in α and β positions to the alkyl end, respectively [81]. When B_{pol} is chosen closely to the maximum efficiency of ST$_-$-transitions ($B_{pol} \approx 2 \left| J_{ex} \right| \gamma_e$), the polarization is all emissive, irrespective of the sign of hyperfine interactions of the individual protons, because in the vicinity of the electronic level crossing the conditions for $T_{-\alpha}$–S_β-transitions are most favourable (here, α and β denote the projections of the nuclear spin), thus leading to a very efficient depletion of α, and enrichment in β-spins in the products [82].
In magnetic fields much lower than the individual HFC's in the biradical, the polarization pattern differs significantly. During CIDNP formation, all electron and nuclear spin states are coupled strongly by the hyperfine interaction. Singlet-triplet transitions occur according to the

magnitude of the total spin and the electronic transitions are accompanied by nuclear transitions with conservation of the total spin momentum. Because of the selection rules, only multiplet polarization is expected to form in the absence of an external magnetic field, and the nuclei in the multi-spin system are polarized according to their total spin projection quantum numbers, J_z,

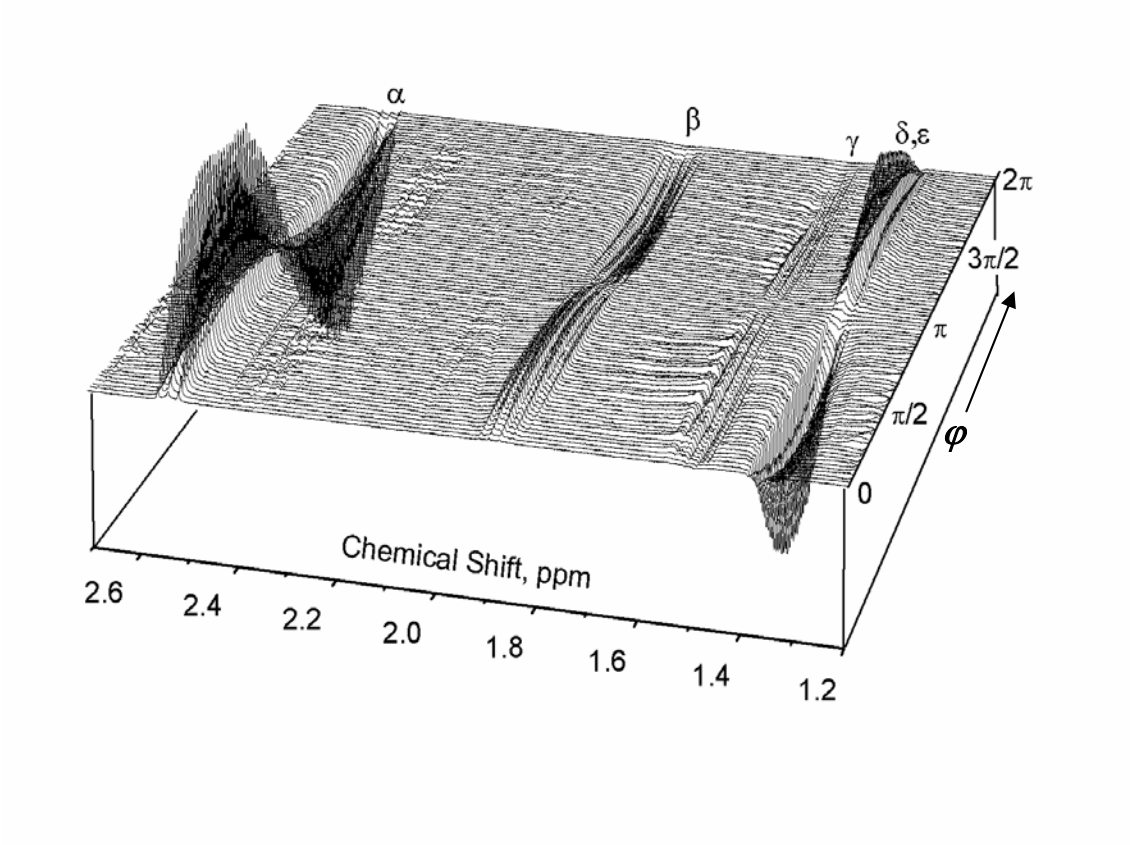

Figure 5.0.1: 2-D NMR spectra of cyclodecanone after CIDNP formation at "zero-field" (B_{pol} = 0.1mT). One axis corresponds to the NMR frequency, the other one to the RF flip angle φ.

Even in the absence of unpaired electrons the nuclear spins are coupled strongly in low fields by their spin-spin interactions, and the energy levels are the collective states of the entire multi-spin system. When all spins are strongly coupled multiplet effects of high order can be expected (see chapter 2.2.3).

Fig. 5.0.1 shows the aliphatic region of the flip angle dependent spectra of cyclodecanone after CIDNP formation in zero-field ($B_{pol} \leq$ 0.1mT). All protons in the product of the cyclic reaction path (cyclodecanone) are polarized irrespective of the hyperfine couplings in the biradical state. The polarization pattern looks highly symmetric: While the protons in δ and ε positions to the carboxylic group (~1.4ppm) are in strong emission at a flip angle $\varphi = \pi/2$, the emission is smaller in the γ-position and gradually turns into strong enhanced absorptive polarization on the α-protons at 2.5ppm. This pattern is interpreted in terms of high order

multiplet polarization that stretches along the whole polymethylene chain of the molecule. In 'zero-field', similar polarization patterns are observed in other multi-spin systems, such as the aromatic amino acids tyrosine [41] , histidine [40] and tryptophan (this work) where all protons are coupled strongly (in low magnetic field).

When looking at the nutation pattern of e.g. the β-protons in fig. 5.0.1, slight deviations from a single sine-function are notable: the signal reaches its maximum amplitude at $\varphi < \pi/2$ at higher field values and at $\varphi > \pi/2$ at lower ones. In order to confirm the interpretation of the observed zero-field polarization pattern, the set of spectra taken at different flip angles in fig. 5.0.1 was decomposed into its Fourier components along the φ-axis.

For the analysis of higher spin orders the signal at 2.5ppm (the signal of the α-proton) was chosen because it has the largest intensity in the CIDNP spectrum. Signals well above the noise level are detected up to a harmonic order of ten, indicating that in zero-field all protons are involved simultaneously in the singlet-triplet conversion irrespective of their hyperfine couplings in the bi-radical. In fig. 5.0.2 a) the spectra for the harmonics $n = 1$ to $n = 6$ are displayed. The absorptive spectrum at $n = 1$ corresponds to the net-CIDNP of the α-proton, and reflects the expectation value for the CIDNP of a single nucleus, $\langle I_{1z} \rangle$. It actually coincides with the NMR spectrum taken at thermal equilibrium. The orders with $n > 1$ reflect the fractions of the signal that nutate with double, triple, and so forth the frequency of the signal with $n = 1$. With considerably weaker amplitude they display the antiphase structure inherent to the multiplet effects of higher orders, with the tendency that the odd orders have lower intensities than even orders. Displaying the expectation values of these higher orders, e.g. $\langle I_{1z} I_{2z} \rangle$, *J*-couplings are resolved that are non-resolvable by ordinary NMR.

In the same way, the product of the type II photolysis (dec-9-enal) was analyzed and the result is displayed in figure 5.0.2 b). The signals around 5ppm are assigned to the CH_2-protons in the unsaturated aldehyde formed during H-atom transfer from the β-position to the alkyl end. While the net CIDNP spectrum of ($n = 1$) is all emissive, the spectra of higher orders ($n > 1$) also display an antiphase structure characteristic for the average mutual alignment of the coupled spins. Strong multiplet order up to $n = 3$ and weaker signals up to $n = 5$ are detected. Thus, in zero-field both the Norrish type I and type II reactions proceed with CIDNP formation of high multiplet order. CIDNP redistribution at low magnetic field by isotropic mixing leads to significant polarization of all protons in the diamagnetic product [56], which manifests itself in the NMR spectra as multiplet polarization of different orders after the sample is transferred to the detection field.

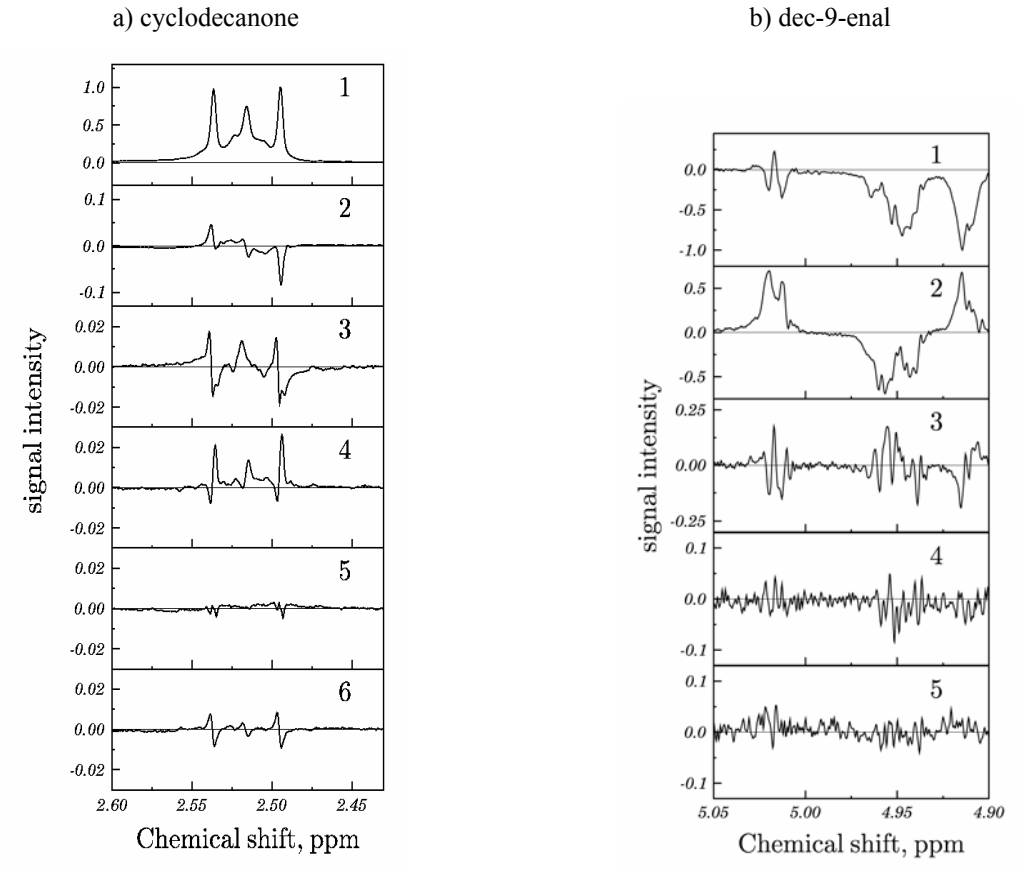

Figure 5.0.2: CIDNP spectra of a) α-protons in cyclodecanone and b) protons of dec-9-enal at different harmonics. The numbers indicate the order *n* of harmonics.

Analysis of β-protons in NATrpH polarized at variable magnetic field. The second example for the analysis of nutation patterns by Fourier expansion is closely related to the polarization transfer phenomena discussed in chapter 4, because it deals with the nuclear spin energy levels of NATrpH at variable magnetic field. CIDNP formation during quenching reactions of NATrpH with different triplet excited dyes is discussed in more detail in chapter 6.2. The observed CIDNP pattern on the protons of NATrpH changes significantly with the external magnetic field. While in high magnetic fields, the spin sorting process ($S\text{-}T_0$ mechanism) prevails and the CIDNP pattern roughly reflects the spin density distribution in the tryptophanyl cation radical, in lower magnetic fields all the protons acquire polarization according to the magnitude of the total nuclear spin projection in the coupled spin system. Depending on the external magnetic field and the parameters of the sample transfer, the polarization can be redistributed among the individual nuclear spin levels in the diamagnetic product molecule. In chapter 4 the energies of the nuclear spin eigen-states in the NATrp molecule were calculuated for two different spin sub-systems at arbitrary magnetic field.

Here, the spin sub-system that consists of the β-protons, the α-proton and the H2-proton shall be analysed in more detail.

Because the two β-protons have relatively large hyperfine couplings (see table 6.2.3) and show strong multiplet polarization in low magnetic fields, their signals were chosen for the anaylysis of field dependent nutation patterns. Their spin-spin coupling among each other is about 15 Hz. Because their difference in chemical shift is only 0.2 ppm, they remain strongly coupled in the whole magnetic field range considered here (0.1 mT to 0.32 T). In addition, they exhibit spin-spin couplings to the proton in α-position (~ 8 Hz) and to the H2-proton (~ 0.8 Hz) of the indole ring. The large range of spin-spin couplings and strong polarization in low magnetic fields renders them a particulary attractive canditate for an analysis of the higher order hamonics at variable strength of the magnetic field.

The multi-spin orders in NATrpH were probed by the Fourier expansion of three sets of flip angle dependent spectra. For these experiments, characteristic field values have been chosen: Around 0.065T and 0.32T level anti-crossings occur in the sub-manifold with total nuclear spin projection M_z = -1 in the spin-system with the two β-protons, the α-proton and the H2 proton (see fig. 4.0.4). In addition spin order at zero-field (B_{pol} = 0.01mT) was investigated. In fig. 5.0.3 the results for the harmonics n = 1 to n = 4 are displayed for the β-protons. When the multi spin order is probed in zero-field (B_{pol} = 0.01mT), even orders higher than n = 4 are detected, while in higher fields, only the net effect (n = 1) and the mutual alignmet of the two strongly coupled β-protons at n = 2 are clearly present.

Qualitatively, the two double doublets observed for n = 1 (net-polarizations) are the same in all three magnetic fields, however the intensity of the four lines assigned to the β1-proton centered at 3.025 ppm is significantly reduced at 0.32T as compared to 0.065T and in zero-field (the intensities of different harmonics for one field value were normalized with respect to the intensity of the highest line observed at n = 1). Interestingly, the intensitiy on the β1-proton is only lowered in the first, but not in the second order spectrum in the level anti crossing at 0.32T, meaning that rather net-CIDNP, but no multiplet-CIDNP is reduced. The loss of spectral intensity at n = 1 is attributed to an efficient transfer of net-polarization to the α-proton in the level anti-crossing; the α-proton shows an absorptive peak in the CIDNP field dependence at 0.32T. It is due to the relatively strong coupling between the two β-protons ($J_{\beta 1\text{-}\beta 2}$ = -14.8Hz) that the characteristic features of the "(n-1) multiplet effect" or zero-field multiplet [83] remain in the entire range of magnetic field investigated.

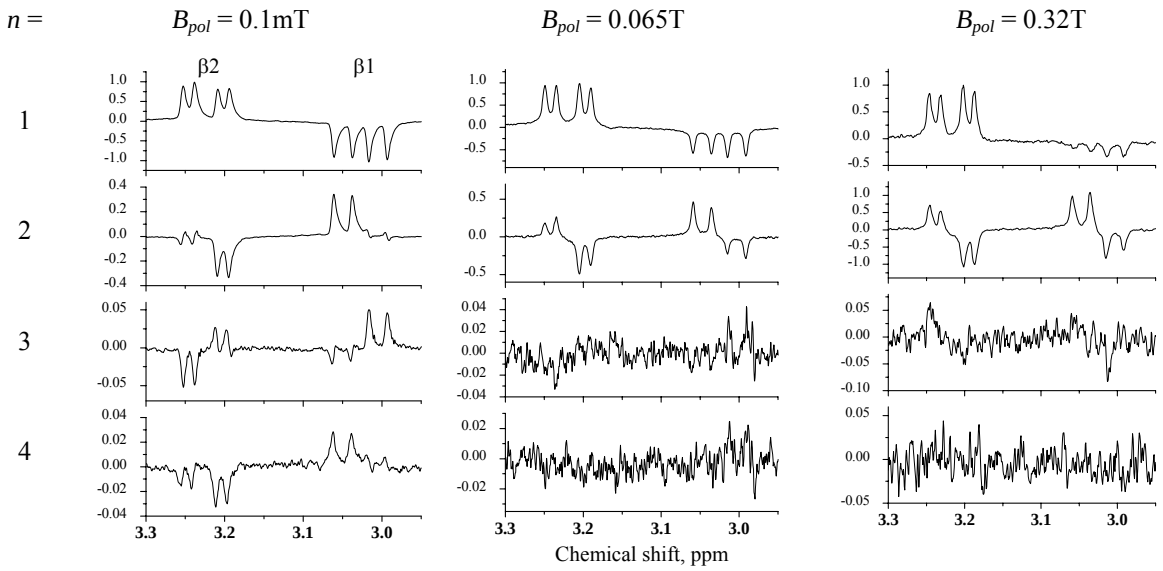

Figure 5.0.3: Multiplet effects of the orders n = 1 to n = 4 in the β-protons of NATrpH at variable magnetic field: B_{pol} = 0.1mT, sample b); B_{pol} = 0.065T and 0.32T, sample c).

At n = 2 the spectral patterns at 0.065T and 0.32T are identical and resemble the mutual alignment of the two β-protons. This is in accord with the expectation that the expectation value $\langle I_{1z}I_{2z}\rangle$, does not depend on the external magnetic field [41]. In zero-field, however, the second harmonic obviously also displays the multiplet effect with H2 on the outer lines (fig. 5.0.3, B_{pol} = 0.1mT, n = 2). Concomitantly, the sign of the signal for the H2-proton changes from emission to absorption between n = 1 and n = 2 (not shown). These couplings (0.8 and 0.7Hz for β1-H2 and β2-H2, respectively) are seen in the NMR spectrum in fig. 4.0.1. Here, the couplings are resolved due to the antiphase structure in the harmonic spectrum of second order (n = 2) at zero-field. The signs of the spin-spin couplings between the β-protons and H2 are -0.8Hz (β1-H2) and +0.7Hz (β2-H2) when determined from the phases of multiplet polarizations in the zero-field spectrum at n = 2.

The harmonic spectrum at n = 3 in zero-field exhibits mainly the multiplet effect between the two β-protons, and only small contributions from the spin-spin couplings to the H2-proton. The phase of this β1-β2 multiplet structure is opposite to that in the second order harmonics observed at higher magnetic fields. Obviously, the changes in odd even order harmonics, and the different grouping of nuclear spin levels at variable magnetic field lead to multiplet effects of opposite sign. The signs of individual spin-spin couplings thus do not reveal themselves in straightforward manner. Changes in the grouping of nuclear spin levels in the level anti-crossings during the field change have to be taken into account numerically. At B_{pol} = 0.32T the coupling of the β-protons to the α-proton shows up in the third harmonics, while the

coupling to H2 is not present in any of the harmonics n = 1 to n = 4. The absence of the multiplet polarization between the β-protons and H2 at higher fields is attributed to their coupling being in the weak limit, i.e. their relatively large chemical shift difference. Inspection of the nuclear spin energy levels with total spin J_Z = -1 of the four-spin system under consideration in figure 4.0.4 suggests, that the proximity of energy levels near zero-field is responsible in the appearance of the β1-H2 and β2-H2 multiplet effects at n =2 at 0.1mT.

Conclusions

The analysis of nutation patterns by Fourier expansion of the flip angle dependent CIDNP spectra turns out as a convenient method for distinguishing the contributions of multiplet polarizations of different orders. In the present study, multiplet CIDNP effects of the order n > 2 are evaluated for the first time. In low magnetic fields, the technique is capable of analyzing multiplet effects of high orders, because all strongly coupled nuclei are commonly involved in the singlet-triplet conversion and are polarized due to their average mutual alignment.

Generally, in higher fields the alignment of nuclear spins is less pronounced. The changes in multiplet CIDNP patterns at variable magnetic field are related to the differing NMR parameters, i.e. the chemical shifts and the spin-spin couplings among the nuclei. The multiplet effects observed here are not unique to CIDNP, and resemble those observed in PHIP experiments after hydrogenation reactions of multiple bonds when performed in low and high magnetic fields (PASADENA and ALTADENA), and the approach of the analysis of multi-spin orders in the FT-NMR spectra is in principle not limited to CIDNP. The new technique allows further elucidation of pathways for an efficient polarization transfer among coupled spins and might add important pieces of information on the mechanisms for redistribution and transfer polarization and coherences.

In the examples presented coherences formed during the non-adiabatic development of product formation are known to exist and are in part transferred into polarization by the non-adiabatic field switch (see chapter 4 and ref. [55]). In addition, the amplitude of these oscillations is expected to depend characteristically on the flip angle of detection [57]. Restricting the discussion to non-equilibrium states of the first kind is thus not sufficient, and a more detailed understanding of the observed multiplet patterns requires considering the full

density matrix and its evolution during all steps of the field cycling experiment. However, the disappearance of higher orders with increasing field strength in the spin sub-system of NATrpH is rationalized with the energetic changes in the nuclear spin states calculated in chapter 4, and in principle the method for elucidating the different multiplet contributions may be useful for the optimization of polarization and coherence transfer experiments.

The dependence of the efficiency of the transfer of multiplet polarization into net polarization on the applied detection pulse angle and the external field during the formation of polarization is of particular practical interest. Multiplet type polarization is, in principle, not very attractive for enhancing the sensitivity of NMR (or of functional or morphological MRI), because the lines with opposite polarization may overlap and thus compensate each other. By adjusting both, the external magnetic field during the stage of the spin evolution, and the pulse angle of the detection these problems may be overcome.

6 Light-induced Processes Studied by CIDNP

CIDNP is of considerable interest for mechanistic and structural chemistry of transient radicals, adding valuable information to the methods of paramagnetic resonance and standard nuclear magnetic resonance. The last part of this work deals with the photophysical and photochemical aspects of the formation of nuclear polarization in different systems. It is divided into three sub-chapters which have in common that in all cases radicals are produced by means of irradiating the samples with 308nm laser light (XeCl excimer laser).

Analysing photochemical events has always been an important application of the CIDNP technique. Besides of the unambiguous determination of the electron spin multiplicity from which the radicals have been formed, CIDNP offers the possibility of the identification of reaction products by their highly specific NMR parameters. In particular when combining available information from CIDNP field dependence with that from time resolved CIDNP, the method allows following the pathways of photochemical reactions that elude the investigation by other methods. The radicals can originate from various chemical events such as electron and hydrogen transfer reactions, the cleavage of covalent bonds or by ionization.

Measuring the dependence of CIDNP as a function of the external field allows the identification of radicals by the extraction of their magnetic interaction parameters (g-factors and hyperfine couplings). Ideally, the position of the high field maximum is given by the matching condition $B_{max} = \hbar a/2\Delta g\beta$ (formula 2.1.11), where small hyperfine couplings, a, on one radical can often be approximated by an effective hyperfine coupling, a_{eff} (see chapter 2, equation 2.1.19).

The first section (6.1) deals with the simple event of photo-ionization of the aromatic amino acids tyrosine and tryptophan; it leads to radical pairs in which the solvated electron acts as a counter radical. It is shown that the solvated electron (e^-_{aq}) can be treated the same way as other radicals in radical pairs to model the CIDNP field dependence. Electron and hydrogen atom transfer reactions of amino acids as quenchers of different triplet excited sensitizers are the subject of the second section in this chapter (6.2). Investigating amino acid radicals in aqueous media is generally aimed at a better understanding of the underlying photochemistry for potential biophysical investigations and applications.

In the last section (6.3), the photochemical α-cleavage of ketones (Norrish type I and II) is compared in liquid and solid solutions of cyclohexane-d_{12}. Changes in the field dependence of CIDNP allow distinguishing between different mechanisms of CIDNP formation. It is shown

that upon cooling to the plastic crystalline phase, polarization is formed by predominantly by S-T$_-$-transitions for all ketones under study, and that the electronic exchange interaction, J_{ex}, tends to be dominated by the matrix dimensions.

6.1 Photolysis of Aromatic Amino Acids

The aromatic amino acids tyrosine and tryptophan act as the mayor chromophores in proteins, absorbing light in the near UV region. Whereas the mechanisms of the action of UV radiation have been studied comprehensively for nucleic acids, for the second group of important biological molecules, the amino acids, the primary photochemical events, such as formation and decay of solvated electrons (e^-_{aq}) are still poorly understood. Some decades ago the general aspects of the near UV photolysis of tyrosine [84] and tryptophan [85] have been summarized in a series of reviews, and not much knowledge has been added afterwards. This is probably because most of the studies involve optical spectroscopy only, and the excitation of the amino acids is usually performed at wavelength shorter than 308nm, since their maximum of absorption is centred at ~280nm. It is however known that excitation at the long wavelength edge of the absorption bands also produces radicals of the parent amino acids via photo-ionization.

Tyrosyl and tryptophanyl radicals are known to play important roles in many biological systems. In the reaction centers of photosystem II (PS II) of plants, algae and cyanobacteria, two radicals of tyrosine have been detected [86, 87]. They are involved in the coupling of light induced charge separation to the oxidation of H_2O to O_2 and the reduction of plastoquinone. Tyrosine acts as the precursor to neurotransmitters like dopamine and epinephrine, and tryptophan or tryptamine take part in the in the oxidation chemistry of neurotransmitters and neurotoxins [88]. Hence, the radical reactions of both, tyrosine and tryptophan play key roles in neurochemistry. Tryptophan and tryptamine further act as endogenous radical scavengers to protect proteins from oxidative damage, associated with carcinogenicity and aging.

Besides of their appearance in chemically and radiatively damaged proteins, the radicals of tyrosine and tryptophan have been recognized as catalytically active redox agents in a number of enzymes, e.g. ribonucleotide reductase, DNA photolyase or cytochrome c peroxidase [89]. Photoionization of tyrosine and tryptophan is also of interest because of the possible role of

the solvated electron (e^-_{aq}) in the mechanisms of radiation induced damage of enzymes and DNA.

The following CIDNP study on the photolysis of the aromatic amino acids aims to contribute to the general understanding of photochemical events in proteins and their roles in biochemistry. In the present work the N-acetylated derivatives of tyrosine and tryptophan (NATyrOH and NATrpH) are photolyzed because they lack a primary amine group which is the final locus of electron attack in small peptides [90], thus providing simple models for larger peptides. An obvious benefit of the CIDNP technique with respect to previously applied (optical) methods lays in the unambiguous identification of the precursor states (singlet or triplet) of the radical pairs that evolve from the photochemical events.

Because the CIDNP field dependences are obtained under pseudo cw-conditions, they do not allow distinguishing between polarization formed in the primary reaction cage on the time scale of tens of nanoseconds and polarization formed in the bulk on much longer timescales. Therefore, the investigation of $NATyrO^-$ is amended with a time resolved CIDNP experiment under comparable conditions, thus allowing a direct comparison to the results obtained by field cycling.

It was further mandatory to perform a study on the photolysis of the amino acids in the absence of sensitizers, in order to obtain an idea of its influence on the CIDNP field dependences observed in quenching reactions of different photo sensitizers by tryptophan and tyrosine (chapter 6.2). During the experiments with sensitizers, significant CIDNP was detected on the solvent line (HDO) and the studies presented in this chapter will clarify the origin of this polarization, i.e. if it is of a chemical (formed in a photo reaction) or physical (formed by polarization and/or coherence transfer) origin.

The high content of information inherent to NMR spectroscopy allows the identification of products and their way of formation by the analysis of the shape of their CIDNP field dependence and dynamics from time resolved CIDNP measurements. The reaction mechanisms leading to formation of CIDNP will be discussed in the light of available results.

Experimental

Field dependent CIDNP. The experimental set-up and the timing scheme to obtain CIDNP field dependences are described in chapter 3.2. For the experiments discussed here, the probe head was transferred rapidly to the detection field ($\tau_{fv} \leq 350$ms) immediately after irradiation.

Apart from the CIDNP on HDO, the effects discussed in this chapter are rather small as compared to the enhancement observed in the presence of photo sensitizers. Therefore, relatively long irradiation times ($\tau_L \leq$ 1.5s, 50 Hz) were used, facilitating particularly the observation of CIDNP on HDO given its long relaxation time. Changes in pH and optical density resulting from irradiation limit the number of experiments to about ten experiments per sample.

In order to have reproducible starting conditions for observing the CIDNP field dependence of the HDO signal (~4.7ppm), it is necessary to introduce waiting times of about 180s in low field (roughly five to six times T_1 of the HDO signal) in-between subsequent measurements, since here, the polarization is not destroyed by application of particular pulse sequences applied prior to the experiment.

Time resolved CIDNP. The experimental set-up for time resolved CIDNP measurements was described in chapter 3.1. It employs the same optical wavelength for excitation (308nm) and magnetic field for the NMR detection (B_0 = 7T) as the field dependent CIDNP experiments. CIDNP kinetics are obtained by the variation of the delay time, τ_d, between a single laser pulse and the RF detection pulse by averaging over 32 experiments and scrambling the delay times in order to avoid potential systematic errors from an incomplete correction of the signal decay due to aging of the sample. Because of the small signal enhancement in the present experiments, a 90°-pulse (3μs) was used for the detection in order to obtain the maximal signal amplitude, sacrificing time resolution. It turned out that a reproducible pre-saturation to observe the signal of HDO can be obtained by applying a single RF-pulse of ~3 ms prior to the laser pulse.

Sample preparation. Field dependent CIDNP measurements were done on basic (pH~11) solutions of N-acetyl tryptophan (NATrpH) and on basic solutions of NATyrOH (pH~11) at different concentrations (2mM to 10mM). Here, the CIDNP field dependences shall be discussed for basic NATyrOH (5mM) and NATrpOH (11mM) solutions of roughly equal optical densities for 308nm light ($OD_{308} \approx$ 0.7-0.8).

The TR-CIDNP experiment was performed with a 5mM solution of N-acetyl tyrosine (NATyrOH) in D_2O. The pH was adjusted by addition of NaOD and the samples were purged with N_2 prior to use in order to remove dissolved oxygen.

6.1.1 CIDNP Formation in aqueous N-acetyl tyrosine (NATyrOH)

Product identification by cw-CIDNP spectra. Besides volatile products resulting from the decay of the backbone during the photolysis of N-acetylated amino acids (CO_2, CO, H_2O and to a minor extent CH_4 and H_2) [91], various stable products have been reported in the literature, e.g. 3,4-dihydroxyphenylalanine (3,4-DOPA), 2,2'-bityrosyl (BITYR), and 2-amino-4-ethenyl-hex-4-enic acid (AEHEA) [92]. In addition, very recently also deuterated derivatives of tyrosine (mainly 5-deutero tyrosine) were reported [93]. In the present study, some of these products are identified by inspection of the aromatic region of the cw-CIDNP spectrum.

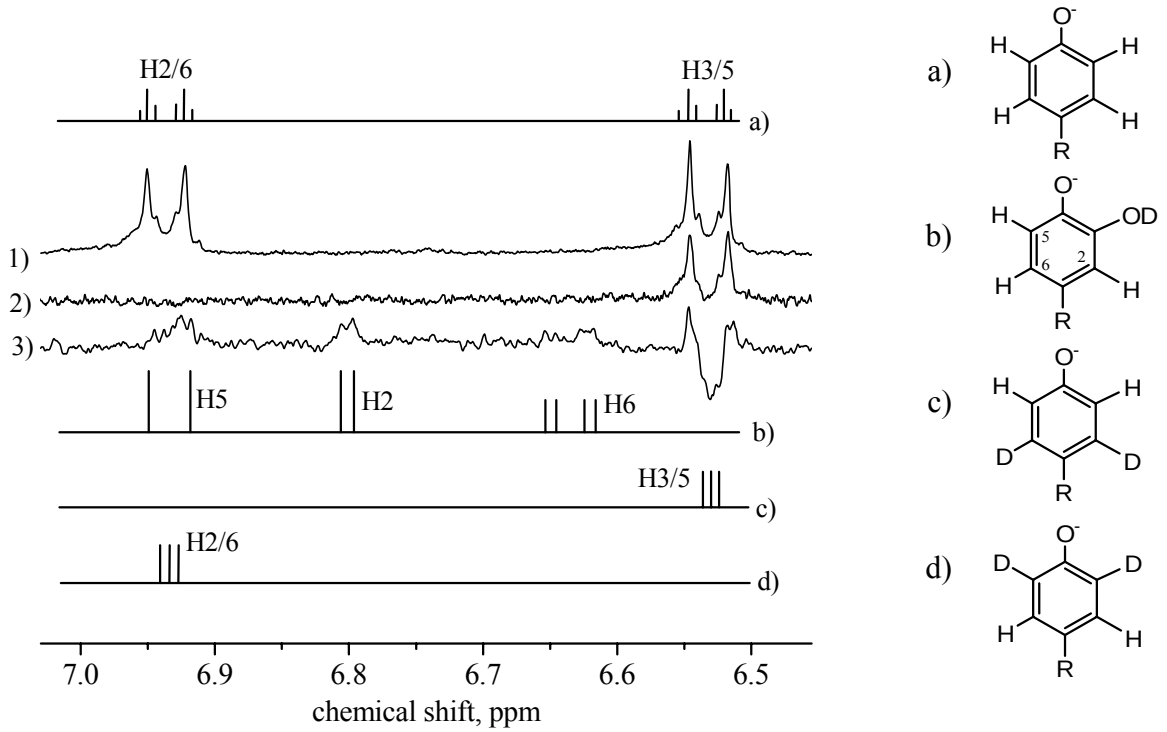

Figure 6.1.1: 1) aromatic fraction of the NMR spectrum of $NATyrO^-$; 2) averaged CIDNP spectrum (B_{pol} = 1T) of 2mM $NATyrO^-$; 3) averaged CIDNP spectrum of 5mM $NATyrO^-$. For comparison, the stick spectra and structures expected for a) parent compound ($NATyrO^-$) b) 3,4-dihydroxyphenylalanin c) 2,6-dideutero tyrosine d) 3,5-dideutero tyrosine are shown (R = $-CH_2-CH(NDAc)(COOH)$).

Figure 6.1.1 displays NMR spectra of the aromatic region of basic $NATyrO^-$ solutions under different conditions. The first trace in figure 6.1.1 (trace 1) shows the NMR-spectrum at Boltzmann equilibrium. The four protons in the phenolic ring consist of two pairs of equivalent protons. They give rise to two doublets in the aromatic region of the NMR spectrum, which are further split due to smaller couplings to the other protons in the

molecule. They are assigned to the two pairs of equivalent protons in positions 2 and 6 (H2/6: 6.94ppm), and in the positions 3 and 5 (H3/5: 6.53ppm). Between 2 and 5ppm the NMR spectrum of $NATyrO^-$ resembles that of NATrpH (see e.g. fig. 4.0.1), showing a single line at ~2.05ppm for the three equivalent protons of the N-acetyl group, and twelve lines for the ABX spin system formed by the two diastereotopic β-protons (β1: 2.71ppm and β2: 2.95ppm) and the α-proton (4.27ppm).

The averaged high field CIDNP spectrum (B_{pol} = 1T) of a 2mM solution of $NATyrO^-$ in trace 2) shows absorptive polarization of the protons H3 and H5 of the parent compound. It is attributed to ionization of $NATyrO^-$, yielding the tyrosyl radical and the solvated electron. According to the rules of Kaptein [39], the absorptive high field CIDNP on the protons in positions 3 and 5 is consistent with a radical pair formed from a singlet precursor state. Thus, ionization at the excitation wavelength of 308nm occurs from a singlet excited state, presumably S_1:

$$NATyrO^- \xrightarrow{h\nu} {}^1NATyrO^- \longrightarrow NATyrO^\bullet + e^-_{aq} \quad . \qquad (6.1.1)$$

Support for this conclusion is provided in the field dependent and time resolved CIDNP studies presented further down.

When a higher concentration (5mM) is photolyzed, the CIDNP spectrum in trace 3) is obtained, in which the polarization pattern is complicated by the superposition of the NMR signals of various products formed during the photolysis. It displays absorptive CIDNP on the resonances, tentatively assigned to 3,4-dihydroxyphenylalanine, a precursor of 3,4-DOPA (structure b) in fig. 6.1.1). For comparison, the expected stick spectrum is displayed (see fig. 6.1.1b)). On the basis of the assignment of lines it is concluded, that a hydroxylation of the parent compound occurs in the absence of O_2 in a radical reaction. It is, however, likely that 3,4-DOPA is formed in a two-step photoreaction, e.g. the absorption of light by an intermediate, because these signals were not detected during the experiments with a single laser pulse (in the time resolved CIDNP measurements).

Furthermore, the CIDNP spectrum in fig 6.1.1 (trace 3) shows an emissive signal with exactly the same chemical shift (6.53ppm) as that of the parent $NATyrO^-$ signal of H3/5. It is attributed to the product of photochemical H/D-exchange in tyrosine [93]. The exchange obviously occurs without further structural changes of $NATyrO^-$, because for any change in structure at least a small change in chemical shift would be expected. Additionally, characteristic changes in the pattern of spin-spin couplings from H-H to H-D are expected: As indicated in the stick spectra c) and d) in fig. 6.1.1, a change from a doublet (spectrum a))

with a coupling of $J_{H\text{-}H}$ = 8.5Hz to a triplet with $J_{H\text{-}D}$ = 8.5Hz/6.5 = 1.3Hz according to the ratio of the gyromagnetic constants of the proton and the deuteron are seen in the CIDNP spectrum in trace 3) for the deuteration of both ortho and meta positions of the parent compound. The intensity of CIDNP signals suggests that the exchange preferably takes place in the ortho-position (position 2 and 6), over that in the meta-position (compare expected stick spectra c) and d) in fig. 6.1.1).

The ratio of CIDNP observed on H3/5 of the parent $NATyrO^-$ and its derivative deuterated in ortho-position depends on the initial tyrosine concentration used in the photolysis. At higher tyrosine concentrations (5mM), the resonances of the deuterated compound are clearly seen, while in a more dilute solution of 2mM only absorptive CIDNP on H3/5 of the parent $NATyrO^-$ is observed. This observation indicates the involvement of a further tyrosine molecule in the formation of deuterated tyrosine. A solution of 10mM $NATyrO^-$ gives roughly the same pattern as that observed for a 5mM solution (not shown).

It is known from pulse radiolysis studies, that e^-_{aq} reacts with tyrosine with a bimolecular rate constant close to the diffusion limit (10^8 $M^{-1}s^{-1}$ at pH 11) [94]. In the same work it was further concluded that both, e^-_{aq} and H-atoms add predominantly to the phenol ring. The addition of electrons to the aromatic moiety is known to the organic chemist as a so-called Birch reduction [95], providing access to substituted 1,4-cyclohexadienes. Thus, addition of e^-_{aq} to $NATyrO^-$ may lead to the formation of a cyclohaxadienyl anion radical which is rapidly protonated (actually deuterated) to the cyclohexadienyl radical ($CHD^\bullet$) as indicated in scheme 6.1.1. The cyclohexadienyl radical can then undergo transformations, such as decarboxylation or deamination. An emissive signal is observed at 2.26ppm, but could not be assigned unambiguously and in scheme 6.1.1 the rest R therefore remains unidentified. It presumably stems from a product of the decay of the backbone of $NATyrO^-$.

Strong emissive polarization is observed for the residual protons of the solvent (HDO: 4.7ppm), which was also observed in the experiments with triplet sensitizers discussed in chapter 6.2. In previous CIDNP studies of the near UV photolysis of phenolic compounds the polarization of HDO was related to the hydroxylation of the aromatic ring, leading to 3,4-dihydroxyphenylalanine (precursor of 3,4-DOPA) [96, 97]. However, in the present study the lines of this compound are not very pronounced (see fig. 6.1.1), and the polarization on HDO is rationalized by the disproportionation of the cyclohexadienyl radical with a phenoxyl radical. This reaction gives rise to the selectively deuterated tyrosine, and explains the polarization of the solvent via the proton marked with an asterisk in scheme 6.1.1. The

involvement of a second tyrosine molecule in scheme 6.1.1 is in accord with the increasing polarization of the deuterated tyrosine with increasing concentration of the photolyte.

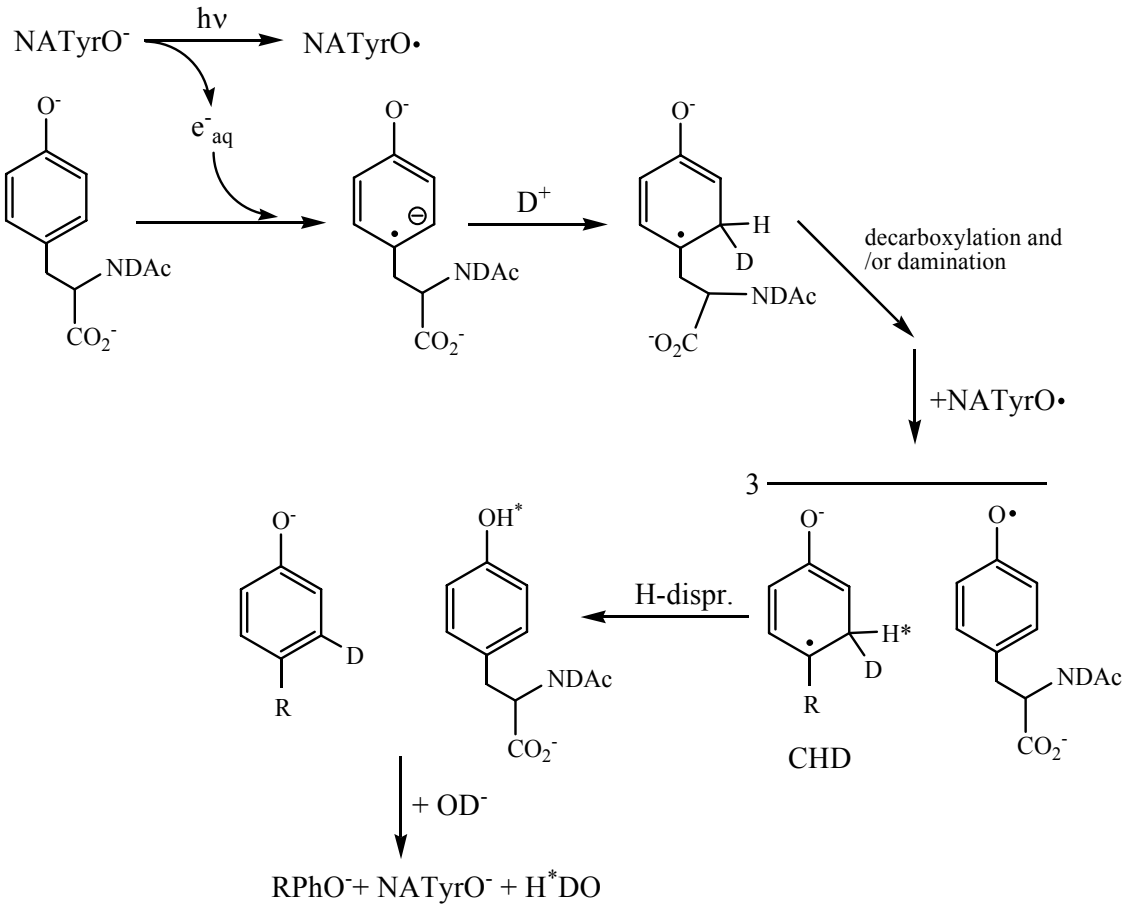

Scheme 6.1.1: CIDNP formation on HDO by photochemical H/D-exchange in tyrosine. In part adopted from ref. [93]. Here, R indicates either a transformed (absorptive CIDNP at 2.26ppm), or the intact N-acetylated amino acid backbone.

Very recently, London and Gabel [93] proposed this kind of H/D-exchange to occur in aqueous tyrosine solutions, and the following field dependent and time resolved CIDNP experiments shall be analyzed to support or disprove scheme 6.1.1. The authors of ref. [93] analyzed conventional NMR spectra taken after prolonged UV-irradiation (up to hours) by a mercury flash lamp and found an ortho/meta-ratio of about 1.6/1 at pH 11. The highest selectivity of H/D-exchange was found around pH 9.

Singlet-triplet mixing in the cycloxhexadienyl/phenoxyl radical pair upon random encounter provides a likely path for the polarization of water via the proton indicated with an asterisk after disproportionation and subsequent deprotonation of NATyrOH by the solvent. Alternatively, H-atoms could be transferred from one tyrosine to another to yield the radical pair proposed in scheme 6.1.1. Bussandri and van Willigen studied the photolysis of phenol in D_2O at a wavelength of 266 nm by FT-EPR and observed a cyclohexadienyl radical ($CHD^{\bullet}$)

in which the deuterated position is meta (note, that in scheme 6.1.1 it is ortho) to the hydroxyl substituent [98]. They interpreted their finding in terms of H-atom transfer from one tyrosine to another to yield a phenoxyl/cyclohexadienyl radical pair. H-atoms may add to the phenol ring to yield $CHD^{\bullet}$, but no cyclohexadienyl radical arising from this process could be identified by the CIDEP study of Bussandri and van Willigen [98]. A similar reaction path was also assumed as a source of an identified cyclohexadienyl radical during the photolysis of single crystals of NATyrOH [99]. Whereas at low pH this mechanism may be feasible, the phenolic proton is unavailable under the experimental conditions used in the present work, and this mechanism becomes inoperative above the phenolic pK_a of tyrosine ($pK_a \sim 9.1$).

At low pH, photolysis of the aromatic amino acids also yields H-atoms (actually D-atoms); at least in part due to scavenging of e^-_{aq} by protons:

$$e^-_{aq} + H_3O^+ \longrightarrow \dot{H} + H_2O \quad . \tag{6.1.2}$$

Reaction 6.1.2 is usually formulated to account for the production of H_2 during the photolysis. Another source of H_2 would be the disproportionation of two electrons to yield H_2 and OH^-:

$$e^-_{aq} + e^-_{aq} \xrightarrow{H_2O} H_2 + 2OH^- \quad . \tag{6.1.3}$$

Although the rate constant of reaction 6.1.2 is $2.4 \cdot 10^{10}$ $M^{-1}s^{-1}$ [100], for experiments at high pH the conversion of e^-_{aq} to $H^{\bullet}$ by reaction 6.1.2 may be neglected in comparison with the reaction with other scavengers, namely the aromatic amino acids themselves and e^-_{aq}. At pH 10.5, the rate of reaction 6.1.3 is $4.5 \cdot 10^9$ $M^{-1}s^{-1}$ and somewhat faster at even higher pH [101]. A significant increase in pH (pH 11 to pH 11.5) after prolonged irradiation ($\tau_L \sim 100$s, 50Hz) was indeed observed in the present study and may be attributed to reaction 6.1.3.

Strong emissive CIDNP was observed on the residual protons in the solvent (HDO in D_2O). The polarized water line appears to be shifted to slightly higher field upon irradiation, depending on the duration of light irradiation. The observed shift of the polarized HDO line in the spectra of the irradiated solutions can be explained by the strong temperature dependence of the HDO chemical shift. The chemical shift, σ, depends roughly linear on temperature, T, with: σ(in ppm) = 5.051-0.0111·T (in °C) [102]. The HDO in the CIDNP spectra shifts by about 3.7Hz with respect to the non-irradiated solution, corresponding to $\Delta\sigma = 0.012$ ppm. The above formula allows estimating a temperature change of about 1°C in the irradiated spot of the solution. Since the sample was irradiated for 1.5 s with a repetition rate of 50 Hz (75 laser pulses) with an approximate energy of 15 mJ per pulse reaching the sample, the 'hot spot' collects about 1.1 J over the whole irradiation time. After the photo reaction is accomplished, the solute molecules dissipate fast, giving virtually all this energy to the lattice

(D_2O). With a heat capacity of about 4.2 kJ/kg · K, the irradiated spot is estimated to contain about 0.24 g of water solution. This number will be used further down, to estimate the efficiency of ionization. In the following, the CIDNP signals will be analyzed in more detail by their dependence on the external magnetic field.

Field dependent CIDNP. For the acquisition of the CIDNP field dependences a 5mM solution of $NATyrO^-$ at pH 11 ($OD_{308} \approx 0.8$) was irradiated for τ_L = 1.5s (50Hz), and subsequently the NMR spectra were recorded with a 90° flip angle at B_0 = 7T. CIDNP field dependences of the protons in $NATyrO^-$ are shown in figure 6.1.2. For the absorptive signals of the protons in positions 3 and 5 (see fig.: 6.1.1) the use of narrow integration windows allows to separate the signal from that assigned to the deuterated compound. The different resonances at 6.94ppm, however could not be integrated separately and the field dependence in figure 6.1.2 (H2/6) represents a mixture of the CIDNP observed for different compounds. In low field (at least up to 0.3T) the signal is a doublet with the splitting of approximately 8.5Hz and is assigned to H2/6 of the parent $NATyrO^-$, while above B_{pol} = 2T, the absorptive polarization does not resemble the doublet structure of H2/6 (see fig. 6.1.1).

In low field, both H3/5 and H2/6 are equally polarized. Both pairs of aromatic protons display a distinct minimum at B_{pol} = 1mT, and the field dependences are identical up to B_{pol} = 0.3T. Their similarity may be attributed to the efficient redistribution of CIDNP via spin-spin coupling between the aromatic protons of $NATyrO^-$ ($J \approx 8.5$Hz) during the long irradiation time because in the present case, the criterion $J^{-1}\tau_L > 1$ is fulfilled [56]. The field dependences of the aromatic protons appear to be similar until roughly B_{pol} = 0.3T, a field range in which they can be considered strongly coupled ($\Delta\sigma \approx 0.4$ ppm, $J \approx 8.5$ Hz). Hence, the field dependences modelled for the aromatic protons were added up, and the result is displayed as a dashed line in fig. 6.1.2. The phenomenon of CIDNP redistribution due to strong coupling of spins was discussed in chapter 4.

In contrast, the β-protons display a pronounced multiplet effect in low-field, and do not acquire any significant polarization in high field. Their coupling is in the order of 14Hz, and thus about twice as high as in the case of the aromatics. A prerequisite for the observation of zero-field multiplet CIDNP is an adiabatic sample transfer. Taking $J\tau_{fv} \geq 1$ as a crude criterion for adiabaticity, we obtain 5.6 and 3.4 for the β-protons and for the aromatic protons respectively and rather expect the transfer to occur in the adiabatic regime for both cases. However, the experimental field dependences suggest that CIDNP is redistributed during the long irradiation of 1.5s in both cases, and that the sample transfer is still in the adiabatic

regime in case of the β-protons while it might occur non-adiabatically for the aromatic protons, since for the former a multiplet effect is observed and for the latter not (see fig. 2.1.6). The above criterion for the adiabaticity of the field switch is thus too crude, and the inclination of different spin levels at variable field during the transfer would in principle have to be taken into account. However, the simulations in figure 6.1.2 agree quite well with the experimental data, allowing a discussion of the photo-chemistry.

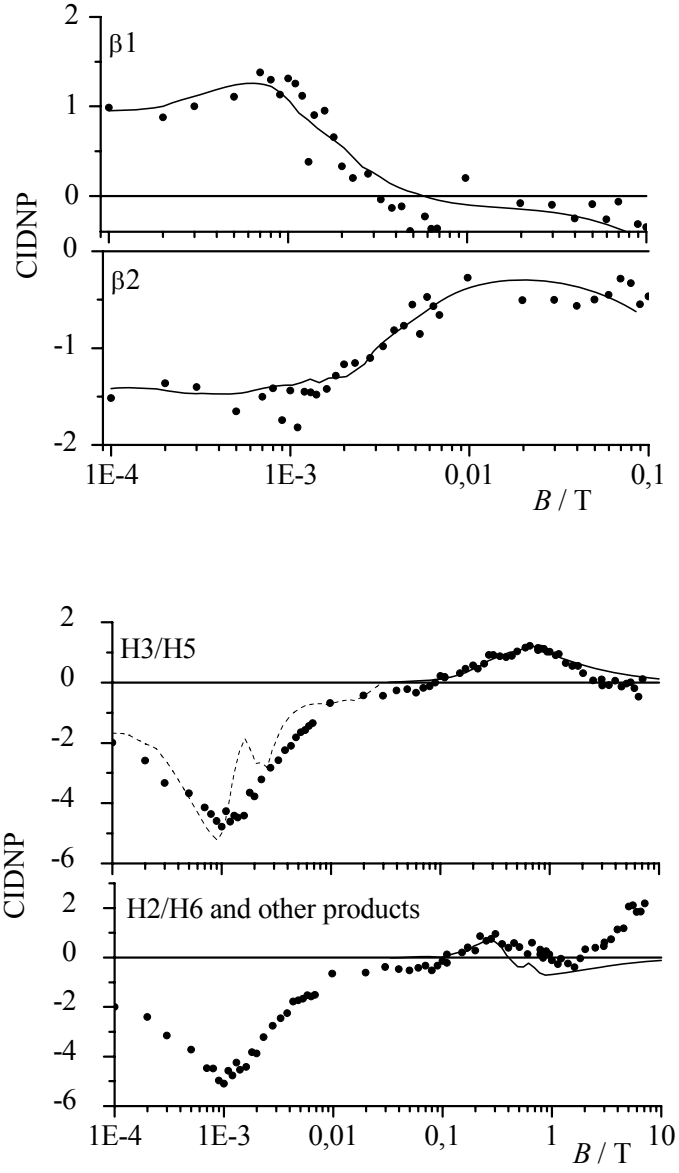

Figure 6.1.2: CIDNP field dependences of 5mM $NATyrO^-$ in D_2O at pH 11. Simulation parameters: g(NATyrO•) = 2.0045, a(H3/5) = -0.69mT, a(H2/6) = 0.19mT, a(β1) = 0.84mT, a(β2) = 0.56mT; $g(e^-_{aq})$ = 2.00049 [103], a_{eff} = 0.001mT. For the low field part of H3/5 (dashed line) the calculated field dependences of the strongly coupled aromatic protons were added and scaled separately according to the experimental data.

From the shape of the field dependence of H3/5, and its absorptive high field maximum located at $B_{pol} \approx 0.6$T, the most probable present radical pair is identified by comparison with the simulation, which is also displayed in figure 6.1.2 (solid lines). This radical pair consists of a tyrosyl radical and a solvated electron (e^-_{aq}), according to reaction 6.1.1. Both, the absorptive CIDNP of H3/5 and the shape of the field dependence of H2/6 at high magnetic fields are consistent with the polarization being formed from a singlet precursor. Taking the relatively well determined (single line in the EPR spectrum) g-factor of the solvated electron in D_2O ($g(e^-_{aq}) = 2.00049$) as a reference [103], a g-factor difference of $\Delta g = -0.0040 \pm 0.0008$ is obtained from the simulation of the high field CIDNP. The analysis thus allows a crude estimation of $2.0035 < g_{iso} < 2.0055$ for the tyrosyl radical in aqueous solution, since the error Δg is estimated to about 15% (see chapter 6.2.2). However, because the difference in g-factors is quite large, no other radical pair is considered for the maximum occurring at such low polarization field. For the simulation in figure 6.1.2, the HFC's for the individual proton sites in NATyrO• were taken from ref. [104].

The g-factor obtained for NATyrO$^\bullet$ may be compared to g-factors of tyrosyl radicals reported in the literature, some of which are summarized in table 6.1.1. The table shows, that there is a significant difference between the g-factors of tyrosyl radicals, depending whether they are generated in hydrogen bonding media or not, and the value obtained here agrees with isotropic g-factors observed in H-bonding media before [105-107]. This shall be corroborated by a more precise determination of its value (see table 6.1.1) from high field maxima observed with triplet sensitizers in chapter 6.2.

H-bonded				non-H-bonded		
NATyrO$^\bullet$ liq. D_2O[a)]	Tyr-HCl crystal[b)]	PMP calc.[c)]	spinach-TyrD in PSII[d)]	NATyr crystal[e)]	PMP calc.[c)]	RNR[f)]
2.00445	2.0045	2.0044	2.00455	2.0055	2.0052	2.00500

Table 6.1.1: Isotropic g-factors of tyrosyl radicals in different systems. a) this work (see table 6.2.3), b) Fassanella and Gordy [105], c) PMP: para-methyl-phenoxyl radical calculated by Un *et al.* [106], d) in *Synechocystis* 6803 by Un *et al.* [107], e) Mezzetti *et al.* [99], f) in *Escherichia coli* by Hoganson *et al.* [108].

A CIDNP field dependence was also obtained for the signal of HDO (~4.7ppm). It is shown in fig. 6.1.3 together with the field dependences of side products, which do not show any significant polarization in low magnetic field and considerably less polarization than HDO at high magnetic field. (The amplitude of CIDNP on HDO was reduced by a factor of twelve in fig. 6.1.3 to allow a convenient comparison to the signal at 2.26ppm.) The CIDNP field dependences of the signals at 2.26ppm, 6.80ppm and at 6.58ppm do not provide sufficient

signal to noise ratio to discuss a correlation with the polarization of HDO. Apparently, the CIDNP on the protons in the solvent altogether shows a field dependence as it would be expected from the radical pair mechanism (S-T_0) being operative, with minor polarization in the intermediate field range, a characteristic high field maximum at B_{pol} = 4.5T, and low field polarization governed by HFC. Thus, for the current discussion alterative mechanisms, e.g. cross polarization, shall be disregarded. This conclusion is in accord with CIDNP studies on the photolysis of phenol [96] and tyrosine [97] reported in the literature, in which the concentration of protons in the solvent was altered to show that always the same fraction of water molecules is polarized. Dimerization of the phenoxyl type radical can be ruled out to lead to the polarization in HDO since Δg is zero for this radical pair, and hence no net polarization is expected in this case [22].

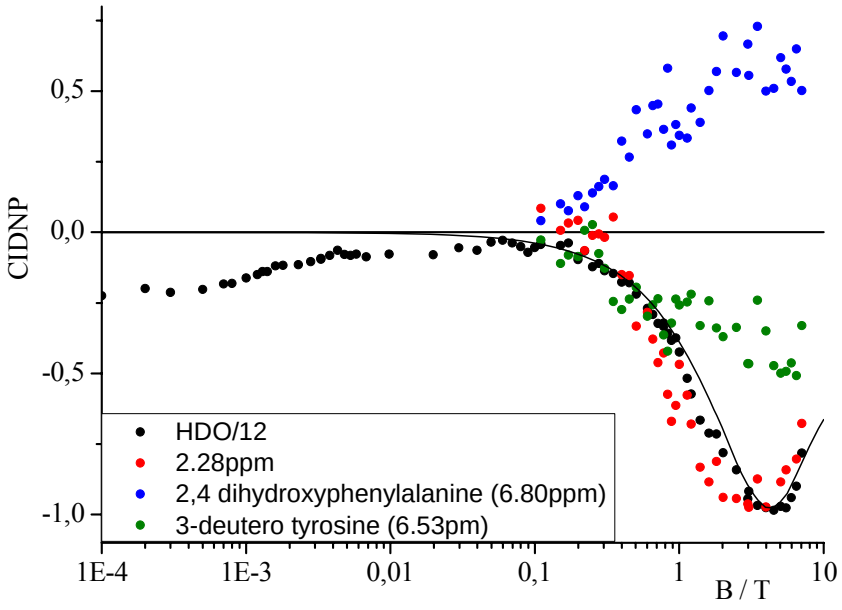

Figure 6.1.3: CIDNP field dependences of HDO and other signals of side products observed during photolysis of 5mM $NATyrO^-$ in D_2O at pH 11. Simulation parameters: g(NATyrO•) = 2.00445, a(H3/H5) = -0.62mT, a(H2/H6) = 0.17mT, a(β1) = 0.56mT a(β2) = 0.84mT; g(CHD•) = 2.00328, a = 3mT.

The high field part of the HDO field dependence is simulated by Adrians model [28], and the result is displayed in figure 6.1.3 as a solid line, in order to extract the g-factor difference in the radical pair in which the water acquired CIDNP. The best agreement with the measured data is achieved with Δg = 0.0012±0.0003. According to reaction scheme 6.1.1, the solvent acquires polarization during random encounters of tyrosyl and cyclohexadienyl radicals, and the HDO field dependence supports this assumption. The simulation yields a value of g = 2.0033±0.0004 for the cyclohexadienyl radical ($CHD^{\bullet}$), which is in accord with reported

values for radicals of this type [109, 110]. This value, however, does not provide conclusive evidence for scheme 6.1.1 and the presence of the cyclohexadienyl radical, since C-centered radicals of the type H(NAc)NC•RCO_2^- have comparable g-factors [111].

Neither the N-acetyl group, nor the carboxyl group of $NATyrO^-$ provide a source for polarized protons ending up in the solvent, but the proton in α-position may be considered. In CIDNP experiments of the photolysis of phenol (without the α-proton available), Cocivera *et al.* [96] also observed CIDNP of the solvent protons. In their experiments, the solvent was not polarized, when 2,4,6-trideuterophenol was photolyzed instead of phenol. This finding is important for the interpretation of the present results, because it rules out the α-proton as the source of CIDNP on HDO, and lends further support to scheme 6.1.1.

The large polarization on HDO, its CIDNP field dependence, and the dependence of CIDNP on deuterated tyrosine on the concentration of $NATyrO^-$ support reaction scheme 6.1.1, which has been proposed by London and Gabel [93]. Here, the polarization of HDO is particularly efficient because of the large hyperfine coupling of the methylene protons in cyclohexadienyl radicals (a_{iso} ≈ 2-4mT [98, 110, 112]). In addition, the long relaxation time of HDO in D_2O (~30s) also helps to accumulate CIDNP on the solvent line under pseudo-cw-conditions.

Time resolved CIDNP. The field dependent CIDNP spectra are obtained upon continuous irradiation (train of laser pulses) and can not discriminate the effects originating from geminate pairs (~10^{-10}s) from those caused by random encounters of free radicals (F-pairs). The interpretation of steady state CIDNP experiments alone in terms of scheme 6.1.1 still depends on several assumptions and thus remains highly indirect. Therefore, the validity of reaction channels considered in the previous section are supported by variation of the delay time between a single laser pulse and the RF-pulse at high magnetic field (B_{pol} = 7T). Time resolved CIDNP spectra of a basic 5mM $NATyrO^-$ solution are shown in figure 6.1.4 a). Immediately after the laser pulse (upper line, delay: 1.5μs), only the resonances assigned to $NATyrO^-$ are observed. The phase of all lines is opposite to that observed in experiments with $NATyrO^-$ as a triplet quencher (see chapter 6.2 and refs. [113] and [41]). The inverted phase of the geminate high field CIDNP spectrum with respect to these spectra clearly identifies the electron spin multiplicity of the precursor to be of singlet character, given the fact that the g-factor of e^-_{aq} is smaller than that of the tyrosyl radical. Thus, the suggestion of a triplet state to be involved [114] should be refuted.

The spectrum, taken with the shortest delay time (1.5μs, fig.: 6.1.4 a)) reflects the ratio of hyperfine couplings, *a*, in the primary tyrosyl radical, though keeping in mind that one deals

with a somewhat crude estimation being far away from the high field maximum of CIDNP intensity located at $B_{pol} \approx 0.6$T (see fig.: 6.1.2). Integration of the individual signals yields the following ratios: H3/5 : H2/6 : β2 : β1 ≈ 1 : -0.27 : -0.62 : -0.4, respectively. The largest HFC is found for the protons in positions 3 and 5. The sign of the HFC of H3 and H5 is known from the experiments with triplet sensitizers (see chapter 6.2 and refs. [113] and [41]), where the precursor multiplicity is well-known, and the magnitude is taken from that obtained by EPR [104]. From this value, a_{iso}(H3 and H5) = -0.62mT , and the ratios of intensities in the geminate CIDNP spectrum the other HFC's in the primary tyrosyl radical are determined to a_{iso}(H2 and H6) = 0.17mT, a_{iso}(β2) = 0.75mT and a_{iso}(β1) = 0.50mT. These numbers agree with those extracted from high field EPR spectra of the phenoxyl type NATyrO$^{\bullet}$ in the literature [97, 104], which were also taken for the simulation of the CIDNP field dependence above (fig. 6.1.2).

Tomkievicz *et al.* [97] interpreted the observed 1.54mT splitting in their EPR spectrum from the UV photolysis of tyrosine at pH 11 as the sum of two 0.77mT splittings from two equivalent methylene protons, broadened beyond detection because of restricted rotation. However, the present study consistently reveals a significant difference in the HFC's of the two β-protons in both, the integrals of the geminate CIDNP spectrum in fig. 6.1.4 and the low field part of their CIDNP field dependence in fig. 6.1.2. One should be aware, that the methylene protons are located adjacent to a chiral center, an environment which renders these protons magnetically inequivalent, irrespective of any rotation that may be present.

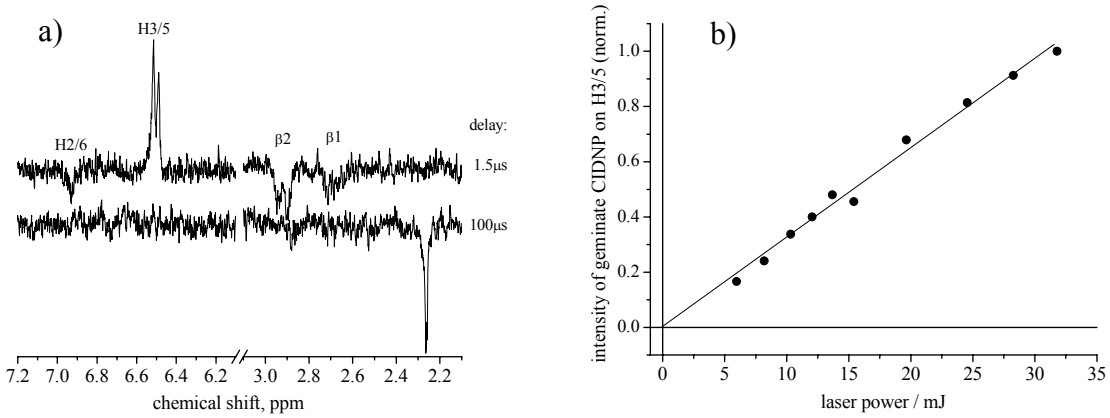

Figure 6.1.4: a) Time resolved CIDNP spectra of a 5mM solution of NATyrO$^-$ at pH 11 taken with a 3µs RF-pulse (90°). 64 spectra are averaged for each trace. b) Dependence of geminate CIDNP (delay: 0.1µs) of NATyrO$^-$ (H3/5) on the laser power (output power per pulse measured behind liquid light guide).

The lower trace in figure 6.1.4 a) shows a CIDNP spectrum taken with a delay of 100µs. Here, the resonances of NATyrO$^-$ have decayed completely. At delay times longer than

several tens of microseconds only the signal at 2.26ppm and the HDO signal (~4.7ppm) are observed.

While the sign of CIDNP depends upon whether the RP stems from a singlet or triplet precursor, the light intensity dependence of the signals can be analyzed to determine whether electron ejection occurs after the absorption of one or two photons. In a further experiment, the output power of the laser was reduced, in order to acquire the dependence of the geminate CIDNP intensity of the largest signal (H3/5) on the light intensity, and the result is presented in figure 6.1.4 b). The linear response clearly suggests that a single photon of 308nm suffices to ionize $NATyrO^-$. This finding is in accord with that of Clancy and Forbes [114] who also concluded a monophotonic ionization in their CIDEP study. However, the present study identifies the monophotonic ionization to occur from a singlet state (see reaction 6.1.1), yielding the phenoxyl type radical, $NATyrO^{\bullet}$, with the largest spin density on the protons in the vicinity of the phenoxyl-group and the β-protons, whereas a triplet state was concluded to contribute in ref. [114]. The unusual polarization found in their CIDEP experiments might be the consequence of an inverted ordering of the electronic states in the radical pair (triplet below singlet, $J_{ex} > 0$).

In principle, a quantitative analysis of the CIDNP kinetics as introduced by Vollenweider *et al.* in 1985 [37] employs the following processes according to scheme 6.1.1 (neglecting the additional decay pathways 6.1.2 and 6.1.3 for e^-_{aq}):

$$NATyrO^- \xrightarrow{h*\nu_{308}} {}^{S1}NATyrO^- \longrightarrow {}^{1}\overline{NATyrO^{\bullet} + e^-_{aq}} \qquad (6.1.1)$$

$${}^{1}\overline{NATyrO^{\bullet} + e^-_{aq}} \xrightarrow{k_{gem}} NATyrO^- \qquad (6.1.4)$$

$${}^{1}\overline{NATyrO^{\bullet} + e^-_{aq}} \xrightarrow{k_{isc}} {}^{3}\overline{NATyrO^{\bullet} + e^-_{aq}} \qquad (6.1.5)$$

$$NATyrO^{\bullet} + e^-_{aq} \xrightarrow{k_t} NATyrO^- \quad \text{(F-pairs)} \qquad (6.1.6)$$

$$NATyrO^{\bullet} + NATyrO^- \xrightarrow{k_{ex}} NATyrO^- + NATyrO^{\bullet} \qquad (6.1.7)$$

$$NATyrO^{\bullet} \xrightarrow{T_{1n}^{para}} NATyrO^{\cdot} \qquad (6.1.8)$$

$$NATyrO^- + e^-_{aq} \xrightarrow{k_a} CHD^{\bullet} \qquad (6.1.9)$$

$${}^{3}\overline{NATyrO^{\bullet} + CHD^{\bullet}} \xrightarrow{k_{d,\,eff}} 2\ NATyrO^- + HDO\ \text{(polarized)} \qquad (6.1.10)$$

$$CHD^{\bullet} \xrightarrow{T_{1n}^{para}} CHD^{\bullet} \qquad (6.1.11)$$

After ionization from a singlet excited state of $NATyrO^-$ (reaction 6.1.1), CIDNP is formed by spin sorting ($S\text{-}T_0$-mechanism) during geminate recombination (reaction 6.1.4) and intersystem crossing to the triplet state (reaction 6.1.5). Reaction 6.1.6 is the termination of the primary radicals after random encounters in so-called F-pairs.

In the literature, two different types of CIDNP kinetics have been observed for the protons H3 and H5 of tyrosine in reversible electron and hydrogen transfer reactions with the sensitizer 2,2'-dipyridyl (DP) [113]. It was shown that significant stationary CIDNP can only be observed in acidic and neutral solutions, whereas above the phenolic p*K* of 9.1 the CIDNP decays rather fast, and the rate of decay depends on the initial $NATyrO^-$ concentration. The kinetics of CIDNP in basic solutions is determined by the rate of degenerate exchange, k_{ex}. Reaction 6.1.7 represents the transfer of an electron from ground state $NATyrO^-$ molecule to a tyrosyl radical upon random encounter. This exchange does not result in a net chemical change but it transfers polarization from a neutral radical to a parent $NATyrO^-$ anion with a considerably longer spin-lattice relaxation time. This way, CIDNP is cancelled out very efficiently when it has been formed by a radical pair mechanism, i.e. in high magnetic fields, since the transferred polarization is of opposite sign to that in the initial radical pair. In low field however, CIDNP intensities will not be influenced by it.

Reaction 6.1.8 is the spin lattice relaxation in the paramagnetic tyrosyl radical. Closs and Miller [115] first recognized that paramagnetic spin lattice relaxation is essential for the observation of CIDNP effects in cyclic reactions by cw-techniques. The equations 6.1.9 and 6.1.10 are the electron attachment to the parent $NATyrO^-$ molecule to give $CHD^\bullet$, and the disproportionation of $CHD^\bullet$ with the tyrosyl radical, with rate constants k_a and $k_{d,eff}$, respectively. Here, $k_{d,eff}$, is the effective rate constant for polarizing HDO by exchange of the proton (not the deuteron) in $CHD^\bullet$. CIDNP on HDO and on the signal at 2.26ppm is presumed to form in the radical pair in equation 6.1.10. Spin lattice relaxation in $CHD^\bullet$ is accounted for in equation 6.1.11.

In figure 6.1.5 the CIDNP kinetics obtained for a 5mM solution of NATrpH are displayed. Only the signals of H3/5 of the parent $NATyrO^-$, the signal at 2.26ppm and HDO give appreciable polarization in the TR-CIDNP experiment (see also fig.: 6.1.4). It turns out that the fast decay kinetics of $NATyrO^-$ is only sensitive to the rate of electron exchange (reaction 6.1.7) and the initial radical concentration, R_0. Tsentalovich *et al.* [113] determined the pseudo first order rate constant for the degenerate electron exchange k_{ex} *to* $3.6\cdot10^5 s^{-1}$ by altering the concentration of the solute. In the same work, $T_1^{NATyrO^\bullet}$ was determined to 63µs. In the present work CIDNP kinetics were obtained for a 5mM solution of $NATyrO^-$ only.

Taking the values for k_{ex} and for $T_1^{NATyrO\bullet}$ from ref. [113], the best agreement with the experimental decay of $P_{NATyr\text{-}}$ is obtained with an initial radical concentration of R_0 = $1.7 \cdot 10^{-7} \pm 5 \cdot 10^{-7}$ M. This is about three orders of magnitude less than in other CIDNP experiments and can be rationalized by a low quantum yield of ionization on one hand, and on the high probability of geminate recombination of the singlet born radical pair on the other. The value of R_0 allows estimating the quantum yield of escaped radicals to about 0.001. (15mJ laser energy per pulse corresponds to about $2.3 \cdot 10^{16}$ photons of λ = 308nm, and $1.7 \cdot 10^{-7}$M radicals in 0.24g[1] are about $2.3 \cdot 10^{13}$ escaped radicals) Thus, about 1000 photons are necessary to yield one radical pair that escapes geminate recombination. The deviations between the experimental data and the fitted curves at short (<20µs) times may be attributed to the length of the applied RF-pulse (3µs).

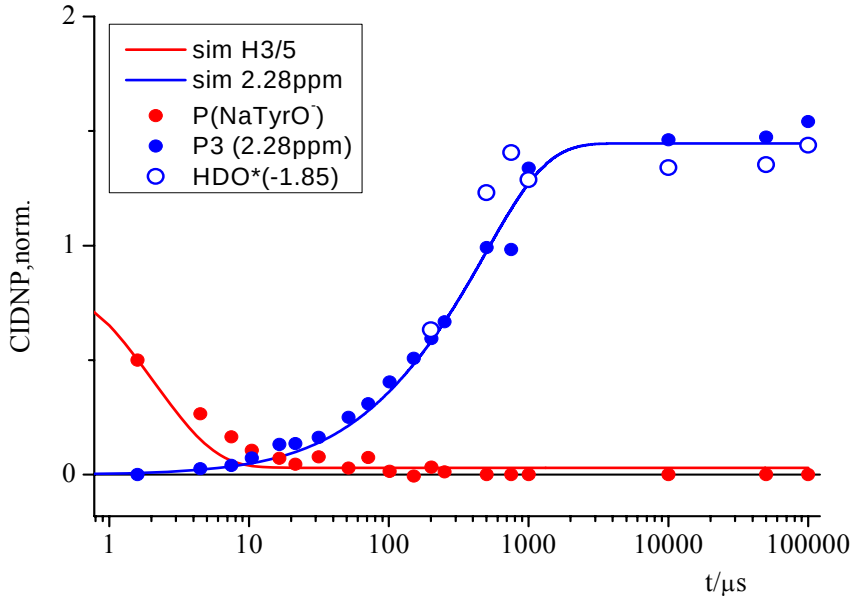

Figure 6.1.5: CIDNP transients of a 5mM solution of NATyrO$^-$ at pH 11 taken with a 3µs RF-pulse. The experimental values are normalized to the initial polarization of H3/5 (●), and the integrals of the HDO line (○) are scaled to those of the product peak at 2.26ppm (x-1.85) (●). Solid lines: fitted curves (see text)

Because of insufficient suppression of the HDO signal, it was only possible to obtain CIDNP signals for longer times (≥200µs). However, obviously the HDO signal rises together with the signal at 2.26ppm, indicating that they are polarized in the same reaction. Thus, both experiments, TR-CIDNP and FD-CIDNP indicate that CIDNP on HDO is formed together with the peak at 2.26ppm. These transients depend on the rate of electron capture by NATyrO$^-$, k_a, and to the rate of disproportionation, $k_{d,eff}$ (reactions 6.1.9 and 6.1.10). Neither the decay

[1] This value was obtained from the shift of the HDO line upon 1.5s of irradiation (see above).

of CIDNP on H3/5 nor the rise of the signal at 2.26ppm is sensitive to k_t, the rate constant of termination (reaction 6.1.6). Besides of these parameters, the spin-lattice relaxation in $CHD^{\bullet}$, and the so-called CIDNP enhancement factors (statistical factors), usually expressed by the ratios β/R_0 with different values for β for each step responsible for CIDNP formation, have to be accounted for. Because a single CIDNP transient is insufficient for a quantitative evaluation of all these parameters, the present analysis is restricted to a crude estimation whether CIDNP formation on HDO in terms of scheme 6.1.1 does not contradict the results of the TR-CIDNP experiment.

For this estimation, the value of $5 \cdot 10^5\ s^{-1}$ for the pseudo first order rate of electron attachment to $NATyrO^-$, k_a, is taken from the literature [94]. Further, the spin-lattice relaxation in $CHD^{\bullet}$ is estimated to ~100μs, and for β in singlet and triplet radical pairs (equations 6.1.4 and 6.1.10), values of -1 and 3 are taken, respectively. Under these presumptions, the simultaneous fitting of the two CIDNP transients in figure 6.1.5 indicates the disproportionation of $CHD^{\bullet}$ and $NATyrO^{\bullet}$ to occur at the diffusion controlled limit ($k_{d,eff} = 1.1 \cdot 10^{10} \pm 0.2 \cdot 10^{10}\ M^{-1}s^{-1}$).

A successful fitting of the CIDNP kinetics with reasonable parameters supports the notion that CIDNP is formed in RP's consisting of the tyrosyl-radical and a second radical formed by the uptake of e^-_{aq}, but it does *not* prove the assignment of this second radical to be $CHD^{\bullet}$. Without a definite assignment of the signal at 2.26ppm and further evidence from a variation of starting concentration, neither the reaction scheme nor the involved rate constants are determined confidently, and alternative mechanisms for CIDNP formation in HDO may be considered that also fit into the kinetic scheme. Finally, HDO is obviously polarized in a (secondary) radical reaction, and a photochemical H/D-exchange in tyrosine as outlined in scheme 6.1.1 is likely, since both, the results of FD-CIDNP and those of TR-CIDNP are in accord with it, but the present results can not provide conclusive evidence for it.

6.1.2 CIDNP Formation in aqueous N-acetyl tryptophan (NATrpH)

The molar absorptivity of tryptophan is about five times higher than that of tyrosine (at the absorption maximum, $\lambda \approx 275$nm) rendering tryptophan residues the most important chromophore among natural amino acids. Photo-ionization of tryptophan is believed to be a major pathway of photo-oxidation of many proteins. Besides ionization, the photophysics and chemistry of tryptophan is more complex than that of tyrosine and the chemical pathways

following light excitation of NATrpH in the near UV can be rather diverse. A detailed discussion of the vast literature on this topic is certainly beyond the scope of the present work and we shall restrict ourselves to an interpretation of the CIDNP results in comparison to those obtained with basic tyrosinate solutions discussed in the previous section.

In basic solution, the cation radical may form upon photo-ionization of NATrpH:

$$NATrpH \xrightarrow{h\nu} {}^1\overline{NATrpH^{\bullet+} + e^-_{aq}} \qquad (6.1.12)$$

The initially formed tryptophan radical cation ($NATrpH^{+}\cdot$) produced by photo-ionization in neutral and moderately basic solution is relatively short lived ($k \approx 1.5*10^6 s^{-1}$) [74, 116, 117], and in alkaline solutions it is much shorter lived due, presumably, to an OH^- mediated H-abstraction:

$$NATrpH^{\bullet+} \longrightarrow NATrp^{\bullet} + H^+ \qquad pK_a = 4.3 \qquad (6.1.13)$$

In acidic solution, at pH 3-4, the cation radical was reported to be comparably long lived ($\tau >$ 100µs) [116], the pK of reaction 6.1.13 is 4.3 [118]. The spin density distribution in the tryptophanyl radicals depends on whether the indole N is protonated or not. DFT calculations by Kiryutin *et al.* [72] predict the most significant differences in proton HFC's for the protons attached to C2 (see table 6.1.3).

	H2	H4	H5	H6	H7	β1	β2
$Trp^{\cdot}$ in H_2O	-0.053	-0.447	0.079	-0.368	-0.034	1.542	2.787
$TrpH^{+\cdot}$ in H_2O	-0.421	-0.504	0.124	-0.412	-0.050	1.189	2.544
CIDNP at pH 13.2	-	A	-	A	-	E	E
CIDNP at pH 11.6	A	A	-	A	-	E	E

Table 6.1.2: Comparison of observed CIDNP patterns for NATrpH at pH 13.2 and pH. 11.6 with calculated isotropic hyperfine couplings for protonated and deprotonated radicals of Trp from ref. [72].

Figure 6.1.6 compares the high field CIDNP patterns observed at pH 11.6 and pH 13.2 in high magnetic field. Qualitatively, the most pronounced difference in these two CIDNP spectra is found for H2. This change in spectral pattern is thus attributed to the rapid deprotonation of $NATrpH^{+\bullet}$ (reaction 6.1.13), producing the neutral radical species with less spin density on H2. Table 6.1.2 compares the predicted isotropic hyperfine couplings to the CIDNP patterns observed in the present work. Hence, the spectra may be interpreted in terms of radical pairs consisting of the solvated electron (e^-_{aq}) with $NATrpH^{+\bullet}$ and with $NATrp^{\bullet}$ at pH 11.6 and pH 13.2, respectively. The g-factor of $NATrpH^{\bullet+}$ (g = 2.00295) is between the radicals of the triplet dyes (g = 2.0030 and g = 2.0041, see table 6.2.3) used in chapter 6.2, and that of e^-_{aq} (g

= 2.00049 [103]). According to the known empirical rules for the analysis of CIDNP effects (see chapter 2.1.3 and ref. [39]) the precursor multiplicity of photo-ionization is thus identified as singlet (reaction 6.1.12).

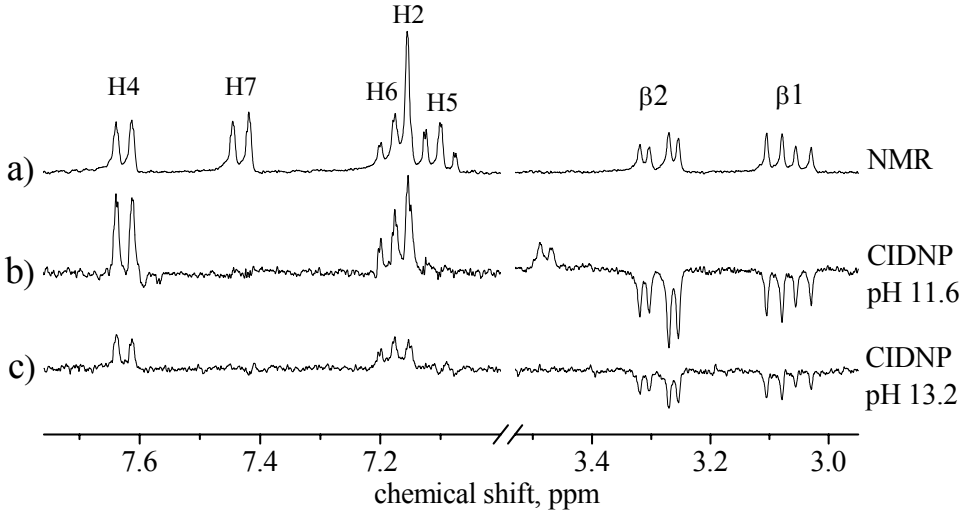

Figure 6.1.6: a) NMR spectrum of NATrpH (pH 11.6); b) and c) CIDNP spectra obtained upon pseudo-cw conditions. For each CIDNP spectrum, three spectra with irradiation (1s at 50Hz) and without irradiation were averaged and subtracted. The two CIDNP spectra are scaled the same way.

Furthermore, signals of side products are seen at pH 11.6, namely a doublet in absorption centred at 3.48ppm, and another signal that also appears as a doublet at 7.58ppm in the vicinity of the signal assigned to H4. Without further spectroscopic evidence, possible assignments for these signals remain too speculative to be discussed here.

The largest CIDNP is obtained around pH 10. When going to lower pH, the intensity of high field CIDNP decreases, and around pH 7 no significant polarization is detected (not shown). Furthermore, no CIDNP is seen in acidic solutions. In low field, however, multiplet CIDNP for the β-protons is still observed at pH 7. It is concluded, that the small value of polarization in high field is a consequence of CIDNP cancellation during degenerate electron exchange (reaction 6.1.14), in which only the cationic radical, $NATrpH^{\bullet+}$, can participate:

$$*NATrpH^{\bullet+} + NATrpH \rightarrow *NATrpH + NATrpH^{\bullet+} \qquad (6.1.14)$$

(With the asterisk denoting the nuclear spin polarization) Hence, the lack of high field CIDNP is taken as further evidence for the protonated radical $NaTrpH^{\bullet+}$ to contribute significantly to CIDNP formation in neutral and moderately basic solution.

However, when taking a closer look at the CIDNP spectrum at pH 11.6 in fig. 6.1.6 there is a significant qualitative discrepancy to the HFC's calculated by Kiryutin *et al.* [72]: The proton

in position 5 of the indole ring rather shows absorptive CIDNP, whereas emission would be expected from the predicted HFC's. Small emission for H5 is also seen in the high field CIDNP spectra with triplet sensitizers (chapter 6.2), which also reflect the spin density in the tryptophanyl radicals. The DFT calculations shall therefore be considered trustworthy, and another reason has to be found for absorption on H5. In addition, reactions 6.1.12 to 6.1.14 can not account for the large nuclear spin polarization observed for the residual protons in the solvent (HDO). In the following the CIDNP field dependence is discussed, and a possible explanation is given.

CIDNP field dependence of aqueous NATrpH at pH 12. The high field spectra discussed above did not reveal the mechanism of CIDNP formation for HDO. In addition, the CIDNP pattern observed for the protons in NATrpH is not in accord with the pattern expected, when only RP's formed upon ionization of NATrpH are considered. In order to clarify some of the ambiguities, a field dependence of CIDNP was acquired with a 12mM solution of NATrpH at pH 12.

^{1}H-CIDNP for the protons in NATrpH and HDO as a function of the external field are shown in figure 6.1.7, an assignment of NMR signals to the positions in the NATrpH molecule can be seen in figure 6.1.6. The field dependence was acquired with the same time interval for irradiation (τ_L = 1.5s) as in the case of NATyrO$^-$. Polarizations for both, the protons in the amino acid and in HDO are considerably smaller than with NATyrO$^-$.

As may be expected from the results discussed in chapter 4, in low magnetic field the polarization is redistributed among all protons in the molecule due to their strong spin-spin coupling. Upon the long irradiation times used in the present experiment (τ_L = 1.5s), even the relatively weakly coupled protons H2 ($J_{H2\text{-}H6} \approx 0.6$ Hz) and the α-proton show a similar CIDNP field dependence as those of H4, H6, and H7. In addition, at 0.32T, the lines of the α-proton acquire large CIDNP due to a level crossing in the nuclear spin eigen-states of the diamagnetic tryptophan molecule (see chapter 4 and ref. [55]). The present chapter, however, is focussed on the underlying photochemistry, and for its elucidation the CIDNP patterns observed at larger field values should be considered.

For CIDNP formed in radical pairs consisting of a tryptophanyl radical and the solvated electron ($\Delta g \approx 0.005$), a high-field maximum around $B_{pol} \approx 1$T would be expected, and indeed, significant CIDNP is formed in this field range. However, emissive CIDNP for H2, and absorptive polarization for one of the β-protons contradicts the HFC's found in ref. [72] (see

table 6.1.2). Around B_{pol} = 1T CIDNP may be explainable by singlet-triplet mixing of $NATrpH^{+\bullet}$ and/or $NATrp^{\bullet}$ with e^-_{aq}, with the nuclear spin states being populated according to their ordering in the diamagnetic product molecule. For neighbouring protons, the strong coupling condition is still fulfilled in this field region, and the observed polarization patterns depends on the timing of the experiment, i.e. on the time for the irradiation and field cycling. The pattern with emission and absorption for the two strongly coupled β-protons obtained here with $\varphi = 90°$ reflects that observed with n=1 (net-effect) in the nutation analysis in fig.: 5.0.3. However, attempts to model the field dependences under the assumption of an adiabatic sample transfer and in the absence of redistribution of polarization due to strong coupling failed.

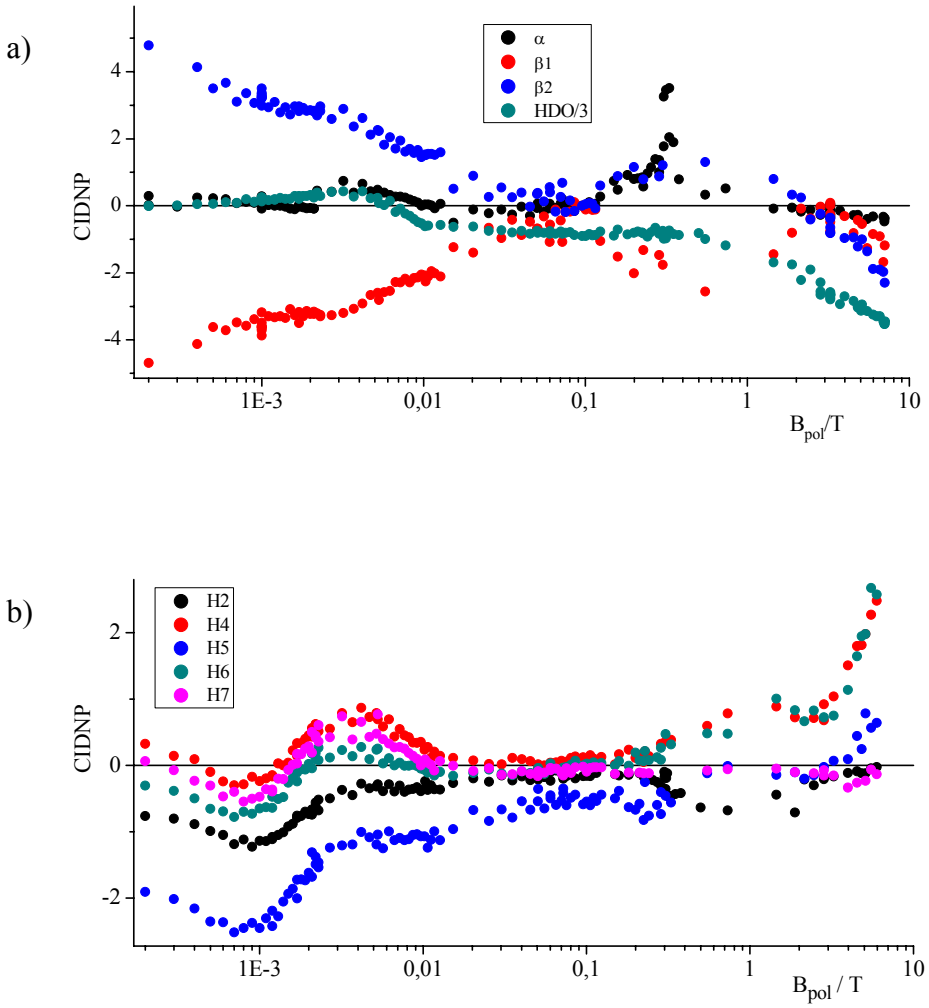

Figure 6.1.7: CIDNP field dependences of 12mM NATrpH at pH 12 (τ_L = 1.5s, $\tau_{fv} \leq$ 0.3s, $\varphi = 90°$), a) HDO (intensity divided by 3), α- and β-protons; b) aromatic protons (indole ring).

Above B_{pol} = 3T the polarization pattern changes, the protons in β-position are both in emission, and absorptive CIDNP is observed for the ring protons in positions 4, 6, (and 5). The shape of the field dependence of the HDO is also typical for a radical pair mechanism to be operative. Between B_{pol} = 3T and 7T the polarizations for the all these protons increases, suggesting that the maximum efficiency for S-T_0 transitions via Δg is reached above 7T. Hence, CIDNP is formed most efficiently in radical pairs with a very small difference in g-factors. These findings may be rationalized with reactions that follow the escape of radicals from the primary reaction cage as follows: The fate of e^-_{aq} produced by photoionization (reaction 6.1.12) parallels that in the case of its production via ionization of $NATyrO^-$. Reactions 6.1.2 and 6.1.3 thus constitute two possible pathways for its disappearance. In addition, ground state NATrpH reacts faster with solvated electrons than most other amino acids.[2] For zwitterionic tryptophan, the rate constant of reaction 6.1.15 has been determined to $4.1*10^8$ $M^{-1}s^{-1}$ at pH 6.8 and $1.5*10^8$ $M^{-1}s^{-1}$ at pH 11.5 [119].

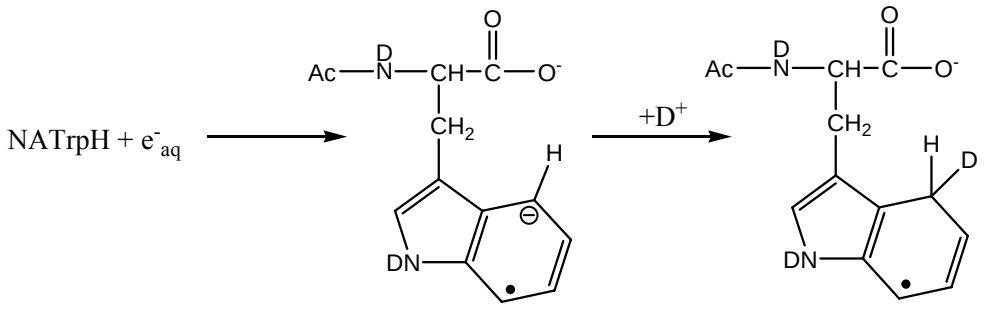

(6.1.15)

In analogy to the cyclohexadienyl radical formed from $NATyrO^-$ (see scheme 6.1.1), the anion radical of NATrpH formed in reaction 6.1.15 is expected to be rapidly deuterated. Alternatively, e^-_{aq} may attach to the carboxyl group of NATrpH, causing other side reactions, e.g. decarboxylation. This, however, will not give rise to CIDNP in the parent NATrpH molecule. Because the increasing CIDNP of HDO above B_{pol} = 2T parallels that of the protons in NATrpH, it is suggestive that CIDNP on HDO is formed in a radical reaction that recovers the original NATrpH molecule, and in the following only this path shall be considered.

Besides of the geminate recombination of the primary radicals (reaction 6.1.12), a further source for CIDNP in parent NATrpH molecules is available through radical pairs consistingof two different kinds of tryptophanyl radicals. H-atom transfer from the radical formed upon electron attachment (reaction 6.1.15) and the neutral tryptophanyl radical from reaction 6.1.13 recovers two NATrpH molecules:

[2] Exceptions are cysteine, cystine reacting about one order of magnitude faster, histidine reacts faster only at low pH, and tyrosine and phenylalanine that react with a comparable rate.

3, 1

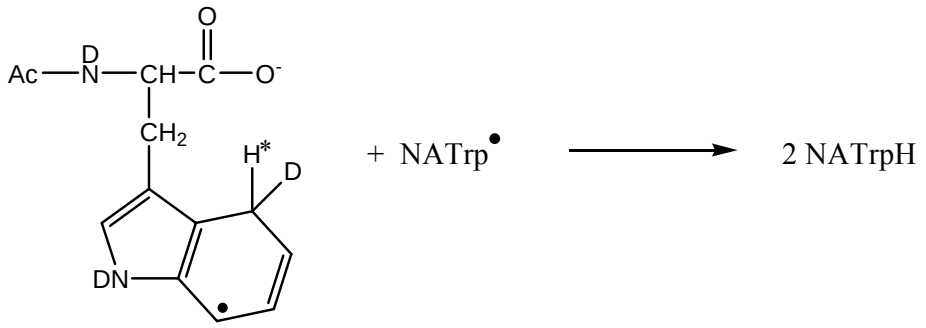

(6.1.16)

The polarization pattern of NATrpH observed at B_{pol} = 7T is thus reconciled with CIDNP formed during disproportionation of two different radicals of NATrpH (reaction 6.1.16). Random encounters of the radical formed by electron attachment (reaction 6.1.15) with NATrp$^{\bullet}$ lead to formation of a radical pair, in which the two radicals have almost similar structures and therefore probably rather similar g-factors. The slight difference in g-factors gives a high field maximum in the CIDNP field dependence which is far beyond 7T, and explains both, the rise of polarization in the field dependences of HDO and the protons in NATrpH. In this reaction path, the parent NATrpH molecule is recovered after H-transfer from one type of tryptophanyl radical to another, and the protons in the solvent then acquire CIDNP after H/D-exchange of the indole N-H in the product via the proton marked with an asterisk in reaction 6.1.16. The high field CIDNP pattern of NATrpH then represents a mixture of (at least) two different tryptophanyl radicals.

The small absorptive CIDNP for H5 is then attributed to the radical formed in reaction 6.1.15. Reaction 6.1.16 leads to incorporation of deuterium in position 4 of NATrpH. This kind of photochemical H/D-exchange results in the collapse of the double doublet for H5 (at 7.10 ppm) into a doublet, which has been observed by NMR after several hours of irradiation with a mercury flash lamp before by Saito et al. [120]. In the present study, the small absorptive CIDNP signals for H5 in figure 6.1.6 b) and c), which could not be reconciled with the signs of HFC's predicted in ref. [72], do not resemble the double doublet structure of the NMR signal for H5 in fig. 6.1.6 a) either, thus lending support to the mechanism proposed above. However, Saito *et al.* [120] actually ruled out that a radical reaction is involved in their H/D-exchange, since it was still observed in the presence of N_2O as a radical scavenger.

Finally, the discussion shows that CIDNP studies that rely on spectra polarized at a single value for the external field can easily be misinterpreted. In the present case, the field dependence of CIDNP could show that a mayor part of polarization observed on NATrpH is

not due to radical pairs containing e^-_{aq}, but is formed in radical pairs with rather small Δg-values.

Conclusions

The photolysis (λ = 308 nm) of the aromatic amino acids tyrosine and tryptophan in aqueous solutions was investigated by different CIDNP techniques. The initial conditions such as concentration of photolyte and pH of the solution have significant influence on the observed spectral patterns, indicating different kinds of tyrosyl and tryptophanyl radicals to contribute to the formation of CIDNP. In principle, these additional reaction pathways can complicate the extraction of quantitative information from CIDNP studies of tyrosine and tryptophan residues with triplet sensitizers (see chapter 6.2), when the wavelength of the applied light lies within the absorption band of the amino acids under study. In order to eliminate the effects that result from ionization of the parent amino acids it is thus recommendable to operate at $\lambda \geq 350$nm (in presence of suitable dyes).

CIDNP is formed most efficiently in basic solutions, and both, tyrosine and tryptophan are found to undergo ionization from singlet precursor states producing solvated electrons (e^-_{aq}). This finding is in accordance with the primary process identified by Bussandri and van Willingen [98] or Ichino and Fessenden [121]. No indication for the involvement of a triplet excited state in the photolysis of tyrosinate as suggested by Clancy and Forbes [114] was found, and the unusual polarization found in their CIDEP experiments might be the consequence of an inverted ordering of the electronic states in the radical pair (triplet below singlet, $J_{ex} > 0$). In the experiments with $NATyrO^-$ it was further shown, that e^-_{aq} is formed upon absorption of a single photon by the variation of light intensity.

It turns out, that e^-_{aq} can be treated as a counter radical within the frame of the radical pair theory to explain CIDNP formation, and the CIDNP field dependence was modelled in good agreement with magnetic interaction parameters reported in the literature for the radical pair consisting of the phenoxyl type tyrosyl radical and e^-_{aq}. The geminate high field spectrum reflects the ratio of hyperfine couplings in the tyrosyl radical.

The CIDNP spectra of $NATyrO^-$ give evidence for the formation of ortho-d_1-$NATyrO^-$ in a reaction involving radicals, and the results lend support to the involvement of the cyclohexadienyl anion radical, formed by electron attachment to $NATyrO^-$, as proposed by London and Gabel [93], which is rapidly protonated. From the CIDNP field dependence of

the solvent (HDO) it was possible to estimate the g-factor of this radical in aqueous solution to g ($CHD^{\bullet}$) ≈ 2.0033±0.0004.

The slow formation of CIDNP in HDO and the signal at 2.26ppm in the time resolved measurement is rationalized by the low concentration of radicals escaping from geminate recombination. Thus, the present study also reveals a source of a particularly efficient polarization of solvent HDO, which may be of potential interest for applications in magnetic resonance imaging. The facile uptake of e^-_{aq} by aromatic moieties of the ground state amino acids produces anion radicals of the parent amino acids. The solvent (HDO) is suggested to acquire CIDNP in the course of disproportionation of different kinds of amino acid radicals. This reaction recovers the parent amino acids, which transfer the polarization via H/D-exchange to the solvent. Mechanistically, the polarization of HDO is suggested to proceed in a similar way for both, tyrosine and tryptophan.

Virtually every DNA-binding protein which is present in biological systems, e.g. histone in the cell nucleus, has a basic potential for protecting the genetic information from excess charges (radicals) present in the DNA [122]. The particularly low oxidation potential of the aromatic amino acids tyrosine and tryptophan is assumed to play an important role in the trapping of radicals by charge transfer processes via the DNA-protein interface. Finally, it can be expected that a facile formation of the anion radicals of tyrosine and tryptophan by the uptake of e^-_{aq} is also of considerable significance, thus enabling the trapping of both, holes *and* excess electrons. This aspect suggests a very general biochemical role of this kind of radicals.

6.2 CIDNP Field Dependences of Amino Acid / Dye Systems

Photoreactions, in which triplet excited sensitizers are quenched by so-called "CIDNP active amino acids" are of particular significance because of their potential biophysical applications. There has constantly been some interest in this kind of reactions since R. Kaptein *et.al.* proposed to use the CIDNP technique as a surface probe for proteins [123]. The idea is simple in its essence: A protein is brought into aqueous solution together with a suitable dye. Upon irradiating the solution with the appropriate light, the excited dye undergoes singlet-triplet inter-conversion, and is subsequently 'quenched' by certain amino acids in the protein which are accessible for the dye. The resulting triplet born radical pair, consisting of a dye and an amino acid radical, can diffuse apart and undergo nuclear spin dependent inter system crossing into the reactive singlet state. After back reaction the NMR spectrum is measured, which shows enhanced absorption and emission lines (CIDNP) for specific amino acid residues, thereby simplifying the assignment of lines. Information on the surface topology of the protein can be extracted from these NMR spectra. A key point in such studies is the dependence of accessibility of the protein surface on the structure of the sensitizing reagent. More recently, it has been shown that the dynamics of protein folding can be probed by measuring the CIDNP spectrum with a variable delay after a folding or refolding process has been initiated in stopped-flow type experiments [124].

Only three out of the twenty naturally occurring amino acids, namely histidine, tyrosine, and tryptophan are commonly referred to as 'CIDNP-active', meaning that they are capable of quenching suitable triplet excited dyes (sensitizers). Depending on the sensitizer, methylated lysines and methionine can also exhibit CIDNP [125]. It is known, that amino groups in general are capable of quenching triplet excited carbonyl sensitizers such as quinones or benzophenone derivatives by electron transfer upon formation of N-centred radicals to give rise to CIDNP [126, 127].

The dyes on the other hand, are chosen according to the requirements of the experimental set-up, i.e. the wavelength of the applied light. They should be water-soluble and undergo a reversible reaction path, with the quenching amino acid, meaning that both, the sensitizing dye and the quenching amino acid are recovered after the reaction. Most commonly flavins are used for initiating the photochemical reaction at wavelength longer than the 308 nm applied in the present experiments.

Here, the efficiency of CIDNP formation as a function of the external magnetic field is investigated for different combinations of aromatic amino acids and photoactive dyes, with the aims of i) establishing the mechanisms of the quenching processes, ii) extracting the magnetic interaction parameters (hyperfine couplings and isotropic g-factors) of the involved amino acid radicals, and iii) optimizing the conditions for potential biophysical applications.

In the present work, radical pairs (RP's) are formed by electron transfer from the aromatic amino acids N-acetyl tyrosine (NATyrOH) and N-acetyl tryptophan (NATrpH) to the triplet excited dyes anthraquinone-2-sulfonic acid (AQ2S) and 2,2'-dipyridyl (DP). Other triplet sensitizers have also been employed (e.g. p-benzoquinone (BQ) and 4-carboxy benzophenone (4-CBP)), but shall not be discussed here. Triplet benzoquinone is quenched by ground-state benzoquinone giving rise to formation of hydroquinone, and 4-CBP gives large CIDNP on NATrpH (see chapter 4) but a complete CIDNP field dependence was not acquired. 4-CBP is commonly used in experiments with methionine [43, 128, 129].

All reaction systems discussed in this chapter involve excitation of a dye molecule (*D*) by 308nm laser light, followed by inter system crossing into a triplet state:

$$^{S}D \overset{h\nu, ISC}{\rightarrow} {}^{T}D \quad . \tag{6.2.1}$$

The radical pairs are then formed by subsequent electron or hydrogen transfer reactions between the triplet excited dye molecule with the amino acid. Because each reaction system has its own peculiarities they are discussed separately.

The amino acids have been investigated with DP as a sensitizer at 308nm by field dependent CIDNP before [11, 130], but a reliable determination of the magnetic interaction parameters of the involved radicals remained difficult, because it relies solely on the g-factor of DP for which only a single value obtained from an EPR spectrum taken in 1962 is available [131]. Moreover, the small difference in g-factors between the radicals of dipyridyl and tryptophan prevented the determination of the g-factor of the tryptophanyl radical. Probing the different amino acid radicals with the same sensitizers allows the comparison and refinement of magnetic interaction parameters obtained from simulations of the CIDNP field dependences in the different RP's. This strategy further allows confirming the validity of the method for extracting these parameters from the CIDNP field dependence which has been developed and applied [40, 41] and is briefly outlined in the theoretical section (chapter 2.1). However, it was shown in chapter 4, that it is subject to certain limitations. The determination of hyperfine couplings from the low-field part of the field dependence is obstructed by the redistribution of polarization among those spins that are strongly coupled ($J \geq \Delta\nu$) in low magnetic fields [56]. In the previous chapter, the strategy for the extraction of hyperfine couplings has therefore

been modified. From the ratio of intensities in the TR-CIDNP spectrum taken immediately after the laser pulse (geminate spectrum) at high magnetic field, the ratios between hyperfine couplings were obtained. However, only if the spectrum contains a signal for which the value of hyperfine coupling is known, the absolute values become accessible. The present discussion will thus be restricted to relative CIDNP intensities observed at high magnetic field in comparison to hyperfine structures reported in the literature.

Taking the g-factor of the solvated electron (e^-_{aq}) as reference (g = 2.00049 [103]), the g-factor of the tyrosyl radical (phenoxyl type) was estimated from the high field maximum in the CIDNP field dependence obtained upon photolysis of N-acetyl tyrosine (g ≈ 2.0045) in the previous chapter (6.1). In the following, this value is refined by comparison with other g-values from the literature, namely those for the radicals of the sensitizers DP and AQ2S. Finally, the short lived radical cation of tryptophan ($NATrpH^{+\bullet}$) in aqueous solution shall be studied with the same dyes, in order to extract a reliable value for its g-factor.

Experimental

CIDNP field dependences were measured with the field cycling set-up described in chapter 3, and a typical timing scheme for the experiments is sketched in fig. 3.2.4. The sample was transferred from B_{pol} to B_0 immediately after pulsed laser irradiation (~15mJ at the sample, 50Hz) with $\tau_{fv} \leq 350$ms.

sample	chapter/ ref.	*AA*	*D*	*c*(*AA*)/ mM	*c*(*D*)/ mM	pH	τ_L / s	φ
1	6.2.1	NATyrOH	DP	12.4	2	10.5; Na_2HPO_4, NaOD	1.2	45°
2	[11, 41]	NATyrOH	DP	50	2	3.5	2	45°
3	6.2.2	NATyrOH	AQ2S	12.1	0.65	10.5; Na_2HPO_4, NaOD	1.3	45°
4		NATyrOH	AQ2S	10	0.65	3	1	45°
5	6.2.3	NATrpH	DP	3.5	12	13; NaOD	1	45°
6	6.2.4	NATrpH	AQ2S	8.1	0.6	3	1	45°
7		NATrpH	AQ2S	2.5	0.6	3	1	90°
8		NATrpH	AQ2S	8.1	0.6	7; Na_2HPO_4	1	90°
9		NATrpH	AQ2S	8.1	0.6	11.5; NaOD	1	45°

Table 6.2.1: Experimental conditions for amino acid (*AA*)/ dye (*D*) systems studied.

Chemicals: N-acetyl-tryptophan (NATrpH), N-acetyl-tyrosine (NATyrOH), 2,2'-dipyridyl (DP) (all Sigma Aldrich) were used as received. Anthraquinone-2-sulfonic acid (AQ2S) was recrystallized from D_2O. The concentrations of quenching amino acids and dye molecules in aqueous solutions are listed in table 6.2.1. All samples were purged with dry nitrogen to remove dissolved oxygen prior to use.

6.2.1 Reaction of NATyrOH with DP

Depending on the concentrations of the compounds and the pH of the solution, different pathways of the photoreaction and formation of CIDNP have been established in a combined study of laser flash photolysis and time resolved CIDNP for this reaction system [113]. In acidic and basic solutions triplet DP is quenched by electron transfer, whereas in neutral and moderately basic solutions, the process was found to be hydrogen atom transfer. This is due to the different protonation states of the reacting compounds:

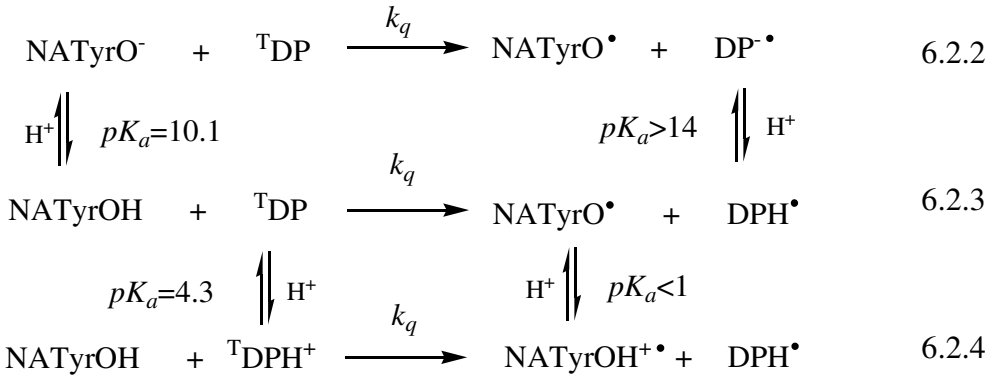

Scheme 6.2.1: Quenching processes and subsequent protonation and deprotonation steps in solutions of NATyrOH with DP at different pH values.

The different quenching processes summarized in scheme 6.2.1 have quenching rate constants, k_q, near the diffusional limit ($\sim 2 \cdot 10^9 M^{-1}s^{-1}$) for the electron transfer reactions at pH > 10.5 and pH < 5, and about two orders of magnitude smaller for H-atom transfer in neutral and moderately basic solutions [113]. Despite these significant differences, the radical pairs that lead to CIDNP formation are the same at any pH, consisting of the neutral tyrosyl and dipyridyl radicals ($NATyrO^{\cdot}$ / $DPH^{\cdot}$). This is due to the anion radical of DP being a strong base, and the cation radical of NATyrOH being a strong acid. Both undergo rapid protonation and deprotonation steps as indicated in scheme 6.2.1. Changes in the absorption coefficient of the different forms of DP are summarized in ref. [113]. The total charge of the radicals formed at different pH can have electrostatic influence on the rate of the recombination reaction. The carboxyl groups of NATyrOH and $NATyrO^{\cdot}$ have pK_a's of about 2.2 and the neutral radical of DP is further protonated in strongly acidic solutions:

(6.2.5)

For the tyrosine protons the CIDNP kinetics are significantly different at high and low pH values [113]. In basic solution the signal decays fast and depends on the initial tyrosine

concentration, because the polarization is transferred from the radical to the diamagnetic ground state molecule in the reaction:

$$NATyrO^- + {}^*NATyrO^\bullet \xrightarrow{k_{ex}} {}^*NATyrO^- + NATyrO^\bullet \qquad (6.2.6)$$

Here, the asterisk denotes the polarization; reaction 6.2.6 is usually referred to as a 'degenerate electron exchange'; its rate constant has been determined to $k_{ex} = 9\ 10^{-7}\ M^{-1}s^{-1}$ by time resolved CIDNP [113], and was used for fitting the CIDNP kinetics obtained upon photolysis of a basic $NATyrO^-$ solution in chapter 6.1.1.

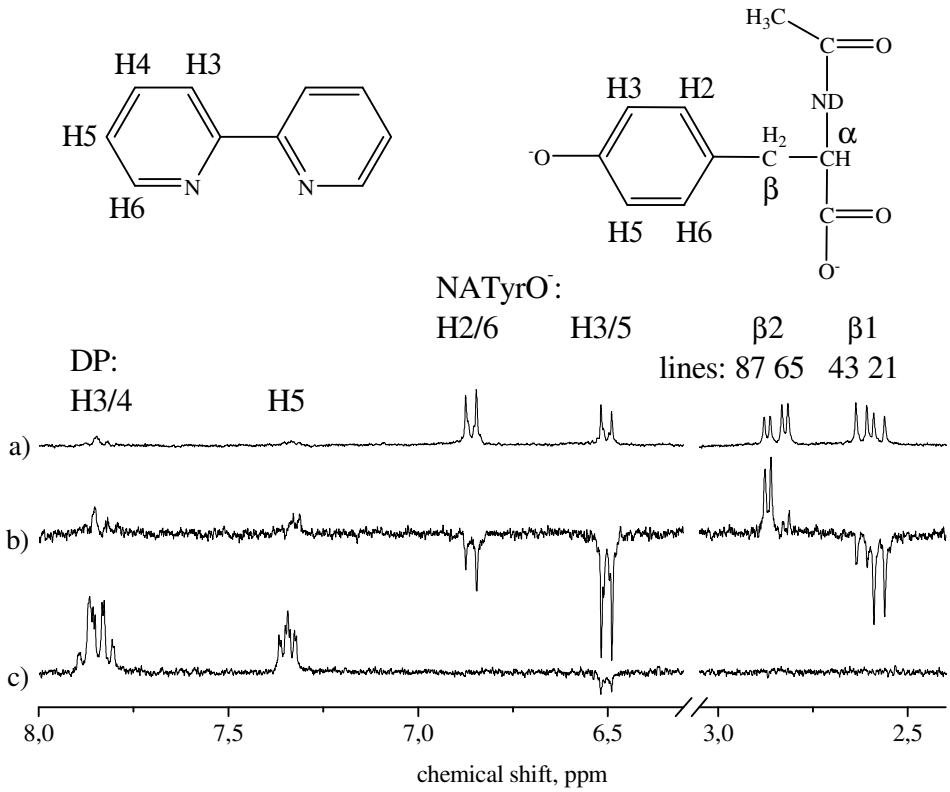

Figure 6.2.1: a) NMR-spectrum of $NATyrO^-$ and DP at pH 10.5 (sample 1, table 6.2.1). b) CIDNP spectrum (τ_L = 1.2 s) of the same solution at B_{pol} = 2.2 mT and c) B_{pol} = 2 T.

Because the radical pairs formed in acidic and basic solutions are essentially the same, it is expected that qualitatively similar CIDNP field dependences are observed in acidic and basic solutions of NATyrOH with DP. In basic solutions, less polarization is expected at high magnetic fields only, because reaction 6.2.6 reduces the stationary value of CIDNP formed during the spin sorting process ($S\text{-}T_0$).

Figure 6.2.1 displays typical CIDNP spectra obtained with a basic solution; field dependent spectra of acidic solutions were obtained in ref. [11], and a detailed theoretical treatment was

undertaken and published in ref. [41]. In low magnetic fields (B_{pol} = 2.2mT, fig. 6.2.1), the β-protons display the typical (n-1) multiplet effect [11, 130], which monotonously decays with increasing B_{pol} until no significant polarization is detected above 0.2T. This effect has been extensively discussed for the cases of histidine [40] and tyrosine [41] and the shall not be repeated here, because it does not bear useful information on the magnetic interaction parameters of the involved radicals. For the β-protons, CIDNP field dependences are shown in figure 6.2.2. For the pair of β-protons, the field variation obviously occurs rather adiabatically, since this is a prerequisite for observing the n-1-multiplet effect.

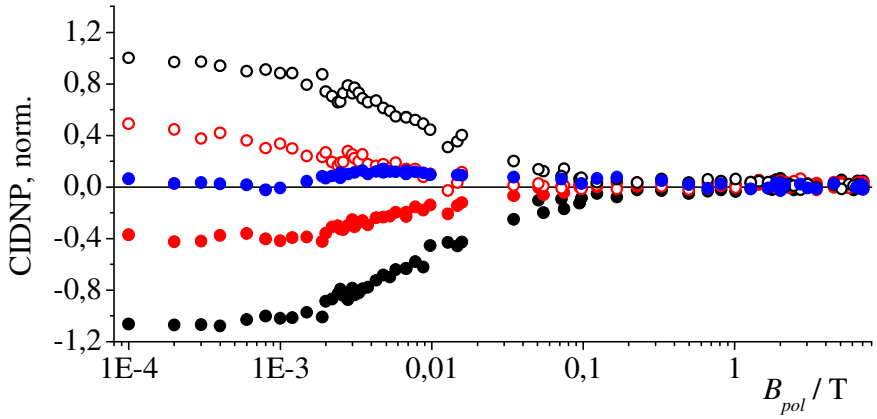

Figure 6.2.2: CIDNP field dependences of α-proton and β-protons in NATyrOH sensitized with DP in basic solution (sample 1, table 6.2.1). Full black circles: lines 1 and 2, full red circles: lines 3 and 4, open red circles: lines 5 and 6, Open black circles: lines 7 and 8, blue circles: α-proton. For the assignment of lines see fig.: 6.2.1.

In addition, a field dependence for the α-proton is shown in fig. 6.2.2, which was not reported in ref. [11]. Because of its small hyperfine coupling in the tyrosyl radical, no polarization is expected for the α-proton, and its reason remains unclear. CIDNP might be transferred from the β-protons via scalar coupling, or the α-proton may be polarized directly in a radical reaction. In the present case only small CIDNP is observed, and the former possibility seems more likely, the latter possibility is briefly discussed in section 6.2.3 (NATrpH / DP).

The following discussion shall be reduced to the CIDNP field dependences of the ring protons of NATyrOH observed in acidic [11] and basic solutions (present work); because they reflect the most prominent differences and allow the extraction of a g-factor for the neutral dipyridyl radical ($DPH^{\bullet}$). CIDNP field dependences observed for the ring positions (H2/6 and H3/5) are compared in figure 6.2.3.

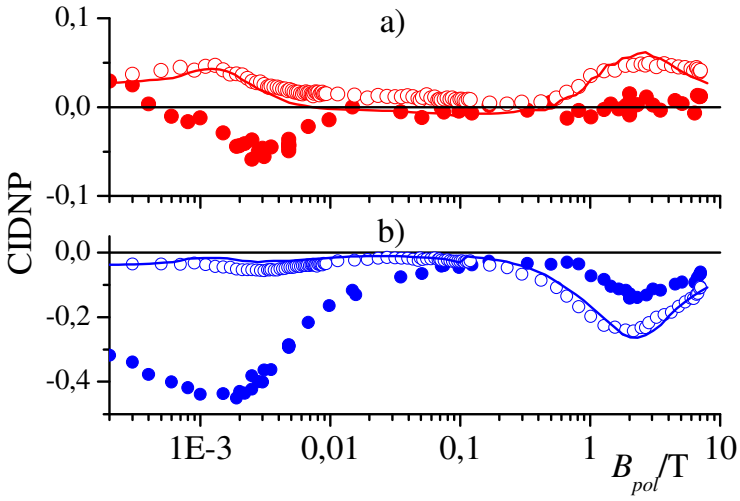

Figure 6.2.3: CIDNP field dependences of NATyrOH sensitized with DP in basic (sample 1, full circles) and acidic (sample 2, open circles) solution from ref. [11]. Solid lines: Simulation with the parameters listed in table 6.2.3. a) H2 and H6; b) H3 and H5.

Despite the fact, that CIDNP is expected to be formed in the same RP, both pairs of aromatic protons show significantly different field dependences for acidic and basic solutions. In low field, between 0.4mT and 15mT, the two curves for H2/6 (fig. 6.2.3 a)) even differ in the sign of CIDNP. Because no systematic study was performed on the present reaction system it can only be speculated that coherent polarization transfer processes during τ_L gives rise to these differences. In ref. [11], the sample was irradiated for τ_L = 2s with significantly lower power and a higher repetition rate (2mJ, 200Hz), whereas in the present work polarization is generated within a much shorter time (τ_L = 1s, 15mJ, 50Hz), complicating a direct comparison of the low field parts in fig. 6.2.3. The large emissive polarization observed on H 3/5 at low magnetic fields has its maximum around 2mT. This value will be compared to the low field maxima observed with AQ2S and e^-_{aq} in the conclusions in the end of this chapter.

The hyperfine interactions in $DPH^{\cdot}$ have been calculated by N. P. Gritsan, and are given in refs. [11] and [41]. Taking these HFC's, satisfactory fits for the observed field dependences in acidic solutions were obtained with Δg = 0.0015±0.0003 and the other parameters listed in table 6.2.3 in the end of the chapter. Thus, taking g_{iso} = 2.0045 for the tyrosyl radial, an isotropic g-value of 2.0030±0.0004 is obtained for $DPH^{\cdot}$, which agrees with the only available experimental value obtained by EPR [131]. The CIDNP field dependences obtained in acidic solutions are published in ref. [41].

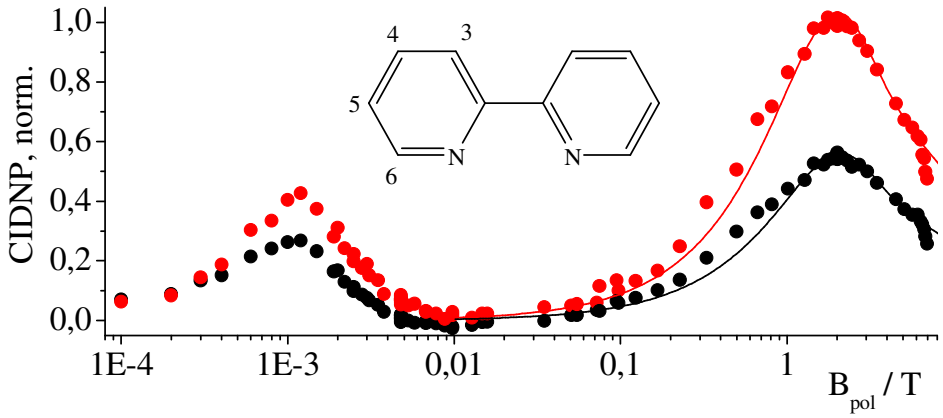

Figure 6.2.4: CIDNP field dependences of DP-protons (sample 1, table 6.2.1) red circles: H3 and H4, black circles: H5. The parameters for the simulation with Adrians model are listed in table 6.2.3. The calculated values of HFC's for $DPH^{\cdot}$ were taken from ref.: [41].

Field dependences obtained with basic solutions are also displayed in fig. 6.2.3; due to degenerate electron exchange (reaction 6.2.6), the polarization at high magnetic fields is significantly smaller in basic than in acidic solution. Only the protons with larger HFC, namely those in the positions 3 and 5 reveal a high field maximum. This *emissive* maximum is slightly shifted with respect to that in the field dependence observed in acidic solutions, which is attributed to ionization of the parent $NATyrO^{\cdot}$ giving an *absorptive* maximum around B_{pol} = 1T (see chapter 6.1.1, fig. 6.1.2). The contribution of this reaction path may shift the maximum observed on H3/5 from about B_{pol} = 2T to B_{pol} = 2.3T. This conclusion is corroborated by the high-field maximum observed for the protons of DP also occurring around 2T in basic solutions, as can be seen in figure 6.2.4.

6.2.2 Reaction of NATyrOH with AQ2S

It is instructive to compare the magnetic interaction parameters obtained for the tyrosyl radical in the previous sections (6.1.1 and 6.2.1) to those that can be obtained from other radical pairs. The photochemistry of the sulphate derivatives of 9,10-anthraquinone has been studied in more detail than that of 2,2-dipyridyl (DP), as their configuration isomers such as the 1- and 2-sufonates have been used as simple model compounds representing 'weak' and 'strong' sensitizers [132, 133]. The sodium salt of anthraquinone-2-sulfonic acid can be easily

dissolved in water, and is known for its high triplet yield (ϕ_{ISC} > 0.9) [134]; its photo-reactivity has received some attention, e.g. as a photo-catalyst in solar energy storage and photo-oxidation of chloride into chlorine and for the splitting of water. Anthraquinone sulfonates are further used quite frequently for generating radicals of bio-molecules such as nucleosides, simple amino acids, and small peptides [135-138].

In basic solution, ^{T}AQ2S is expected to be quenched by NATyrO$^-$ via electron transfer to yield triplet radical pairs consisting of the anthraquinone anion radical and the neutral tyrosyl radical:

$$^{T}\text{AQ2S} + \text{NATyrO}^- \longrightarrow {}^{T}\overline{\text{AQ2S}^{-\bullet} + \text{NATyrO}^{\bullet}} \quad . \qquad (6.2.7)$$

The anion radical AQ2S$^{-\bullet}$ can be protonated to AQ2SH$^{\bullet}$ in acidic solutions (pK ~ 3.2) [139], while protonation of the -SO_3^- group in the parent AQ2S molecule occurs only around pH ~ 0.

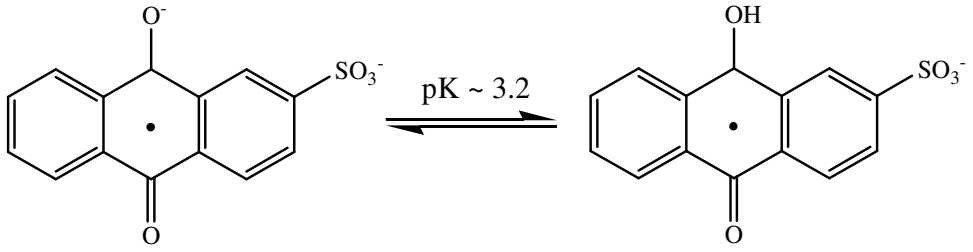

(6.2.7)

For the reaction system of ^{T}AQ2S and NATyrOH two pH regions can thus be distinguished, namely above and below the pK of about 3.2 in the protonation equilibrium in equation 6.2.7. At low pH values, triplet AQ2S may be quenched by H-atom transfer from neutral NATyrOH to yield the radical pair NATyrO$^{\cdot}$/AQ2SH$^{\cdot}$:

$$^{T}\text{AQ2S} + \text{NATyrOH} \longrightarrow {}^{T}\overline{\text{AQ2SH}^{\bullet} + \text{NATyrO}^{\bullet}} \quad . \qquad (6.2.8)$$

The magnetic interaction parameters of AQ2S$^{-\bullet}$ have been investigated in more detail than those of DPH$^{\cdot}$. Hyperfine couplings of the anion radical were determined by ENDOR and TRIPLE resonance techniques [140] and are given in figure 6.2.5. In the same work, the g-factor of AQ2S$^{-\bullet}$ was estimated to g = 2.0040.

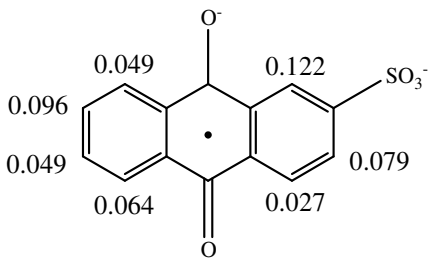

g = 2.0040; a_{eff} = 0.141mT

Figure 6.2.5: Magnetic interaction parameters of AQ2S$^{-\cdot}$ from ref. [140]

The α- and β-protons of NATyrOH do not acquire significant polarization at high magnetic field. Again, multiplet CIDNP of the β-protons is observed up till B_{pol} ~ 0.3T and monotonously decreases with growing field. It reflects the strong coupling (J) in the diamagnetic product rather than properties of the radical pair state.

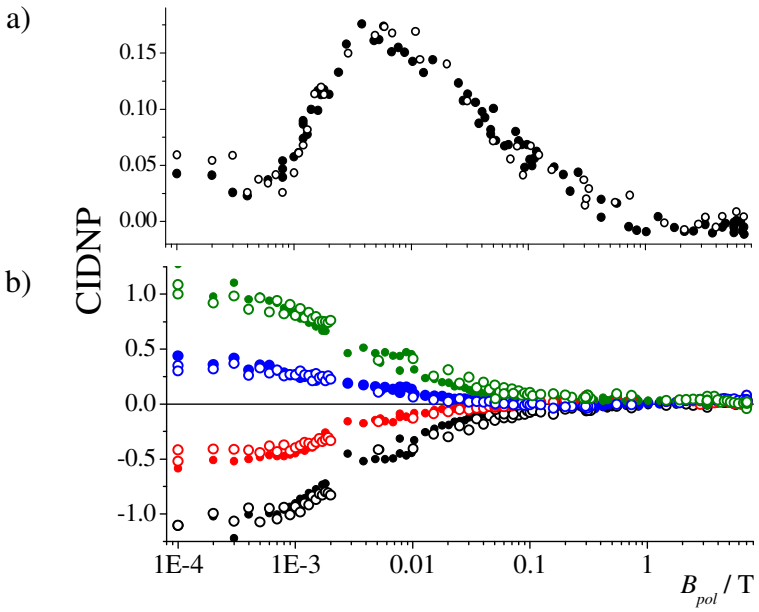

Figure 6.2.6: CIDNP field dependences of NATyrOH (see structure in fig. 6.2.1) sensitized with AQ2S in basic (sample 3, full circles) and acidic (sample 4, open circles) solution. a) α-proton (four lines) b) β-protons: black: lines 1 and 2; red: lines 3 and 4; blue: lines 5 and 6; lines 7 and 8. (For the assignment of lines see fig. 6.2.1, and for sample preparation table 6.2.1)

Polarization of the α-proton is also observed up till 0.3T only. It is attributed to the redistribution of CIDNP within the ABX-system formed by the two β-protons and the α-proton. The similarity of the field dependences for the α-proton at both pH-values supports the conclusion that 'low-field CIDNP' is observed, since 'high field CIDNP' is i) influenced by degenerate exchange and ii) obviously varies with the change of pH (see below). For the other protons in NATyrOH, the field dependences obtained after quenching of ^{T}AQ2S at pH 10.5 and pH 3 are shown in figure 6.2.7.

As in the case with DP as a sensitizer, low field CIDNP of similar sign is observed for the ring protons (H3/5 and H2/6) in basic solution, and is again explained with the redistribution of polarization between the individual proton positions that exhibit strong coupling in low field. Here, the intensity and repetition of laser irradiation is the same in the two experiments (~15mJ, 50Hz), and the efficiency of CIDNP re-distribution reflects the difference in τ_L. Up

till B_{pol} = 0.3T, the curves for H3/5 and H2/6 are clearly more similar with τ_L = 1.3s (pH 10.5) than those obtained with τ_L = 1s (pH 3).

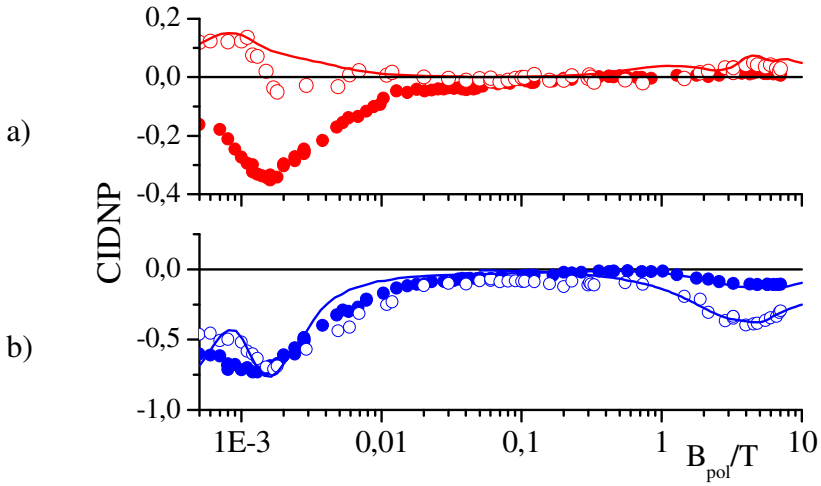

Figure 6.2.7: CIDNP field dependences of NATyrOH (see structure in fig. 6.2.2) sensitized with AQ2S in basic (sample 3, full circles) and acidic (sample 4, open circles) solution. Solid lines: Simulation with the parameters listed in table 6.2.3. a) H2 and H6, b) H3 and H5 (For sample preparation see table 6.2.1)

At high magnetic field in both, basic and acidic solutions, emissive polarization is observed for the protons in position 3/5, and absorptive polarization for those in position 2 and 6. This result is in accordance with Kaptein's rules [39] for a triplet born radical pair, a larger g-factor for $NATyrO^{\cdot}$ than for $AQ2S^{\cdot -}$, and the hyperfine couplings taken from chapter 6.1 (positive for H2/6 and negative for H3/5). In basic solution, the high field maximum occurs close to the maximum available field, and in acidic solutions it shifts to slightly lower field. Because no change in the protonation state of the tyrosyl radical is expected, the shift is attributed to the protonation state of AQ2S (reaction 6.2.7). A slight decrease of the isotropic g-factor upon protonation of the radical of 2,6-anthraquinone disulfonic acid has been observed in ref. [139], supporting this assumption.

The CIDNP field dependences were simulated with the same values of magnetic interaction parameters for the tyrosyl radical (g = 2.00445) as taken for the previously discussed cases (chapter 6.1 and chapter 6.2.1). The high field part of H 3/5 of $NATyrO^{\cdot}$ yields g = 2.0041 and g = 2.0039 for the deprotonated and protonated forms of AQ2S radicals, respectively (reaction 6.2.7), which is in excellent agreement with the value stated in ref.: [140].

The value of g_{iso} for the tyrosyl-radical in aqueous solution is now determined on the basis of Δg-values obtained with four different counter radicals: e^{-}_{aq} (chapter 6.1), $DPH^{\bullet}$ (chapter 6.2.1), $AQ2S^{\bullet}$ and $AQ2SH^{+\bullet}$ (present chapter). In order to obtain an idea about the precision of the Δg-values extracted from FD-CIDNP, different simulations for acidic and basic

solutions are compared in figure 6.2.8. Here, the value for NATyrO$^{\bullet}$ was fixed to g_{iso} = 2.00445 and the g-values of the counter radicals AQ2S$^{\bullet}$ and AQ2SH$^{+\bullet}$ are varied in a reasonable range. On the basis of this comparison, a relative error for Δg is estimated to ±15%. This means that the determination of g-factors becomes considerably more precise with increasing B_{max}, making an extension of the available field range above B_{pol} = 7T desirable.

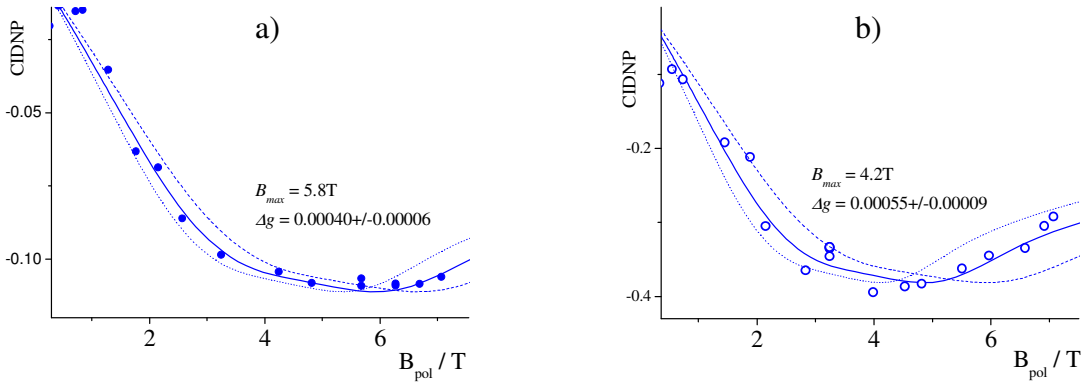

Figure 6.2.8: Comparison of simulations with different Δg-values for CIDNP field dependences of H3/5-protons obtained in acidic and basic solutions of NATyrO- with AQ2S (g_{iso}(NATyrO$^{\bullet}$)=2.00445). a) basic solution (full circles, sample 3, table 6.2.1) g_{iso}(AQ2S$^{\bullet}$)=2.00400 (solid line), 2.00405 (dashed line), 2.00395 (dotted line). b): acidic solution (open circles, sample 4, table 6.2.1) g_{iso}(AQ2SH$^{+\bullet}$)=2.00390 (solid line), 2.00410 (dashed line), 2.00380 (dotted line).

Another reason for the observed shift of the high field maximum could be a contribution of ionization of NATyrO^{-}, as stated in the case of (NATyrOH/DP). The lower value of high field polarization in basic solution is the consequence of degenerate electron exchange (reaction 6.2.6).

The use of AQ2S as a sensitizer has obvious advantages over that of DP, namely the significantly smaller value of a_{eff} that renders the approximation of the individual couplings by one effective HFC's more reliable on one hand, and gives a higher value of CIDNP on the amino acid under investigation on the other hand. In contrast to DP, AQS does not show any significant CIDNP due to its small hyperfine interaction. In reversible reactions of NATyrO^{-} with different counter radicals the g-factors of the dye-radicals are now determined. In the following, these numbers shall be taken for the determination of the unknown g-factor of the short lived tryptophanyl radical in aqueous solution.

6.2.3 Reaction of NATrpH with DP

The reaction of triplet DP with NATrpH has been investigated in some detail by laser flash photolysis and time resolved CIDNP before [74], and a CIDNP field dependence has also been measured [11]. In these works, also the reactions between excited DP and NATrpH were established. In basic solution, the radical cation, $NATrpH^{+\bullet}$, is formed by electron transfer to triplet DP and can subsequently deprotonate to give the neutral tryptophanyl radical, $NATrp^{\bullet}$. In parallel, $DP^{-\bullet}$ is protonated to give $DPH^{\bullet}$. One of the main problems of the experimental work applied on tryptophanyl radicals was, to determine whether the indole-N is protonated or not in the species under investigation. For the present reaction system the protonation/deprotonation steps are summarized in scheme 6.2.2:

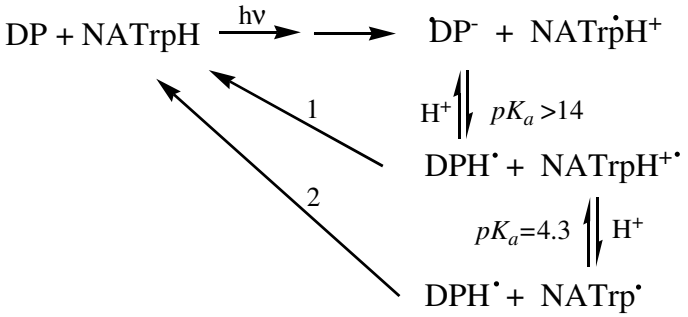

Scheme 6.2.2: Protonation and deprotonation steps in the reaction system NATrpH / DP.

Depending on the protonation state of the radicals in the pair, back reaction to the starting compounds either occurs via electron transfer with subsequent deprotonation of DPH (path 1 in scheme 6.2.2), or by H-atom transfer from $DPH^{\bullet}$ to $NATrp^{\bullet}$ (path 2). Because protonation equilibrium cannot be established within the short lifetime of the radical pairs, the pK-values given in scheme 6.2.2 might be of minor importance. Under the present conditions, the geminate pairs react on the timescale of about 10ns, whereas of a solvent exposed tryptophan residue in *E. coli* DNA photolyase was reported to deprotonate with a time constant of 300ns (at pH 5.4-8.6) [141]. Consequently, singlet-triplet mixing occurs in geminate pairs containing $NATrpH^{+\bullet}$, while CIDNP formed in bulk reactions will always involve the deprotonated tryptophanyl radical. It is thus unclear to which extent the protonated and deprotonated radical species are observed in the CIDNP experiments under pseudo-cw conditions.

In acidic solutions, degenerate electron exchange prevents the observation of considerable high field polarization:

$$^{*}NATrpH^{+\bullet} + NATrpH \longrightarrow {}^{*}NATrpH + NATrpH^{+\bullet} \qquad (6.2.9)$$

Here, the asterisk denotes the polarization. Because only the cation radical of NATrpH participates in CIDNP cancellation, the CIDNP field dependence for this reaction system was first probed in basic solution with DP. However, in section 6.2.4 it will be seen that considerable high field CIDNP is also detected in neutral solution.

The NMR spectrum and typical CIDNP spectra obtained with a 45° RF-flip angle for NATrpH with DP are shown in figure 6.2.9 together with the structure and the assignments NMR signals to the protons in NATrpH. CIDNP is observed in the entire field region with different intensity for the individual protons of NATrpH. In the following first the field dependences for the α-proton and β-protons shall be discussed and then, those of the protons in the indole ring.

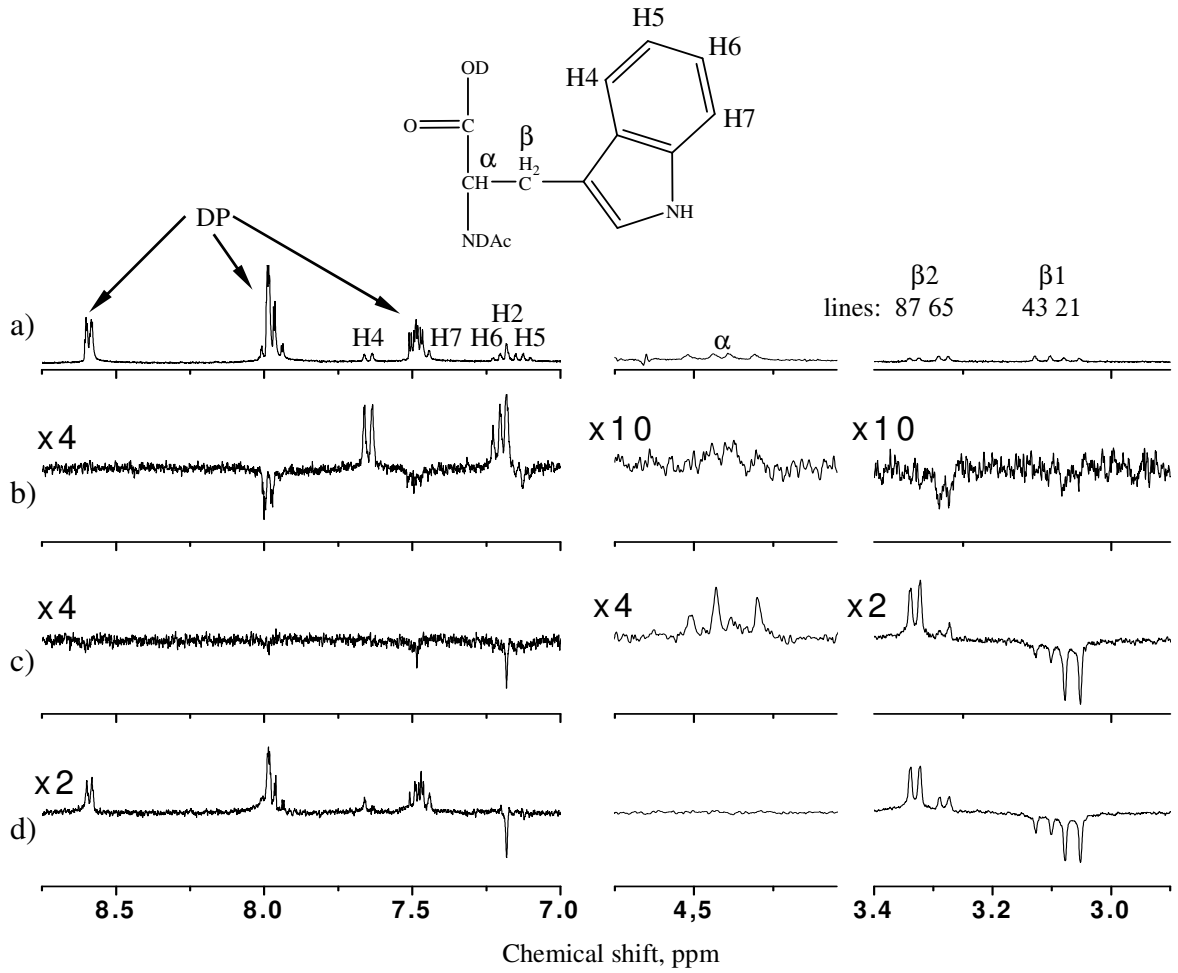

Figure 6.2.9: NMR and field dependent CIDNP spectra of NATrpH with DP (sample 5, table 6.2.1) a) NMR (B_0 = 7T); b) CIDNP at B_{pol} = 7T; c) CIDNP at B_{pol} = 12mT; d) CIDNP at B_{pol} = 1.6mT.

As expected, the low field parts of CIDNP field dependences obtained in this reaction do not reveal peculiarities of the involved radicals. Results for the α-proton and the β-protons are displayed in fig. 6.2.10 a) and b), respectively. In case of the β-protons it appears that CIDNP

is dominated by the multiplet effect in the entire field region. This multiplet effect can be modelled in fair agreement with the experimentally observed field dependences using a quantum mechanical treatment [40, 41] of the pair of coupled β-protons ($J_{\beta 1\text{-}\beta 2}$ = -14.8 Hz, see table 4.0.1) in NATrpH, assuming an adiabatic sample transfer. The calculated field dependences in figure 6.2.10 b) were obtained with the magnetic interaction parameters listed in table 6.2.3 and are shown as solid lines. The qualitative agreement of experiment and theory lends further support to the approach of treating low-field CIDNP as described in refs. [40, 41].

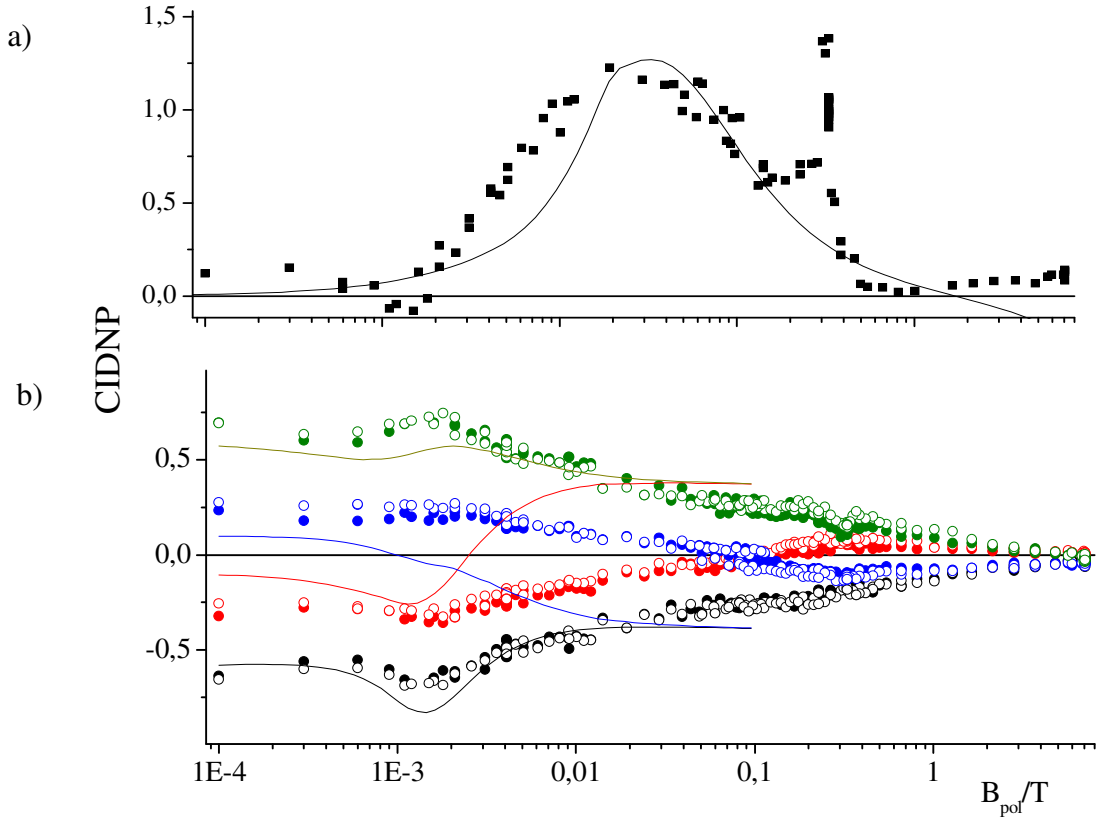

Figure 6.2.10: CIDNP field dependence of obtained upon quenching of DP with NATrpH and (sample 5, table 6.2.1). a) α-proton (four lines) and b) β-protons: full black circles: line 1; open black circles: line 2; full red circles: line 3; open red circles: line 4; full blue circles: line 5; open blue circles: line 6; full green circles: line 7; open green circles: line 8 (see fig. 6.2.8).

However, the DFT calculations listed in table 6.2.2 (p.173) predict significantly different HFC's for the two β-protons in both types of tryptophanyl radicals. In contrast, the CIDNP field dependences appear to be very symmetric. However, being dominated by the multiplet effect in low magnetic field, they are relatively insensitive to HFC's in the radical pair state. The discrepancies between experiment and theory may be overcome by accounting for the

redistribution of CIDNP and for the actual changes in energies of all individual levels in the entire spin sub-system also containing the α-proton and H2 (see table 4.0.1) during the field switch. For the simulations in fig. 6.2.9 and 6.2.10, six protons of NATrpH were considered quantum mechanically, and coupled in pairs by single *J*-couplings. This approach may still give reasonable agreement with the experimental data when the coupling between two spins is much larger than all others as in the case of the β-protons. In case of the aromatic protons discussed further down, it can certainly not describe the results satisfactorily.

The field dependence of the α-proton in figure 6.2.10 a) shows a narrow peak at B_{pol} = 0.32T, which is accompanied by a dip in the CIDNP intensity of some of the β-lines (fig. 6.2.10 b)). This observation is rationalized by a level anti-crossing in the nuclear spin energy levels (see fig. 4.0.4) and was discussed in chapter 4.2.

In addition, significant polarization on α-C-H is observed between 2mT and 0.5T, with a maximum around 55mT. This maximum can be modelled with the hyperfine coupling of the hydrogen atom (*a*(H) = 50.38mT [142]), which is shown as a solid line in figure 6.2.10 a). The reasonable agreement with the experimental curve raises the question whether a parallel reaction path involving the H-radical should be considered, or if the observed field dependence reflects solely the efficiency of polarization transfer from protons carrying hyperfine coupling (as stated above in the case of NATyrOH). The second possibility alone seems improbable in the present case because of the low polarization of all other protons in NATrpH in this range.

The origin of the hydrogen atom would indubitably be one of the dissolved compounds (NATrpH or DP) when working in a deuterated solvent, and the polarized product is obviously the chemically unmodified NATrpH molecule, since NMR parameters are very sensitive to changes in the molecular structure. Thus, the precursor RP leading to this CIDNP field dependence must be the H-atom with the C_α-centred tryptophanyl radical:

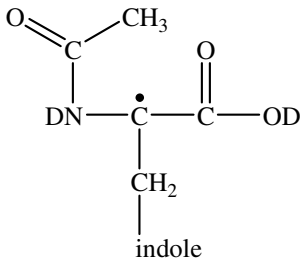

A possible recombination reaction of the H-atom with C_α-centered radicals is the only point that can be made from the available data, whereas the source of the RP proposed remains unclear. The simulation shown in figure 6.2.10 a) (solid line) assumes a larger g-factor for the resulting α-centred radical than that of the H-atom (g = 2.00223, [142]) and a triplet born RP.

However, only the low-field maximum of the resulting field dependence appears in the range of the experimentally available field, which is insensitive to parameters other than the large HFC in the H-atom. Despite the large polarization observed in the intermediate field (due to the large HFC in $H^{\bullet}$), the contribution of this reaction path may be small as compared to the primary reaction path.

CIDNP field dependences of indole protons obtained in basic solution of NATrpH with DP are shown in figure 6.2.11. Like in the previously discussed cases, low-field CIDNP appears to be redistributed among the protons in the six-membered ring (H4, H5, H6 and H7), masking the properties of individual proton positions in the tryptophanyl radical. In addition a sharp feature is seen around B_{pol} = 60mT in the field dependence of H2 (fig. 6.2.10 a)), which is attributed to a level crossing in the nuclear spin states of the diamagnetic product molecule and discussed in chapter 4. There, the kinetics of the coherent transfer of CIDNP where shown to proceed with a frequency that coincides with the energy difference between the two anti-crossing nuclear spin sublevels (see fig. 4.3.3). This feature, however, is unique to the reaction with DP at high pH, and hardly seen in the experiments with AQ2S, which is rationalized with the significantly smaller value of CIDNP on the α-proton with AQ2S in this field range.

At high magnetic fields, absorptive CIDNP is observed on the aromatic protons in positions H2, H4, and H6, while in positions H7 and H5 no polarization is seen. Calculated HFC's for both, cationic and neutral indolyl radicals is summarized in table 6.2.2. The observed CIDNP ratios only fairly agree with spin density distributions of the radicals calculated by DFT methods by Himo and Erickson [143] and by Walden and Wheeler [144, 145]. According to these calculations the neutral tryptophanyl radical may be distinguished from its cationic counterpart by its significantly lower spin density on H2 *and* H7. In the present experiments H2 is polarized but H7 not, thus according to these calculations the spectral pattern does neither resemble the HFC pattern in $NATrpH^{+\bullet}$ nor in $NATrp^{\bullet}$.

Recently, this dilemma was solved by recalculation of the couplings in zwitterionic $TrpH^{+\bullet}$ and $Trp^{\bullet}$ radicals explicitly including a hydration shell, showing that H7 neither exhibits significant HFC in the protonated nor in the unprotonated radical when solvated [72]. In these calculations *only* H2 shows a significant difference. The lack of CIDNP observed on H7 thus emphasizes the importance of including surrounding solvent molecules in DFT calculations and lends support to the calculations by Kyriutin *et al*.[72]. From the moderate polarization observed on H2 in the present experiments it is concluded that a mixture of the two radical

species is detected at pH 13, because at B_{pol} = 7T, CIDNP of H2 has roughly half the intensity of H4[1].

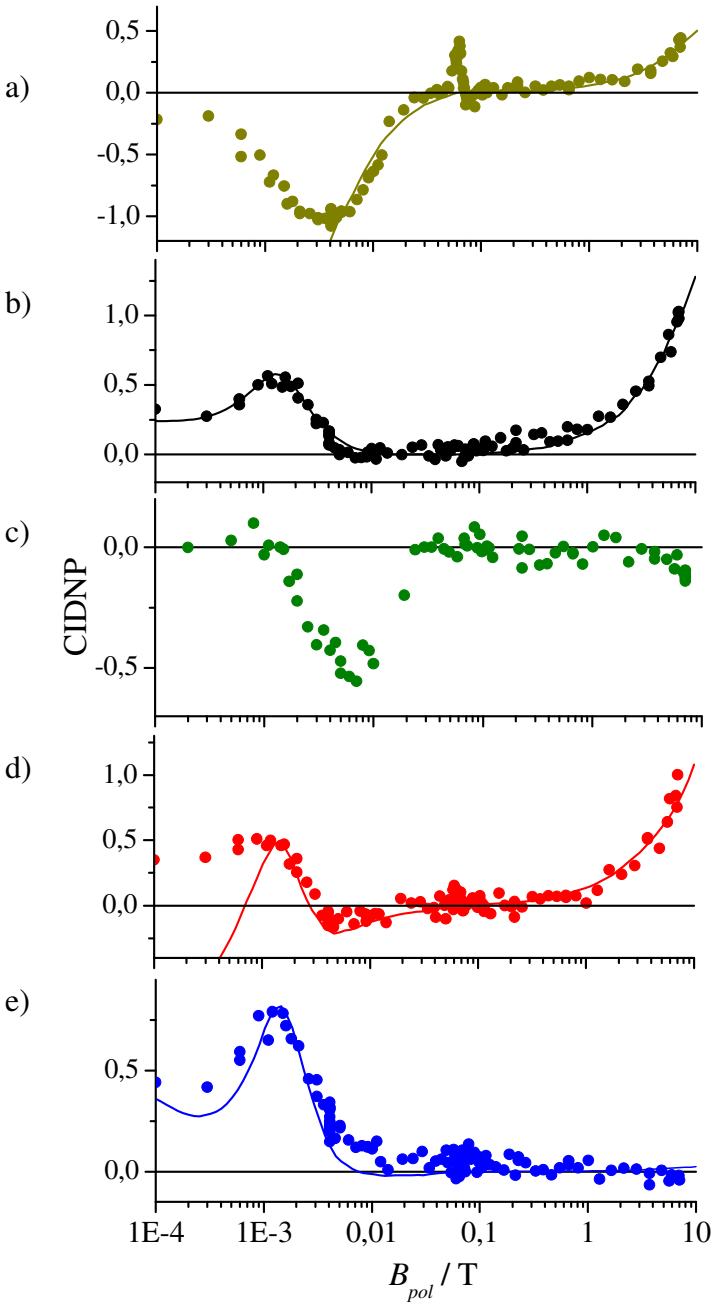

Figure 6.2.11: CIDNP field dependences of aromatic protons in NATrpH sensitized with DP (sample 5, table 6.2.1). a) H2, b) H4, c) H5, d) H6 e) H7. (signal assignment: fig. 6.2.9; simulation parameters: table 6.2.3)

The high field maximum of CIDNP is presumably located beyond the available field range because the signal intensity grows at B_{pol} = 7T, suggesting a very small difference in g-values ($\Delta g < 0.0004$). According to the rules of Kaptein [39], the absorptive CIDNP on H2, H4 and H6 (negative HFC's, see table 6.2.2) indicates the g-factor of the typtophanyl radical to be slightly below that of $DP^{-\bullet}$. The high field part thus allows at least a rough estimation of the g-

[1] Because of the overlapping signals of H2 and H6, the CIDNP ratios shall not be stated more precisely here.

factor of the tryptophanyl radical, and the knowledge of g-factors of the dye radicals from previous sections further allows predicting the high field maximum with AQ2S as a sensitizer to occur in the available field range.

species	ref.	N-H	H2	H3	H4	H5	H6	H7
$In^{\cdot}$	[144]	-	0.00	-1.19	-0.47	0.031	-0.38	-0.12
$InH^{+\cdot}$	[144]	-0.37	-0.42	-0.77	-0.62	0.08	-0.46	-0.29
$In^{\cdot}$	[145]	-	-0.086	-0.89	-0.36	-0.025	-0.29	-0.14
$InH^{+\cdot}$	[145]	-0.30	-0.34	-0.61	-0.47	-0.03	-0.35	-0.25
$InCH_2CH_3^{\cdot}$	[143]	-	-0.05	-	-0.40	0.03	-0.32	-0.08
$InHCH_2CH_3^{+\cdot}$	[143]	-0.34	-0.47	-	-0.51	0.06	-0.35	-0.21
$Trp^{\cdot}$ in water	[72]	-	-0.053	-	-0.447	0.079	-0.368	-0.034
$TrpH^{+\cdot}$ in water	[72]	-0.413	-0.421	-	-0.504	0.124	-0.412	-0.050
$Trp^{\cdot}$	[72]	-	0.048	-	-0.437	0.064	-0.356	-0.057
$TrpH^{+\cdot}$	[72]	-0.598	-0.278	-	-0.488	-0.040	-0.208	-0.364

Table 6.2.2: Calculated literature values of proton hyperfine coupling constants (in mT) in neutral and cationic indolyl radicals (In = Indole) from the literature.

6.2.4 Reaction of NATrpH with AQ2S

There are several advantages for investigating the tryptophanyl radicals with AQ2S rather than with DP as a triplet sensitizer. The resonances of AQ2S do not overlap with those of NATrpH, while the H7-signal of NATrpH partly overlaps with some of the DP resonances. The fact that a smaller effective HFC on the dye results in a larger polarization on the amino acid under investigation was already mentioned above. Most importantly, however, AQ2S was chosen as a sensitizer because it enables the determination of the g-factor of the tryptophanyl radical due to the larger difference in g-factors between the counter radicals than in the case of NATrpH with DP.

The photochemistry in reactions of ^{T}AQ2S with NATrpH follows the previously discussed reactions: ^{T}AQ2S is presumably quenched by electron transfer from NATrpH, thus generating triplet radical pairs of $NATrpH^{+\bullet}$ and $AQ2S^{-\bullet}$:

$$^{T}AQ2S + NATrpH \longrightarrow \overline{^{T}AQ2S^{-\bullet} + NATrpH^{+\bullet}} \qquad (6.2.10)$$

The radicals can undergo protonation and deprotonation reactions according to reaction 6.2.7 and scheme 6.2.2. Several CIDNP field dependences were acquired at different pH-values and RF-flip angles (see table 6.2.1), since the reasons for the similarity of the low field parts for the individual protons was unknown at that point.

For the α- and β-protons in NATrpH, field dependences are displayed in figure 6.2.12, and resemble those obtained with DP. When the polarization is read out with a 90°-pulse (pH 7, fig. 6.2.12 b)), the four lines for each β-proton have roughly equal intensity in emission (β1) and absorption (β2) in low field, and were therefore integrated together. In this case, CIDNP shows maximum intensity around B_{pol} = 1.5mT, which coincides with the maximum calculated for the β2-proton, i.e. the β-proton with the larger HFC (see table 6.2.3). Qualitatively, the observed field dependences can again be rationalized in terms of CIDNP re-distribution caused by strong scalar coupling during τ_L, which renders HFC's for individual β-protons non-accessible, in combination with subsequent adiabatic sample transfer. For the α-proton, polarization is also detected up to 0.3T and tentatively attributed to CIDNP transferred from the β-protons.

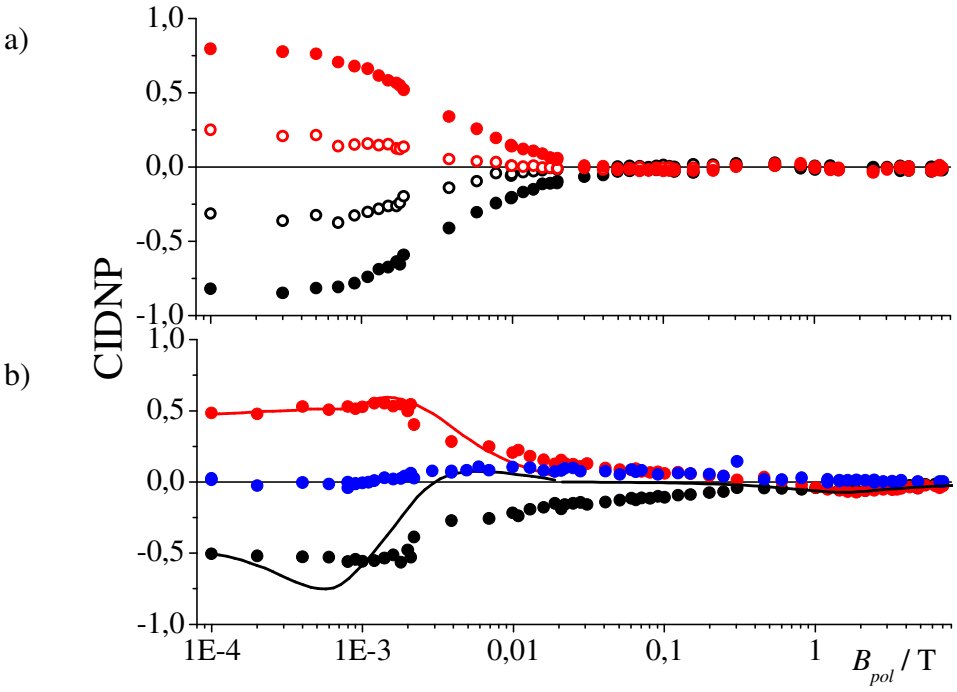

Figure 6.2.12: CIDNP field dependences of α and β-protons in NATrpH sensitized with AQ2S at a) pH 3 ,φ = 45° (sample 6): lines 1 and 2: ●, lines 3 and 4:○, lines 5 and 6:○ , lines 7 and 8:●; b) pH 7, φ = 90° (sample 8), ●β1-proton, ●β2-proton, ●: α-proton. (Assignment of lines: fig. 6.2.1; sample preparation: table 6.2.1; simulation parameters table 6.2.3.)

When CIDNP is probed at pH 7 both β-protons show emission at high field with a maximum centred at $B_{pol} \approx 1.85$T, while in acidic solution no high field polarization is observed due to degenerate exchange (reaction 6.2.9).

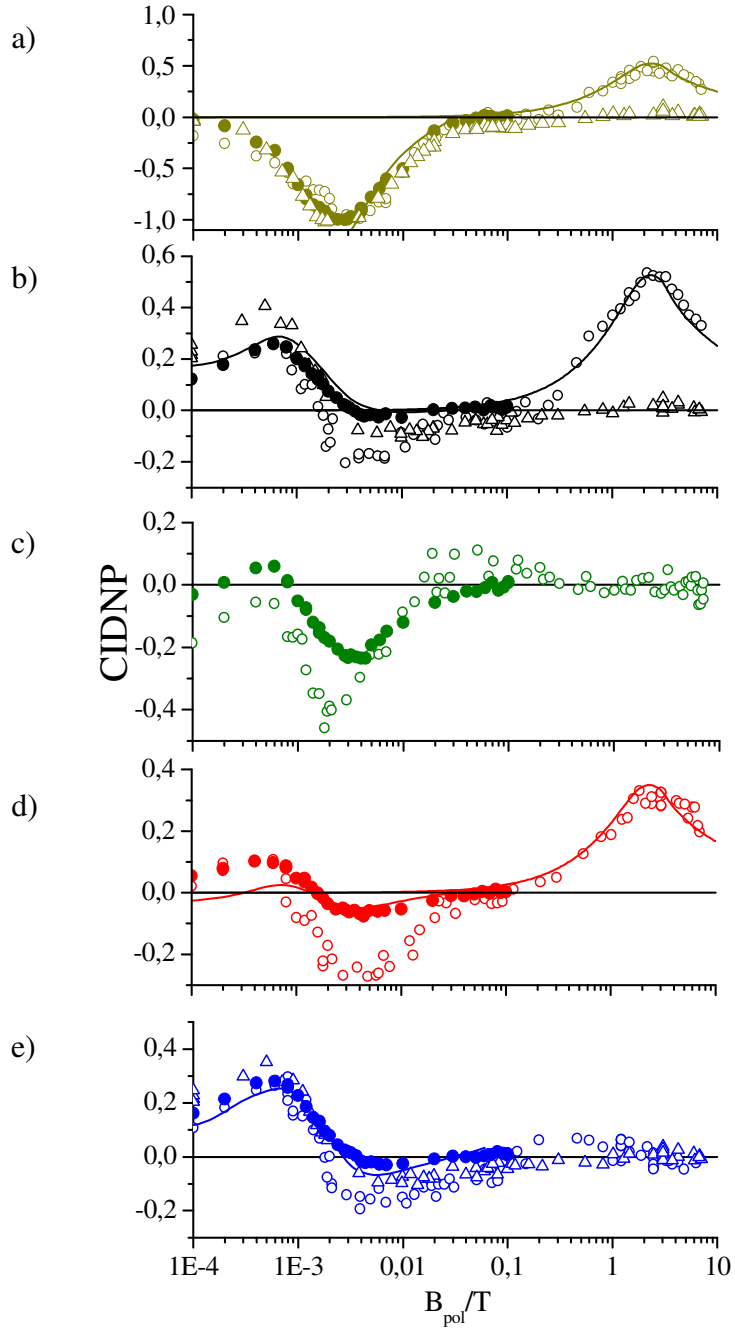

Figure 6.2.13: CIDNP field dependences of aromatic protons in NATrpH sensitized with AQ2S (open trangles: sample 6, φ = 45°; open circles: sample 8, φ = 90°; full circles: sample 9), φ = 45°; solid lines: simulation with φ = 45°. a) H2 (triangles: H2 and H6), b) H4, c) H5, d) H6, e) H7 (normalized to the emissive CIDNP of H2 at $3*10^{-3}$T). For sample preparation see table 6.2.1 and for simulation parameters table 6.2.3.

For the aromatic protons the field dependences are shown in figure 6.2.13. With the relatively long irradiation times used (τ_L ~ 1s), the efficient CIDNP redistribution renders the low field

parts for protons in the six-membered ring (H4, H5, H6, and H7) very similar to each other. Upon variation of the RF flip angle (90°/45°), a different shape of the CIDNP field dependences is seen in low fields for the protons in the six-membered ring (H4, H5, H6 and H7) but not for H2, reflecting the small coupling of H2 to all other protons in the molecule. However, the remaining discussion shall be restricted to high field CIDNP, i.e the extraction of the g-factor of $NATrpH^{+\bullet}$ since the low field CIDNP does not reveal properties of the involved radicals.

The most prominent difference upon variation of pH is the lack of high field CIDNP in acidic solution due to degenerate exchange (reaction 6.2.9). In order to diminish its contribution and reveal a possible difference in g-factors of the protonated and unprotonated tryptophanyl radicals, the concentration of NATrpH was lowered from 8mM to 2mM NATrpH in acidic solution (sample 7, table 2.6.1). However, no difference in the position of the high-field maximum of CIDNP to that obtained in neutral solution was discernable, indicating that similar RP's are responsible for the formation of CIDNP in the whole pH range.

The CIDNP field dependence of a neutral solution (pH 7) of NATrpH and AQ2S displays its high field maximum around $B_{pol} \approx 2.2$T, and the polarization pattern of NATrpH at pH 7 differs from that observed with DP (pH 13) showing roughly equal intensity on H4 and H6 and H2, but no polarization on H5 and H7. According to the calculations in ref. [72], this CIDNP pattern is expected for $NATrpH^{+\bullet}$. Thus, in neutral solution the deprotonation of $NATrpH^{+\bullet}$ is too slow for the deprotonated form to contribute to CIDNP formation, and the polarization is attributed to the radical pair consisting of $NATrpH^{+\bullet}$ and $AQ2S^{\cdot-}$.

Taking the hyperfine couplings for the protonated tryptophanyl radical from ref. [72], and g = 2.0041 for the $AQ2S^{\cdot}$-radical from above (section 6.2.2.), a reasonable fit is obtained with a Δg-value of 0.00115±0.00020. Thus, the g-factor of the tryptophanyl radical cation is determined to 2.00295, a value which supports the assignments of EPR-signals detected in enzymes like peroxidases [146, 147] and in ribonucleotide reductase [148] in this field range to tryptophanyl radicals.

Conclusions

This comparison of CIDNP field dependences obtained in amino acid dye systems served several purposes. The strategy of combining different types of amino acid radicals with different dye radicals under well defined conditions, allows a self-consistent extraction of Δg-

values obtained in each of the combinations because of their interdependence. As compared to high field EPR, the FD-CIDNP method benefits from the fact that g-factor differences are measured instead of the g-factors themselves, because one inherently gains accuracy. In order to establish the method for this more accurate determination of g-values the comparison of different RP's was necessary. As the starting point, the g-factor of the solvated electron was taken from ref. [103] and the magnetic interaction parameters of $NATyrO^{\bullet}$ were determined in chapter 6.1. In this chapter, the extraction of g-factors was extended to different sensitizers (DP and AQ2S) and a good agreement with literature values for these sensitizers from EPR was achieved, thus allowing a more precise determination of $g_{iso}(NATyrO^{\bullet})$. In this context, the electron transfer reactions between triplet AQ2S and the amino acids tryptophan and tyrosine are reported for the first time.

Finally, the strategy allowed to extract an accurate value for the g-factor of $NATrpH^{+\bullet}$, which was hitherto unknown in liquid aqueous media. No difference in *g*-factors for the protonated and unprotonated forms of tryptophanyl radicals could be detected. Comparison of the ratios of CIDNP intensities in high field to DFT calculations of HFC's in protonated and unprotonated tryptophanyl radicals suggest that a mixture of the two radical species is observed at high pH, while in neutral and acidic solutions only the cationic radical contributes to CIDNP formation. The Δg-values used for the simulations of CIDNP field dependences are summarized in table 6.2.3.

	e^-_{aq} g = 2.00049 (ref. [103]) a_{eff} = 0.001mT	$DPH^{\bullet}$ g = 2.0030 +/-0.0002 a_{eff} = 1.17mT	$AQ2SH^{+\bullet}$ g = 2.0039 +/-0.0002 a_{eff} = 0.16mT	$AQ2S^{\bullet}$ g = 2.0041 +/-0.0002 a_{eff} = 0.16mT
$NATyrO^{\bullet}$ g = 2.00445+/-0.00010 a_{eff} = 1.01mT a(H3/H5) = -0.69mT a(H2/H6) = 0.19mT $a(\beta 1)$ = 0.56mT $a(\beta 2)$ = 0.84mT	$B_{max} \approx 0.6$T Δg = -0.0040 +/-0.0006	$B_{max} \approx 2.0$T Δg = 0.0015 +/-0.00025	$B_{max} \approx 4.2$T Δg = 0.00055 +/-0.00009	$B_{max} \approx 5.8$T Δg = 0.00035 +/-0.00006
$NATrpH^{+\bullet}$ g = 2.00295+/-0.00010 a_{eff} = 2.06mT a(H2) = -0.525 mT a(H4) = -0.495 mT a(H5) = 0.145 mT a(H6) = -0.49 mT a(H7) = -0.07 mT $a(\beta 1)$ = 1.00 mT $a(\beta 2)$ = 0.69 mT	not detected	$B_{max} > 7$T $\Delta g \leq 0.0003$	not detected	$B_{max} \approx 2.4$T Δg = 0.00115 +/-0.00018

Table 6.2.3: Summary of the magnetic interaction parameters used for simulations of CIDNP field dependences in chapters 6.1 and 6.2. HFC's were taken from ref. [72] for $NATrpH^{+\bullet}$ (experimental), ref. [104] for $NATyrO^{\bullet}$ and ref. [140] for $AQ2SH^{+\bullet}$ and $AQ2S^{\bullet}$.

Combining the same amino acid radicals in pairs with different counter radicals has provided new insight into the effects responsible for the observed CIDNP field dependences. The importance of spin evolution in the diamagnetic products discussed in chapter 4 was noticed upon the observation of common features that appeared in the field dependences of certain nuclei independent of the radical partner.

It was further shown, that CIDNP when probed at the fixed field of the spectrometer only, the method is relatively insensitive to unravel parallel reaction pathways (such as the formation of the H-atom), because not every radical reaction gives significant CIDNP at high magnetic field. When aiming at magnetic interaction parameters of particular radicals, one has to be aware that the method is highly indirect, and take into account that parallel reaction pathways may contribute that distort the extracted values of both HFC's from CIDNP ratios and g-factors from B_{max}.

Individual HFC's of the radicals involved are not accessible from the low field part of the field dependence when the method is performed under steady state illumination, because of the efficient redistribution of polarization among strongly coupled spins. This drawback may be circumvented or overcome in the future, e.g. by accumulation of experiments with single laser shots and subsequent fast probe transfer.

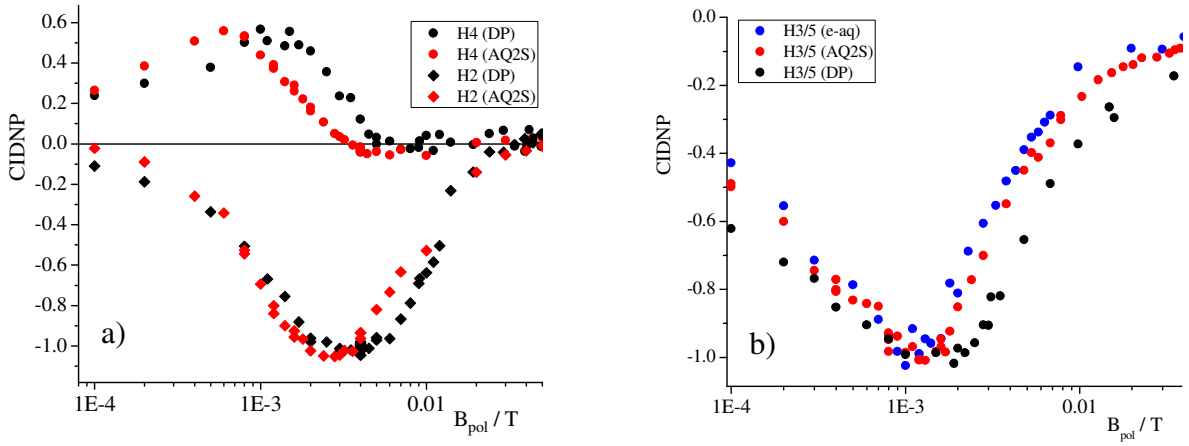

Figure 6.2.14: Comparison of low field CIDNP of a) NATrpH and b) NATyrOH in radical pairs with different counter radicals.

It is shown that the magnetic interaction parameters of the involved radicals, i.e. hyperfine couplings and g-factors, in the RP are sufficient for a full description of the observed CIDNP field dependences. In particular, no exchange coupling between counter radicals needs to be considered for their description. Moreover, the applicability of the concept of a semi-classical hyperfine field i.e. that of an effective HFC for the counter radical, for describing low field

CIDNP is applicable. The influence of its value on the low field CIDNP is seen in figure 6.2.14 a) for NATrpH and b) $NATyrO^{\cdot}$. Because of differences in timing schemes for the experiments with different counter radicals (in particular different τ_L) CIDNP is distributed among coupled nuclei to varying extent, and the curves can not be compared quantitatively. However, the trend that for larger values of a_{eff} of the counter radical the field of maximum polarization shifts to higher values is clearly seen. In principle, the approach of calculating low field CIDNP presented by Ivanov *et al.* [40, 41] is valid, but it is recommended to chose counter radicals with small values of a_{eff}, e.g. deuterated sensitizers. Also, a restriction to pairs of coupled nuclei can not work in a molecule such as NATrpH, where several spins in the network exhibit comparable couplings. Therefore, the present discussion was restricted to the extraction of *g*-values from high field CIDNP of the involved radicals. Here, it is fully sufficient to restrict the calculations to the much simpler Adrian model instead of using the more time-consuming, exact quantum mechanical approach with a more exact treatment of the diffusing radicals.

6.3 CIDNP of Ketones in Liquids and Plastic Crystalline Matrix - Effect of Molecular Mobility on CIDNP Formation

The application of the CIDNP-technique to study the structural dynamics of biological systems has been suggested in 1978 by Kaptein [123]. Investigating the dynamics of larger proteins by CIDNP, however, necessitates detecting the effect in so-called 'soft matter'. There are only few examples, where a photo-CIDNP effect has been observed in solids. One is the detection CIDNP of several ketones in the plastic crystalline matrix of cylohexane [149-152], and the other are the polarized NMR signals detected during irradiation of photosynthetic reaction centers [153-155]. In particular the latter case stimulated further experiments [156-159], and a discussion about the possible mechanisms of CIDNP formation in systems with restricted mobility. New mechanisms were formulated besides the well established radical pair mechanism [160, 161]. These mechanisms invoke the anisotropy of the hyperfine tensor, and do not need molecular mobility. The aim of the work performed in this chapter is to reveal the underlying mechanisms of CIDNP formation in solids and to probe the dependence of their efficiency on the change of molecular mobility.

There are basically two different ways established by which CIDNP may be formed; they have been introduced in chapter 2. In the framework of the radical pair mechanism the CIDNP effect arises from either S-T_0 or S-$T_\pm$ transitions. These mechanisms have been introduced in chapter 2. In organic solids the broadening of NMR lines is usually connected with intramolecular dipole-dipole interaction between proton spins. In principle, S-T_0 transitions do not create a total net polarisation, but the products of radical reactions are sorted due to their spin states. In addition, the formation of CIDNP due to the S-T_0 transitions relies on the diffusive separation of radical centres. A low mobility of radicals in solid solutions is expected to lead to a sharp decrease in the efficiency of S-T_0 mixing in radical pairs, and other mechanisms may be considered responsible for the polarization of nuclei. The multiplet effect is practically not accessible in solids either, due to the broadening of NMR lines once dipolar interaction is not averaged out by fast isotropic rotational diffusion.

In contrast, the S-T- mechanism of CIDNP formation involves spin flips, thereby creating a net nuclear spin polarization that manifests itself in the NMR spectra of the reaction products. An eventual redistribution of this net polarisation may tend to equalize the effect over all molecules with overlapping NMR lines by spin diffusion, but it will not be eliminated like in the case of S-T_0 transitions. In order to see CIDNP due to S-$T_\pm$ transitions it is necessary that

the exchange integral J_{ex} differs from zero, i.e. that the distance r between the radical centres does not exceed a certain value which is around several nanometers, because the exchange interaction between the radicals is expected to decay exponentially with their distance.

Different mechanisms are considered for the electronic exchange interaction, and their contributions are difficult to separate. It can be transferred through a network of chemical bonds, through space (vacuum), or a so-called 'super-exchange' can contribute through the surrounding solvent molecules. In particular the through bond mechanism is expected to depend crucially on the molecular geometry, i.e the orders and angles of chemical bonds between the radical centres. Nevertheless, the effective exchange interaction $J_{ex,eff}$ decreases exponentially with increasing radical distance r and is usually written as a sum over all contributions, i, with different amplitudes $J_{ex,0i}$ and exponents α_i (see formula 2.1.8). The exchange integral is modulated in time by the molecular mobility, i.e. the variation of distance between the radical centres during conformational changes or the constrained diffusive separation.

Both, CIDNP due to S-T_- and S-T_0 transitions show a characteristic dependence on the external magnetic field at which the polarization is formed most efficient. The conditions for most effective CIDNP formation in a spin sorting process (S-T_0) is given by the difference in g-factors between the radical partners in the pair with respect to their HFC, leading to a maximum at $B_{max} = a/2\Delta g\beta\hbar^{-1}$ (formula 2.1.11). This is typically the case for radical pairs in liquid solution that undergo diffusive separation, like the amino acid/dye combinations discussed in chapter 6.2 and the overwhelming majority of CIDNP signals reported in the literature. For the S-$T_\pm$ mechanism strongest nuclear spin polarization of the products is observed around the magnetic field of singlet-triplet level crossing, where the electronic Zeeman interaction matches the exchange interaction, J_{ex} : $B_{max} = 2|J_{ex}|/g\beta$ (formula 2.1.9). Here, negative and positive sign of J_{ex} result for crossing with T_- and T_+, respectively [1, 82, 162].

Hence, field-dependent CIDNP opens the unique possibility to determine the electronic exchange interaction J_{ex} in both sign and magnitude. In addition, the technique might be capable of distinguishing between different mechanisms for J_{ex} by an appropriate change of experimental conditions, e.g. the temperature the solvent or the solute.

The present study was stimulated by the observation of CIDNP of several ketones in plastic crystalline matrix [149-152]. Obinochny et al. suggested that the high rotational mobility of the cyclohexane host molecules plays an important role for CIDNP formation [150], because some molecular mobility can be expected to be necessary for the modulation of exchange

interaction to facilitate the S-T$_-$ transitions. However, the experiments were performed at a fixed magnetic field and did not allow the unambiguous identification of the polarizing mechanism. In particular, the reported CIDNP of different sign in the homologous series of cyclic ketones [151] that is in contradiction to the proposed S-T$_-$ mechanism supposes that the mechanism of CIDNP formation remains unclear, and that a systematic study of the influence of molecular mobility on CIDNP formation is required. In the present study, both the temperature and the magnetic field are varied over a wide range in order to elucidate the influence of molecular mobility on the mechanism of CIDNP formation during the photolysis of several ketones in liquid and solid solutions of cyclohexane-d_{12}.

Photochemistry of ketones. The photolysis of carbonyl compounds, and in particular that of ketones is probably one of the most extensively studied photoreactions in the literature because of their use as photosensitizers for chain reactions of industrial interest. In order to elucidate the mechanism of CIDNP formation upon restriction of molecular mobility the photolysis of different ketones was investigated. Cyclic ketones of the general formula $C_nH_{2n-2}O$ with n = 7-11 have been photolysed, and the non-cyclic ketone acetone. Both classes of compounds share a common photochemistry which is classified into two different processes which are commonly referred to as Norrish type I and type II reaction. For cyclic ketones, the type I reaction is outlined in scheme 6.3.1.

Excitation by the 308nm light causes $n\rightarrow\pi^*$ transition in the C=O double bond of the parent ketone, followed by the scission of the bond in α-position to the carbonyl function (Norrish type I cleavage). The type I cleavage leads to the formation of an acyl-alkyl biradical in the case of the cyclic ketones, and to freely diffusing acyl and alkyl radicals in the case of aliphatic ketones (acetone). In either case the radicals will recombine and give rise to CIDNP. For liquid solution it is known from previous investigations that in the first case CIDNP is formed by S-T$_-$ transitions [11], whereas in the latter case spin sorting provides the path for CIDNP formation [163], because the exchange interaction vanishes upon diffusive separation of the alkyl and acyl radicals. In both cases the reaction is cyclic, i.e. it restores the educts of the reaction. The type I cleavage typically goes along with the intramolecular disproportionation reaction yielding an unsaturated aldehyde as indicated in scheme 6.3.1. While the CIDNP of the unsaturated aldeyde has usually been in the focus of the discussion [82], here, mainly the CIDNP formed in the parent ketone in the cyclic reaction path is analysed.

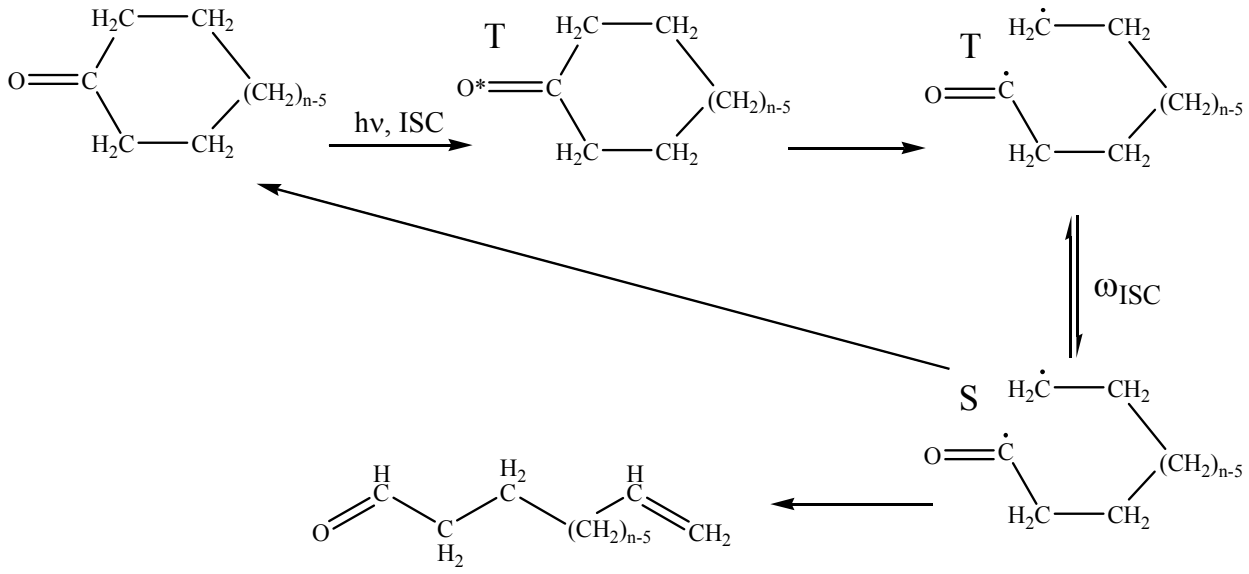

Scheme 6.3.1: Norrish type I photoreaction of cyclic ketones (n=7-11)

In ketones with a hydrogen atom available in γ-position to the carboxyl group, intramolecular photoreduction of the ketone yields another type of biradicals, undergoing type II cleavage to form an olefin and the enol of the ketone. In the photolysis of acetone in cyclohexane the solvent can donate hydrogen atoms for the reduction of the ketone to the enol of acetone [164]. The photolysis of acetone in the liquid phase leads to a greater variety of products than that of the cyclic ketones because of the availability of further reaction pathways, which will be discussed further down.

The Matrix – Cyclohexane-d_{12}. Cyclohexane is a molecule with globular shape which is free to rotate not only in its liquid but also in its upper (cubic) solid phase, where well-defined lattice positions are occupied. The largest intramolecular distance in the molecule, 0.476 nm, measures between opposite equatorial hydrogens in the chair-conformation. Taking the van der Waals radii into account, the largest diameter of the molecule is 0.71 nm. When cooling the neat liquid a phase transition is passed around 6.5°C (289.7K) to the solid rotor phase (also called plastic crystalline phase). The plastic phase extends to -87°C (186.2K) where cyclohexane passes into its rigid phase.

Steric considerations for a cubic model phase with a mean intermolecular distance of 6.09Å yield a negligible overlap of adjacent molecules in the plastic crystal only for rotations around the three-fold axis [165]. According to neutron scattering results, the molecular rotational dynamics is only slightly affected by this phase transition, and in both, liquid and plastic crystal phases relatively strong orientational correlation is present because of significant coupled motions between adjacent molecules [166]. In the plastic phase these motions appear

to be coupled to translational displacements of the molecular centers, and are very sensitive to temperature variation.

Correlation times for both, rotational motions and translational displacements were obtained by field cycling NMR relaxometry [167]. Because the rotational jumps occur around different axis, namely both the two- and the three fold axis of the cyclohexane molecule simultaneously, it is regarded to as an 'almost unhindered' rotator in the plastic phase. The measurements of relaxation dispersion by Stapf and Kimmich [167] were interpreted assuming anisotropic molecular rotation on a short timescale ($\tau_{rot} \approx 2.3 \cdot 10^{-12}$ s at 272 K) and translational diffusion on a far longer timescale leading to the modulation of intramolecular dipole-dipole coupling. Their measurements also allowed the determination of a self-diffusion coefficient of $D = 1.15 \pm 0.10 \cdot 10^{-13}$ m^2s^{-1} at 272K, and no direct indication of ring (chair-to-chair) interconversion process was identified in the plastic phase. Upon comparison to the work of other authors [168] it was concluded, that it is at least 100 times slower than the jump mechanism described by Stapf and Kimmich.

Cyclohexane–d_{12} (C_6D_{12}) has been chosen because it offers the possibility to vary the molecular mobility of its guest molecules in a wide range. The rotor phase is easily accessible because the phase transition occurs close to room temperature, and the ketones chosen for the photoreactions are of a size comparable to that of the host molecule. Likewise, for guest molecules of appropriate size rotational mobility is expected to persist in the plastic phase, while translational motion is restricted. This assumption is further supported by the fact that the cyclic ketones themselves also form plastic crystals with comparable properties to those of the cyclohexane host molecule [169]. Further advantages of C_6D_{12} as a host molecule for the present investigation are its transparency for near UV-light and the appreciable narrowing expected for the NMR-lines of host and guest molecules due to rotational self-diffusion.

Experimental

The experimental setup and the timing scheme of the experiment is described in chapter 3.2 and has been published in ref. [10]. The samples were irradiated with the XeCl excimer laser (308nm) in the pre-selected polarization field (τ_L = 500ms to 1000ms), and then immediately transferred to the detection field ($\tau_T \leq$ 350ms), where the NMR spectrum was measured via the FID after a 90° detection pulse.

Sample cooling is possible down to 160 K using dry nitrogen gas from a liquid N_2 reservoir

and a Bruker B-VT 1000 temperature control unit. The drift of temperature during the experiments and its gradient across the sample does not exceed 2 K.

Sample preparation. Each sample contains 1.2ml of cyclohexane-d_{12} solution of the ketones with the concentrations of 0.9 mM for cycloheptanone, 0.8 mM for cyclooctanone, 0.7 mM for cyclononanone, and 0.6 mM for cyclodecanone, and 14 mM for acetone. The concentrations were chosen to keep the optical density of the liquid samples in the 5 mm standard NMR sample tube below 0.5. The samples were degassed in several freeze-pump-thaw cycles and then sealed in order to remove dissolved oxygen which is an effective quencher of triplet states. This procedure prevents the sample from cracking when cooling it into the rotor phase, and thus allows one to obtain nearly transparent samples upon cooling. Cyclic ketones ($C_nH_{2n-2}O$ with n = 7-11) were obtained from Aldrich; acetone (analytical reagent, purity of 99.5%) was purchased from Riedel-de Haën (Germany), and cyclohexane-d_{12} (enrichment of 99.5%) from Deutero GmbH (Germany). All chemicals were used without further purification.

Results and Discussion

NMR and CIDNP spectra of cyclic ketones in frozen solution.

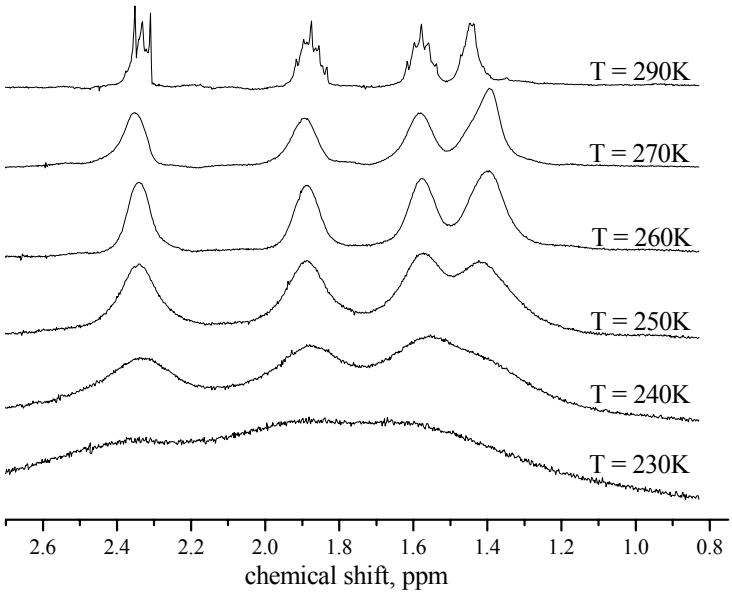

Figure 6.3.1: NMR-spectra of cyclooctanone in C_6D_{12} at variable temperature.

As an example, NMR-spectra of cyclooctanone in C_6D_{12} taken at 300MHz are displayed in figure 6.3.1. Only in the NMR-spectrum of the liquid sample (uppermost line) the lines exhibit the fine structure due to spin-spin coupling. The moderate broadening of lines below the phase transition prevents such resolution but still allows differentiating between the signals for protons at different positions in the cyclooctanone molecule. Upon further cooling, the broadening of the lines increases until a broad unstructured signal is observed at temperatures below 240K. Its width of about 10 kHz indicates that most of the intramolecular contribution of the dipole-dipole interaction to the line width is still averaged out, while the broadening of the signals can be attributed to the upcoming intermolecular dipolar interactions. Because the width of the lines in the NMR-spectra taken at different temperatures directly reflects the molecular mobility of the guest molecules in the matrix, it is concluded that the cyclohexane matrix is well suited for a gradual change of molecular mobility of the guest molecules.

The NMR-signal of the residual protons of the host molecules ($C_6D_{11}H$) appears around 1.45 ppm and is already broadened significantly in the liquid sample. (The solvent line can be seen more clearly in the NMR spectrum of acetone in C_6D_{12} in figure 6.3.6. Its width is attributed to the slow exchange between axial and equatorial positions during chair to chair inter-conversion. Upon lowering the temperature, the lines of the solute molecules broaden significantly more than the solvent line, which explains the apparent shift of the solutes lines around 1.4 ppm upon cooling in figure 6.3.1.

In figure 6.3.2, representative spectra (NMR and CIDNP) for cyclic ketones of different sizes (n = 7 to 11) in plastic crystalline matrix taken at a temperature of 260K are shown. At this temperature, T_1 was determined to 630±50ms at 7T for a sample of cyclononanone. Because of differences in the absorption coefficients for 308nm, the CIDNP spectra do not allow a quantitative comparison of the efficiency of polarization upon irradiation for ketones of different ring size. Nevertheless, some meaningful similarities as well as some interesting differences are obvious. Irrespective of their size, all cyclic ketones under investigation display emissive CIDNP in the plastic crystalline matrix of C_6D_{12}. This observation is inconsistent with the observation of CIDNP of opposite signs in the homologous series of cyclic ketones reported by Obinochny et al. [151], who saw absorptive CIDNP in the case of cyclodecanone in plastic crystalline C_6D_{12}. In a given ketone, all individual lines are emissively polarised with comparable intensities, irrespective of both sign and magnitude of HFC in the corresponding protons. This observation has usually been attributed to spin diffusion the literature [151].

Because the dipole-dipole interactions are not averaged out completely in the plastic crystalline phase, the strong coupling between the protons leads to collective states rather than individual eigenstates for each proton. In contrast to scalar spin-spin couplings as discussed in chapter 4, the coupling may be considered as strong irrespective of B_{pol}. Under these conditions, the protons will almost immediately be polarized together and at least within the finite irradiation time of one second, CIDNP is redistributed between all strongly coupled protons.

However, when it comes to ketones of intermediate size (n = 9 and 10) it is conspicuous, that *not* all the lines detected by NMR are polarized in a similar fashion upon irradiation. In the case of $C_9H_{16}O$ (see fig. 6.3.2, n = 9), the shape of the CIDNP spectrum deviates considerably from that of the NMR spectrum, which may be rationalized in the following way: Different subgroups of molecules exist, and their different local environment and/or conformations give rise to slightly different chemical shifts for the individual positions in the ketone. These protons do not redistribute their polarization, as they belong to different subgroups of molecules. The fact that they are polarized with different efficiency, results in CIDNP-spectra in which not all the lines are polarized with the same efficiency.

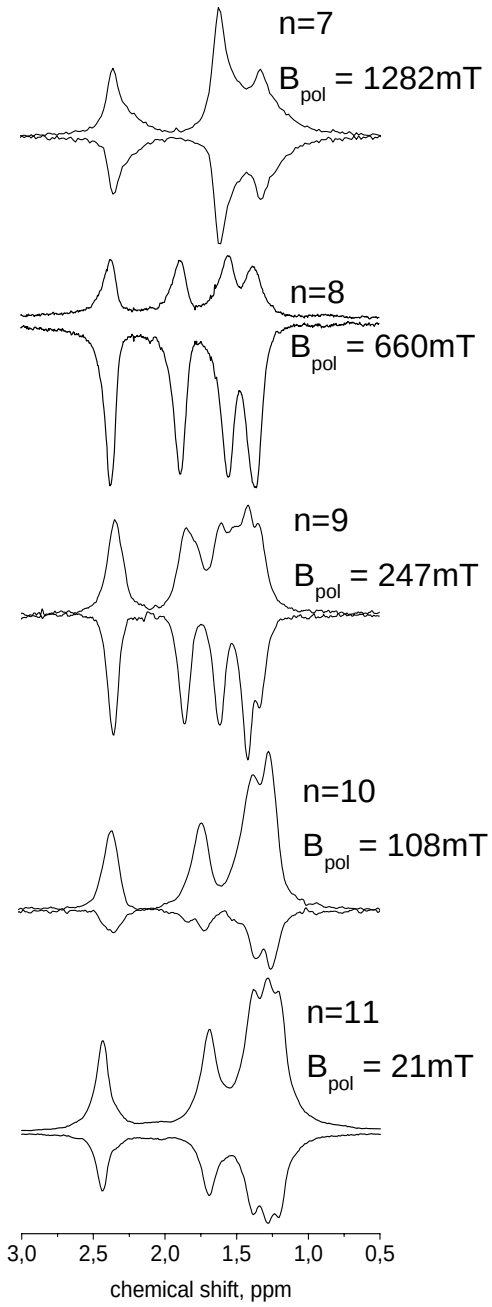

Figure 6.3.2: NMR (absorptive) and CIDNP (emissive) spectra of different cyclic ketones ($C_nH_{2n-2}O$ with n = 7-11) in C_6D_{12} at T = 260K

One of the main tasks of this investigation was the elucidation of the relevant mechanisms of nuclear polarization in condensed matter. The consequences of an almost complete restriction of the biradicals mobility are seen in figure 6.3.3. It shows CIDNP spectra observed in the cycloheptanone photolysis upon stepwise cooling and passing the transition from the rotor phase to the rigid crystalline phase. At 210 K the NMR spectrum does not resolve the

different positions of protons in the cyclic ketone anymore. At this temperature the width of the signal has grown to about 3 kHz and the CIDNP effect becomes gradually smaller upon further cooling. Thus, the amplitude of CIDNP scales with the confinement by the plastic crystalline matrix.

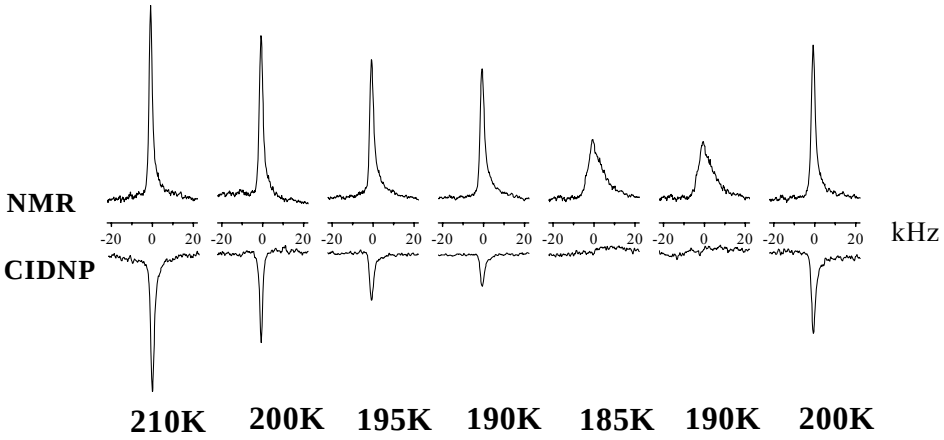

Figure 6.3.3: Cycloheptanone in cyclohexane-d_{12}: Change of Boltzmann NMR (at 7T) and CIDNP (at B_{pol} = 1T) upon temperature variation. The sequential measurements start at the left. The integrals of the NMR signals are scaled to unity and the same scaling factor is used for treating the CIDNP signals.

Upon transition to the rigid crystalline phase the width of the NMR signals leaps to about 10 kHz and in parallel no CIDNP is detectable any longer (Figure 6.3.3, 185 K). This evidences that molecular mobility is a prerequisite for the formation of CIDNP. Upon subsequent cooling and re-heating to 190 K the broad NMR signal is retained, indicating that the structural features are influenced by the thermal history of the sample. Emergence of polarization and reduction of line width, both of comparable size with respect to the case at cooling, are observed with a slight hysteresis when heating the sample further to 200K (figure 6.3.3, 200 K right side). The vanishing CIDNP in the rigid phase is attributed to a lack of modulation of J_{ex}. The singlet-triplet evolution is then probably governed by spin-orbit coupling and the zero-field splittings of the electronic states.

In order to confirm, that the features of the plastic crystalline phase remain in the sample under study, differential scanning calorimetry[1] (DSC) was performed with a sample of a cycloheptanone solution after it has been subjected to the near UV light of the laser. The result is displayed in figure 6.3.4. It should be noted that in the NMR measurements, the

[1] The DSC measurement was kindly provided by the group of Prof. Hartl from the department of inorganic and analytical chemistry of FU-Berlin.

sample was allowed to equilibrate for roughly 20 minutes, whereas in the DSC experiment the sample is continuously heated and cooled with a slew rate of 4K/min.

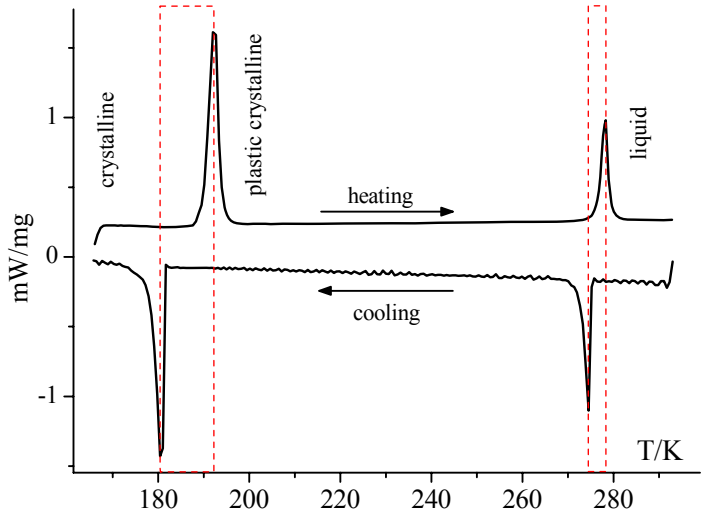

Figure 6.3.4: DSC of C_6D_{12} doped with cycloheptanone (10µl in 1.2ml) after irradiation, the dashed rectangular mark the regions of hysteresis.

The DSC clearly shows two phase transitions in the expected range. Upon cooling, the phase transition from the liquid to the plastic crystalline phase occurs at T = 274.9 K, and the sample becomes crystalline at 180.4K. When coming from the crystalline phase, a pronounced hysteresis is observed. For the transition to the plastic phase; the transition is shifted by about 12 K to higher temperatures with respect to that observed upon cooling. This shift provides the explanation for the second spectrum taken at T = 190 K in figure 6.3.3 not showing any CIDNP, because upon heating the sample remains in the crystalline phase at this temperature. Thus, the temperature intervals of the hysteresis found in the DSC measurement resemble those found in the NMR spectra. For the second phase transition also, a slight hysteresis is observed.

CIDNP field dependence of cyclic ketones at variable temperature. After having discussed the change in the appearance of NMR spectra upon geometrical confinement in the plastic crystalline matrix of C_6D_{12}, the underlying mechanism of CIDNP formation is not yet clarified. Therefore, field dependent CIDNP measurements were performed at variable temperature for ketones of different chain length to provide this information.

In all cyclic ketones under investigation polarization of equal sign and comparable strength is observed for all protons over the whole field range, therefore the intensity integrated over all

lines is used for describing the dependence of CIDNP on the magnetic field at different temperatures in the plastic phase. The magnetic field dependence of integrated CIDNP intensity, and its variation with temperature is shown in fig. 6.3.5 for the cyclic ketones with n = 7-10. The polarization is scaled to unity at the maximum and thus does not reflect the monotonous decrease with decreasing temperature in the plastic crystalline phase as it is seen in fig. 6.3.3.

The general features of the field dependences are strikingly similar for all temperatures and for all ketones. For the individual spectral components in the liquid solution (fig. 6.3.5, solid squares) as well as for the lines in solid phase the polarization has emissive character with its maximum value at intermediate field (0.1 T > B_{max} > 2 T). This maximum position, B_{max}, is different for the four ketones and is shifted toward higher field for smaller ketones as compared to the larger ones. This observation is attributed to the increase of average exchange interaction with closer distance of alkyl and acyl radical centers for smaller ketones. The fact that all protons in the reaction products exhibit CIDNP of emissive phase and have comparable B_{max} is strong evidence that the S-T$_-$ mechanism is operative in both, the liquid and the plastic crystalline phase.

In the case of cycloheptanone (figure 6.3.5a)) the magnetic field dependences show one distinct maximum that can be interpreted as the motionally averaged singlet-triplet splitting in the biradical. This effective *J*-coupling, $J_{ex,eff}$, decreases from about 1 T in the liquid to about 0.5 T in the plastic phase (the field dependencies display their maxima at about 2 and 1T). The curves for cycloheptanone are characterized by a width, ΔB (taken at half height), which decreases from 3.3 T in liquid to about 2.5 T in the plastic crystal. For the larger cyclic ketones (n = 8-10), the field dependencies are displayed in figures 6.3.5b) to 6.3.5d). Here also, motionally averaged field dependences are observed in the liquid phase (T = 300K) and well defined maxima are observed. The value of the average *J*-coupling scales with the size of the ketone: as the mean distance between the alkyl and the acyl moiety in the biradical increases, the maximum in the field dependence is observed at lower field indicating a decrease in J_{eff}. In parallel a decrease in width is observed, indicating different efficiency of motional averaging for the flexible biradicals of variable length. In the liquid state, the maxima of the field dependences and their width are comparable to those observed before in deuterated chloroform [11], indicating that the solvent does not contribute significantly to the exchange interaction.

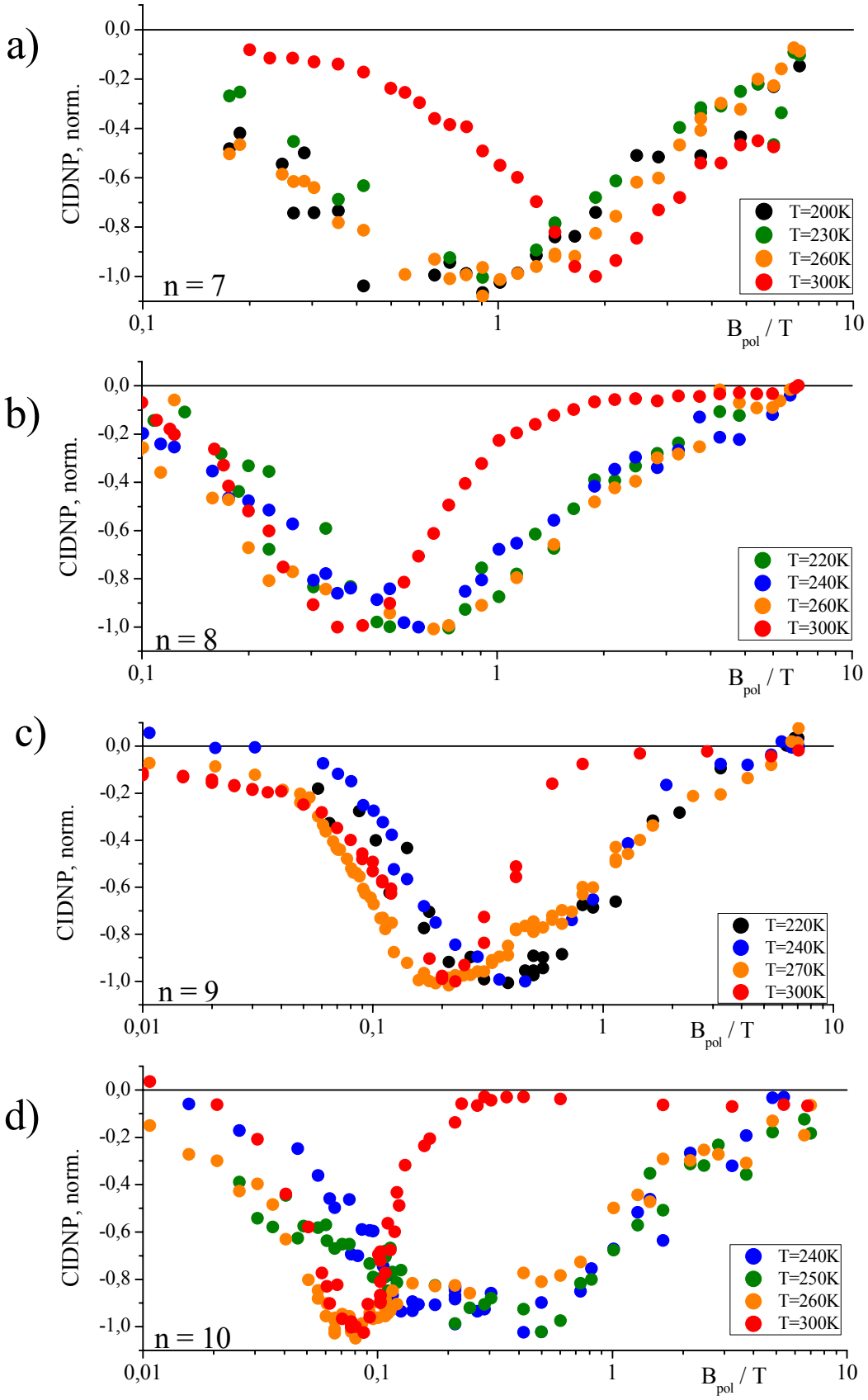

Figure 6.3.5: CIDNP field dependences of a) cycloheptanone, b) cylooctanone, c) cyclononanone, and d) cyclodecanone at variable temperature. All CIDNP field dependences are normalized to unity at the maximum and plotted against a logarithmic field scale.

For cyclodecanone the corresponding field dependences are shown in figure 6.3.5d). The red points represent the motionally averaged case in the liquid state, they display a well resolved maximum at around B_{max} = 0.08 T with a width of ΔB = 0.07 T. Upon the transition to the plastic crystalline phase the averaging differs substantially from that in the liquid state: At 260 K a second polarization maximum appears at around 0.45 T and, upon further cooling, it grows and marks the field of most effective CIDNP formation. The occurrence of more than one maximum in the field dependence is also seen in the case of cyclononanone (fig. 6.3.5c)). In the plastic crystalline phase, the biradicals might be distributed over different subensembles with different J_{eff}, e.g. occupying different number of lattice sites. A similar effect is observed for the ketones with n = 8 and n = 9, but it is less pronounced, probably because the overall shift of the maximum is smaller.

Interestingly, for the ketones with n = 8-10 the maxima shift towards higher field indicating the increase of J_{eff}, whereas in the case of cycloheptanone the effective *J*-coupling between the radical sites decreases. This effect will be discussed in more detail further below together with the CIDNP field dependence of acetone in solid solution, which shows an emissive maximum in a comparable field range.

CIDNP of acetone in liquid C_6D_{12}. CIDNP effects resulting from the photolysis of acetone in liquid solution were studied in detail earlier [163, 170] and S-T_0 mixing was identified as the predominant mechanism. Time resolved CIDNP studies revealed that the following three reaction pathways contribute to the formation of CIDNP [163, 170]. The first is the Norrish type I reaction of triplet acetone leading to formation of acyl and methyl radicals.

$$CH_3COCH_3 \xrightarrow{h\nu} {}^1CH_3COCH_3 \longrightarrow {}^3CH_3COCH_3 \tag{6.3.1}$$

$$CH_3COCH_3 \xrightarrow{h\nu} {}^3CH_3COCH_3 \longrightarrow CH_3\dot{C}O + \dot{C}H_3 \tag{6.3.2}$$

In the presence of hydrogen donors such as cyclohexane, hydrogen (actually deuterium) atom abstraction from the solvent (cyclohexane-d_{12}) by triplet acetone occurs, resulting in the formation of ketyl and cyclohexyl radicals:

$${}^3CH_3COCH_3 + C_6D_{12} \longrightarrow CH_3\dot{C}ODCH_3 + \dot{C}_6D_{11} \tag{6.3.3}$$

The third reaction is the reaction of triplet acetone with ground state acetone. It results in the formation of acetonyl and ketyl radicals:

$${}^3CH_3COCH_3 + CH_3COCH_3 \longrightarrow CH_3\dot{C}OHCH_3 + C\dot{H}_2COCH_3 \tag{6.3.4}$$

Under the present experimental conditions, reaction 6.3.4 is only of minor importance, because of the low concentration of acetone used. However, because of cross termination reactions of the radicals formed in the reactions 6.3.1 to 6.3.4 in the liquid phase, the photolysis of acetone leads to a variety of products that will only be briefly discussed here, since most of the products detected in the present study have been subject to previous CIDNP investigations [163, 170]. Measuring highly resolved CIDNP spectra at variable magnetic field, however, enables the identification of reaction products emerging from the diversity of reaction pathways, some of which have not been reported before.

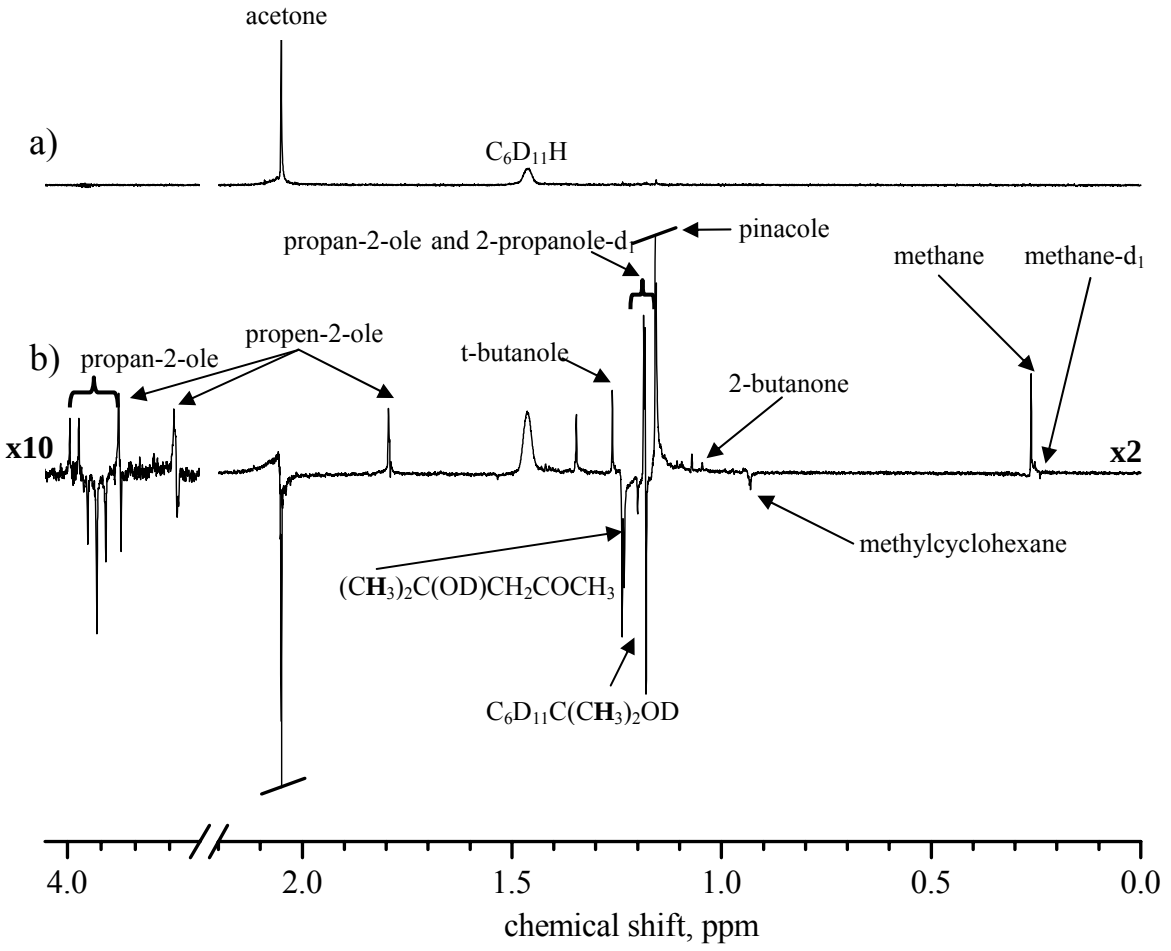

Figure 6.3.6: a) NMR spectrum of acetone in liquid C_6D_{12}; b) CIDNP spectrum at B_{pol} = 7T, τ_l = 2s. Note the different scaling factors for different parts of the CIDNP spectra with respect to the NMR spectrum (x2 and x10).

In figure 6.3.6, the CIDNP spectrum obtained at B_{pol} = 7T is displayed together with the Boltzmann polarized NMR spectrum, which only shows the signals of acetone and $C_6D_{11}H$. The CIDNP spectrum allows the identification of several products formed during the irradiation. The assignment of lines was made by comparison to CIDNP spectra reported in

the literature [163, 170] when available, and additional signals were assigned by comparison to the NMR chemical shifts of purchased compounds.

Time resolved CIDNP studies on the photolysis of acetone in D_2O have revealed that the geminate recombination of acetone leads to the emissive polarization detected for acetone at high magnetic field (see also fig. 6.3.6b)) [163, 170]. This observation is in accordance with the rules of Kaptein for a triplet precursor with the magnetic interaction parameters of the radicals formed in reaction 6.3.3 and 6.3.4. The absorptive net CIDNP for the residual protons in C_6D_{12} (1.46ppm), for enol (3.75, 3.88 and 1.79ppm), isopropanol (3.96 and 1.18ppm), and methane (0.26ppm) is also in accord with ref. [170]. The formation of these products and the additional products assigned in fig. 6.3.6 may all be rationalized in frame reactions 6.3.4 to 6.3.6, the corresponding back reactions, and cross-termination reactions of the involved radicals. The back reaction of reaction 6.3.5 does not exclusively yield acetone, but also its enole (propen-2-ole), which is one of the main reaction products of acetone photolysis in the presence of hydrogen donors.

The observation of emissive CIDNP for acetone (fig. 6.3.6b)) disagrees with the observations reported in refs. [149] and [150], were absorptive CIDNP was reported for acetone and the residual protons in cyclohexane, whereas no signal for the enole form of acetone was detected. The enole converts to acetone on the timescale of about ten seconds at room temperature, and the contradictive observations might be the consequence of different experimental conditions. In the present experiments the sample is irradiated by a pulsed UV laser for less than a second with fast subsequent detection of the NMR spectrum at 7 T. One can assume that under the intensive continuous irradiation by a high-pressure mercury lamp during the detection at 1.88 T in refs. [149] and [150], the equilibrium of the keto-enole tautomerism is established more rapidly. As a consequence, the absorptive net CIDNP of the enole may then be detected as apparent absorptive polarization on acetone. In a later publication Skakovskii et al. [152] report that the absorptive phase of acetone polarization is seen at high temperature of 353 K, while upon cooling to room temperature, it decreases and turns into emissive polarization in rotor phase. In the present experiments the enole signals do not contribute significantly to the acetone polarization, because the enole formed during the laser irradiation decays during the sufficiently long delay time between the experiments.

For some of the signals assigned in fig. 6.3.6, the high field parts of the CIDNP field dependences are displayed in figure 6.3.7. Most of the CIDNP signals do not display a high field maximum and the polarization still grows at B_{pol} = 7 T, while in low field only some of the signals are discernable. Literature values of magnetic interaction parameters for radicals

present during the photolysis are summarized in table 6.3.1, and for some of the radical pairs that form upon random encounter, a high field maximum would be expected in the available field range. An absorptive maximum is seen around B_{pol} = 4 T for the signals appearing at 1.345 and 2.6 ppm that could not be assigned. The similarity of the field dependences of these two signals suggests that they belong to the same product or at least that they share common precursor radicals (acetonyl and cyclohexyl). The signal that is tentatively assigned to acetylcyclohexane (2.25ppm) shows an emissive maximum at 2 T, while the application of Adrians model [28] with the magnetic interaction parameters from table 6.3.1 predicts a high field maximum around 1 T. For the formation of pinacole from symmetrical radical pairs containing two 2-propanol-2-yl radicals (Δg = 0), no CIDNP would be expected at high magnetic field, nevertheless CIDNP is formed quite efficiently. Obviously, many of the products show CIDNP which they inherit from the primary formed RP.

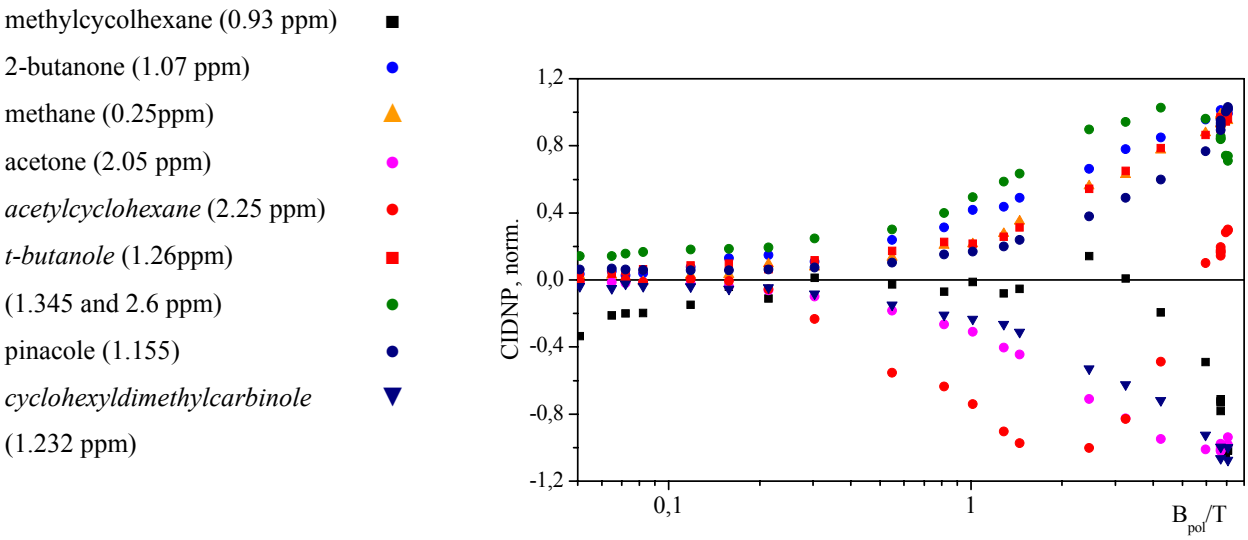

Figure 6.3.7: CIDNP field dependence of products formed during the photolysis of acetone in liquid C_6D_{12}. The compounds in italic letters are to be considered as tentative assignments.

The primary RP can be identified by the CIDNP field dependence of the acetone line, displaying its high field maximum close to B_{pol} =7T, which accords with the small difference in g-factors between the 2-propanol-2-yl radical and the cyclohexyl radical (see table 6.3.1). Assuming triplet acetone as the precursor (μ = +), in cage recombination (ε = +), and a positive Δg for the radical pair formed in reaction 6.3.5, the emissive acetone polarization is allegeable only with a negative hyperfine interaction in the 2-propanol-2-yl radical. This follows from the sign rules of CIDNP and at high magnetic field.

A detailed analysis of the diverse reaction pathways of acetone photolysis and the CIDNP patterns that emerge from them is not the aim of the present study, but rather the elucidation of the mechanism of CIDNP formation as compared to the solid state. The occurrence of different signs of net polarization, the shape of the field dependences and the observed multiplet patterns in low magnetic fields, evidence that spin sorting processes are responsible for the formation of CIDNP in the reaction products in the liquid, because these are characteristic features for the S-T_0 mechanism to be operative.

radical	formula	g_{iso}	HFC / G	ref.
2-propanol-2-yl	$(CH_3)_2COH$	2.0032	19.7G (CH_3); 0.45G (OH)	a)
cyclohexyl	C_6D_{11}	2.0026	2.10 (1); 4.00(2); 0.55(2)	b)
methyl	CH_3	2.00255	-22.8G	c)
methylketyl (acetyl)	CH_3CO	2.0005	+5.1G (A_β)	d)
acetonyl	CH_3COCH_2	2.00446	-19.74G (A_α)	a)
hydrogen	H (D)	2.00223	503.8 (77.5)	c)

Table 6.3.1: Literature values of magnetic interaction parameters of radicals formed during the photolysis of acetone in C_6D_{12}. a) H. Zeldes, R. Livingston [171], b) P. M. K. Leung, J. W. Hunnt [172], c) R. W. Fessenden, R. H. Schuler [142], d) J. E. Bennet, B. Mile [173].

CIDNP of acetone in plastic crystalline C_6D_{12}. Upon cooling the acetone solution into the rotor phase of the host molecule, the NMR lines broaden to roughly 100Hz. The NMR spectrum is seen in 6.3.8a). The CIDNP spectrum at 1.1 T in figure 6.3.8 c) displays emissive lines for acetone and (2.1 ppm) and cyclohexane (1.5 ppm); only net polarization but no multiplet polarization is observed. Furthermore, the CIDNP spectrum shows additional emissive maxima assigned to isopropanol (1.18 ppm) and enol (1,78 ppm), 1-cyclohexylpropan-2-one (1.72ppm) and acetylcyclohexane (1.28 ppm). All these products may be formed without translational displacements of radicals.

The relative intensity of the individual lines changes significantly with the magnetic field, and at high field (see B_{pol} = 6.95 T, fig. 6.3.8b)) most of the spectrum is in absorption. However, in the field range from 0.1 to 5T all lines show emissive polarization irrespective of the signs of hyperfine coupling and g-factors of the individual radicals. When integrating separate fractions between 0.7 and 2.2 ppm, each of them has the same emissive maximum at B_{pol} = 1.25 T. This observation is characteristic for the predominance of the S-T. channel of intersystem crossing and can not be attributed to a transfer of polarization, because the lines are assigned to different products which occupy different lattice sites. The sign of

polarization, Γ, is solely determined by the spin multiplicity of the precursor and the sign of the exchange interaction J_{ex}:

$$\Gamma = \mu \, \mathrm{sign}(J_{ex}) \quad , \tag{6.3.5}$$

where $\mu = 1$ applies for a singlet and $\mu = -1$ for a triplet precursor.

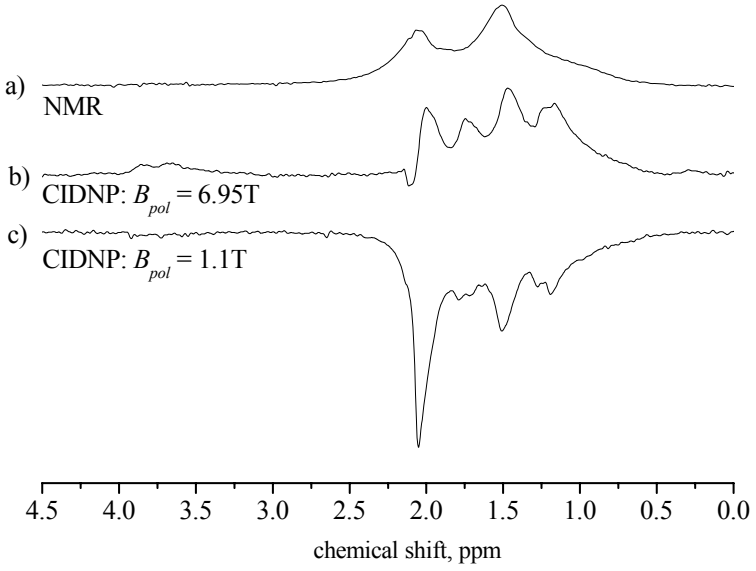

Figure 6.3.8: a) NMR spectrum (absorptive) and CIDNP (emissive) spectra of acetone in C_6D_{12} at B_{pol} = 1.1 T and T = 270 K.

In contrast to case of biradicals the CIDNP field dependence does not change gradually upon cooling, but abruptly at the phase transition of the solvent as can be seen in figure 6.3.9. Slightly below the phase transition, the maximum position is detected at 1.25T, and the amplitude of low field polarization is reduced by a factor of 200 as compared to the high field maximum. The position and the width of the CIDNP curve as functions of the external magnetic field in the plastic crystalline phase are very close to those for the cyclic ketones with n = 7-10 at the lowest temperatures.

A closer inspection of the high field CIDNP spectrum (fig. 6.3.8 b)) allows one to see absorptive polarization at 0.26 ppm. It is attributed to methane, and its formation is considered as proof for the occurrence of the Norrish type I photo reaction in the plastic crystalline phase. The signal for methane has an absorptive maximum around B_{pol} = 6.3 T (fig. 6.3.9). The absorptive polarization of methane is explained with a sufficiently high mobility of the methyl radical in the rotor phase of cyclohexane to allow CIDNP to be formed via the S-T_0 mechanism. For the spin sorting process to become efficient, the exchange coupling must become zero ($J_{ex} \approx 0$), and the absorptive polarization of the other signals in high field (fig.

6.3.8 b)) is also attributed to S-T_0 transitions. The exchange interaction in radical pairs involving the cyclohexyl radical may become sufficiently small upon rotational displacement of the radical centres. When the temperature is lowered from 270K to 250K, the contribution of the S-T_0 mechanism to CIDNP formation becomes smaller. In figure 6.3.9 the CIDNP intensity is normalized at the emissive maxima attributed to S-T.-transitions for two temperatures in the plastic crystalline phase (250K and 270K). Because of the reduced mobility, the absorptive high field part is significantly reduced upon lowering the temperature.

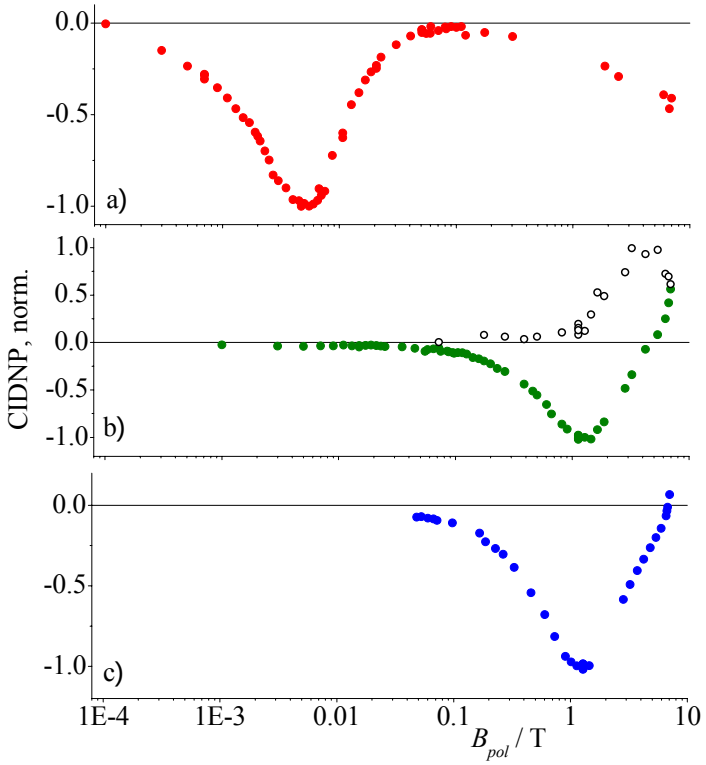

Figure 6.3.9: CIDNP field dependences observed during the photolysis of acetone in liquid and plastic crystalline C_6D_{12} at variable temperature. a) ● acetone line (2.05 ppm) at T = 295 K; b) ●: 0.5 to 2.25ppm at T = 270K, ○: 0.25ppm at T = 270K, b) ●: 0.5 to 2.25ppm at T = 250K.

A diffusional displacement of most radicals during the lifetime of the radicals is improbable and the contribution from diffusional radical pairs (F-pairs) to polarization is negligible. On the basis of the emissive sign of the CIDNP signals for both acetone and cyclohexane and their CIDNP field dependence with an emissive maximum at B_{pol} = 1.25 T detected in the solid the CIDNP is attributed to the predominance of S-T.-transitions, as they are seen in the photocleavage of the cyclic ketones with n = 7 to 10 with acyl-alkyl biradical as intermediates.

Geometrical interpretation of the CIDNP field dependences in solid matrix. The size of the observed effective exchange interaction $J_{ex,eff}$ can be understood in the frame of a simple geometrical model and on the basis of the assumption that the radical intermediates keep the high rotational mobility in the rotor phase of C_6D_{12}. In the solid matrix, the average distance of 0.87nm between C_6D_{12} neighbours in the fcc lattice serves as an effective size of the cage that is left for the guest to occupy individual lattice sites. With Monte Carlo statistics for the description of the conformational motion of the polymethylene chain [162, 174], for the 1,7-biradical formed during the photolysis of cycloheptanone the average distance of radical centers is estimated to about 0.7nm. One can further assume that the biradical is rather flexible and moves fast in its cage when substituting one C_6D_{12} molecule. It is known that the exchange interaction has an exponential dependence on the distance r between the paramagnetic centers (see formula 2.1.8). Accordingly with the exchange interaction parameters $J_{ex,0}$ = -7·10^5 T (taking $\alpha \approx (R_B)^{-1}$ = 0.214 nm^{-1}, where R_B is the Bohr radius) obtained earlier for acyl alkyl biradicals [175], the size of the cage leads to a minimum J_{eff} of about 0.019 T, while the observed $J_{ex,eff}$ = 0.67 T corresponds to a reasonable average distance of about 0.0707 nm.

The cyclic ketones with n = 9 and n = 10 have a considerably larger volume and it can be assumed that they hardly fit into a single lattice site. Its corresponding 1,10-biradical for instance reduces in average size from 0.83 nm (J_{eff} = 0.04 T) in the liquid phase to 0.74 nm corresponding to an increase of J_{eff} to 0.25 T under the confinement in the rotor phase. Under these steric constraints it is rather obvious to assume that a fraction of these biradicals occupies two lattice sites, leading to a larger average r and thus smaller J_{eff} = 0.04 T for them. This explains the cyclodecanone field dependence with two maxima, which can also be seen in the case of cyclononanone.

In the case of the acetone photolysis the ketone molecule itself and consequently any of the radical formed from the triplet acetone molecule are smaller than the 0.87 nm of the matrix cage and therefore can rotate without much constraint. Similarly the cyclohexyl radical, which is known to have a shape close to that of cyclohexane is expected to rotate in the matrix. Assuming that J_0 and α of the ketyl-alkyl pair are close to those of the acyl-alkyl pair, the maximum position of B_{max} = 1.25 T corresponds to an average distance of 0.696 nm for the radical centers. For such distance no distortions of the matrix is expected, and accordingly the position of B_{max} stays constant over the whole rotor phase and only the polarization amplitude decreases with decreasing mobility. The decrease in amplitude is attributed to singlet-triplet evolution induced by spin-orbit coupling.

Conclusions

The present work identifies the mechanism of CIDNP formation in acyl-alkyl biradicals formed in the photolysis of cyclic ketones of the general formula $C_nH_{2n-2}O$ in liquid and plastic crystalline C_6D_{12} by their characteristic field dependences. The starting compounds show strong emissive polarization with decreasing size when lowering the temperature. The polarization remains in the whole temperature range in the rotor phase and vanishes with the phase transition to the rigid crystalline phase. In both liquid and plastic crystalline phase, the S-T$_-$ mechanism is responsible for the CIDNP effects in the reaction products. In the photolysis of acetone the dominating mechanism for CIDNP formation changes from S-T_0 mixing in liquid solution to S-T$_-$ mixing upon phase transition to the plastic crystal. The vanishing polarization upon phase transition to the rigid crystal evidences that sufficient molecular mobility is a prerequisite for polarizing the nuclear spins. In the rotor phase, all systems under investigation show their emissive maximum in a comparable field range, which allows the suggestion that the size of the matrix determines the average value of exchange interaction between the partners in the radical pair ($2\,J_{ex,eff} \approx$ -1.25 T).

The RP's that form during the photolysis of acetone are not connected via a network of chemical bonds. In this case, the exchange interaction is entirely transmitted through space. In the matrix, the larger cyclic ketones exhibit exchange interactions, which is somewhat smaller (up to one order of magnitude). It can be concluded that a through space mechanism is also dominating in the case of the cyclic ketones with n>7, and their smaller $J_{ex,eff}$ is amenable with greater distortions in the lattice leading to larger radical distances. A through bond mechanism might contribute in the case of cycloheptanone. An eventual through solvent contribution may be excluded on the basis that similar positions of maxima are observed in the liquid with cyclohexane as a solvent as with $CDCl_3$ in an earlier study [11].

The investigation shows that measuring CIDNP as a function of the external field opens the unique possibility for the determination of mechanisms of CIDNP formation and the characterization of structures and properties of radical intermediates. It would be particularly interesting to apply the method to the polarization observed in photosystem II, because it opens the possibility to determine the value of $J_{ex,eff}$, and check the influence of molecular mobility. Generally, the technique might allow accessing values for the exchange interactions between redox centers in proteins transmitted along long chemical paths containing sigma and H-bonds.

7 Summary and Outlook

The present work is a comprehensive study of the various factors determining the outcome of field cycling NMR experiments; and in majority it deals with hyper-polarized spin systems generated by means of CIDNP. In the first two chapters the reader is introduced, and the basic principles of spin quantum mechanics necessary to understand the formation of CIDNP at variable magnetic field, and the appearance of NMR spectra after field switching are provided. The experimental techniques are described in chapter 3, and in the remaining part of the thesis, experimental results are discussed in three separate chapters according to the different stages typical for field cycling NMR experiments.

Chapter 4 is devoted to changes in the observed spectra caused by the peculiarities of the nuclear spin systems of diamagnetic species (spin-spin couplings and chemical shifts) at variable field. The collective character of the energy states describing the nuclear spin systems in low fields, being ordered differently from the corresponding Zeeman states at high field, has important implications for field cycling NMR experiments. In particular, the redistribution of hyper-polarization due to strong scalar coupling by isotropic mixing, and the inter-conversion between coherence and polarization by rapid field switches are explored. Coherences generally occur in the nuclear spin density matrix after rapid changes of the Hamiltonian. In addition, NMRD data for the individual proton sites of N-acetyl tryptophan in the fast motional limit are analyzed and shown to also depend on the same parameters.

When hyper-polarization (HP) is formed in low magnetic fields where the nuclear spins are coupled strongly, i.e. when the scalar coupling, J, between them becomes comparable to their difference in Larmor frequency, nuclear spin polarization tends to become equalized within a time corresponding to J. Similarly, the T_1-relaxation times detected for individual protons in strongly coupled spin-system tend to be the same, giving rise to stepwise features in their NMRD data. These effects have to be accounted for when interpreting NMRD curves in terms of molecular mobility or chemical shift anisotropy.

In homo-nuclear spin systems of organic molecules, level anti-crossings among spin states with the same total spin projections, J_z, are frequently present in fields up to several Tesla. In level crossing fields, the effects can become particularly pronounced and give rise to maxima and minima in both, NMRD data, and in the field dependences of HP. Observation of such features is shown to crucially depend on the timing of each step in the field cycling experiment.

Finally, new field cycling schemes are devised that aim to exploit the transfer of coherence into polarization by fast controlled switches through regions of anti-crossings. Both, (0)-quantum-coherences formed during the recombination of radicals and those generated by rapid field switches are employed in polarization transfer experiments. By applying appropriate field cycling schemes, particular coherences in multi-spin systems can be selected in order to transfer polarization from primarily polarized spins to remote target spins of choice via several spacer spins, when the strong coupling condition is fulfilled for neighbouring spins.

The results have implications for the design field cycling NMR experiments in the future. A selective transfer of spin-polarization to hetero-nuclei may become feasible when the available field range is extended to lower fields, where level anti-crossings between nuclei of different gyro-magnetic ratio can be expected. This way the particularly low sensitivity of hetero-nuclei (e.g. ^{13}C or ^{15}N) could be enhanced, which is often detrimental in NMR and imaging (MRI) studies with these nuclei.

The observation of level-crossings in different kinds of field-cycling NMR experiments in the nuclear spin-systems under study further opens a new possibility for determining the signs and magnitudes of very small spin-spin couplings, which have not been accessible hitherto. Conventional 2D-methods can usually not reveal such small couplings due to their limited spectral resolution. Determination of these spin-spin couplings may be helpful for a more thorough understanding of the nature of *J*-coupling and its relation to molecular structure.

A simple modification of the NMRD experiments in terms of an additional pulse prior to the field cycle revealed a source for multi-exponential relaxation behaviour by demonstrating the interdependence of the evolution of magnetization for solvent-protons (HDO) with those in the dissolved amino acid. This approach enables separating the inter-molecular cross-relaxation between solute and solvent spins from the spin-lattice relaxation, thus allowing the extraction of cross-relaxation rates. The factors determining the efficiency of this magnetization exchange may be elucidated in more detail by e.g. varying the proton concentration of the solvent, determining cross-relaxation rates as a function of the external field, and studying larger bio-molecules. A more comprehensive study may open new opportunities to gain insight into location and mobility and thus the function of water in macromolecules.

When low-field CIDNP experiments are aimed at the extraction of HFC's of individual nuclei in a radical under study, the abovementioned effects have to be considered. CIDNP redistribution among strongly coupled spins renders this information unavailable when the

time for light irradiation is chosen too long as compared to the inverse scalar coupling between the nuclei in the diamagnetic products. Furthermore, treating the field switch entirely adiabatic or sudden is usually unrealistic, and can not account for the observed spectral patterns. In principle, the influence of the field switch on the populations and coherences in the nuclear spin density matrices of individual spin-systems has to be accounted for numerically, and may then allow a quantitative evaluation of the spin density distribution in the precursor radicals.

In coupled multi-spin systems, the analysis of polarization patterns is often complicated by the large number of different transitions giving rise to the final NMR spectrum. The energetic ordering of nuclear spin states in low field gives rise to particular polarization patterns in hyper-polarized spin systems. These patterns are termed 'ALTADENA' in the case of PHIP experiments or 'multiplet-effects' in case of CIDNP, and manifest themselves as absorption and emission within the lines of a given spin-multiplet.

Both, the coherences connecting the states of the same total spin quantum number, and the populations of the individual levels reveal themselves in characteristic dependences of individual lines in the spectrum on the RF-flip angle when the spin systems are initially in non-equilibrium states. In chapter 5, a new method for the analysis of hyper-polarized NMR spectra as a function of the RF-flip angle is applied. Fourier decomposition of a series of spectra taken at different flip angles disentangles the contributions of multiplet-effects of different order (number of spins) by their characteristic nutation frequencies. When going to very low fields, eventually all spins in the multi spin system become strongly coupled. This gives rise to multiplet-effects of high order that stretch along entire chains of scalar coupled spins, with NMR signals in emission at one end of the chemical shift scale and absorption on the other. Evaluation of high order multiplet CIDNP is expected to add further information of the coupling topology in the molecule under study and thus help in exploring efficient polarization transfer pathways.

Keeping the abovementioned phenomena in mind, the photo-CIDNP technique can contribute considerably to a thorough understanding of the underlying photo-physics and –chemistry of light induced radical reactions. This is demonstrated in chapter 6, which deals with the analysis of different reaction systems that give rise to CIDNP upon laser irradiation (λ = 308nm).

In chapter 6.1, the photolysis of the aromatic amino acids tyrosine and tryptophan is shown to lead to CIDNP on the parent compounds in the absence of triplet sensitizers. In addition, strong CIDNP on the residual protons in the solvent (HDO) is detected in both cases. Analysis

of CIDNP as a function of time (TR-CIDNP), and as a function of the external field (FD-CIDNP) shows that different radical pairs have to be considered to explain these observations. First, CIDNP is formed in singlet radical pairs consisting of the primary amino acid radicals formed by photo-ionization with the solvated electron (e^-_{aq}), showing that e^-_{aq} can be treated as a diffusing radical within the radical pair model of CIDNP formation.

In addition, the parent aromatic amino acids are easily oxidized by e^-_{aq}, and a second path for the formation of CIDNP becomes available. The radicals formed by electron attachment can disproportionate with the primary amino acid radicals upon recovery of the parent amino acids, giving rise to characteristic shapes of the high field part of their CIDNP field dependences. At the same time, the amino acids undergo a selective H/D-exchange, and the polarization formed on HDO is reconciled with the chemical exchange.

In general, strong nuclear polarization of water molecules is desirable for its potential use as a contrast agent in functional MRI studies. In the abovementioned photo-cycle, nuclear spin polarization could be formed immediately at the place where the water is employed as a contrast agent. The ubiquitous function of water in physiology and the fact that its chemical properties do not depend on its magnetization renders this substance a particularly attractive candidate for *in vivo* sensitivity enhancement.

While the spin density distribution in the precursor radicals is often not available from FD-CIDNP, the determination of isotropic g-factors of individual radicals is not affected by the redistribution of polarization. Reliable values for amino acid and sensitizer radicals were extracted from the positions of most efficient CIDNP formation by the Δg-mechanism (high field CIDNP). Their determination is relatively accurate because of the determination of g-factor differences instead of the g-factors themselves. Hence, the method is well suited for investigating radical species under ambient condition in aqueous solution that are often elusive to other methods.

In a comprehensive study, the abovementioned amino acids are studied in quenching reactions with different triplet sensitizers in chapter 6.2. The radical reactions leading to CIDNP and the protonation steps of the intermediates are discussed in detail. The prerequisite for the determination of isotropic g-factors from the high field part of the CIDNP field dependence is the precise knowledge of one of the g-factors in the RP under study. Here, it is the combination of different amino acids with the same dye molecules that allows a reliable extraction of g-factors by simultaneously extracting the same parameter from several experimental curves. This way, the previously unknown g-factor of the short lived radical of tryptophan in its protonated form ($NATrpH^{\bullet+}$) in aqueous solution is determined. The most

obvious continuation of the present studies would be an extension to further dye molecules and other CIDNP active amino acids and small peptides that allow comparing the extracted quantities to those of other radicals.

The effect of molecular mobility on CIDNP formation is subject to the last chapter (6.3). In majority it deals with polarization formed by nuclear spin dependent S-T$_-$-transitions ($J_{ex} \neq 0$) in cyclic ketones. Analysis of CIDNP and its dependence on the external field in liquid and plastic crystalline solutions of C_6D_{12} and the absence of CIDNP in the crystalline phase showed, that some residual mobility is necessary for the observation of CIDNP. For cyclic ketones of different size, lowering the temperature in the plastic phase induces increasing constraints for the biradicals under study and results in comparable values of J_{ex} which are attributed to the matrix dimensions. In the case of the non-cyclic ketone acetone, the prevailing mechanism of CIDNP formation changes abruptly from S-T$_0$ in liquid to S-T$_-$ in the plastic crystalline phase, indicating that J_{ex} is primarily transmitted 'through space'.

A successful implementation of the MAS technique in combination with the fast field cycling apparatus still remains an open task. The systems of ketones and in particular that of acetone, in plastic crystalline matrices of C_6D_{12} are expected to be well suited as model systems. Here, the lines of individual components could not be assigned unambiguously in the plastic phase, and the MAS technique is expected to provide the resolution necessary to enable an assignment. This may not only provide further insight into the photo-chemistry of the system under study, but also allows one to study the redistribution of non-thermal polarization by dipole-dipole interactions and influences of their suppression by MAS on the efficiency. Implications for the observation of CIDNP in photosynthetic reaction centres are conceivable, and investigating their CIDNP field dependence is anticipated to provide an insight into the mechanisms underlying the formation of nuclear spin polarization in these systems.

Finally, there are numerous possibilities to exploit the phenomena discovered in the present work, and only a few opportunities could be covered within this thesis. It is expected that field cycling NMR techniques with hyper-polarized spin systems will gain more attention in the future for their potential applications of highly selective polarization transfer schemes to particular nuclei of choice. The present studies already initiated further research activities, in particular by extending the investigations of efficient polarization transfer to a larger variety of CIDNP active compounds. These studies are expected to establish far more efficient exploitation of different hyper-polarization phenomena by controlled field switches than hitherto possible, besides of the ongoing investigation of radical reactions and their intermediates by field dependent and time resolved DNP techniques.

8 Bibliography

1. Salikhov, K.M., Molin, Y.N., Sagdeev, R.Z., and Buchachenko, A.L. (1984). Spin Polarization and Magnetic Effects in Chemical Reactions (Amsterdam: Elsevier).
2. Muus, L.T., Atkins, P.W., McLauchlan, K.A., and Pedersen, J.B. (1977). NATO Advanced Study Institute Series, Vol. C34: Chemically Induced Magnetic Polarization (Dordrecht: Kluwer).
3. Ritz, T., Thalau, P., Phillips, J.B., Wiltschko, R., and Wiltschko, W. (2004). Resonance effects indicate a radical-pair mechanism for avian magnetic compass. Nature (London, United Kingdom) *429*, 177-180.
4. Cintolesi, F., Ritz, T., Kay, C.W.M., Timmel, C.R., and Hore, P.J. (2003). Anisotropic recombination of an immobilized photoinduced radical pair in a 50-mT magnetic field: a model avian photomagnetoreceptor. Chemical Physics *294*, 385-399.
5. Ritz, T., Dommer, D.H., and Phillips, J.B. (2002). Shedding light on vertebrate magnetoreception. Neuron *34*, 503-506.
6. Ritz, T., Adem, S., and Schulten, K. (2000). A model for photoreceptor-based magnetoreception in birds. Biophysical Journal *78*, 707-718.
7. van der Horst, M.A., Laan, W., Yeremenko, S., Wende, A., Palm, P., Oesterhelt, D., and Hellingwerf, K.J. (2005). From primary photochemistry to biological function in the blue-light photoreceptors PYP and AppA. Photochemical & Photobiological Sciences *4*, 688-693.
8. Fiedler, B., Borner, T., and Wilde, A. (2005). Phototaxis in the cyanobacterium Synechocystis sp. PCC 6803: role of different photoreceptors. Photochemistry and photobiology *81*, 1481-1488.
9. Kimmich, R., and Editor (1997). NMR-Tomography, Diffusometry, Relaxometry. (Berlin: Springer)
10. Grosse, S., Gubaydullin, F., Scheelken, H., Vieth, H.M., and Yurkovskaya, A.V. (1999). Field cycling by fast NMR probe transfer: design and application in field-dependent CIDNP experiments. Applied Magnetic Resonance *17*, 211-225.
11. Grosse, S. (2000). CIDNP-Untersuchungen an photoinduzierten Radikalpaar-Reaktionen im Magnetfeldbereich von 0 - 7T. PhD thesis, Freie Universität Berlin, Berlin, Germany.
12. Bluemich, B., Kuhn, W., and Editors (1992). Magnetic Resonance Microscopy: Methods and Applications in Materials Science, Agriculture and Biomedicine. (Weinheim: VCH)
13. Natterer, J., and Bargon, J. (1997). Parahydrogen induced polarization. Progress in Nuclear Magnetic Resonance Spectroscopy *31*, 293-315.
14. Jeffries, C.D. (1963). Dynamic Nuclear Orientation (Interscience: New York).
15. Hausser, K.H., and Stehlik, D. (1968). Dynamic nuclear polarization in liquids. In Advances in Magnetic Resonance, Volume 3 pp. 79-139.
16. Salerno, M., Altes, T.A., Mugler, J.P., 3rd, Nakatsu, M., Hatabu, H., and de Lange, E.E. (2001). Hyperpolarized noble gas MR imaging of the lung: potential clinical applications. European journal of radiology *40*, 33-44.
17. Buntkowsky, G., Bargon, J., and Limbach, H.-H. (1996). A Dynamic Model of Reaction Pathway Effects on Parahydrogen-Induced Nuclear Spin Polarization. Journal of the American Chemical Society *118*, 8677-8683.
18. Bowers, C.R., and Weitekamp, D.P. (1987). Parahydrogen and synthesis allow dramatically enhanced nuclear alignment. Journal of the American Chemical Society *109*, 5541-5542.

19. Pravica, M.G., and Weitekamp, D.P. (1988). Net NMR alignment by adiabatic transport of para-hydrogen addition products to high magnetic field. Chemical Physics Letters *145*, 255-258.
20. Bargon, J., Fischer, H., and Johnsen, U. (1967). Nuclear magnetic resonance emission lines during fast radical reactions. I. Recording methods and examples. Zeitschrift für Naturforschung, Teil A: Astrophysik, Physik und Physikalische Chemie *22*, 1551-1555.
21. Ward, H.R., and Lawler, R.G. (1967). Nuclear magnetic resonance emission and enhanced absorption in rapid organometallic reactions. Journal of the American Chemical Society *89*, 5518-5519.
22. Kaptein, R., and Oosterhoff, L.J. (1969). Chemically induced dynamic nuclear polarization. III. Anomalous multiplets of radical coupling and disproportionation products. Chemical Physics Letters *4*, 214-216.
23. Kaptein, R., and Oosterhoff, L.J. (1969). Chemically induced dynamic nuclear polarization. II. Relation with anomalous ESR spectra. Chemical Physics Letters *4*, 195-197.
24. Closs, G.L. (1969). Mechanism explaining nuclear spin polarizations in radical combination reactions. Journal of the American Chemical Society *91*, 4552-4554.
25. Closs, G.L., and Trifunac, A.D. (1970). Theory of chemically induced nuclear spin polarization. V. Comparison of coupling reactions in singlet and triplet derived radical pairs and of radicals not generated in pairs. Journal of the American Chemical Society *92*, 2186-2187.
26. Atkins, P.W. (1977). The Triplet Mechanism. In ref. [2] pp. 191-203
27. Adrian, F.J. (1970). Role of diffusion-controlled reaction in chemically induced nuclear spin polarization. Journal of Chemical Physics *53*, 3374-3375.
28. Adrian, F.J. (1971). Role of diffusion-controlled reaction in chemically induced nuclear-spin polarization. II. General theory and comparison with experiment. Journal of Chemical Physics *54*, 3912-3917.
29. Claude Cohen Tannoudji, B.D., Frank Laloë (1977). Quantum Mechanics, Volume 1. (Berlin: deGruyter)
30. Closs, G.L., and Trifunac, A.D. (1970). Theory of chemically induced nuclear spin polarization. III. Effect of isotropic g shifts in the components of radical pairs with one hyperfine interaction. Journal of the American Chemical Society *92*, 2183-2184.
31. Redfield, A.G. (1966). The theory of relaxation processes. Advan. Magn. Resonance *1*, 1-32.
32. Angerhofer, A., and Bittl, R. (1996). Radicals and radical pairs in photosynthesis. Photochemistry and Photobiology *63*, 11-38.
33. Lowdin, P.O. (1962). Exchange correlation, and spin effects in molecular and solid-state theory. Reviews of Modern Physics *34*, 80-87.
34. Herring, C., and Flicker, M. (1964). Asymptotic exchange coupling of two hydrogen atoms. Physical Review *134*, 362-366.
35. Goldberg, A.H., and Dougherty, D.A. (1983). Effects of through-bond and through-space interactions on singlet-triplet energy gaps in localized biradicals. Journal of the American Chemical Society *105*, 284-290.
36. Miesel, K., Yurkovskaya, A.V., and Vieth, H.-M. (2004). Field dependence of CIDNP in photoreactions in plastic crystalline matrix. Applied Magnetic Resonance *26*, 51-64.
37. Vollenweider, J.K., Fischer, H., Hennig, J., and Leuschner, R. (1985). Time-resolved CIDNP in laser flash photolysis of aliphatic ketones. A quantitative analysis. Chemical Physics *97*, 217-234.
38. Noyes, R.M. (1954). A treatment of chemical kinetics with special applicability to diffusion-controlled reactions. Journal of Chemical Physics *22*, 1349-1359.

39. Kaptein, R. (1971). Simple rules for chemically induced dynamic nuclear polarization. Journal of the Chemical Society D: Chemical Communications, 732-733.
40. Ivanov, K.L., Lukzen, N.N., Vieth, H.-M., Grosse, S., Yurkovskaya, A.V., and Sagdeev, R.Z. (2002). Investigation of the magnetic field dependence of CIDNP in multinuclear radical pairs. 1. Photoreaction of histidine and comparison of model calculation with experimental data. Molecular Physics *100*, 1197-1208.
41. Ivanov, K.L., Vieth, H.-M., Miesel, K., Yurkovskaya, A.V., and Sagdeev, R.Z. (2003). Investigation of the magnetic field dependence of CIDNP in multi-nuclear radical pairs.Part II. Photoreaction of tyrosine and comparison of model calculation with experimental data. Physical Chemistry Chemical Physics *5*, 3470-3480.
42. Kaptein, R., and Den Hollander, J.A. (1972). Chemically induced dynamic nuclear polarization. X. Magnetic field dependence. Journal of the American Chemical Society *94*, 6269-6280.
43. Korchak, S.E., Ivanov, K.L., Yurkovskaya, A.V., and Vieth, H.-M. (2004). Structure and magnetic resonance parameters of the cation-radicals of methionine as studied by the CIDNP magnetic field dependence. ARKIVOC (Gainesville, FL, United States), 121-131.
44. Purtov, P.A., and Doktorov, A.B. (1993). The Green function method in the theory of nuclear and electron spin polarization. I. General theory, zero approximation and applications. Chemical Physics *178*, 47-65.
45. Osintsev, A.M., Purtov, P.A., and Salikhov, K.M. (1993). Calculation of SNP effects in weak magnetic fields. Chemical Physics *174*, 237-245.
46. Schulten, K., and Wolynes, P.G. (1978). Semiclassical description of electron spin motion in radicals including the effect of electron hopping. Journal of Chemical Physics *68*, 3292-3297.
47. Osintsev, A.M., Purtov, P.A., and Salikhov, K.M. (1992). Semiclassical calculations of the effect of nuclear chemical polarization in weak magnetic fields for radical pairs with large number of magnetic nuclei. Khimicheskaya Fizika *11*, 1192-1201.
48. Seurig, M. (2005). Entwurf und Konstruktion eines magnetisch neutralen Probenkopfes für Messungen der chemisch induzierten dynamischen Kernspinpolarisation mit schneller Feldzyklisierung. Diploma thesis, TFH Berlin, Berlin, Germany.
49. Levitt, M.H. (2002). Spin Dynamics - Basics of Nuclear Magnetic Resonance (Chichester: Wiley).
50. Ernst, R.R., Bodenhausen, G., and Wokaun, A. (1987). Principles of Nuclear Magnetic Resonance in One and Two Dimensions (Oxford: Clarendon Press).
51. Schäublin, S., Höhener, A., and Ernst, R.R. (1974). Fourier spectroscopy of nonequilibrium states, application to CIDNP, Overhauser experiments, and relaxation time measurements. Journal of Magnetic Resonance (1969-1992) *13*, 196-216.
52. Vollenweider, J.K., and Fischer, H. (1986). Time-resolved CIDNP in laser flash photolysis of di-tert-butyl ketone. Multiplet versus net effects. Chemical Physics *108*, 365-372.
53. Ivanov, K.L., Miesel, K., Vieth, H.M., Yurkovskaya, A.V., and Sagdeev, R.Z. (2003). 2D NMR nutation analysis of non-thermal polarization of coupled multi-spin systems. Zeitschrift fuer Physikalische Chemie (Muenchen, Germany) *217*, 1641-1659.
54. De Kanter, F.J.J., and Kaptein, R. (1979). CIDNP transfer via nuclear dipolar relaxation and spin-spin coupling. Chemical Physics Letters *62*, 421-426.
55. Miesel, K., Ivanov, K.L., Yurkovskaya, A.V., and Vieth, H.-M. (2006). Coherence transfer during field-cycling NMR experiments. Chemical Physics Letters *425*, 71-76.

56. Ivanov, K.L., Miesel, K., Yurkovskaya, A.V., Korchak, S.E., Kiryutin, A.S., and Vieth, H.-M. (2006). Transfer of CIDNP Among Coupled Spins at Low Magnetic Field. Applied Magnetic Resonance *30*, 513-534.
57. Schäublin, S., Wokaun, A., and Ernst, R.R. (1976). The creation of off-diagonal elements in chemically induced dynamic nuclear polarization experiments. Chemical Physics *14*, 285-293.
58. Schäublin, S., Wokaun, A., and Ernst, R.R. (1977). Pulse techniques applied to chemically induced dynamic nuclear polarization. Journal of Magnetic Resonance (1969-1992) *27*, 273-302.
59. Salikhov, K.M. (1993). Creation of spin coherent states in the course of chemical reactions. Chemical Physics Letters *201*, 261-264.
60. Landau, L. (1932). Theory of energy transfer. II. Physikalische Zeitschrift der Sowjetunion *2*, 46-51.
61. Zener, C. (1932). Non-Adiabatic Crossing of Energy Levels. Proceedings of the Royal Society of London. Series A *137*, 696-702.
62. Wittig, C. (2005). The Landau-Zener formula. The journal of physical chemistry. B *109*, 8428-8430.
63. Ivanov, K.L., Yurkovskaya, A.V., and Vieth, H.-M. (2008). High resolution NMR study of T1 magnetic relaxation dispersion. I. Theoretical considerations of relaxation of scalar coupled spins at arbitrary magnetic field. Journal of chemical physics, *submitted*.
64. Kiryutin, A.S., Ivanov, K.L., Yurkovskaya, A.V., and Vieth, H.-M. (2008). High-resolution study of nuclear magnetic relaxation dispersion of purine nucleotides: Effects of spin-spin coupling. Solid State Nuclear Magnetic Resonance, *doi: 10.1016/j.ssnmr.2008.03.004*, *in press*.
65. Abragam, A. (1987). The Principles of Nuclear Magnetism, 5th Edition (Oxford: Clarendon Press).
66. Hore, P.J., Zuiderweg, E.R.P., Kaptein, R., and Dijkstra, K. (1981). Flash photolysis NMR. CIDNP time dependence in cyclic photochemical reactions. Chemical Physics Letters *83*, 376-383.
67. Closs, G.L., and Miller, R.J. (1981). Laser flash photolysis with NMR detection. Submicrosecond time-resolved CIDNP: kinetics of triplet states and biradicals. Journal of the American Chemical Society *103*, 3586-3588.
68. Morozova, O.B., Yurkovskaya, A.V., Sagdeev, R.Z., Mok, K.H., and Hore, P.J. (2004). Time-resolved CIDNP study of native-state bovine and human a-lactalbumins. Journal of Physical Chemistry B *108*, 15355-15363.
69. Goez, M. (1990). Evaluation of flash CIDNP experiments by iterative reconvolution. Chemical Physics Letters *165*, 11-14.
70. Korchak, S. (2004). Investigation of Short Lived Radicals of Methionine in Aqueous Solutions by CIDNP. Diploma thesis, Novosibirsk State University, Novosibirsk, Russia.
71. Buntkowsky, G. (1991). Untersuchungen an organischen Festkörpern mit optischer Kerspinpolarisation und Multiquanten-NMR. PhD thesis, Freie Universität Berlin, Berlin, Germany.
72. Kiryutin, A.S., Morozova, O., Kuhn, L.T., Yurkovskaya, A., and Hore, P.J. (2007). 1H and 13C hyperfine coupling constants of the tryptophanyl cation radical in aqueous solution from time-resolved CIDNP. J. Phys. Chem. B *111* 11221-11227.
73. Solomon, I. (1955). Relaxation processes in a system of two spins. Physical Review *99*, 559-565.
74. Tsentalovich, Y.P., Morozova, O.B., Yurkovskaya, A.V., and Hore, P.J. (1999). Kinetics and mechanism of the photochemical reaction of 2,2'-dipyridyl with

tryptophan in water: Time-resolved CIDNP and laser flash photolysis study. Journal of Physical Chemistry A *103*, 5362-5368.
75. Miesel, K., Ivanov, K.L., Köchling, T., Yurkovskaya, A.V., and Vieth, H.-M. (2008). Field Cycling Effects on Dynamic Nuclear Polarization. Applied Magnetic Resonance *in press*.
76. Born, M., and Fock, V. (1928). Proof of the adiabatic principle. Zeitschrift für Physik *51*, 165-180.
77. Kuhn, L.T., Bommerich, U., and Bargon, J. (2006). Transfer of Parahydrogen-Induced Hyperpolarization to ^{19}F. Journal of Physical Chemistry A *110*, 3521-3526.
78. Boelens, R., Podoplelov, A., and Kaptein, R. (1986). Separation of net polarization and multiplet effect in coupled spin systems by two-dimensional CIDNP. Journal of Magnetic Resonance (1969-1992) *69*, 116-123.
79. Ivanov, K.L., and Sagdeev, R.Z. (2006). Using the spin echo technique for separation of spin orders in CIDNP spectra. Doklady Physical Chemistry *409*, 221-223.
80. Wang, J., Doubleday, C., Jr., and Turro, N.J. (1989). Negative temperature dependence in the decay of triplet biradicals. Journal of the American Chemical Society *111*, 3962-3965.
81. Fischer, H., and Hellwege, K.-H. (1977). Magnetic Properties of Free Radicals, Landolt-Börnstein (Berlin: Springer).
82. Closs, G.L., and Doubleday, C.E. (1973). Determination of the average singlet-triplet splitting in biradicals by measurement of the magnetic field dependence of CIDNP. Journal of the American Chemical Society *95*, 2735-2736.
83. Fischer, H., and Lehnig, M. (1971). Nuclear and electron spin polarizations during radical reactions. Journal of Physical Chemistry *75*, 3410-3416.
84. Creed, D. (1984). The photophysics and photochemistry of the near-UV absorbing amino acids. II. Tyrosine and its simple derivatives. Photochemistry and Photobiology *39*, 563-575.
85. Creed, D. (1984). The photophysics and photochemistry of the near-UV absorbing amino acids. I. Tryptophan and its simple derivatives. Photochemistry and Photobiology *39*, 537-562.
86. Debus, R.J., Barry, B.A., Babcock, G.T., and McIntosh, L. (1988). Site-directed mutagenesis identifies a tyrosine radical involved in the photosynthetic oxygen-evolving system. Proceedings of the National Academy of Sciences of the United States of America *85*, 427-430.
87. Barry, B.A. (1993). The role of redox-active amino acids in the photosynthetic water-oxidizing complex. Photochemistry and photobiology *57*, 179-188.
88. Dryhurst, G. (1990). Applications of electrochemistry in studies of the oxidation chemistry of central nervous system indoles. Chemical Reviews (Washington, DC, United States) *90*, 795-811.
89. Stubbe, J.A. (1989). Protein radical involvement in biological catalysis? Annual review of biochemistry *58*, 257-285.
90. Simic, M., and Hayon, E. (1971). Reductive deamination of oligopeptides by solvated electrons in aqueous solution. Radiation Research *48*, 244-255.
91. Hill, D.J.T., O'Donnell, J.H., Pomery, P.J., and Whittaker, A.K. (1986). The UV photolysis of N-acetyl amino acids studied by ESR as models for biological polypeptides. Polymer Photochemistry *7*, 13-25.
92. Jin, F., Leitich, J., and von Sonntag, C. (1995). The photolysis (λ = 254 nm) of tyrosine in aqueous solutions in the absence and presence of oxygen. The reaction of tyrosine with singlet oxygen. Journal of Photochemistry and Photobiology, A: Chemistry *92*, 147-153.

93. London, R.E., and Gabel, S.A. (2006). Photoactivated H/D Exchange in Tyrosine: Involvement of a Radical Anion Intermediate. Journal of the American Chemical Society *128*, 2268-2275.
94. Birch, A.J. (1944). Reduction by dissolving metals. I. Journal of the Chemical Society, 430-436.
95. Feitelson, J., and Hayon, E. (1973). Electron ejection and electron capture by phenolic compounds. Journal of Physical Chemistry *77*, 10-15.
96. Cocivera, M., Tomkiewicz, M., and Groen, A. (1972). Electron paramagnetic resonance and nuclear spin polarization study of the photooxidation of phenol in water. Journal of the American Chemical Society *94*, 6598-6604.
97. Tomkiewicz, M., McAlpine, R.D., and Cocivera, M. (1972). Photooxidation and decarboxylation of tyrosine studied by EPR and CIDNP techniques. Canadian Journal of Chemistry *50*, 3849-3856.
98. Bussandri, A., and van Willigen, H. (2002). FT-EPR Study of the Wavelength Dependence of the Photochemistry of Phenols. Journal of Physical Chemistry A *106*, 1524-1532.
99. Mezzetti, A., Maniero, A.L., Brustolon, M., Giacometti, G., and Brunel, L.C. (1999). A Tyrosyl Radical in an Irradiated Single Crystal of N-Acetyl-L-tyrosine Studied by X-band cw-EPR, High-Frequency EPR, and ENDOR Spectroscopies. Journal of Physical Chemistry A *103*, 9636-9643.
100. Anbar, M., and Neta, P. (1967). A Compilation of Specific Bimolecular Rate Constants for the Reactions of Hydrated Electrons, Hydrogen Atoms and Hydroxyl Radicals with Inorganic and Organic Compounds in Aqueous Solution. International Journal of Applied Radiation and Isotopes *18*, 193-523.
101. Matheson, M.S., and Rabani, J. (1965). Pulse radiolysis of aqueous hydrogen solutions. I. Rate constants for reaction of e^-_{aq} with itself and other transients. II. The interconvertibility of e^-_{aq} and H. Journal of Physical Chemistry *69*, 1324-1335.
102. Gottlieb, H.E., Kotlyar, V., and Nudelman, A. (1997). NMR chemical shifts of common laboratory solvents as trace impurities. Journal of Organic Chemistry *62*, 7512-7515.
103. Jeevarajan, A.S., and Fessenden, R.W. (1989). ESR studies of solvated electron in liquid solution using photolytic production. Journal of Physical Chemistry *93*, 3511-3514.
104. Sealy, R.C., Harman, L., West, P.R., and Mason, R.P. (1985). The electron spin resonance spectrum of the tyrosyl radical. Journal of the American Chemical Society *107*, 3401-3406.
105. Fasanella, E.L., and Gordy, W. (1969). Electron spin resonance of an irradiated single crystal of L-tyrosine-HCl. Proceedings of the National Academy of Sciences of the United States of America *62*, 299-304.
106. Un, S., Atta, M., Fontecave, M., and Rutherford, A.W. (1995). g-Values as a Probe of the Local Protein Environment: High-Field EPR of Tyrosyl Radicals in Ribonucleotide Reductase and Photosystem II. Journal of the American Chemical Society *117*, 10713-10719.
107. Un, S., Tang, X.-S., and Diner, B.A. (1996). 245 GHz High-Field EPR Study of Tyrosine-D Deg and Tyrosine-Z Deg in Mutants of Photosystem II. Biochemistry *35*, 679-684.
108. Hoganson, C.W., Sahlin, M., Sjoeberg, B.-M., and Babcock, G.T. (1996). Electron Magnetic Resonance of the Tyrosyl Radical in Ribonucleotide Reductase from Escherichia coli. Journal of the American Chemical Society *118*, 4672-4679.

109. Hayashi, H., Sakaguchi, Y., Murai, H., and I'Haya, Y.J. (1986). CIDEP studies of the formation of cyclohexadienyl-type radicals in the photoreduction of aromatic ketones. Journal of Physical Chemistry *90*, 4403-4407.
110. Eiben, K., and Schuler, R.H. (1975). ESR spectra of the carboxylated cyclohexadienyl radicals. Carbon-13 hyperfine constants and the effect of carboxylation on the g-factors and proton hyperfine constants. Journal of Chemical Physics *62*, 3093-3108.
111. Neta, P., and Fessenden, R.W. (1971). Electron spin resonance study of radicals produced in irradiated aqueous solutions of amines and amino acids. Journal of physical chemistry *75*, 738-748.
112. Fessenden, R.W., and Schuler, R.H. (1963). E.S.R. spectrum of the cyclohexadienyl radical. Journal of Chemical Physics *38*, 773-774.
113. Tsentalovich, Y.P., and Morozova, O.B. (2000). Laser flash photolysis and time resolved CIDNP study of photoreaction of 2,2'-dipyridyl with N-acetyltyrosine in aqueous solutions. Journal of Photochemistry and Photobiology, A: Chemistry *131*, 33-40.
114. Clancy, C.M.R., and Forbes, M.D.E. (1999). Time-resolved electron paramagnetic resonance study of photoionization of tyrosine anion in aqueous solution. Photochemistry and Photobiology *69*, 16-21.
115. Closs, G.L., and Miller, R.J. (1979). Laser flash photolysis with NMR detection. Microsecond time-resolved CIDNP: separation of geminate and random-phase processes. Journal of the American Chemical Society *101*, 1639-1641.
116. Bent, D.V., and Hayon, E. (1975). Excited state chemistry of aromatic amino acids and related peptides. III. Tryptophan. Journal of the American Chemical Society *97*, 2612-2619.
117. J. F. Baugher, L.I.G. (1977). Photolysis Mechanism of Aqueous Tryptophan. The Journal of Physical Chemistry *81*, 1349-1354.
118. Posener, M.L., Adams, G.E., Wardman, P., and Cundall, R.B. (1976). Mechanism of tryptophan oxidation by some inorganic radical-anions: a pulse radiolysis study. Journal of the Chemical Society, Faraday Transactions 1: Physical Chemistry in Condensed Phases *72*, 2231-2239.
119. Braams, R. (1966). Rate constants of hydrated electron reactions with amino acids. Radiation research *27*, 319-329.
120. Saito, I., Sugiyama, H., Yamamoto, A., Muramatsu, S., and Matsuura, T. (1984). Photoinduced reactions. 158. Photochemical hydrogen-deuterium exchange reaction of tryptophan. The role of nonradiative decay of singlet tryptophan. Journal of the American Chemical Society *106*, 4286-4287.
121. Ichino, T., and Fessenden, R.W. (2003). Energy Requirements for Inverted CIDEP in Reactions between e^-_{aq} or Radical Anions and Phenoxyl Radicals. Journal of Physical Chemistry A *107*, 9257-9268.
122. Wagenknecht, H.-A. (2006). Electron transfer processes in DNA: mechanisms, biological relevance and applications in DNA analytics. Natural Product Reports *23*, 973-1006.
123. Kaptein, R., Dijkstra, K., and Nicolay, K. (1978). Laser photo-CIDNP as a surface probe for proteins in solution. Nature (London, United Kingdom) *274*, 293-294.
124. Hore, P.J., Winder, S.L., Roberts, C.H., and Dobson, C.M. (1997). Stopped-Flow Photo-CIDNP Observation of Protein Folding. Journal of the American Chemical Society *119*, 5049-5050.
125. Stob, S., and Kaptein, R. (1989). Photo-CIDNP of the amino acids. Photochemistry and Photobiology *49*, 565-577.
126. Roth, H.D. (2006). Nuclear-spin polarization in electron-transfer reactions of amines. Helvetica Chimica Acta *89*, 2847-2860.

127. Roth, H.D., and Manion, M.L. (1975). Photoreactions of ketones with amines. CIDNP criteria for the intermediacy of aminoalkyl radicals and aminium radical ions. Journal of the American Chemical Society *97*, 6886-6888.
128. Goez, M., Rozwadowski, J., and Marciniak, B. (1998). CIDNP spectroscopic observation of $(S\text{-}N)^+$ radical cations with a two-center three-electron bond during the photooxidation of methionine. Angewandte Chemie, International Edition *37*, 628-630.
129. Goez, M., and Rozwadowski, J. (1998). Reversible Pair Substitution in CIDNP: The Radical Cation of Methionine. Journal of Physical Chemistry A *102*, 7945-7953.
130. Fabian, H., Grosse, S., Onnen, M., Vieth, H.-M., and Yurkovskaya, A. (2002). Chemically induced dynamic nuclear polarization (CIDNP) in the photoreaction of N-acetyl histidine, tyrosine, and tryptophan with 2,2'-dipyridyl and its dependence on the magnetic field. RIKEN Review *44*, 134-136.
131. Koenig, E., and Fischer, H. (1962). Electron spin resonance (E.S.R.) studies on the anion radical of 2,2'-dipyridyl. Zeitschrift für Naturforschung *17a*, 1063-1066.
132. Loeff, I., Treinin, A., and Linschitz, H. (1983). Photochemistry of 9,10-anthraquinone-2-sulfonate in solution. 1. Intermediates and mechanism. Journal of Physical Chemistry *87*, 2536-2544.
133. Loeff, I., Treinin, A., and Linschitz, H. (1984). The photochemistry of 9,10-anthraquinone-2-sulfonate in solution. 2. Effects of inorganic anions: quenching vs. radical formation at moderate and high anion concentrations. Journal of Physical Chemistry *88*, 4931-4937.
134. Tickle, K., and Wilkinson, F. (1965). Photoreduction of anthraquinone in isopropanol. Transactions of the Faraday Society *61*, 1981-1990.
135. Ma, J., Lin, W., Wang, W., Han, Z., Yao, S., and Lin, N. (1999). Characterization of reactive intermediates in laser photolysis of nucleoside using of sodium salt anthraquinone-2-sulfonic acid as photosensitizer. Radiation Physics and Chemistry *54*, 491-497.
136. Lu, J.-M., Wu, L.M., Geimer, J., and Beckert, D. (2001). Time resolved FT-EPR study of the decarboxylation following photo-induced electron transfer between α-amino acids and anthraquinone-2,6-disulfonic acid in aqueous solution. Physical Chemistry Chemical Physics *3*, 2053-2058.
137. Tarabek, P., Bonifacic, M., and Beckert, D. (2006). Time-pesolved FT EPR and optical spectroscopy study on photooxidation of aliphatic α-amino acids in aqueous solutions; Electron transfer from amino vs carboxylate functional group. Journal of Physical Chemistry A *110*, 7293-7302.
138. Tarabek, P., Bonifacic, M., and Beckert, D. (2004). Photooxidation of Glycylglycine. Two-Channel Reaction Mechanism as Studied by Time-Resolved FT EPR. Journal of Physical Chemistry A *108*, 3467-3470.
139. Geimer, J., and Beckert, D. (1998). Study of radical pairs generated by photoreduction of anthraquinone-2,6-disulfonic acid with thymine by Fourier transform electron paramagnetic resonance. Chemical Physics Letters *288*, 449-458.
140. Makela, R., and Vuolle, M. (1989). Electron spin resonance, ENDOR and TRIPLE resonance of some 9,10-anthraquinone radicals in solution. 2. Anthraquinonesulfonates. Journal of the Chemical Society, Faraday Transactions 1: Physical Chemistry in Condensed Phases *85*, 4011-4017.
141. Byrdin, M., Sartor, V., Eker, A.P.M., Vos, M.H., Aubert, C., Brettel, K., and Mathis, P. (2004). Intraprotein electron transfer and proton dynamics during photoactivation of DNA photolyase from E. coli: review and new insights from an "inverse" deuterium isotope effect. Biochimica et Biophysica Acta, Bioenergetics *1655*, 64-70.

142. Fessenden, R.W., and Schuler, R.H. (1963). Electron spin resonance studies of transient alkyl radicals. Journal of Chemical Physics *39*, 2147-2195.
143. Himo, F., and Eriksson, L.A. (1997). Theoretical Study of Model Tryptophan Radicals and Radical Cations: Comparison with Experimental Data of DNA Photolyase, Cytochrome c Peroxidase, and Ribonucleotide Reductase. Journal of Physical Chemistry B *101*, 9811-9819.
144. Walden, S.E., and Wheeler, R.A. (1996). Distinguishing features of indolyl radical and radical cation: implications for tryptophan radical studies in proteins. Journal of Physical Chemistry *100*, 1530-1535.
145. Walden, S.E., and Wheeler, R.A. (1997). First Evidence of Anchimeric Spin Delocalization in Tryptophan Radical Cation. Journal of the American Chemical Society *119*, 3175-3176.
146. Jakopitsch, C., Obinger, C., Un, S., and Ivancich, A. (2006). Identification of Trp106 as the tryptophanyl radical intermediate in Synechocystis PCC6803 catalase-peroxidase by multifrequency Electron Paramagnetic Resonance spectroscopy. Journal of Inorganic Biochemistry *100*, 1091-1099.
147. Ivancich, A., Jakopitsch, C., Auer, M., Un, S., and Obinger, C. (2003). Protein-based radicals in the catalase-peroxidase of Synechocystis PCC 6803: A multifrequency EPR investigation of wild-type and variants on the environment of the heme active site. Journal of the American Chemical Society *125*, 14093-14102.
148. Bleifuss, G., Kolberg, M., Poetsch, S., Hofbauer, W., Bittl, R., Lubitz, W., Graeslund, A., Lassmann, G., and Lendzian, F. (2001). Tryptophan and Tyrosine Radicals in Ribonucleotide Reductase: A Comparative High-Field EPR Study at 94 GHz. Biochemistry *40*, 15362-15368.
149. Obynochny, A.A., Maryasov, A.G., Purtov, P.A., Salikhov, K.M., and Molin, Y.N. (1994). Proton polarization during acetone photolysis in solid cyclohexane. Doklady Akademii Nauk *337*, 479-482.
150. Obynochny, A.A., Purtov, P.A., Maryasov, A.G., Molin, Y.N., Salikhov, K.M., and Skakovsky, E.D. (1995). CIDNP in photolysis of acetone solutions in plastic crystals of cyclohexane-d12. Applied Magnetic Resonance *9*, 355-365.
151. Obynochny, A.A., Maryasov, A.G., Purtov, P.A., and Salikhov, K.M. (1998). The CIDNP effect in plastic crystals. Applied Magnetic Resonance *15*, 259-268.
152. Skakovskii, E.D., Shirokii, O.V., Tychinskaya, L.Y., Ogorodnikova, M.M., and Rykov, S.V. (2002). Nonequilibrium polarization of nuclei in photolysis of solid cyclohexane solutions of diacyl peroxides and ketones. Journal of Applied Spectroscopy (Translation of Zhurnal Prikladnoi Spektroskopii) *69*, 689-694.
153. McDermott, A., Zysmilich, M.G., and Polenova, T. (1998). Solid state NMR studies of photoinduced polarization in photosynthetic reaction centers: mechanism and simulations. Solid State Nuclear Magnetic Resonance *11*, 21-47.
154. Zysmilich, M.G., and McDermott, A. (1996). Photochemically Induced Nuclear Spin Polarization in Bacterial Photosynthetic Reaction Centers: Assignments of the ^{15}N SSNMR Spectra. Journal of the American Chemical Society *118*, 5867-5873.
155. Zysmilich, M.G., and McDermott, A. (1994). Photochemically Induced Dynamic Nuclear Polarization in the Solid-State ^{15}N Spectra of Reaction Centers from Photosynthetic Bacteria Rhodobacter sphaeroides R-26. Journal of the American Chemical Society *116*, 8362-8363.
156. Prakash, S., Alia, Gast, P., de Groot, H.J.M., Matysik, J., and Jeschke, G. (2006). Photo-CIDNP MAS NMR in Intact Cells of Rhodobacter sphaeroides R26: Molecular and Atomic Resolution at Nanomolar Concentration. Journal of the American Chemical Society *128*, 12794-12799.

157. Prakash, S., Alia, Gast, P., de Groot, H.J.M., Jeschke, G., and Matysik, J. (2005). Magnetic Field Dependence of Photo-CIDNP MAS NMR on Photosynthetic Reaction Centers of Rhodobacter sphaeroides WT. Journal of the American Chemical Society *127*, 14290-14298.
158. Alia, Roy, E., Gast, P., Van Gorkom, H.J., De Groot, H.J.M., Jeschke, G., and Matysik, J. (2004). Photochemically Induced Dynamic Nuclear Polarization in Photosystem I of Plants Observed by ^{13}C Magic-Angle Spinning NMR. Journal of the American Chemical Society *126*, 12819-12826.
159. Prakash, S., Alia, Gast, P., Jeschke, G., de Groot, H.J.M., and Matysik, J. (2003). Photochemically induced dynamic nuclear polarisation in entire bacterial photosynthetic units observed by ^{13}C magic-angle spinning NMR. Journal of Molecular Structure *661-662*, 625-633.
160. Jeschke, G., and Matysik, J. (2003). A reassessment of the origin of photochemically induced dynamic nuclear polarization effects in solids. Chemical Physics *294*, 239-255.
161. Jeschke, G. (1998). A new mechanism for chemically induced dynamic nuclear polarization in the solid state. Journal of the American Chemical Society *120*, 4425-4429.
162. Leuschner, R., and Fischer, H. (1985). Type I cleavage of triplet acetone in solution studied by time-resolved CIDNP. Chemical Physics Letters *121*, 554-558.
163. Porter, G., Dogra, S.K., Loutfy, R.O., Sugamori, S.E., and Yip, R.W. (1973). Triplet state of acetone in solution. Deactivation and hydrogen abstraction. Journal of the Chemical Society, Faraday Transactions 1: Physical Chemistry in Condensed Phases *69*, 1462-1474.
164. Würflinger, A. (1994). Steric considerations in the low temperature phases of cyclohexane. Zeitschrift für Physikalische Chemie (Muenchen, Germany) *186*, 183-194.
165. Farman, H., Coveney, F., Dore, J.C., and Bellissent-Funel, M.C. (1996). Structural studies of cyclohexane C_6D_{12} by neutron diffraction. III. Temperature variation measurements for the liquid and plastic crystal phases. Molecular Physics *87*, 1217-1233.
166. Stapf, S., and Kimmich, R. (1997). Translational versus rotational molecular dynamics in plastic crystals studied by NMR relaxometry and diffusometry. Molecular Physics *92*, 1051-1060.
167. Poupko, R., and Luz, Z. (1981). Dynamic deuterium NMR in liquid crystalline solvents: ring inversion of cyclohexane-d12. Journal of Chemical Physics *75*, 1675-1681.
168. Fried, F. (1973). Molecular motions in four medium-size cyclic ketones. Molecular Crystals and Liquid Crystals *20*, 1-12.
169. Tsentalovich, Y.P., Yurkovskaya, A.V., and Sagdeev, R.Z. (1993). Flash CIDNP measurement of triplet lifetimes and investigation of two-photon processes. Journal of Photochemistry and Photobiology, A: Chemistry *70*, 9-16.
170. Livingston, R., and Zeldes, H. (1966). Paramagnetic resonance study of liquids during photolysis. Hydrogen peroxide and alcohols. Journal of Chemical Physics *44*, 1245-1259.
171. Leung, P.M.K., and Hunt, J.W. (1967). Electron spin resonance spectra of free radicals in irradiated cyclohexanecarboxylic acid. Journal of Physical Chemistry *71*, 3177-3186.
172. Bennett, J.E., and Mile, B. (1971). ESR studies of the acetyl and benzoyl radicals. Transactions of the Faraday Society *67*, 1587-1597.

173. De Kanter, F.J.F., Den Hollander, J.A., Huizer, A.H., and Kaptein, R. (1977). Biradical CIDNP and the dynamics of polymethylene chains. Molecular Physics *34*, 857-874.
174. Lal, M., and Spencer, D. (1973). Monte-Carlo computer simulation of chain molecules. V. Flexibility of n-alkane molecules. Molecular Physics *26*, 1-6.
175. Yurkovskaya, A., Grosse, S., Dvinskikh, S., Morozova, O., and Vieth, H.-M. (1999). Spin and Molecular Dynamics of Biradicals as Studied by Low Field Nuclear Polarization at Variable Temperature. Journal of Physical Chemistry A *103*, 980-988.

Publications

In parts, this work has been published in the following contributions:

Papers:

2D NMR nutation analysis of non-thermal polarization of coupled multi-spin systems
K. L. Ivanov, K. Miesel, H.-M. Vieth, A. V. Yurkovskaya, R. Z. Sagdeev
Zeitschrift für Physikalische Chemie (Muenchen, Germany), **2003** *217*, 1641-1659.

Investigation of the magnetic field dependence of CIDNP in multi-nuclear radical pairs.Part II. Photoreaction of tyrosine and comparison of model calculation with experimental data
K. L. Ivanov, H.-M. Vieth, K. Miesel, A. V. Yurkovskaya, R. Z. Sagdeev
Physical Chemistry Chemical Physics, **2003** *5*, 3470-3480.

Field dependence of CIDNP in photoreactions in plastic crystalline matrix
K. Miesel, A. V. Yurkovskaya, H.-M. Vieth
Applied Magnetic Resonance, **2004** *26*, 51-64.

Coherence transfer during field-cycling NMR experiments
K. Miesel, K. L. Ivanov, A. V. Yurkovskaya, H.-M. Vieth
Chemical Physics Letters, **2006** *425*, 71-76.

Transfer of CIDNP among coupled spins at low magnetic field
K. L. Ivanov, K. Miesel, A. V. Yurkovskaya, S. E. Korchak, A.S. Kiryutin H.-M. Vieth
Applied Magnetic Resonance, **2006** *30*, 513-534.

Field-Cycling Effects on Dynamic Nuclear Polarization
K. Miesel, K. L. Ivanov, T. Köchling, A. V. Yurkovskaya, H.-M. Vieth
Applied Magnetic Resonance, **2008**, *in print.*

Posters (selection):

Magnetic Fied Dependence of CIDNP in Acyl-Alkyl-Biradicals of Different Length in Plastic Crystal Matrices

Miesel, K.; Kurnysheva, O.; Yurkovskaya, A.V.; Vieth, H.-M.

16th European Experimental NMR Conference - EENC (Prague, September 2002)

Magnetic Field Dependence of Photo-CIDNP in the Norrish Type I Reaction with Subsequent H-Transfer in Plastic Crystal-Matrices

K. Miesel, A.Yurkovskaya, H.-M. Vieth

Horizons in Hydrogen Bond Research (Berlin, September 2003)

Determination of magnetic interaction parameters in tryptophan and tyrosine radicals by field dependent CIDNP

K. Miesel,; Nascimento de Carvalho Pinto, V.; Ivanov, K. L.; Yurkovskaya, A. V.; Vieth, H.-M.

9th International Symposium on Spin and Magnetic Field Effects in Chemistry and Related Phenomena (Oxford, September 2005)

Coherent transfer of CIDNP in biologically important molecules at low magnetic field

K. Miesel, K. L. Ivanov, A. V. Yurkovskaya, S. E. Korchak, A. S. Kiryutin, H.-M.Vieth.

22nd International Conference on Magnetic Resonance in Biological Systems, (Goettingen, August 2006)

Electron and Hydrogen Transfer Reactions in the Photolysis of Aromatic Amino Acids Studied by CIDNP

K. Miesel, H.-M. Vieth

70th Annual Meeting of German Physical Society in conjunction with the 21st General Conference of the Condensed Matter Division of the European Physical Society (Dresden, April 2006)

Photochemical H/D Exchange in Tyrosine Revealed by Chemically Induced Dynamic Nuclear Polarization

K. Miesel, A.V. Yurkovskaya, H.-M. Vieth.

Triple Symposium (Freyburg/Unstrut, October 2006)

Talks:

Hydrogen Transfer in Radical Reactions Investigated by Field Dependent CIDNP

Horizons in Hydrogen Bond Research (Berlin, September 2003)

Further Publications:

Papers:

Fluorescence Study of the Coil-Globule Transition of a PEO Chain in Toluene

J. P. S. Farinha, S. Picarra, K. Miesel, J. M. G. Martinho

Journal of Physical Chemistry B, **2001** *105*, 10536-10545.

Posters:

Photo-CIDNP studies of intramolecular charge transfer reactions in rigid donor-spacer-acceptor complexes.

Miesel, K.; Onnen, M.; Vieth, H.-M.; Oliver, A.; Paddon-Row, M. N.

67th Annual Meeting of the German Physical Society (Dresden, March 2003)

Quantitative CIDNP of Biomolecules

K. L. Ivanov, S. E. Korchak, K. Miesel, H.-M. Vieth, A. V. Yurkovskaya

22nd International Conference on Magnetic Resonance in Biological Systems, (Goettingen, August 2006)

Acknowledgements

There are numerous people who helped me finally getting to this point, but most importantly I wish to thank Prof. Dr. Hans-Martin Vieth for the opportunity to perform research independently and for his indefatigable belief in me. He is a very special mentor with quite some patience in explaining complicated phenomena sufficiently descriptive to make them accessible to a chemist.

I thank Prof. Dr. Hans-Heinrich Limbach for his interest in my work and for the opportunity to defend it in the chemistry department of FU-Berlin.

I'm grateful to Prof. Dr. Dietmar Stehlik (†) for many encouraging discussions in our seminars. I will always remember outstanding sociability which went far beyond work.

The scientific expertise of Dr. Konstantin L. Ivanov and the encouragement of Dr. Alexandra V. Yurkovskaya were often indispensable for the interpretation of observations and very instructive for the development of new experiments and the choice of appropriate systems for them. Thanks a lot.

Further, I'm grateful to all current and former members and associates of the workgroup of Mr. Vieth. I'm indebted to the former members for the construction of the unique NMR field cycling set-up. My colleagues Sergey Korchak, Alexey Kyriutin and Talea Köchling have been quite generous with their time and helpful to me. I thank Matthias Seurig, Vitor Nascimento de Carvalho Pinto, Srivats Rajasekaran, and Firdus Gubaydullin for assistance and diversion in the lab.

Thanks to Roswitha Brunn, Ingrid Wallat, Sabine Simon and to all the technicians in the physics department for their availability in various manners, and in particular to Mr. Streuber and Mr. Prüfer who were always there when I was in despair with the machines in the student workshop.

My brother Thorsten Miesel lent his expertise in computer programming, preventing me from spending most of my time with manually changing field cycling parameters. Macej Krzystyniak has been very helpful when programming in MATLAB.

Last but not least, this work would not have been possible without the love and constant encouragement of my entire family. Special thanks to my sons Jascha and Jimi and to my wife Tatjana.

Thanks to all the people I forgot to mention personally.